VOLUME 12 (1959) No. 4

NUCLEAR PHYSICS

JOURNAL DEVOTED TO THE EXPERIMENTAL AND THEORETICAL STUDY OF THE FUNDAMENTAL CONSTITUENTS OF MATTER AND THEIR INTERACTIONS

EDITOR: L. ROSENFELD · COPENHAGEN

KEN KIKUCHI, Distribution of the imaginary part of the optical potential . . 305

I. BIAŁYNICKI-BIRULA, Lee model and the local field theory 309

D. M. BRINK and A. K. KERMAN, Two body forces in light deformed nuclei . . 314

V. I. GOLDANSKY, B. B. GOVORKOV and R. G. VASSILKOV, Photoproduction of neutral pions on hydrogen near the threshold 327

M. L. MEHTA, On the singularities of a generalized Brueckner t-matrix . . . 333

RIAZUDDIN, K^0-K^+ mass excess 342

S. GORODETZKY, P. CHEVALLIER, R. ARMBRUSTER et G. SUTTER, Corrélation angulaire de paires de conversion interne détectées dans un fond de neutrons et de rayonnement γ. Application à ^{14}N, ^{10}Be, ^{10}B 349

S. K. BHATTACHERJEE, BALDEV SAHAI and C. V. K. BABA, Decay of Pm^{148} . . . 356

J. BOWCOCK and D. WALECKA, Analytic properties of the Schrödinger amplitude at a fixed angle 371

P. GREGERS HANSEN, O. B. NIELSEN and R. K. SHELINE, Levels in Gd^{156} excited in the decay of 5.6 d Tb^{156} 389

R. E. BELL and M. H. JØRGENSEN, Half-lives of two excited states of Gd^{156} . . 413

S. K. SRINIVASAN and K. VENKATESAN, Photo-production of pion pairs by a nucleon 418

A. T. G. FERGUSON and E. B. PAUL, A study of the energy levels of A^{37}, Sc^{48} and Cr^{51} 426

BÖRJE PERSSON and SVEN A. E. JOHANSSON, Internal bremsstrahlung from P^{32} 432

Book reviews. 446

NORTH-HOLLAND PUBLISHING COMPANY - AMSTERDAM

August (1) 1959

EDITORIAL BOARD

AUSTRALIA & NEW ZEALAND:	H. Messel (Sydney), M. L. Oliphant (Canberra)
AUSTRIA:	B. Karlik, (Vienna), H. Thirring (Vienna)
BELGIUM:	M. de Hemptinne (Louvain), J. Verhaeghe (Ghent)
CANADA:	G. Volkoff (Vancouver)
DENMARK:	C. Møller (Copenhagen), S. Rozental (Copenhagen)
FINLAND:	L. Simons (Helsinki)
FRANCE:	A. Berthelot (Saclay), S. Gorodetzky (Strasbourg)
GERMANY (DEM. REP.):	G. Hertz (Leipzig)
GERMANY (FED. REP.):	W. Gentner (Freiburg i. B.), J. H. D. Jensen (Heidelberg)
GREAT BRITAIN:	S. Devons (Manchester), T. H. R. Skyrme (Harwell)
HUNGARY:	L. Janossy (Budapest)
INDIA:	H. Bhabha (Bombay), R. Ramanna (Trombay)
IRISH REPUBLIC:	J. McConnell (Maynooth)
ISRAEL:	G. Racah (Jerusalem)
ITALY:	E. Amaldi (Rome)
JAPAN:	S. Kikuchi (Tokyo), S. Tomonaga (Tokyo)
MEXICO:	M. Moshinsky (Mexico)
NETHERLANDS:	H. Brinkman (Groningen), S. R. de Groot (Leiden)
NORWAY:	E. Hylleraas (Oslo), A. Lundby (Oslo), H. Wergeland (Trondheim)
POLAND:	L. Infeld (Warsaw)
PORTUGAL:	J. M. Araújo (Porto), J. R. de Almeida Santos (Coimbra)
SOUTH AMERICA:	G. Beck (Saõ Paulo), J. Leite Lopes (Rio de Janeiro)
SPAIN:	J. M. Otero (Madrid), C. Sanchez del Rio (Madrid)
SWEDEN:	O. Klein (Stockholm), K. Siegbahn (Uppsala), I. Waller (Uppsala)
SWITZERLAND:	P. Huber (Basel), P. Scherrer (Zürich)
U.A.R. & ARAB COUNTRIES:	F. El Bedewi (Alexandria), M. G. Nooh (Cairo)
U.S.A.	H. H. Barschall (Madison, Wisconsin), V. Weisskopf (Cambridge, Mass.)
U.S.S.R.:	M. A. Markov (Moscow), I. S. Shapiro (Moscow), D. V. Skobeltzyn (Moscow)
YUGOSLAVIA:	I. Supek (Zagreb)

CONTRIBUTIONS may be sent to the Editor, Professor L. Rosenfeld, NORDITA, Blegdamsvej 17, Copenhagen Ø, either directly, or preferably through the intermediary of one of the members of the Editorial Board of the country or region in which the author is working. They may be written in English, French or German.

NUCLEAR PHYSICS is published in Fortnightly issues. The subscription price per volume of 700 pages is fl 57.00; 114s; a 15.00. Post-free.

SUBSCRIPTIONS should be sent to the publishers, NORTH-HOLLAND PUBLISHING COMPANY, P.O.Box 103, Amsterdam or to any subscription-agent.

BOOKS FOR REVIEW should be sent to Professor Rosenfeld.

No part of this issue may be reproduced in any form, by print, photoprint, microfilm or any other means without written permission from the publisher. Reprints, photoprints or microfilms are obtainable at cost from the publisher.

Printed in the Netherlands

REPRINTS OF NUCLEAR PHYSICS

Available at the Publishers

NUCLEAR ENERGIES AND THE SHELL MODEL

by

NISSAN ZELDES

Department of Physics, The Hebrew University of Jerusalem, Israël

and

Department of Mathematical Physics, University of Birmingham, England

volume 7 (1958) no. 1,
84 pages, 20s., $ 2.80

PARTICLES AND SYMMETRIES

by

E. CORINALDESI

University College of North Staffordshire, Keele, England

volume 7 (1958) no. 4
68 pages, 17s., $ 2.25

ENERGY LEVELS OF LIGHT NUCLEI. VI

by

E. AJZENBERG-SELOVE

Department of Physics, Haverford College, Haverford, Pennsylvania

and

T. LAURITSEN

Kellog Radiation Laboratory, California
Institute of Technology, Pasadena, California

volume 11 (1959) no. 1
320 pages, 40s., $ 5.30

NORTH-HOLLAND PUBLISHING COMPANY

NIEUWE ZIJDS VOORBURGWAL 68-70 AMSTERDAM-C HOLLAND

2.E *Nuclear Physics* **12** (1959) 305—308; © *North-Holland Publishing Co., Amsterdam*
Not to be reproduced by photoprint or microfilm without written permission from the publisher

DISTRIBUTION OF THE IMAGINARY PART OF THE OPTICAL POTENTIAL

KEN KIKUCHI †
School of Physics, University of Minnesota, Minneapolis, Minnesota ††

Received 20 April 1959

Abstract: The radial dependence of the imaginary part of the nuclear optical potential is calculated by the semi-classical independent particle model with a diffuse nuclear boundary. Our method is completely the same as the one proposed by Harada and Oda, whose results are extended for various energies in this work. It is found that the strong absorption at the nuclear surface is less important for intermediate incident energies.

Recently Harada and Oda [1]) have calculated the radial distribution of the absorption coefficient in a nucleus on the basis of the statistical independent-particle model with a diffuse nuclear boundary. Unfortunately, their calculation has been confined only to the Sn nucleus for incident energies of 4, 7 and 14 MeV. However, since the framework of their method has more implications in view of the fact that the thickness of the nuclear surface is roughly independent of mass number, we can derive further conclusions concerning the behaviour of the absorption coefficient. According to their procedure, we begin with the nuclear density distribution

$$\rho(r) = \rho(0)/(1+e^{(r-R)/d}) \quad \text{for} \quad R \gg d, \tag{1}$$

where $\rho(0)$ is the nuclear density at the centre of the nucleus, R the average radius, and d the diffuseness parameter. Following Harada and Oda, the Fermi energy μ_F is expressed as a function of r in the form

$$\mu_F(r) = \mu_F(0)\{f(r)\}^{\frac{2}{3}} \tag{2}$$

with

$$f(r) = \rho(r)/\rho(0). \tag{3}$$

Here $\mu_F(0)$ is the Fermi energy at the centre of the nucleus and is entirely determined by the magnitude of $\rho(0)$. Within the accuracy of our simplifications, the binding energy B for an incident nucleon may be assumed to be constant over the spatial region in which the absorption takes place. Hence the kinetic energy E of the incident nucleon is given by

$$E(r) = \mu_F(r)+B+E_0, \tag{4}$$

† On leave of absence from the Institute for Nuclear Study, University of Tokyo, Japan.
†† This work was supported in part by the U.S. Atomic Energy Commission.

where E_0 is the incident energy outside of the nucleus. This assumption results in a discontinuous form for the nuclear potential and may be less valid for low incident energies. The cross section $\bar{\sigma}$ for a two-body collision

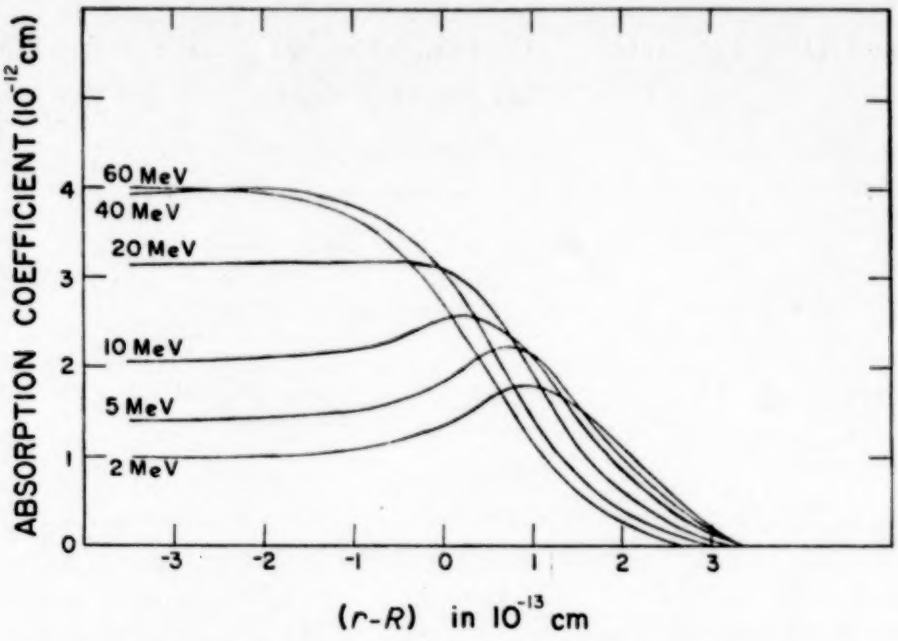

Fig. 1a. Radial distribution of the absorption coefficient calculated for the Fermi energy $\mu_F(0) = 30$ MeV and the nuclear density $\rho(0) = 1.18 \times 10^{38}$ nucleons/cm^3. Figures attached to respective curves indicate the energy of the incident nucleon outside the nucleus.

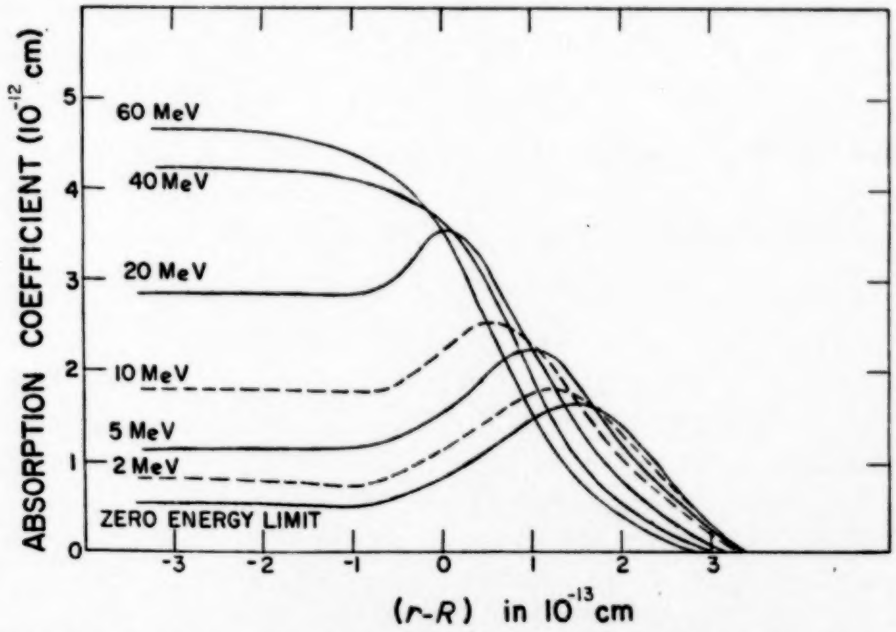

Fig. 1b. Radial distribution of the absorption coefficient calculated for the Fermi energy $\mu_F(0) = 40$ MeV and the nuclear density $\rho(0) = 1.81 \times 10^{38}$ nucleons/cm^3. Figures attached to respective curves indicate the energy of the incident nucleon outside the nucleus.

in the nucleus is given in terms of the cross section for free nucleon-nucleon scattering and of a certain function which takes into account the Pauli principle and depends on the ratio μ_F/E. Thus, for a given value of E_0 and B, the absorption coefficient $K = \rho(r)\bar{\sigma}(r)$ is completely determined by the nuclear density $\rho(r)$, which depends only on $r-R$. Therefore, we can calculate the absorption coefficient K without a specific choice of the nuclear radius. Fig. 1 shows the results calculated for $\mu_F(0) = 30$ MeV and 40 MeV, which correspond to $\rho(0) = 1.18\times10^{38}$ and 1.81×10^{38} nucleons/cm^3, respectively.

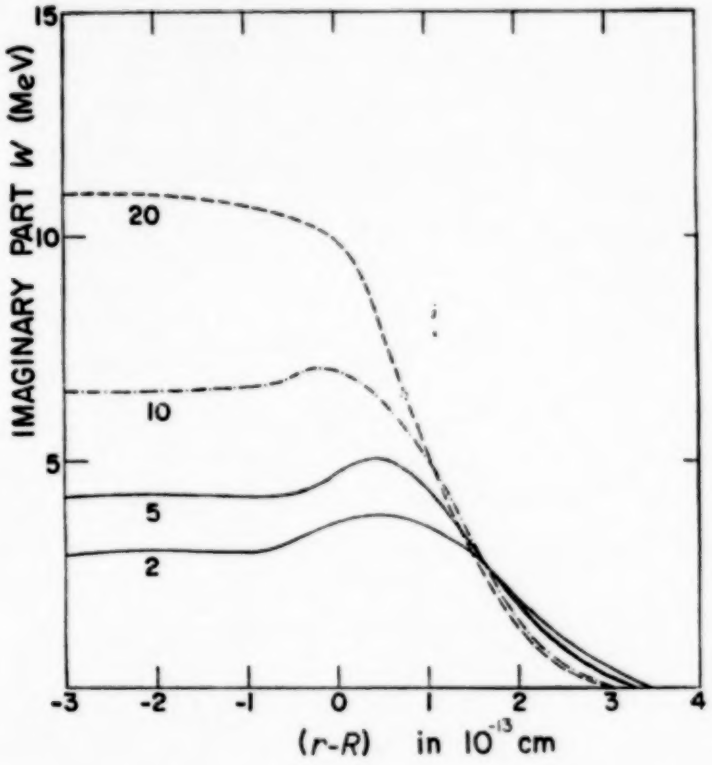

Fig. 2a. Distribution of the imaginary part of the optical potential calculated for the Fermi energy $\mu_F(0) = 30$ MeV and the nuclear density $\rho(0) = 1.18\times10^{38}$ nucleons/cm^3. Figures attached to respective curves indicate the energy of the incident nucleon outside the nucleus.

Here the values $d = 0.57\times10^{-13}$ cm and $B = 8$ MeV are employed. Once the absorption coefficient K is calculated, the imaginary part W of the optical potential can be calculated directly by using the formula

$$W = \sqrt{E\varepsilon}\left(1+\frac{\varepsilon}{4E}\right)^{\frac{1}{2}} \approx \sqrt{E\varepsilon}, \tag{5}$$

where $\varepsilon = \hbar^2K^2/2m$. Fig. 2 shows the calculated distribution of W. From a crude approximation, we can see that the peak of the imaginary part appears only when the following inequality is satisfied:

$$E_0+B \lessapprox \mu_F(0). \tag{6}$$

These results lead to the following conclusions, within the uncertainties of our method:

1. An extremely strong absorption only near the nuclear surface is less realistic for intermediate energies.

2. The peak in the absorption coefficient is important for incident nucleons with energy lower than about 20 MeV.

Conclusion has already been predicted in part by Harada and Oda.

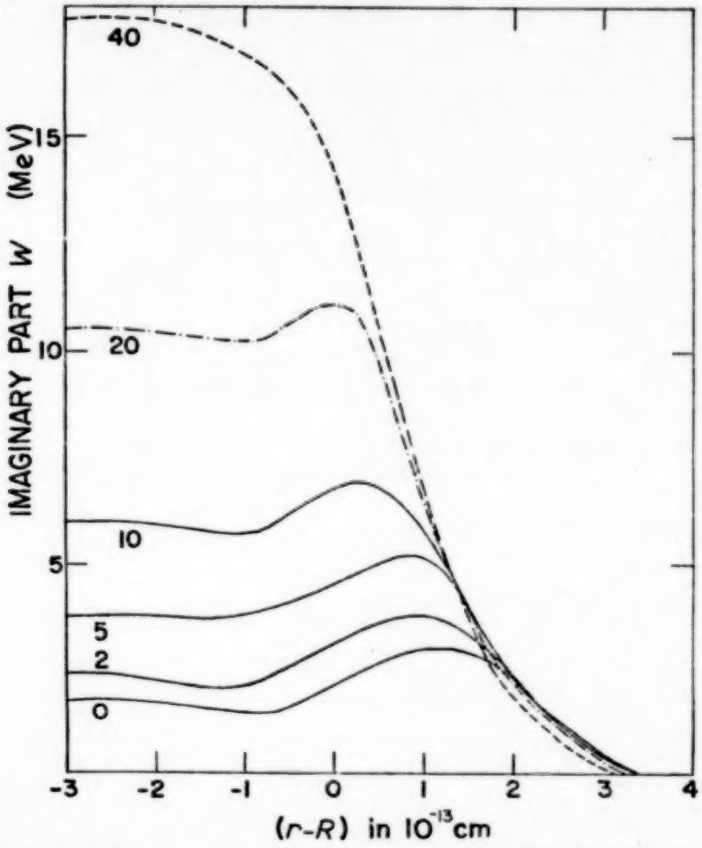

Fig. 2b. Distribution of the imaginary part of the optical potential calculated for the Fermi energy $\mu_F(0) = 40$ MeV and the nuclear density $\rho(0) = 1.81 \times 10^{38}$ nucleons/cm^3. Figures attached to respective curves indicate the energy of the incident nucleon outside the nucleus.

The author expresses his sincere gratitude to Dr. C. E. Porter for helpful discussions and for careful reading of the manuscript.

Reference

1) K. Harada and N. Oda, Prog. Theor. Physics **21** (1959) 260

8.C *Nuclear Physics* **12** (1959) 309—313; © *North-Holland Publishing Co., Amsterdam*
Not to be reproduced by photoprint or microfilm without written permission from the publisher

LEE MODEL AND THE LOCAL FIELD THEORY

I. BIAŁYNICKI-BIRULA
Institute for Theoretical Physics, Warsaw University

Received 31 March 1959

Abstract: The comparison between the Lee model and the usual local field theory is discussed in a certain simple case. The conclusion is that the difficulties associated with the renormalization in the Lee model do not appear in the local field theory.

1. Introduction

The Lee model is the only known model of quantum field theory exactly soluble with renormalization of the coupling constant. However, renormalization of the Lee model in terms of usual concepts of the field theory is impossible if the renormalized coupling constant is greater than a critical coupling constant [1, 2, 3]). In the Lee model without cut-off the critical coupling constant vanishes and thus for any value of the observable coupling constant one must change the fundamental concepts of the field theory. Such a situation in the Lee model implies the possibility that also the usual local field theory is inconsistent for similar reasons [4, 5]). In this paper we want to show that the difficulties which appear in the Lee model are intimately connected with simplifications made in passing from the local field theory to the Lee model. These difficulties disappear when Lee's interaction Hamiltonian is completed by the lacking terms. We give the comparison of the Lee model with the local field theory for a certain simple case.

2. The Model of the Local Field Theory

Let us consider a simple model of non-relativistic quantum field theory which describes the interaction of the fixed fermions V and N with bosons ϑ. We assume the Hamiltonian for this model in the form

$$\begin{aligned} H &= H_0+H_1 \\ &= m_0^{\mathrm{V}}\int \mathrm{d}^3x V^\dagger(\mathbf{x})V(\mathbf{x})+m_0^{\mathrm{N}}\int \mathrm{d}^3x N^\dagger(\mathbf{x})N(\mathbf{x}) \qquad (1) \\ &+\tfrac{1}{2}\int \mathrm{d}^3x[\pi^2(\mathbf{x})+(\nabla\phi(\mathbf{x}))^2+\mu^2\phi^2(\mathbf{x})]-g_0\int \mathrm{d}^3x[V^\dagger(\mathbf{x})N(\mathbf{x})+N^\dagger(\mathbf{x})V(\mathbf{x})]\phi(\mathbf{x}). \end{aligned}$$

With the notations

$$\psi(\mathbf{x}) = \begin{Vmatrix} V(\mathbf{x}) \\ N(\mathbf{x}) \end{Vmatrix}, \qquad \psi^\dagger(\mathbf{x}) = \|V^\dagger(\mathbf{x}),\ N^\dagger(\mathbf{x})\|,$$
$$j(\mathbf{x}) = \psi^\dagger(\mathbf{x})\tau_1\psi(\mathbf{x}) = V^\dagger(\mathbf{x})N(\mathbf{x}) + N^\dagger(\mathbf{x})V(\mathbf{x}), \tag{2}$$
$$m_0 = \tfrac{1}{2}(m_0{}^{\mathrm{V}} + m_0{}^{\mathrm{N}}), \qquad \Delta m_0 = m_0{}^{\mathrm{V}} - m_0{}^{\mathrm{N}},$$

we can write Hamiltonian (1) in the form

$$H = H^0 + H^1 = m_0 \int \mathrm{d}^3x \psi^\dagger(\mathbf{x})\psi(\mathbf{x}) + \tfrac{1}{2}\int \mathrm{d}^3x [\pi^2(\mathbf{x}) + (\nabla\phi(\mathbf{x}))^2 + \mu^2\phi^2(\mathbf{x})]$$
$$- g_0 \int \mathrm{d}^3x j(\mathbf{x})\phi(\mathbf{x}) + \Delta m_0 \int \mathrm{d}^3x \psi^\dagger(\mathbf{x})\tau_3\psi(\mathbf{x}). \tag{3}$$

We shall treat the Schrödinger equation with Hamiltonian (3) by means of the perturbation method with respect to the term

$$H^1 = \Delta m_0 \int \mathrm{d}^3x \psi^\dagger(\mathbf{x})\tau_3\psi(\mathbf{x}). \tag{4}$$

It is well known [1,6]) that we must find only the physical one-particle states to carry out the renormalization, since the renormalization constants are defined in terms of the matrix elements between these states. We denote the one-particle states in zeroth, first and second approximation by $|\psi^0(\mathbf{x})\rangle$, $|\psi^1(\mathbf{x})\rangle$ and $|\psi^2(\mathbf{x})\rangle$ respectively. We then obtain by usual procedure

$$|\psi^1(\mathbf{x})\rangle = \left(1 - \mathrm{P}\frac{1}{H^0 - m}H^1\right)|\psi^0(\mathbf{x})\rangle \tag{5}$$

$$|\psi^2(\mathbf{x})\rangle = N^{-\frac{1}{2}}\left(1 - \mathrm{P}\frac{1}{H^0-m}H^1 + \mathrm{P}\frac{1}{H^0-m}(H^1 - \Delta E)\mathrm{P}\frac{1}{H^0-m}H^1\right)|\psi^0(\mathbf{x})\rangle, \tag{6}$$

where

$$H^0|\psi^0(\mathbf{x})\rangle = m|\psi^0(\mathbf{x})\rangle, \tag{7}$$

$$\delta(\mathbf{x}-\mathbf{x}')N = \langle\psi^0(\mathbf{x})|\left(1 + H^1\mathrm{P}\left(\frac{1}{H^0-m}\right)^2 H^1\right)|\psi^0(\mathbf{x}')\rangle, \tag{8}$$

$$\delta(\mathbf{x}-\mathbf{x}')\Delta E = \langle\psi^0(\mathbf{x})|H^1|\psi^0(\mathbf{x}')\rangle. \tag{9}$$

The vector $|\psi(\mathbf{x})\rangle$ denotes the column with elements $|V(\mathbf{x})\rangle$ and $|N(\mathbf{x})\rangle$ and P denotes the principal value. From (9) we obtain for energy correction

$$\Delta E = \tau_3 \Delta m_0 \exp(-2g_0^2/g_{\mathrm{cr}}^2) = \tau_3 \Delta m. \tag{10}$$

Here $g_{\mathrm{cr}}^2 = [2(2\pi)^3]^{-1}\int \mathrm{d}^3k\omega^{-3}$ and Δm is the observed mass difference in the first approximation. The equation (7) can be solved [7]) upon diagonalizing of the Hamiltonian H^0 by means of the unitary transformation

$$U = \exp\left[ig_0 \int \mathrm{d}^3x j(\mathbf{x})\frac{1}{\omega^2}\pi(\mathbf{x})\right]. \tag{11}$$

The multiplication by ω^{-2} in (11) means multiplication of Fourier transform

of $\pi(\mathbf{x})$. The result of the transformation U is

$$\widetilde{H^0} = UH^0U^{-1}$$
$$= m\int \mathrm{d}^3x\psi^\dagger(\mathbf{x})\psi(\mathbf{x})+\tfrac{1}{2}\int \mathrm{d}^3x[\pi^2(\mathbf{x})+(\nabla\phi(\mathbf{x}))^2+\mu^2\phi^2(\mathbf{x})] \tag{12}$$
$$-\tfrac{1}{2}g_0{}^2\int \mathrm{d}^3x : j(\mathbf{x})\frac{1}{\omega^2}j(\mathbf{x}) : .$$

The colon denotes the Wick normal product and

$$m = m_0-\delta m = m_0-\frac{g_0{}^2}{2(2\pi)^3}\int\frac{\mathrm{d}^3k}{\omega^2}.$$

We can see from (12) that $\psi^\dagger(\mathbf{x})|0\rangle$ is an eigenvector of the operator $\widetilde{H^0}$ belonging to the eigenvalue m. It follows then that the eigenvector of H^0 belonging to the eigenvalue m has the form

$$|\psi^0(\mathbf{x})\rangle = U^{-1}\psi^+(\mathbf{x})|0\rangle. \tag{13}$$

The renormalized (observed) coupling constant can be obtained [1]) from the equation

$$\delta(\mathbf{x}-\mathbf{x}')g\tau_1 = g_0\langle\psi^2(\mathbf{x})|\int \mathrm{d}^3x j(\mathbf{x})|\psi^2(\mathbf{x}')\rangle. \tag{14}$$

The renormalization constants $Z_2{}^{\mathrm{V}}$ and $Z_2{}^{\mathrm{N}}$ of the fermion fields can be obtained from the equations

$$\delta(\mathbf{x}-\mathbf{x}')\sqrt{Z_2{}^{\mathrm{V}}} = \langle 0|V(\mathbf{x})|V^2(\mathbf{x}')\rangle, \tag{15}$$

$$\delta(\mathbf{x}-\mathbf{x}')\sqrt{Z_2{}^{\mathrm{N}}} = \langle 0|N(\mathbf{x})|N^2(\mathbf{x}')\rangle. \tag{16}$$

Now we find the renormalized coupling constant. From (6), (13) and (15) we have

$$\delta(\mathbf{x}-\mathbf{x}')g\tau_1$$
$$= g_0N^{-1}\langle 0|U\left[\int \mathrm{d}^3x j(\mathbf{x})+H^1\mathrm{P}\frac{1}{H^0-m}\int \mathrm{d}^3x j(\mathbf{x})\mathrm{P}\frac{1}{H^0-m}H^1\right]U^{-1}|0\rangle. \tag{17}$$

Using (3), (4) and (11) we find

$$g = g_0N^{-1}[1-\langle 0|\mathrm{e}^{2ig_0\tau_1\omega^{-2}\pi(\mathbf{x})}\mathrm{P}H_{\mathrm{ob}}^{-2}\mathrm{e}^{-2ig_0\tau_1\omega^{-2}\pi(\mathbf{x})}|0\rangle], \tag{18}$$

where

$$H_{\mathrm{ob}} = \int \mathrm{d}^3k\omega(\mathbf{k})a^\dagger(\mathbf{k})a(\mathbf{k}).$$

With the abbreviations

$$a(g_0{}^2) = \langle 0|\mathrm{e}^{2ig_0\tau_1\omega^{-2}\pi(\mathbf{x})}\mathrm{P}H_{\mathrm{ob}}^{-2}\mathrm{e}^{-2ig_0\tau_1\omega^{-2}\pi(\mathbf{x})}|0\rangle \tag{19}$$

$$=\sum_{n=1}^{\infty}\frac{1}{n!}\left[\frac{g_0{}^2}{2(2\pi)^3}\right]^n\int\frac{\mathrm{d}^3k_1}{\omega_1{}^3}\cdots\frac{\mathrm{d}^3k_n}{\omega_n{}^3}\frac{1}{(\omega_1+\cdots+\omega_n)^2}, \tag{20}$$

we obtain finally

$$g = g_0 \frac{1-(\Delta m)^2 a(g_0^2)}{1+(\Delta m)^2 a(g_0^2)} \approx g_0(1-2(\Delta m)^2 a(g_0^2)). \tag{21}$$

It can be shown that the power series (20) is convergent for $g_0^2 < g_{\max}^2$ where $g_{\max}^2 > (2\pi)^2 e^{-1}$. From (15) and (17) we can obtain the renormalization constants Z_2^{V} and Z_2^{N}:

$$\sqrt{Z_2^{\mathrm{V}}} = \exp(-g_0^2/2g_{\mathrm{cr}}^2)N^{-\frac{1}{2}}[1-\Delta m b_1(g_0^2)+(\Delta m)^2 b_2(g_0^2)], \tag{22}$$

$$\sqrt{Z_2^{\mathrm{N}}} = \exp(-g_0^2/2g_{\mathrm{cr}}^2)N^{-\frac{1}{2}}[1+\Delta m b_1(g_0^2)+(\Delta m)^2 b_2(g_0^2)]. \tag{23}$$

The functions $b_1(g_0^2)$ and $b_2(g_0^2)$ are also defined by series which are convergent like (20) in a certain neighbourhood of $g_0^2 = 0$.

The vertex part renormalization constant Z_1 can be find from the well known Dyson equation

$$g = Z_1^{-1}(Z_2^{\mathrm{V}} Z_2^{\mathrm{N}})^{\frac{1}{2}} Z_3^{\frac{1}{2}} g_0. \tag{24}$$

The boson field renormalization constant Z_3 is equal to 1 and we have from (24)

$$Z_1 = \exp(-g_0^2/g_{\mathrm{cr}}^2)[1+(\Delta m)^2 C(g_0^2)], \tag{25}$$

where

$$C(g_0^2) = b_1^2(g_0^2)+2b_2(g_0^2)+a(g_0^2). \tag{26}$$

3. The Lee Model

The Hamiltonian for the Lee model [1]) has the form

$$\begin{aligned} H^{\mathrm{L}} = H_0 + H_1^{\mathrm{L}} &= m_0^{\mathrm{V}} \int \mathrm{d}^3x V^\dagger(\mathbf{x})V(\mathbf{x}) + m_0^{\mathrm{N}} \int \mathrm{d}^3x N^\dagger(\mathbf{x})N(\mathbf{x}) \\ &+ \tfrac{1}{2}\int \mathrm{d}^3x[\pi^2(\mathbf{x})+(\nabla\phi(\mathbf{x}))^2+\mu^2\phi^2(\mathbf{x})] \\ &- g_0 \int \mathrm{d}^3x[V^\dagger(\mathbf{x})N(\mathbf{x})\phi^{(+)}(\mathbf{x})+N^\dagger(\mathbf{x})V(\mathbf{x})\phi^{(-)}(\mathbf{x})]. \end{aligned} \tag{27}$$

The renormalization constants in this model are

$$Z_1 = 1, \quad Z_3 = 1, \quad Z_2^{\mathrm{N}} = 1, \quad (Z_2^{\mathrm{V}})^{-1} = 1 + \frac{g_0^2}{2(2\pi)^3}\int \frac{\mathrm{d}^3k}{\omega}\,\frac{1}{(\omega-\Delta m)^2}. \tag{28}$$

The renormalized coupling constant defined by (25) has the form

$$g = \left[1+\frac{g_0^2}{2(2\pi)^3}\int \frac{\mathrm{d}^3k}{\omega}\,\frac{1}{(\omega-\Delta m)^2}\right]^{-\frac{1}{2}} g_0. \tag{29}$$

It is well known that the equation (29) is the source of all difficulties in the Lee model. In fact, no real solution of this equation exists for g_0 if g is finite.

4. Discussion

The comparison between the Lee model and the model described in § 2 can be carried out in terms of Feynman diagrams. In the model of local field theory described by the Hamiltonian (1) there is an infinite number of self energy and vertex part diagrams. The first few diagrams are the following

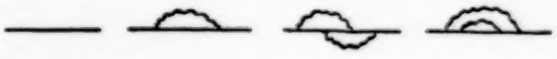

(30)

(31)

The symmetry between self energy and vertex part diagrams leads to the reduction of the infinite parts of renormalization constants Z_1 and Z_2 in the product $Z_1^{-1}(Z_2^{V} Z_2^{N})^{\frac{1}{2}}$. In the particular case of equal masses [7,8]) we have simply the Ward identity $Z_1^{-1} Z_2 = 1$.

In the Lee model this symmetry is disturbed. One diagram appears here as the correction to the self energy but there are no radiation corrections to the vertex part. In the Lee model instead of (30) and (31) we have

(32)

The infinite parts of the constants Z_1 and Z_2 cannot reduce and this leads to the known difficulties in the renormalization procedure.

The author wishes to thank Professors L. Infeld and W. Królikowski for their interest in this work.

References

1) T. D. Lee, Phys. Rev. **95** (1954) 1329
2) W. Heisenberg, Nuclear Physics **4** (1957) 532
3) G. Källén and W. Pauli, Mat. Phys. Medd. Dan. Vid. Selsk **30**, No. 7 (1955)
4) W. Heisenberg, Revs. Mod. Phys. **29** (1957) 269
5) H. Umezawa, Quantum Field Theory (North-Holland Publishing Company, Amsterdam, 1956) p. 354
6) G. Källén, Helv. Phys. Acta **25** (1952) 417
7) O. W. Greenberg and S. S. Schweber, Nuovo Cimento **8** (1958) 378
8) Th. W. Ruijgrok, Physica **24** (1958) 185

1.D.2 *Nuclear Physics* **12** (1959) 314—326; © *North-Holland Publishing Co., Amsterdam*

Not to be reproduced by photoprint or microfilm without written permission from the publisher

TWO BODY FORCES IN LIGHT DEFORMED NUCLEI

D. M. BRINK

Clarendon Laboratory, Oxford University †

and

A. K. KERMAN

Physics Department and Laboratory for Nuclear Science ††,
Massachusetts Institute of Technology, Cambridge, Mass.

Received 11 March 1959

Abstract: There is evidence that the light nuclei in the aluminium region have rotational states. It is well known from studies of heavy rotating nuclei that an independent particle model for a deformed well as used by Nilsson is a surprisingly good approximation for many of the properties of these collective states. However, it has been clear for some time that two body correlations are important for a more complete understanding of the situation. Because the number of single particle states for the light nuclei is relatively small and because isobaric spin is a good quantum number, we have undertaken some studies on the effect of two body forces on binding energies and energy levels. In particular we have employed the method of Bacher and Goudsmit to find relations among binding energies which depend only upon the existence of two body forces and the assumption that the deformed wave function coupling scheme is a good first approximation. The relations so obtained are remarkably well fulfilled by the data while corresponding relations obtained for the spherical shell model are not. Some of the possible excited states in these nuclei are also discussed and estimates made of their energies.

1. Introduction

Recently it has been suggested that the spectra of some light nuclei can be interpreted according to the rotational model of Bohr and Mottelson [1]). All levels up to 4 MeV in Al^{25} and Mg^{25} can be ascribed to low rotational bands [2]), while it has been suggested that the spectrum of F^{19} can be explained in terms of mixed rotational bands [3]) using Nilsson's [7]) model of an ellipsoidal harmonic oscillator well. Rakavy [4]) shows that nuclei following O^{16} should have prolate deformations, and that in nuclei of mass 18 these deformations are already as large as those in the heavy nuclei which show the characteristic rotational spectrum. According to these calculations the deformations begin to decrease again after Mg^{24}. Beyond S^{32} the deformations

† This work was done in the spring of 1957 while D. M. Brink was with the Laboratory for Nuclear Science.

†† This work is supported in part through AEC Contract AT(30—1)-2098, by funds provided by the U.S. Atomic Energy Commission, the Office of Naval Research and the Air Force Office of Scientific Research.

are probably too small for the rotational model to have any validity.

Besides investigating the excited states corresponding to rotational levels in these nuclei, it is of interest to try to make some statements about binding energies and particle excitations. These quantities are strongly dependent on interparticle forces. In the (j, j) coupling shell model, binding energies with two body forces have been discussed by Talmi and Thieberger [5]) using the methods of Bacher and Goudsmit [6]) with considerable success. They succeed in expressing nuclear binding energies in terms of a few parameters, which in turn depend upon the actual nuclear forces. If the nuclear forces were known it would be possible to determine the above mentioned parameters, hence nuclear binding energies. Talmi and Thieberger [5]) however, shortcut this program and use the parameters determined from one group of data to make predictions about another group. In this work we follow a similar program with the deformed nucleus shell model [7]).

2. The Particle Coupling Scheme

Levels which are degenerate in the (j, j) coupling shell model are split in the deformed nucleus model. If the nucleus has an axially symmetric deformation, the resultant single particle levels can be classified by the component of particle angular momentum along the nuclear symmetry axis. For light nuclei where isobaric spin is a good quantum number, each level in this deformed shell model has four independent states, according as to whether the occupying particle is a proton or a neutron, with its angular momentum either parallel or antiparallel to the nuclear symmetry axis. We have a modified shell model with each level fourfold degenerate and with "closed sub-shells" occurring at O^{16}, Ne^{20}, Mg^{28} and Si^{28} respectively.

For nuclei with a positive deformation this scheme makes definite predictions about ground state angular momenta, since the ground state angular momentum is equal to the component K of the particle angular momentum about the nuclear symmetry axis. This scheme gives spin $I = K = \frac{1}{2}$ for odd mass nuclei in the range of mass numbers $16 < A < 20$, $I = \frac{3}{2}$ for $20 < A < 24$; $I = \frac{5}{2}$ for $24 < A < 28$ and $I = \frac{1}{2}$ for $28 < A < 32$. In all cases except O^{17} and F^{17} these predictions are verified, and these two nuclei are very close to the O^{16} closed shell. In both nuclei, however, there is a low spin $\frac{1}{2}$ state which may be the collective state.

In odd nuclei the last two particles may couple with their angular momenta parallel or anti-parallel giving the possibilities:

F^{18}:	$K = 0,1$	Na^{24}:	$K = 1,4$
F^{20}:	$K = 1,2$	Al^{26}:	$K = 0,5$
Na^{22}:	$K = 0,3$	Al^{28}:	$K = 2,3$.

These states are degenerate in the deformed shell model without inter-particle forces. In practice the states of high spin are always the ground states †, thus nuclear forces must favour the angular momentum parallel configurations. It is found that a wide range of reasonable forces reproduces this behaviour.

3. Particle Interactions Within a Sub-Shell Model

The binding energy of one particle outside a closed sub-shell is due entirely to the interaction of this last particle with the core. Two, three or four particles in a sub-shell have a mutual or pairing energy, in addition to their interaction with the core. If we assume isobaric spin is still a good quantum number in these nuclei and subtract out Coulomb energies, we see that two particles in a sub-shell outside a closed shell can exist in three different configuarations. Corresponding to each of these two particle configurations there is a pairing energy. The states, with their pairing energies, are

$T = 1$, angular momenta anti-parallel, pairing energy A;
$T = 0$, angular momenta anti-parallel, pairing energy B;
$T = 0$, angular momenta parallel, pairing energy C.

Provided the nuclear forces are two body forces, the interaction energy of three or four particles in a sub-shell can be expressed in terms of the parameters A, B and C. For three particles, say two protons and one neutron, we must add up the energy of pairs. The proton-proton interaction contributes a pairing energy A. The proton-neutron interaction gives a pairing energy C from the proton with its angular momentum parallel to that of the odd neutron, and a pairing $\frac{1}{2}(A+B)$ from the anti-parallel proton, giving a total of $\frac{1}{2}(3A+B+2C)$. A complete shell of four particles has a mutual interaction exactly twice this, as can be seen by counting up the energies of pairs.

This result gives the possibility of making some binding energy predictions, since the binding energy of a closed shell of four particles can be predicted from the binding energy of nuclei with one and with three particles in that shell. For example in the shell $20 \leqq A \leqq 24$ we have for the binding energy of Mg^{42}:

$$B(Mg^{24})-B(Ne^{20}) = B(Mg^{23})+B(Na^{23})-B(Na^{21})-B(Ne^{21}). \qquad (1)$$

In this way of writing, the Coulomb corrections are already subtracted. The relation (1) has been checked in the shells ending with Ne^{20}, Mg^{24} and Si^{28} and the results given in table 1(a) together with values of A, B and C.

† If the same table is made for the odd nuclei below O^{16} one sees the same regularity (Li^6, Li^8, B^{10}, N^{14}).

TABLE 1(a)

Binding energies of closed-shell nuclei

	Predicted B.E.	Observed B.E.	A	B	C
O^{16}	36.12	35.30			
			4.5	1.6	5.5
Ne^{20}	32.93	33.03			
			2.5	1.6	4.3
Mg^{24}	37.74	37.60			
			2.3	1.6	4.3
Si^{28}	38.15	38.28			
			1.9	1.2	2.7
S^{32}	35.38	35.22			

TABLE 1(b)

Neutron binding energies for nuclei in a sub-shell

$Be^8(J=\frac{1}{2})$	19.32	$He^5(J=\frac{1}{2})$	−3.55	15.77 †
$Li^7(J=\frac{1}{2})$	6.75	$Li^6(J=\frac{1}{2})$	8.01	14.76
C^{12}	18.711	Be^9	1.666	20.377 ††
B^{11}	11.459	B^{10}	8.436	19.895
O^{16}	15.57	C^{13}	4.88	20.45
N^{15}	10.75	N^{14}	10.52	21.27
Ne^{20}	16.908	$O^{17}(J=\frac{1}{2})$	3.271	20.179 †††
F^{19}	10.408	$F^{18}(J=\frac{1}{2})$	9.669	20.077
Mg^{24}	16.580	Ne^{21}	6.756	23.336
Na^{23}	12.418	Na^{22}	11.042	23.460
Si^{28}	17.191	Mg^{25}	7.324	24.515
Al^{27}	13.1	Al^{26}	11.3	24.4
S^{32}	15.0	Si^{29}	8.473	23.5
P^{31}	12.372	P^{30}	11.278	23.650

† The notation ($J = \frac{1}{2}$) beside Be^8, Li^7, He^5 and Li^6 means that we have used neutron binding energies taken from the $J = \frac{1}{2}$ excited states of He^5, Li^5, Li^7 and Be^7, which are at 2.6, 2.5, 0.48 and 0.43 MeV above the ground states. These would be the states corresponding to the $J = \frac{1}{2}$ level if a deformed structure is appropriate for these nuclei. The shell model predicts that the sums should be equal for $J = \frac{3}{2}$ states, but they are off by 6.3 MeV. This is not surprising because it is well known that the j-j coupling shell model does not work in this region.

†† The same sum relation can be shown to hold for the first four and the last four nucleons in a $j = \frac{3}{2}$ shell, and therefore these are included here for comparison.

††† The notation ($J=\frac{1}{2}$) beside O^{17} means that we have used the neutron binding in the $J = \frac{1}{2}$, 872 keV excited state of O^{17}. The same notation beside F^{18} means that the binding of the last neutron in F^{18} is taken with respect to the $J = \frac{1}{2}$, 510 keV excited state of F^{17}. The shell model predicts that the sums should be equal for the $J=\frac{5}{2}$ states, but they are off by 1.4 MeV.

The relation (1) can be written in a more compact way in terms of neutron binding energies. Thus, for example, if each symbol stands for a neutron binding energy we have

$$Mg^{24}+Ne^{21} = Na^{23}+Na^{22}. \tag{1a}$$

In table 1(b) the neutron binding energies of the interesting nuclei are given. Relation (1a) means that the sums of the rows in each section of the table must be equal.

The above binding energy relation is a property of the four particle structure of the levels in the deformed nucleus shell model, and also holds for $j = \frac{1}{2}$ shells in the (j, j) coupling model. Such shells occur between C^{12} and O^{16} and between Si^{28} and S^{32}. Figures for these shells are also given in table 1.

4. Zero Point Energy of Precession

At this stage two corrections should be made to the remarks of section 3. The first concerns the zero point energy of precession of the deformed nucleus. An even deformed nucleus in its lowest state has spin zero and its deformation is oriented at random, giving no zero point energy of precession. On the other hand an odd-mass nucleus has a resultant particle angular momentum which tends to line up the nuclear deformation in the direction of the total angular momentum of the nucleus. This partial specification of the orientation of the nucleus gives rise to a zero point precession, with an associated zero point energy

$$E = \frac{1}{2\mathscr{I}}(Q_x^2+Q_y^2+Q_z^2)$$

where Q is the precession angular momentum and $\mathscr{I}$ is the moment of inertia of the deformed nucleus about an axis perpendicular to its symmetry axis. The precession angular momentum is associated with the collective motion of the nucleus and is equal to the difference between the total angular momentum I and the particle angular momentum j. In the lowest state of a rotational band $I = I_z = j_z = K$ and $Q_z = 0$. Hence

$$\begin{aligned} E &= \frac{1}{2\mathscr{I}}[(I-j)^2] \\ &= \frac{1}{2\mathscr{I}}[I(I+1)-K^2-2(I_xj_x+I_yj_y)+j_x^2+j_y^2] \\ &= \frac{1}{2\mathscr{I}}[K-2(I_xj_x+I_yj_y)+j_x^2+j_y^2] \end{aligned} \tag{2}$$

in the lowest state when $K = I$. In the above the total angular momentum I is resolved along the z axis, which is the symmetry axis of the deformed

nucleus. In the expression (2), $K/2\mathscr{I}$ is the zero point precession energy associated with a rigid body with total angular momentum K, and component K along the symmetry axis. It effectively reduces the binding energy in states with $K \neq 0$. Provided, however, the moment of inertia is the same in nuclei with one and with three particles outside a closed shell, the effect of the zero point energy cancels in the binding energy relation (1). In calculating the constants A, B and C, however, the zero point precession energy has been subtracted out.

The second term in (2) is the Coriolis force acting on a nucleon in the nucleus, but is has diagonal elements only in the $K = \frac{1}{2}$ case,

$$2\langle I = \tfrac{1}{2}|I_x j_x + I_y j_y|I = \tfrac{1}{2}\rangle = a,$$

where a is the "decoupling factor" [1]).

The third term in (2) can be expanded in the form

$$\frac{1}{2\mathscr{I}}(j_x^2+j_y^2) = \sum_i \frac{1}{2\mathscr{I}}(j_{ix}^2+j_{iy}^2) + \sum_{i\neq k}\frac{1}{2\mathscr{I}}(j_{ix}j_{kx}+j_{iy}j_{ky}). \tag{3}$$

The first term in this expression is a sum over one-body operators and can be included in the interaction with the core; while the second term is a sum over two-body operators, hence is an effective two-body interaction.

5. Deformation Energy

The second correction concerns the deformation energy of the nucleus. Rakavy estimates that the binding energy of deformation can change as much as one MeV from nucleus to nucleus as a result of the change of deformation. Energies of this order are far greater than the energy differences in table 1, hence demand investigation.

Suppose we have a closed sub-shell nucleus with an equilibrium deformation β_0. The energy of this core for a deformation β near β can be represented approximately by

$$E(\beta) = E_0 + \tfrac{1}{2}E_1(\beta-\beta_0)^2.$$

The energy of a single particle outside the closed sub-shell will also depend upon the deformation and for small deviations from the deformation β_0 can be expressed as

$$\varepsilon(\beta) = \varepsilon_0 + \varepsilon_1(\beta-\beta_0).$$

With n particles in the shell outside the core the binding energy is

$$\begin{aligned} E &= E(\beta) + n\varepsilon(\beta) \\ &= E_0 + \tfrac{1}{2}E_1(\beta-\beta_0)^2 + n\varepsilon_0 + n\varepsilon_1(\beta-\beta_0). \end{aligned} \tag{4}$$

Minimising this expression gives a new equilibrium deformation

$$\beta = \beta_0 - n\varepsilon_1/E_1$$

and equilibrium energy

$$E = E_0+n\varepsilon_0-\tfrac{1}{2}\frac{n^2\varepsilon_1^2}{E_1}$$
$$= E_0+n\left(\varepsilon_0-\frac{\varepsilon_1^2}{2E_1}\right)-\tfrac{1}{2}n(n-1)\frac{\varepsilon_1^2}{E_1}. \qquad (5)$$

The part $-\varepsilon_1^2/2E_1$ in the binding energy (5) appears as an additional interaction with the core while the part $-\frac{1}{2}n(n-1)\varepsilon_1^2/E_1$ is proportional to the number $\frac{1}{2}n(n-1)$ of pairs of particles in the last shell, hence is an effective two-body interaction independent of spin and isobaric spin. This pairing energy is estimated to be 1.2 MeV in the $16 \leqq A \leqq 20$ shell, 0.2 MeV in the $20 \leqq A \leqq 24$ shell and 0.7 MeV in the $24 \leqq A \leqq 28$ shell, an appreciable fraction of the total interactions as given in table 1.

6. Interactions of Particles in Different Sub-Shells

In section 3 pairing energies have been investigated in states where the odd nucleons are all in the same level. In order to discuss excited states of these nuclei, or ground states of nuclei in which the odd nucleons are filling different sub-shells, it is necessary to study pairing interactions between nucleons in different levels. If nuclear forces conserve angular momentum and isobaric spin, two nucleons, one in level x_1 and another in level x_2, can exist in four different states with isobaric spin $T = 0$ or $T = 1$, and with angular momenta along the nuclear symmetry axis parallel or anti-parallel. With a two-body interaction the pairing energy of n_1 particles in level x_1 and n_2 particles in level x_2 can be expressed in terms of the pairing energies in these four basic states.

In calculating this pairing energy we make use of the fact that a two-body operator is determined by its matrix elements in two-body states. If V and V^1 are two-body potentials which have the same matrix elements in each of the four basic states of two nucleons, one in level x_1 and the other level x_2, then the two potentials have equal matrix elements between general states with n_1 nucleons in level x_1 and n_2 nucleons in level x_2. Let V be the given two-body potential and put

$$V^1 = \sum_{k=1}^{4} a_k V_k, \qquad (6)$$

where V_k are four independent two-body operators. If the four coefficients a_k are determined so that V and V^1 have the same matrix elements in each of the four basic states of two nucleons, V^1 has the same matrix elements as V between many particle states of nucleons in levels x_1 and x_2. The state of a particle in a level is specified by giving the isobaric spin and the component of

angular momentum $\Omega = \pm|\Omega|$ along the nuclear symmetry axis. In the following it is convenient to introduce an operator $p = \Omega/|\Omega|$ instead of Ω. It takes the value 1 when the angular momentum is parallel to the nuclear symmetry axis and -1 when anti-parallel. In the following the suffix i refers to nucleons in level x_1 and the suffix j to nucleons in level x_2. Put

$$P_1 = \sum_i p_i, \qquad P_2 = \sum_j p_j;$$
$$\mathbf{T}_1 = \sum_i \boldsymbol{\tau}_i, \qquad \mathbf{T}_2 = \sum_j \boldsymbol{\tau}_j;$$

the sums are taken over particles in the levels x_1 and x_2 respectively; $\mathbf{T}_i$ is the isobaric spin operator for the i^{th} particle and p_i is the reduced angular momentum operator introduced above. A complete set of states for n_1 particles in level x_1 and n_2 particles in level x_2 is specified by giving $\mathbf{T}_1$, $\mathbf{T}_2$, P_1, P_2 and the total isobaric spin T. We choose for the V_k

$$\begin{aligned} V_1 &= n_1 n_2, \\ V_2 &= \sum_{ij} p_i p_j = P_1 P_2, \\ V_3 &= 4 \sum_{ij} \boldsymbol{\tau}_i \cdot \boldsymbol{\tau}_j = 4\mathbf{T}_1 \cdot \mathbf{T}_2, \\ V_4 &= 4 \sum_{ij} p_i \boldsymbol{\tau}_i \cdot p_j \boldsymbol{\tau}_j = 4\mathbf{Q}_1 \cdot \mathbf{Q}_2, \end{aligned} \tag{7}$$

where $\mathbf{Q}_1 = \sum_i p_i \boldsymbol{\tau}_i$ and $\mathbf{Q}_2 = \sum_j p_j \boldsymbol{\tau}_j$.

It may be shown that for diagonal matrix elements $\mathbf{Q}_1$ may be replaced by

$$\begin{aligned} \mathbf{Q}_1 &= P_1 \mathbf{T}_1 && \text{for } n_1 = 1 \\ \mathbf{Q}_1 &= 0 && \text{for } n_1 = 2 \\ \mathbf{Q}_1 &= P_1 \mathbf{T}_1 && \text{for } n_1 = 3 \\ \mathbf{Q}_1 &= 0 && \text{for } n_1 = 4; \end{aligned} \tag{8}$$

similar results hold for $\mathbf{Q}_2$. Finally eq. (6) for V^1 may be written

$$V^1 = an_1 n_2 + bP_1 P_2 + 4c\mathbf{T}_1 \cdot \mathbf{T}_2 + 4d\mathbf{Q}_1 \cdot \mathbf{Q}_2. \tag{9}$$

Putting $P = P_1 + P_2$ and $\mathbf{T} = \mathbf{T}_1 + \mathbf{T}_2$ the basic particle states can be labelled by P and T, and the corresponding pairing energy by V_{PT}. The V_{PT} can be expressed in terms of the parameters of eq. (9):

$$\begin{aligned} V_{00} &= a - b - 3c + 3d, \\ V_{10} &= a + b - 3c - 3d, \\ V_{01} &= a - b + c - d, \\ V_{11} &= a + b + c + d. \end{aligned} \tag{10}$$

The binding energies of a further set of nuclei can be correlated with the help of expression (9) for the pairing energy between particles in different levels. First we consider the ground states of three nuclei with one neutron in

level x_2, two neutrons in level x_1, and zero, one, or two protons in level x_1. These states have isobaric spins $T = \frac{1}{2}$, 1 and $\frac{1}{2}$ respectively, and pairing energies between the levels x_1 and x_2 as follows:

$$\begin{aligned} T &= \tfrac{3}{2}: \quad E = 2a+2c; \\ T &= 1: \quad E = 3a+c\pm(b-d) (\pm \text{ according as } P = 2 \text{ or } 0); \\ T &= \tfrac{1}{2}: \quad E = 4a. \end{aligned} \tag{11}$$

In obtaining these results from (9) we make use of the relation $2\mathbf{T}_1 \cdot \mathbf{T}_2 = \mathbf{T}^2 - \mathbf{T}_1^2 - \mathbf{T}_2^2$.

The ground states of the set of three nuclei with four neutrons, four neutrons and one proton, and four neutrons and two protons form a second group whose binding energies can be correlated by calculating pairing forces between sub-shells. The states have isobaric spins $T = 2$, $T = \frac{3}{2}$ and $T = 1$ respectively, with pairing energies between the levels x_1 and x_2:

$$\begin{aligned} T &= 2: \quad E = 4a+4c; \\ T &= \tfrac{3}{2}: \quad E = 6a+2c; \\ T &= 1 \quad\quad E = 8a. \end{aligned} \tag{12}$$

Making use of the relations (11) and (12) along with the results of section 3 we can prove the following relation between *neutron binding energies* (assuming the moments of inertia are all the same)

$$\begin{aligned} O^{20}+Ne^{21} &= O^{19}+Ne^{22} = F^{20}+F^{21}, \\ Ne^{24}+Mg^{25} &= Ne^{23}+Mg^{26} = Na^{24}+Na^{25}, \\ Mg^{28}+Si^{29} &= Mg^{27}+Si^{30} = Al^{28}+Al^{29}. \end{aligned} \tag{13}$$

These binding energies are listed in table 2 along with the sums of eq. (13).

TABLE 2

Pairing energies between sub-shells

O^{19}	3.96	Ne^{22}	(10.36)	14.32
F^{20}	6.60	F^{21}	(7.73)	—
Ne^{21}	6.75	O^{20}	(7.57)	—
Ne^{23}	5.19	Mg^{26}	11.12	16.31
Na^{24}	6.96	Na^{25}	9.24	16.20
Mg^{25}	7.33	Ne^{24}	8.97	16.10
Mg^{27}	6.44	Si^{30}	10.61	17.05
Al^{28}	7.72	Al^{29}	9.03	16.75
Si^{29}	8.47	Mg^{28}	8.50	16.97

Binding energy of the last neutron in MeV (Predicted values in brackets).
The last column gives the sums of corresponding neutron binding energies (cf. eq. (13)).

One sees that the agreement is again very good. Predicted values for O^{20} and F^{21} neutron binding energies are in brackets.

More detailed examination of the energies enable one to evaluate some of the parameters. For example, $a-c = 1.1$ MeV, and $b-d$ is small and positive.

7. Particle Excitations

The nuclei in the region we are considering have energy levels corresponding to particle excitations in addition to the collective rotational levels. In the approximation of the present model and if we neglect configurational mixing, the positions of these levels depend on the single particle level spacings and on the pairing energies between and within sub-shells. These particle excitations are of two main types, the first corresponding to excitation of particles in the unfilled sub-shell, and the second to the excitation of particles in filled sub-shells into vacancies in unfilled sub-shells.

In order to calculate the energies for particle excitations it is necessary to know values of the four parameters occurring in the expression for the interaction energy between sub-shells. From the analysis of section 6 it is possible to determine $a-c$. There is also an indication that $a+c$ and $b-d$ are small; but it is not possible to get values for all the parameters from experimental data. In the following we do not attempt to predict level positions exactly, but rather to get a qualitative picture of the particle excitation spectrum. We consider explicitly the nuclei from Mg^{24} to Se^{28} and assume $a = -b = -c = -d = 0.5$ MeV. This choice of parameters follows if the nuclear force is spin-independent and if it is required that $a+c = b-d = 0$.

7.1. $4n$ NUCLEI: Mg^{24}

The lowest group of excited states corresponds to the excitation of one particle from the $\Omega = \frac{3}{2}$ level to the $\Omega = \frac{5}{2}$ level. To break the closed $\Omega = \frac{3}{2}$ sub-shell requires an energy $\frac{1}{2}(3A+B+2C)$, plus the single particle excitation energy between the levels $\Omega = \frac{3}{2}$ and $\Omega = \frac{5}{2}$. On the other hand there is a gain in binding energy due to the between-level pairing energy. The particle excitations can be classified according to the total isobaric spin T and total z-component of the angular momentum K. The levels with their excitation energies are:

$T = 1$,	$K = 4$:	$E = 3a+c+b-d$,	$\varepsilon = 10$ MeV;
	$K = 1$:	$E = 3a+c-(b-d)$,	$\varepsilon = 10$ MeV;
$T = 0$,	$K = 4$:	$E = 3a+b-3c+3d$,	$\varepsilon = 10$ MeV;
	$K = 1$:	$E = 3a-b-3c-3d$,	$\varepsilon = 5$ MeV;

E are the between- level pairing energies and ε are excitation energies. All two-particle and three-particle excitations lie at energies greater than 8 MeV.

7.2. $(4n+1)$ NUCLEI: Al^{25}, Mg^{25}

The lowest excited state is $I = \frac{1}{2}$ arising from the excitation of the odd nucleon from the $\Omega = \frac{5}{2}$ level to the $\Omega = \frac{1}{2}$ level. The excitation energy corresponds to the spacing between the single particle levels. There may be other low excited states coming from the excitation of the odd nucleon to the other unoccupied single particle levels $\Omega = \frac{1}{2}$ and $\Omega = \frac{3}{2}$. Besides these single particle excitations, there are states corresponding to core-excitations where $\Omega = \frac{3}{2}$ nucleon is excited to the unfilled $\Omega = \frac{1}{2}$ state. Denoting the isobaric spin of the two odd nucleons in the $\Omega = \frac{1}{2}$ state by T_2, the levels with their predicted excitation energies are:

$T_2 = 1$,	$T = \frac{3}{2}$,	$K = \frac{3}{2}$:	$E = 2a+2c$,	$\varepsilon = 7.6$ MeV;
	$T = \frac{1}{2}$,	$K = \frac{3}{2}$:	$E = 2a+4c$,	$\varepsilon = 4.6$ MeV;
$T_2 = 0$,	$T = \frac{1}{2}$,	$K = \frac{13}{2}$:	$E = 2a+2b$,	$\varepsilon = 7.6$ MeV;
		$K = \frac{7}{2}$:	$E = 2a-2b$,	$\varepsilon = 5.6$ MeV;
		$K = \frac{3}{2}$:	$E = 2a$,	$\varepsilon = 6.6$ MeV.

There is a strong matrix element, with value $6d$, of the pairing potential, mixing the two $T = \frac{1}{2}$, $\Omega = \frac{3}{2}$ states, and with the above energy spacings the lowest $T = \frac{1}{2}$, $K = \frac{3}{2}$ state should have an excitation energy of $\varepsilon = 2.5$ MeV.

7.3. $(4n+3)$ NUCLEI: Al^{27}, Se^{27}

There is a considerable analogy between the core excitations of $(4n+3)$ nuclei and the particle excitations of $(4n+1)$ nuclei and vice-versa. There are particle excitations of Al^{27} and Se^{27} which correspond to lifting a nucleon from the closed $\Omega = \frac{3}{2}$ level into the $\Omega = \frac{5}{2}$ level. The pairing lost in the $\Omega = \frac{3}{2}$ level is regained in the $\frac{5}{2}$ level, while the pairing between the levels remains unchanged. Thus the excitation energy is roughly the spacing between the single particle levels, i.e. 1.5 MeV. On the other hand a particle in the $\Omega = \frac{5}{2}$ level may be excited corresponding to the various values for the isobaric spin T_1 of the two nucleons remaining in the $\Omega = \frac{5}{2}$ state. The levels with the predicted energies are:

$T_1 = 1$,	$T = \frac{3}{2}$,	$K = \frac{1}{2}$:	$E = 2a+2c$,	$\varepsilon = 6.5$ MeV;
	$T = \frac{1}{2}$,	$K = \frac{1}{2}$:	$E = 2a-4c$,	$\varepsilon = 3.5$ MeV;
$T_1 = 0$,	$T = \frac{1}{2}$,	$K = \frac{11}{2}$:	$E = 2a+2b$,	$\varepsilon = 6.5$ MeV;
		$K = \frac{9}{2}$:	$E = 2a-2b$,	$\varepsilon = 4.5$ MeV;
	$T = \frac{1}{2}$,	$K = \frac{1}{2}$:	$E = 2a$,	$\varepsilon = 5.5$ MeV.

Again there is a strong matrix element mixing the two $T = \frac{1}{2}, K = \frac{1}{2}$ states, and one state arising from this mixing is predicted to have an excitation of $E \approx 1.4$ MeV. This state may give rise to the $I = \frac{1}{2}$ level and $I = \frac{3}{2}$ level at

0.8 and 1.01 MeV excitation energy in Al^{27}. Rakavy predicts a close similarity between the spectra of $(4n+1)$ and $(4n+3)$ nuclei, but the basis of his prediction neglects pairing energies. As seen above, the details of the particle excitation spectrum is sensitive to the strength of the pairing forces and Rakavy's prediction does not necessarily follow.

7.4. $(4n+2)$ NUCLEI: Mg^{26}, Al^{26}, Se^{26}

The nucleus Al^{26} has three states with two particles in the $\Omega = \frac{5}{2}$ level. They are as discussed in section 3: $T = 1$, $K = 0$; $T = 0$, $K = 0$; $T = 0$, $K = 5$. There are rotational levels built on each of these single particle states and in particular there is a sequence $I = 0, 2, 4, \ldots$ built on the $T = 1$, $K = 0$ level and a sequence $I = 1, 3, 5, \ldots$ built on the $T = 0$, $K = 0$ level. The odd rotational states are excluded in the first case because the internal wave function is symmetric for rotations through 180° about an axis perpendicular to the symmetry axis. In the second case even rotational states are excluded because the internal wave function is odd under such rotation.

Excitation of a single particle from the $\Omega = \frac{5}{2}$ to the $\Omega = \frac{1}{2}$ level produces the states:

$$
\begin{array}{llll}
T = 1, & K = 3: & E = a+b+c+d, & \varepsilon = 5.5 \text{ MeV}; \\
 & K = 2: & E = a-b+c-d, & \varepsilon = 3.5 \text{ MeV}; \\
T = 0, & K = 3: & E = a+b+3c-3d, & \varepsilon = 1.5 \text{ MeV}; \\
 & K = 2: & E = a-b-3c+3d, & \varepsilon = 3.5 \text{ MeV}.
\end{array}
$$

In Al^{26} there is a low $\varepsilon = 0.5$ MeV, $I = 3$ state which may be the $T = 0$, $K = 3$ state. In addition there is a set of states coming from the excitation of one nucleon from the $\Omega = \frac{3}{2}$ level to the $\Omega = \frac{5}{2}$ level. These are states with three particles in the $\Omega = \frac{3}{2}$ level and three particles in the $\Omega = \frac{5}{2}$ level. They have a similar classification to the states coming from exciting one nucleon from the $\Omega = \frac{5}{2}$ level to the $\Omega = \frac{1}{2}$ level but with $K = 4$ and $K = 1$ and with excitation energies about 1 MeV higher.

8. Configuration Mixing

The question of configuration mixing has been completely neglected in the preceding discussion. It may therefore seem somewhat surprising that the pairing relation (1) of section 3 is so accurately verified. The discussion of single particle excitations in section 7 provides some reason for this.

Firstly the $4n$ nuclei have a very low density of excited states. The lowest $I = 0$ excited state is predicted to occur at an excitation of 9 MeV. This low density of excited states should mean that the configuration mixing in the ground state is small. The major factor contributing to configurational

mixing in the $(4n+1)$ and $(4n+3)$ nuclei is the Coriolis force or rotation particle coupling [8]), and it has been shown by Rakavy [4]) and Paul [3]) that this force modifies the energy spectrum of light odd-mass nuclei in an important way. This work shows, however, that the energy shift of the ground state due to rotation particle coupling is always rather small, for it almost never happens that a low excited state has the same angular momentum as the ground state.

We have argued that the configuration mixing should be small in the ground state of $4n$, $(4n+1)$ and $(4n+3)$ nuclei, and thus provide a reason for the validity of eq. (1). On the other hand $(4n+2)$ nuclei have a much higher density of excited states, and it is possible that here configuration mixing is much stronger. In particular the value of $\frac{1}{2}(3A+B+2C)$ obtained from the binding of the lowest states of $(4n+2)$ nuclei may easily be larger than the value found from relation (1).

This is because the first approximation to the energy in the projected wave functions only involves matrix elements of one and two body operators in the deformed well wave functions. Recent detailed work by Redlich [11]) and Levenson [12]) shows that the projected wave functions in fact agree with the detailed shell model wave functions obtained by configuration mixing.

Finally, it may be worth remarking that the above theory fits perfectly [9]) into the framework of the projection theory for rotational states considered by Wheeler, Wigner, Peierls and others [10]).

References

1) A. Bohr and B. Mottelson, Mat. Fys. Medd. Dan. Vid. Selsk. **27**, No. 16 (1953)
2) Litherland *et al.*, Phys. Rev. **102** (1956) 208
3) E. B. Paul, Phil. Mag. **2** (1957) 311;
E. B. Paul and J. H. Montague, Nuclear Physics **8** (1958) 61
4) G. Racavy, Nuclear Physics **4** (1957) 375
5) I. Talmi and R. Thieberger, Phys. Rev. **103** (1956)
6) R. F. Bacher and S. Goudsmit, Phys. Rev. **46** (1934) 948
7) S. G. Nilsson, Mat. Fys. Medd. Dan. Vid. Selsk. **29**, No. 16 (1955);
K. Gottfried, Phys. Rev. **103** (1956) 1017;
S. A. Moszkowski, Phys. Rev. **99** (1955) 803
8) A. K. Kerman, Mat. Fys. Medd. Dan. Vid. Selsk. **30**, No. 15 (1956)
9) A. K. Kerman, Nuclear Reactions, Vol. I, edited by P. M. Endt and M. Demeur (North Holland Publishing Co., Amsterdam 1959) Ch. X, section 15
10) D. L. Hill and J. A. Wheeler, Phys. Rev. **89** (1953) 1102;
M. Redlich and E. P. Wigner, Phys. Rev. **95** (1954) 122;
R. E. Peierls and J. Yoccoz, Proc. Phys. Soc. A **70** (1957) 381
11) M. Redlich, Phys. Rev. **110** (1958) 468
12) C. A. Levinson, private communication

7.C *Nuclear Physics* **12** (1959) 327—332; © *North-Holland Publishing Co., Amsterdam*
Not to be reproduced by photoprint or microfilm without written permission from the publisher

PHOTOPRODUCTION OF NEUTRAL PIONS ON HYDROGEN NEAR THE THRESHOLD

V. I. GOLDANSKY, B. B. GOVORKOV and R. G. VASSILKOV
P. N. Lebedev Physical Institute of the USSR Academy of Sciences, Moscow

Received 11 February 1959

Abstract: The angular distribution of photo-π^0-mesons produced on protons is studied near the threshold for γ-ray energies of 160—220 MeV. The distribution can be represented by the formula

$$\frac{d\sigma}{d\Omega} = A + B\cos\theta + C\cos^2\theta,$$

which corresponds to creation of π^0 mesons in the S- and P-states.

Absolute values of the coefficients A, B, C in the indicated energy region are presented. The experimental values of B/A and C/A are compared with the theoretical formulas of Watson and Feld.

The ratio of the cross sections for photoproduction of π^+ and π^- mesons near the threshold has been derived from the value of the γ-ray energy corresponding to $B = 0$ (260^{+20}_{-10} MeV) and on basis of data on π meson-nucleon scattering. The ratio thus found is $\sigma+/\sigma- = 1.30\pm^{0.19}_{0.05}$.

1. Introduction

Photoproduction of π^0-mesons on protons, being of particular importance for meson-nucleon interaction theory, has recently been studied in a number of experiments [1–6]). Most of the adequately accurate measurements [4–6]), however, have been performed at incident γ-ray energies above 260 MeV, i.e., far away from the π^0-photoproduction threshold.

Relatively accurate results in the energy range near the threshold were actually obtained only in one experiment [2]), in which the total cross section (σ_T) was measured for the process

$$\gamma + p \rightarrow \pi^0 + p \qquad (1)$$

and which showed that near the threshold (up to $\approx$ 180 MeV) σ_T varies proportionally to $\tilde{q}^3$, where $\tilde{q}^3$ is the pion momentum in the centre-of-mass system (c.m.s). An asymmetry in the angular distribution with respect to an angle of 90° was demonstrated in the same work, this asymmetry being due to photoproduction of π^0-mesons in the S-state near the threshold.

The purpose of the present work was to study in more detail the angular distribution of π^0 photoproduction near the threshold. The method used in the experiment — detection of single π^0-decay γ-rays — was determined by the

small cross section of the process (1) near the threshold and by the low energy of the recoil protons. It can be shown that the counting rate of single γ-rays is uniquely related to the angular coefficients of the π^0 angular distribution which, in the analysed energy range, must have the form

$$\frac{d\sigma(\theta)}{d\Omega} = A + B\cos\theta + C\cos^2\theta, \tag{2}$$

where θ is the angle in the c.m.s. between the incident photon and the π^0 meson directions.

2. Experimental Method

The experiments were performed on the 265 MeV synchrotron of the P. N. Lebedev Physical Institute (USSR Academy of Sciences). Two telescopes consisting of four scintillation counters of the type described before [7]) were used to register single π^0-decay photons. They were placed simultaneously at angles of 90° and 135° or 45° and 90° in the laboratory system.

In every set of measurements the yield of decay photons at both angles was determined simultaneously for several (five) maximum bremsstrahlung energies by the method described in ref. [8]). For this purpose the synchrotron pulses were lengthened up to 3000 microseconds by gradually decreasing the amplitude of the accelerating h.f. voltage; this was accompanied by a marked change in the magnetic field strength (at the point at which the synchrotron target was located) which controlled the five-channel time analyzer.

By-channel detection of decay photons by the telescopes was combined with by-channel measurement of pulses with aid of a differential monitor which was simply a single scintillation counter placed in the field of the scattered gamma radiation. The measurements were performed for the following seven values of the maximum bremsstrahlung energies in the different channels: 130, 150, 170, 190, 210, 230 and 250 MeV.

Liquid hydrogen was used to fill a nitrogen-cooled styrofoam target with a cylindrical channel 12 cm in diameter and 30 cm long directed along the beam. The diameter of the incident gamma ray beam was 6 cm. The averaged background counting rate with the target empty was 30 % (45°), 8 % (90°) and 4 % (135°) of the counting rate in the basic experiments.

Absolute monitoring of the incident bremsstrahlung beam was carried out by activating graphite detectors in the reaction $C^{12}(\gamma, n)C^{11}$.

The cross sections for π^0-decay γ-ray emission in the laboratory system were obtained from the measured integral yields at angles of 45°, 90° and 135° with the help of the "photon difference" method, and were used to determine the coefficients A, B and C in the equation (2).

TABLE 1

Values of coefficients A, B and C

γ-ray energy (MeV)	A (10^{-30}cm^2/sr)	B (10^{-30}cm^2/sr)	C (10^{-30}cm^2/sr)	σ_T (10^{-29}cm^2)
160	0.28±0.03	0.13±0.03	0.09±0.12	0.31±0.06
180	0.95±0.02	0.39±0.06	0.5 ±0.1	0.98±0.04
200	2.10±0.05	0.56±0.07	1.3 ±0.2	2.08±0.08
220	4.5 ±0.1	0.7 ±0.1	2.9 ±0.4	4.5 ±0.2
240	8.4 ±0.2	0.9 ±0.2	6.0 ±0.6	8.1 ±0.3

3. Discussion of Results

A phenomenological analysis by Watson's method [13]) was carried out by comparing the data on the energy dependence and absolute values of coefficients A, B, C with the corresponding results for π^+-meson photoproduction [9–12]) and also by taking into account published data on π^0-photoproduction at higher energies [4–6]). The resultant values of S- and P-wave contributions to pion photoproduction were then used to compute the ratio B/A for the π^0 angular distribution coefficients. Since in the measured energy range the magnitudes of the phase shifts α_1 and α_3 are small, the expression for B reduces to

$$B = -\tfrac{4}{3}(A_S A_{K_0})^{\frac{1}{2}}[(\alpha_3-\alpha_1)\sin\alpha_{33}+\tfrac{3}{2}(r+\sqrt{2}r_0)\cos\alpha_{33}] \qquad (3)$$

(see notations in ref. [13])).

The first term in the square brackets refers to π^0 production in the S-state due to "charge-exchange" scattering of π^+-mesons in the field of the nucleon; the second term refers to direct π^0 production in the S-state due to the photoelectric effect connected with the existence of an electric dipole moment in the final state.

The value of $r+\sqrt{2}r_0$ in relation (3) can be determined for that energy of incident gamma rays at which B vanishes. Evidently, the following equation is satisfied at this energy:

$$\operatorname{tg}\alpha_{33} = -\tfrac{3}{2}\frac{1}{\alpha_3-\alpha_1}(r+\sqrt{2}r_0). \qquad (4)$$

The data on B/A obtained in the present work as well as the results reported by McDonald *et al.* [4]) (fig. 1) show that B vanishes at an incident gamma ray energy of $260\pm^{20}_{10}$ MeV. This corresponds to $r+\sqrt{2}r_0 = 0.140\pm^{0.080}_{0.020}$, if for phase shifts α_3 and α_1 we accept the values given by Orear [14]) and for phase shift α_{33} the value reported by K. Brueckner [15]).

The dispersion relations indicate that near the threshold $r_0 = 0$, and $r = \mu/M = 0.144$. Furthermore, as shown, for instance, by Baldin [16]), the values r and r_0 must be constant in a broad energy interval. Thus, the value

obtained above, $(r+\sqrt{2}r_0)_{B=0} = 0.14$, is in good agreement with the predictions of the field theory. One should note that the parameter r is directly related to the threshold ratio of the cross sections for π^- and π^+ photoproduction on nucleons: $(\sigma^-/\sigma^+)_{\text{threshold}} = (1+r)^2$. According to our data $(\sigma^-/\sigma^+) = 1.30\pm^{0.19}_{0.05}$ which agrees with the experimental results of Adamovich and coworkers [17]). Assuming that $r+\sqrt{2}r_0 = \mu/M = \text{Const.}$, we derived the curve (plotted in fig. 1) which shows the dependence of B/A on the gamma ray energy up to 450 MeV. The bulk of the experimental data seems to be satisfactorily described by this curve.

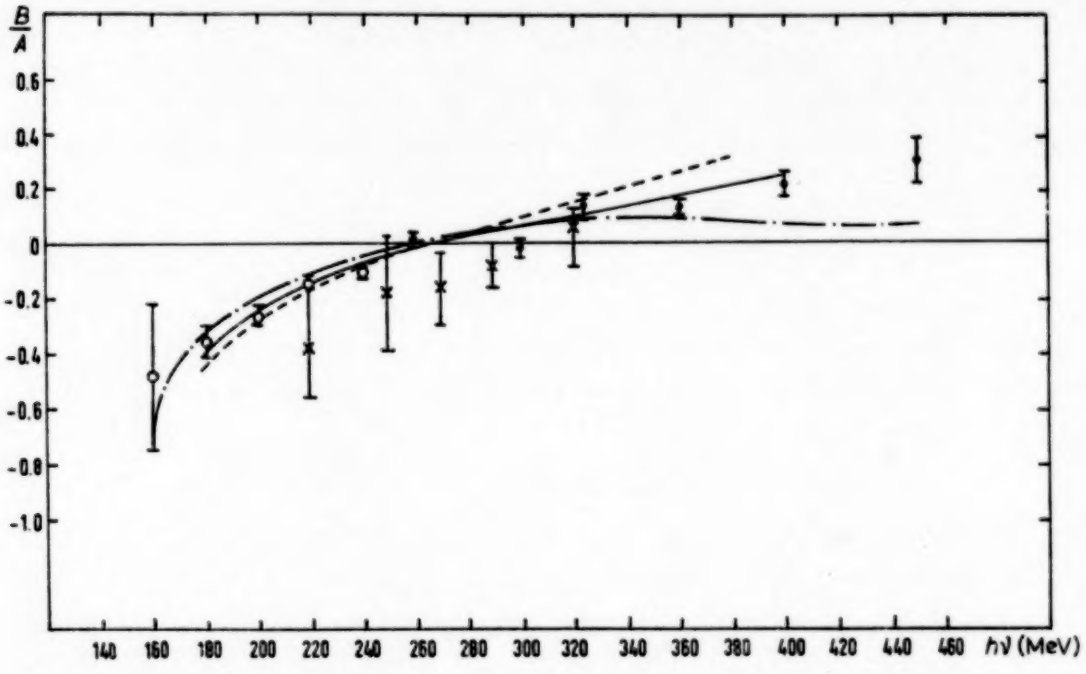

Fig. 1. The data of McDonald *et al.* [4]) are shown by dots. The data of Koester and Mills [2]) are represented by triangles. The circles are our data. The dot-dashed curve is derived by Watson's method [13]). The solid and dotted curves were respectively calculated by Feld [18]) with and without consideration of "retardation" effects.

Two other curves for B/A in fig. 1 were calculated by Feld [18]) by perturbation theory methods on the basis of a semiphenomenological "atomic" model of a nucleon (the solid line was computed with account of "retardation" effects and the dotted line without account of them). It can be seen that our experimental results are in good accord with B. Feld's calculations. The ratio of the real part ξ_r of the electrical dipole amplitude for S-state π^0 photoproduction (direct photoproduction) to the imaginary part ξ_i (charge-exchange production) is $\xi_r/\xi_i = 0.8\tilde{q}^{-1}$ and in the measured energy range is near to one. The experimental results and the curves for C/A calculated by Feld's theory are plotted in fig. 2. For pure M1 transitions $C/A = -0.6$; however, as was pointed out by Feld [18]), the small magnitude of the electric quadruple contribution E2 results in a marked change of this ratio. The

influence of "retardation" effects on this ratio is very small up to $\approx$ 300 MeV. Fig. 2 shows that the experimental results obtained so far are not sufficiently accurate to permit one to draw any definite conclusions regarding the E2 contribution to meson photoproduction in this range of energies.

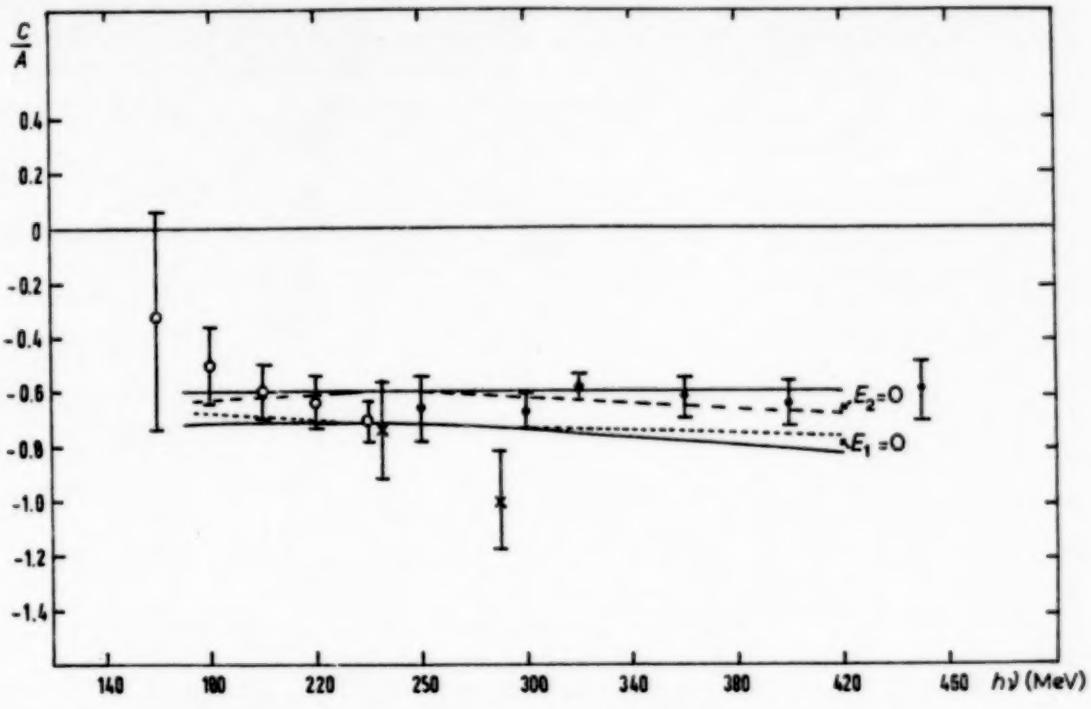

Fig. 2. Experimental data plotted as in fig. 1. The upper solid line is −0.6, the lower curve is derived in Feld's theory.

The authors wish to thank V. V. Pavlovskaya, O. A. Karpukhin, A. V. Kutsenko and I. A. Erofeev for assistance in performing the experiment and to acknowledge A. M. Baldin's instructive comments in discussing the experimental results.

We are also indebted to the operations crew of the P. N. Lebedev Institute 265 MeV synchrotron.

References

1) G. Cocconi and A. Silverman, Phys. Rev. **88** (1952) 1230
2) L. Koester and F. Mills, Phys. Rev. **105** (1957) 1900
3) Y. Goldschmidt-Clermont, L. Osborn and M. Scott, Phys. Rev. **97** (1955) 188
4) W. McDonald, V. Peterson and D. Corson, Phys. Rev. **107** (1957) 577
5) D. Oakley and R. Walker, Phys. Rev. **97** (1955) 1283
6) R. Walker, D. Oakley and A. Tollestrup, Phys. Rev. **97** (1955) 1279
7) B. B. Govorkov, V. I. Goldansky, O. A. Karpukhin, A. V. Kutsenko and V. V. Pavlovskaya, Doklady **111** (1956) 988
8) R. G. Vassilkov, B. B. Govorkov and A. V. Kutsenko, Pribory Tekh. Exper. (in press)
9) M. Beneventano, G. Stoppini, L. Tau and G. Bernardini, CERN Symposium on High-Energy Accelerators and Pion Physics (Geneva, 1956) p. 259

10) R. Walker, J. Teasdale, V. Peterson and J. Vette, Phys. Rev. **99** (1955) 210
11) A. Tollestrup, J. Keck and R. Worlock, Phys. Rev. **99** (1955) 220
12) T. Jenkins, D. Luck, T. Palfrey and R. Wilson, Phys. Rev. **95** (1954) 179
13) K. Watson, J. Keck, A. Tollestrup and R. Walker, Phys. Rev. **101** (1956) 1159
14) J. Orear, Phys. Rev. **96** (1954) 176; **100** (1955) 288
15) K. Brueckner, Phys. Rev. **87** (1952) 1026
16) A. M. Baldin, Nuovo Cimento **8** (1958) 569
17) M. I. Adamovich, G. V. Kuzmicheva, V. G. Larionova and S. P. Kharlamov, JETP **35** (1958) 27
18) B. Feld, Annals of Phys. **4** (1959) 189

1.C *Nuclear Physics* **12** (1959) 333—341; © *North-Holland Publishing Co., Amsterdam*
Not to be reproduced by photoprint or microfilm without written permission from the publisher

ON THE SINGULARITIES OF A GENERALIZED BRUECKNER *t*-MATRIX

M. L. MEHTA †
Centre d'Études Nucléaires de Saclay, Gif-sur-Yvette (*S & O*)

Received 10 April 1959

Abstract: It is shown that the *t*-matrix defined by taking hole-hole interactions together with particle-particle interactions has the same singularity as the original *t*-matrix of Brueckner, and in addition a symmetrical singularity above the Fermi-surface.

1. Introduction

Much progress has been made in the study of large interacting systems after the difficulties due to hard core potentials were removed by Brueckner's [1]) idea of making a summation of all particle-particle interactions. However the *t*-matrix introduced by Brueckner may have in the case of an attractive potential several singularities below the Fermi-surface which yield divergent integrals in the expression for the binding energy [2]).

Since progress was possible by a partial summation, it is natural to think that a more complete summation would remove the remaining difficulty also. Chisholm and Squires [3]) have considered the summation of all hole-hole interactions along with all particle-particle interactions. We shall show, however, that this method leads to a difficulty of exactly the same nature as the original summation of Brueckner.

In section 2 we use time-independent formalism as Chisholm and Squires do and give an explicit solution for the case they considered (separable potential); while in section 3 time dependent theory has been used to derive the result. The equivalence of the two results is not obvious, but, however, easy to show, thus making it clear why such a simple solution exists in the first case.

2. Time-Independent Formalism

In the case of a separable potential of strength g, considering the states of total momentum zero only, the binding energy in the approximation of Chisholm and Squires can be written as [3])

† On leave of absence from Tata Institute of Fundamental Research, Apollo Pier, Bombay.

$$\Delta E_0 = \sum_m \langle m|t|m\rangle, \tag{1}$$

where

$$\langle m|t|m\rangle = \langle m|v|m\rangle + \sum_k \frac{\langle m|v|k\rangle\langle k|t|m\rangle}{m^2-k^2}, \tag{2}$$

and

$$\langle k|t|m\rangle = -g\{v(k)t_1(m)+v(m)t_2(k)\}.$$

The functions $t_1(m)$ and $t_2(k)$ are the solutions of the coupled system of integral equations

$$t_1(m)\left\{1-\frac{g}{L^3}\sum_k \frac{v^2(k)}{k^2-m^2}\right\} - \frac{g}{L^3}\sum_k \frac{v(k)t_2(k)}{k^2-m^2}v(m) = Xv(m), \tag{3}$$

$$t_2(k)\left\{1-\frac{g\lambda}{L_1^3}\sum_m \frac{v^2(m)}{k^2-m^2}\right\} - \frac{g\lambda}{L_1^3}\sum_m \frac{v(m)t_1(m)}{k^2-m^2}v(k) = (1-X)v(k). \tag{4}$$

where $k \geqq k_F$, $m \leqq k_F$, if k_F is the Fermi-momentum; and X is a separation constant.

For convenience, we introduce the notations

$$t_1(m) = v(m)\vartheta_1(m), \qquad t_2(k) = v(k)\vartheta_2(k),$$

$$V(k) = \frac{g}{L^3}v^2(k), \qquad V(m) = \frac{g\lambda}{L_1^3}v^2(m).$$

The equations (1), (3) and (4) then become

$$\begin{aligned}\Delta E_0 &\approx -\sum_m V(m) - \sum_{k,m} V(k)V(m)\frac{\{\vartheta_1(m)+\vartheta_2(k)\}}{k^2-m^2} \\ &= -\sum_m V(m) - \sum_m V(m)\{\vartheta_1(m)-X\}, \\ &= -\sum_m V(m) - \sum_k V(k)\{\vartheta_2(k)-(1-X)\};\end{aligned} \tag{1'}$$

$$\vartheta_1(m)\left\{1-\sum_k \frac{V(k)}{k^2-m^2}\right\} - \sum_k \frac{V(k)}{k^2-m^2}\vartheta_2(k) = X, \tag{3'}$$

$$\vartheta_2(k)\left\{1-\sum_m \frac{V(m)}{k^2-m^2}\right\} - \sum_m \frac{V(m)}{k^2-m^2}\vartheta_1(m) = 1-X. \tag{4'}$$

Following Chisholm and Squires it is convenient to consider $\vartheta_1(m)$ and $\vartheta_2(k)$ as components of a vector ϑ:

$$\vartheta = \begin{pmatrix}\vartheta_1(m) \\ \vartheta_2(k)\end{pmatrix},$$

and to write the equations (3′) and (4′) in matrix form as

$$A\vartheta = Y, \tag{5}$$

where the matrix elements of A are given by

$$A_{mm'} = \delta_{mm'}\left\{1-\sum_k \frac{V(k)}{k^2-m^2}\right\}, \qquad A_{mk} = -\frac{V(k)}{k^2-m^2},$$
$$A_{km} = -\frac{V(m)}{k^2-m^2}, \qquad A_{kk'} = \delta_{kk'}\left\{1-\sum_m \frac{V(m)}{k^2-m^2}\right\}, \tag{6}$$

and where the components of Y are

$$Y_m = X, \qquad Y_k = (1-X). \tag{7}$$

We shall also need the two functions

$$\phi(x) = \sum_m \frac{V(m)}{x-m^2}, \qquad \psi(x) = \sum_k \frac{V(k)}{k^2-x}, \tag{8}$$

and the a_i satisfying the equation

$$\phi(a_i) = \psi(a_i) = c_i, \qquad i = 1, 2, \ldots, n-1,$$

where n = number of single particle energy levels (both above and below the Fermi-surface).

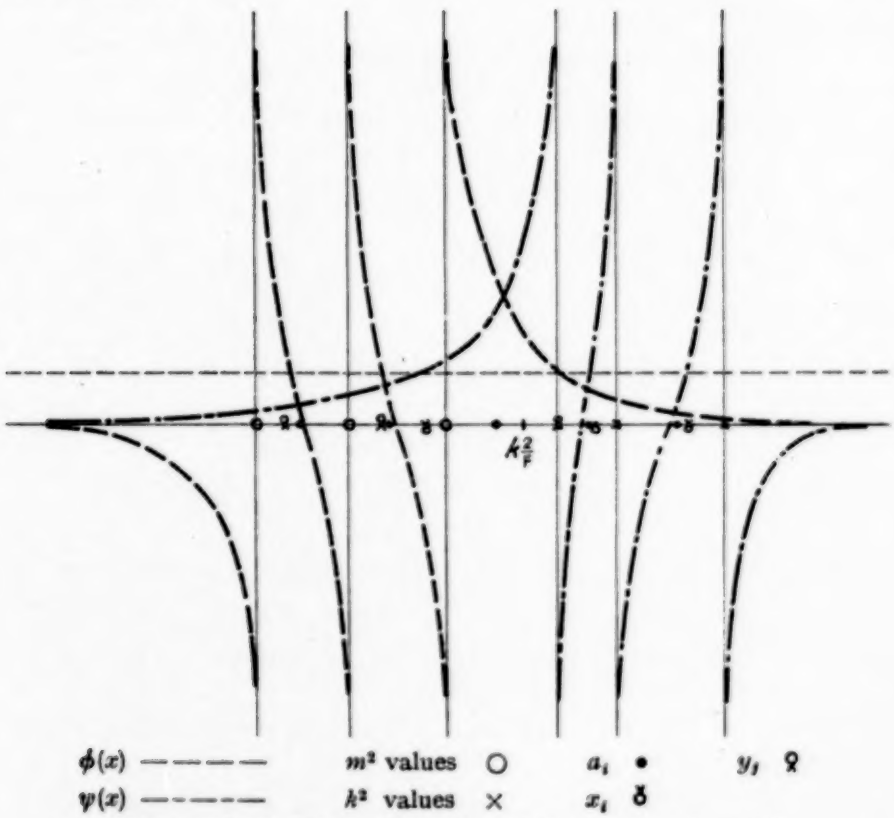

Fig. 1. The functions $\phi(x)$ and $\psi(x)$ for the case $\lambda = +1$.

It will also be convenient to write

$$V_i = \left(\frac{d\psi}{dx}\right)_{x=a_i} - \left(\frac{d\phi}{dx}\right)_{x=a_i} = \psi'(a_i) - \phi'(a_i), \tag{9}$$

$$V_0 = \sum_k V(k) + \sum_m V(m). \tag{10}$$

The functions $\phi(x)$ and $\psi(x)$ are plotted in fig. 1. We note from the figure that

1) Between every pair of energy levels, there lies one and only one a_i. As both $\phi(x)$ and $\psi(x)$ are proportional to g, the a_i are fixed as long as the energy levels are fixed.

2) The common values of ϕ and ψ, i.e. the c_i, vary continuously from 0 to $+\infty$ as g does so, at most two of the c_i being equal when $g > 0$.

Now we may proceed to solve. Define the matrix A' by

$$\begin{aligned}
A'_{mm'} &= \sum_i \frac{1}{V_i}\,\frac{1}{1-c_i}\,\frac{V(m')}{(a_i-m^2)(a_i-m'^2)} + \frac{1}{V_0}V(m'),\\
A'_{mk} &= \sum_i \frac{1}{V_i}\,\frac{1}{1-c_i}\,\frac{V(k)}{(a_i-m^2)(k^2-a_i)} - \frac{1}{V_0}V(k),\\
A'_{km} &= \sum_i \frac{1}{V_i}\,\frac{1}{1-c_i}\,\frac{V(m)}{(k^2-a_i)(a_i-m^2)} - \frac{1}{V_0}V(m),\\
A'_{kk'} &= \sum_i \frac{1}{V_i}\,\frac{1}{1-c_i}\,\frac{V(k')}{(k^2-a_i)(k'^2-a_i)} + \frac{1}{V_0}V(k').
\end{aligned} \tag{11}$$

It is a straightforward matter to verify that A' is the inverse of A. For instance,

$$\begin{aligned}
(AA')_{mm'} &= \sum_{m''} A_{mm''}A'_{m''m'} + \sum_k A_{mk}A'_{km'}\\
&= \sum_i \frac{1}{V_i}\,\frac{V(m')}{(a_i-m^2)(a_i-m'^2)} + \frac{1}{V_0}V(m').
\end{aligned}$$

To see that this is nothing but $\delta_{mm'}$, consider

$$I = \frac{1}{2\pi i}\oint \frac{V(m')}{(z-m^2)(z-m'^2)} \times \frac{1}{\psi(z)-\phi(z)}\,\mathrm{d}z,$$

where the contour encloses all the singularities of the integrand except that at ∞. There are simple poles at the a_i. Note that m^2(or m'^2) is not a pole if $m \neq m'$; and a simple pole if $m = m'$. There are no other singularities in the finite part of the z-plane. Therefore, by the residue theorem,

$$I = \sum_i \frac{1}{V_i}\,\frac{V(m')}{(a_i-m^2)(a_i-m'^2)} - \delta_{mm'}.$$

We may evaluate I also by taking the contour as a large circle whose radius $\to \infty$. So

$$I \to \frac{1}{2\pi i}\oint \frac{V(m')}{z^2} \times \frac{\mathrm{d}z}{\dfrac{\sum V(k)}{-z} - \dfrac{\sum V(m)}{z}} = -\frac{V(m')}{V_0}.$$

Equating these two expressions of I, we get

$$(AA')_{mm'} = \delta_{mm'}.$$

Proceeding in a straightforward fashion, we get, finally,

$$\begin{aligned} \vartheta_1(m) &= (A^{-1}Y)_m = \sum_i \frac{1}{V_i}\,\frac{c_i}{1-c_i}\,\frac{1}{a_i-m^2} + X - \frac{1}{V_0}\sum_k V(k), \\ \vartheta_2(k) &= (A^{-1}Y)_k = \sum_i \frac{1}{V_i}\,\frac{c_i}{1-c_i}\,\frac{1}{k^2-a_i} + (1-X) - \frac{1}{V_0}\sum_m V(m), \end{aligned} \tag{12}$$

and

$$\Delta E_0 = -\sum_i \frac{1}{V_i}\,\frac{c_i^2}{1-c_i} + \frac{1}{V_0}\sum_{m,k} V(m)V(k) - \sum_m V(m).$$

This may be put in a more symmetrical form by noting that

$$\frac{1}{V_0}\sum_{m,k} V(m)V(k) = \sum_i \frac{1}{V_i}\,c_i^2$$

(by evaluating $(1/2\pi i)\oint \psi\phi/(\psi-\phi)\mathrm{d}z$ in two different manners and equating, as done in the previous case). Thus,

$$\Delta E_0 = -\sum_i \frac{1}{V_i}\,\frac{c_i^3}{1-c_i} - \sum_m V(m). \tag{13}$$

Now, as g increases, each of the c_i crosses the value $+1$ one by one. Thus we get a set S_1 of values of g for which the energy expression diverges.

In the ordinary t-matrix case, we face the difficulty when $\psi(m^2) = 1$, giving a set S'_2 of g values. We may add to S'_2 the points at which $\phi(k^2) = 1$ and call this sum the set S_2. Now, it may be seen, by a more detailed analysis of the properties of ψ and ϕ, that every pair of successive points of S_2 contains a point of S_1 and vice-versa. And as we go to the limit of a continuum, both sets S_1 and S_2 become everywhere dense.

3. Time Dependent Theory

Following Bloch [4]) we form the quantity

$$\langle 0|U(\beta)|0\rangle_c = \langle 0|\sum_{p=0}^{\infty}(-)^p \int_{\beta>\beta_1>\ldots\beta_p>0} \mathrm{d}\beta_1 \ldots \mathrm{d}\beta_p H_1(\beta_1)\ldots H_1(\beta_p)|0\rangle_c$$

where

$$H_1(\beta) = \mathrm{e}^{\beta H_0} V \mathrm{e}^{-\beta H_0}$$

and we take the subscript c to mean that only the diagrams with all particle-particle and hole-hole interactions with a separable potential of strength g are summed over. Next, we study the behaviour of this quantity as $\beta \to \infty$ and see whether it is linearly divergent. If it is so, we pick up the coefficient

of $-\beta$, when β is large, which is the energy:

$$\Delta E_0 = -\operatorname*{Lim}_{\beta\to\infty}\frac{1}{\beta}\langle 0|U(\beta)|0\rangle_c .$$

Denoting the variables over particle lines as $\beta_2, \beta_3, \ldots \beta_n$, over hole lines as

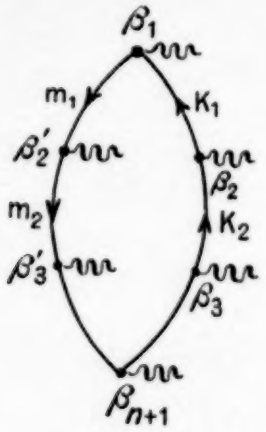

Fig. 2. A graph contributing to the binding energy in the approximation considered.

$\beta'_2, \beta'_3, \ldots \beta'_s$, and β_1 at the highest and β_{n+1} at the lowest of the graph (fig. 2), we have

$$\langle 0|U(\beta)|0\rangle_c = \sum_{n,s} V(m_1)\ldots V(m_s)V(k_1)\ldots V(k_n)\int d\beta_1 \ldots d\beta_{n+1} d\beta'_2 \ldots d\beta'_s$$

$$\exp\{-\beta_1(k_1^2-m_1^2)-\beta_2(k_2^2-k_1^2)-\ldots-\beta_n(k_n^2-k_{n-1}^2)+\beta'_2(m_2^2-m_1^2)$$
$$+\ldots+\beta'_s(m_s^2-m_{s-1}^2)+\beta_{n+1}(k_n^2-m_s^2),$$

with the inequalities

$$\beta > \beta_1 > \beta_2 > \ldots > \beta_n > \beta_{n+1} > 0,$$
$$\beta_1 > \beta'_2 > \ldots > \beta'_s > \beta_{n+1}.$$

To account for the inequalities while integrating we introduce the new variables [5])

$$\beta_1 = \beta_1, \quad \beta_2-\beta_3 = w_2, \quad \beta_3-\beta_4 = w_3, \ldots, \beta_n-\beta_{n+1} = w_n, \quad \beta_{n+1} = \beta_{n+1},$$
$$\beta'_2-\beta'_3 = w'_2, \ldots, \beta'_s-\beta_{n+1} = w'_s,$$

and two step functions:

$$\frac{1}{2\pi i}\int_{-a'+i\infty}^{-a'-i\infty}\frac{1}{\varepsilon}e^{(w_2+\ldots+w_n+\beta_{n+1}-\beta_1)\varepsilon}d\varepsilon,$$

and

$$\frac{1}{2\pi i}\int_{b'+i\infty}^{b'-i\infty}-\frac{1}{\varepsilon'}e^{-(w'_2+\ldots+w'_s+\beta_{n+1}-\beta_1)\varepsilon'}d\varepsilon',$$

the integration over ε and ε' being taken along two straight lines parallel to

the imaginary axis, of abscissae $-a'$ and b' respectively. These step functions serve to reduce the restrictions over w's and w''s to only the following:

$$w_i > 0, \qquad w'_i > 0, \qquad \beta_{n+1} > 0, \qquad \beta_1 < \beta.$$

We now integrate in a straightforward manner to get

$$\langle 0|U(\beta)|0\rangle_c = \sum_{n,s} V(m_1)\dots V(m_s)V(k_1)\dots V(k_n)\int\frac{d\varepsilon}{2\pi i}\int\frac{d\varepsilon'}{2\pi i}\,d\beta_1 d\beta_{n+1}$$
$$e^{-(\beta_1-\beta_{n+1})(k_1^2-m_1^2+\varepsilon-\varepsilon')}\,\frac{1}{-\varepsilon'}\times\frac{1}{\varepsilon}\times\frac{-1}{k_1^2-k_2^2+\varepsilon}\times\dots$$
$$\times\frac{-1}{k_1^2-k_n^2+\varepsilon}\times\frac{-1}{m_2^2-m_1^2-\varepsilon'}\times\dots\times\frac{-1}{m_s^2-m_1^2-\varepsilon'},$$

where a', b' are chosen to satisfy, $-a'+k_1^2-k_i^2<0$, $-b'-m_1^2+m_i^2<0$. By a change of axes,

$$\langle 0|U(\beta)|0\rangle_c$$
$$=\sum_{n,s} V(m_1)\dots V(m_s)V(k_1)\dots V(k_n)\,\frac{(-1)^{n+s}}{(2\pi i)^2}\int_{-a+i\infty}^{-a-i\infty}d\varepsilon\int_{b+i\infty}^{b-i\infty}d\varepsilon'\,d\beta_1 d\beta_{n+1}$$
$$e^{-(\beta_1-\beta_{n+1})(\varepsilon-\varepsilon')}\times\frac{1}{\varepsilon-k_1^2}\times\dots\times\frac{1}{\varepsilon-k_n^2}\times\frac{1}{-\varepsilon'+m_1^2}\times\dots\times\frac{1}{-\varepsilon'+m_s^2};$$

and

$$-a<k_i^2, \qquad b>m_i^2, \qquad \beta_1<\beta, \qquad \beta_{n+1}>0.$$

Thus,

$$\langle 0|U(\beta)|0\rangle_c$$
$$=\int_{-a+i\infty}^{-a-i\infty}\frac{d\varepsilon}{2\pi i}\int_{b+i\infty}^{b-i\infty}\frac{d\varepsilon'}{2\pi i}\,d\beta_1 d\beta_{n+1}\,e^{-(\beta_1-\beta_{n+1})(\varepsilon-\varepsilon')}\times\frac{1}{1-\phi(\varepsilon')}\times\frac{1}{1-\psi(\varepsilon)}.$$

One thing is to be noted while the last summation is made. Since one pole of $\{1-\psi(\varepsilon)\}^{-1}$ lies to the left of every k_i^2, and nothing restricts us in choosing a in relation to this pole, there is an ambiguity. But as this expression equals the series only when the later converges, it is more natural to take $-a$ to the left of this pole also. A similar situation is met in the relative positions of b and a pole of $\{1-\phi(\varepsilon')\}^{-1}$ and we take b to the right of this pole also.

For $\beta_1-\beta_{n+1}<0$, the integral is zero, as is seen by closing the contour of ε on the left. For $\beta_1-\beta_{n+1}>0$, we may close the contour by a large semi-circle on the right for ε and on the left for ε'. As no singularities are left outside these contours in the finite parts of the complex ε and ε'-planes, we may take these contours to be large circles described in opposite senses.

Denoting by x_i and y_j the roots of the equations

$$\psi(x)=1, \qquad \phi(y)=1,$$

we get by the residue theorem

$$\langle 0|U(\beta)|0\rangle_c = \sum_{i,j} \frac{-1}{\phi'(y_j)} \times \frac{1}{\psi'(x_i)} \int_{\beta>\beta_1>\beta_{n+1}>0} e^{-(x_i-y_j)(\beta_1-\beta_{n+1})}\, d\beta_1 d\beta_{n+1}.$$

Integrating finally over β_1 and β_{n+1}, and picking the linear term in β, for large β,

$$\Delta E_0 \sim \sum_{i,j} \frac{1}{x_i - y_j} \times \frac{1}{\psi'(x_i)} \times \frac{1}{\phi'(y_j)}.$$

We may easily verify that this result is the same as that of section 2, as follows:

$$\begin{aligned}
&\sum_{i,j} \frac{1}{x_i-y_j} \frac{1}{\psi'(x_i)} \frac{1}{\phi'(y_j)} \\
&\quad = \sum_i \frac{1}{2\pi i} \oint \frac{1}{x_i-y} \frac{\phi(y)}{\phi(y)-1} dy \frac{1}{\psi'(x_i)} + \sum_i \frac{1}{\psi'(x_i)} \times \frac{\phi(x_i)}{\phi(x_i)-\psi(x_i)} \\
&\quad = \frac{1}{2\pi i} \sum_i \frac{1}{\psi'(x_i)} \oint \frac{1}{x_i-y} \frac{\phi(y)}{\phi(y)-1} dy + \frac{1}{2\pi i} \oint \frac{\psi(x)}{\psi(x)-1} \times \frac{\phi(x)}{\phi(x)-\psi(x)} dx \\
&\quad - \sum_i \frac{\phi(a_i)\psi(a_i)}{\{\psi(a_i)-1\}\{\phi'(a_i)-\psi'(a_i)\}};
\end{aligned}$$

therefore,

$$\begin{aligned}
&\sum_{i,j} \frac{1}{x_i-y_j} \frac{1}{\psi'(x_i)} \frac{1}{\phi'(y_j)} + \sum_i \frac{1}{V_i} \frac{c_i^2}{1-c_i} \\
&\qquad = \frac{1}{2\pi i} \sum_i \frac{1}{\psi'(x_i)} \oint \frac{1}{x_i-y} \frac{\phi(y)}{\phi(y)-1} dy + \frac{1}{2\pi i} \oint \frac{\psi\phi}{\{\psi-1\}\{\phi-\psi\}} dx.
\end{aligned}$$

The last two contour integrals, where the contour is a large circle containing all singularities, except possibly at infinity, can be evaluated by taking the limit when the contour approaches ∞.
Thus,

$$\frac{1}{2\pi i} \oint \frac{1}{x_i-y} \frac{\phi(y)}{\phi(y)-1} dy \sim \frac{1}{2\pi i} \oint \frac{1}{-y} \times \frac{0}{-1} dy \to 0,$$

and

$$\frac{1}{2\pi i} \oint \frac{\psi\phi}{\{\psi-1\}\{\phi-\psi\}} dx \sim \frac{1}{2\pi i} \oint \frac{\sum V(k)V(m)}{-x^2 \frac{V_0}{x}} \times \frac{1}{-1} dx \to \frac{\sum V(k)V(m)}{V_0}.$$

4. Conclusion

Thus, the inclusion of hole-hole interactions along with particle-particle interactions makes things symmetric about the Fermi-surface, but fails to

remove the divergence of the original summation. It simply rotates the frame in the abstract space, and moreover introduces new points of divergence, which are the symmetrical points of those existing in the original theory, with respect to the Fermi-surface.

It is a pleasure to acknowledge my debt to Prof. C. Bloch, who not only suggested the problem but constantly guided and encouraged me throughout the work. I wish also to express my thanks to Dr. C. De Dominicis and Mr. M. Gaudin for many helpful discussions; and the Service de Coopération Technique for a maintenance grant.

References

1) Reviews of the method and lists of references are given by H. A. Bethe, Phys. Rev. **103** (1956) 1353; and K. A. Brueckner and J. L. Gammel, Phys. Rev. **109** (1958) 1023
2) L. N. Cooper, Phys. Rev. **104** (1956) 1189;
A. Bohr, B. R. Mottelson and D. Pines, Phys. Rev. **110** (1958) 936;
J. Goldstone, Thesis, Cambridge University;
K. Gottfried, CERN Report (unpublished)
3) J. S. R. Chisholm and E. J. Squires, Nuclear Physics, in the press
4) C. Bloch, Nuclear Physics **7** (1958) 451
5) C. Bloch and C. De Dominicis, Nuclear Physics **7** (1958) 459

8.B *Nuclear Physics* **12** (1959) 342—348; © *North-Holland Publishing Co., Amsterdam*

Not to be reproduced by photoprint or microfilm without written permission from the publisher

K^0-K^+ MASS EXCESS †

RIAZUDDIN

Department of Mathematics, Imperial College of Science and Technology, London

Received 2 April 1959

Abstract: It is attempted to explain the recently measured K^0-K^+ mass difference in terms of the self-energies of the K-mesons due to K-baryon interaction. Two cases are considered: (1) K^0-K^+ relative parity is assumed to be odd and there arises a non-electromagnetic mass split; (2) K^0-K^+ relative parity is taken to be even and the doublet nature of K is maintained: the mass difference for this case is calculated via the renormalisation of K-baryon coupling constants due to electromagnetic field. It is shown that in either case K^0 may be heavier than K^+. Both cases favour pseudoscalar K^+ with respect to ΛN and ΣN systems. But while case (1) (with pseudoscalar K^+) favours even $\Xi-N$ relative parity, the opposite holds for case (2). Further, for case (1), scalar K^+ together with odd $\Xi-N$ relative parity is also possible.

1. Introduction

Recently it has been shown [1]) experimentally that K^0 is heavier than K^+ by about 8 electron masses. This is contrary to what one would expect for spinless particles of the same charge multiplet. In fact if one assumes K^+ and K^0 to be members of a charge doublet and neglects the effect of strong interactions, it has been shown [2]) that the mass difference between K^+ and K^0 in terms of their electromagnetic self-energies is positive by about 3 electron masses, which is in contradiction with the above-mentioned experimental result. The purpose of this note is to consider the effect of strong K-baryon interaction on K^+-K^0 mass difference and see whether such an effect can make K^0 heavier than K^+. We consider two cases: (1) K^0-K^+ relative parity is odd as suggested by Pais [3]). This invalidates the assumption that K^0 and K^+ are members of a charge doublet unless the K's are weakly coupled. (2) K^0-K^+ relative parity is even. Here the doublet nature of K is retained. Case (1) is discussed in section 2 and the other in section 3. It is shown that in either case K^0 may be heavier than K^+. We conclude this section by writing the K-baryon interaction lagrangian:

$$L = L_N + L_\Xi \tag{1}$$

where

$$L_N = g_1[\bar{p}\Gamma\Lambda K^+ + \bar{n}\Gamma\eta\Lambda K^0] + g_2[\bar{p}\Gamma\Sigma^0 K^+ - \bar{n}\Gamma\eta\Sigma^0 K^0 + 2^{\frac{1}{2}}\bar{n}\Gamma\Sigma^- K^+ + 2^{\frac{1}{2}}\bar{p}\Gamma\eta\Sigma^+ K^0] + \text{H.C.}$$

† Research supported by Department of Scientific and Industrial Research.

and

$$L_{\Xi} = h_1[\bar{\Xi}^- \Gamma' \Lambda \bar{K}^+ - \bar{\Xi}^0 \Gamma' \eta \Lambda \bar{K}^0] + h_2[-\bar{\Xi}^- \Gamma' \Sigma^0 \bar{K}^+ - \bar{\Xi}^0 \Gamma' \eta \Sigma^0 \bar{K}^0 + 2^{\frac{1}{2}} \bar{\Xi}^0 \Gamma' \Sigma^+ \bar{K}^+ - 2^{\frac{1}{2}} \bar{\Xi}^- \Gamma' \eta \Sigma^- \bar{K}^0] + \text{H.C.}$$

Here $\Gamma = 1$ or $i\gamma_5$; $\Gamma' = 1$ or $i\gamma_5$. $\eta = 1(i\gamma_5)$ corresponds to even (odd) $p(K)$, where $p(K)$ denotes the parity of K^0 relative to K^+. $\Gamma = 1$ $(i\gamma_5)$ corresponds to even (odd) $P(K^+)$, where $P(K^+)$ denotes the parity of K^+ relative to $\Lambda-N$ and $\Sigma-N$ systems. And $\Gamma = \Gamma'$ if Ξ-nucleon parity, denoted by $P(\Xi)$, is even. If the latter is odd, one has $\Gamma = 1$, $\Gamma' = i\gamma_5$ or $\Gamma = i\gamma_5$, $\Gamma' = 1$ according as $P(K^+)$ is even or odd.

Although we are here dealing with strong interactions, nevertheless we shall employ second order perturbation theory to compute K-meson self-energy due to the interaction lagrangian (1). Use of second order perturbation theory for the computation of self-charge and self-mass effects is, perhaps, not too misleading as discussed by Salam and Tiomno [4]). Using perturbation theory, the second order contribution to K-meson self-mass, when it interacts with a baryon B_1 and an antbaryon $\bar{B}_2$, equals

$$\Delta m_K^2 = (g^2/4\pi)(-4X^2 \pm 4M_{B_1} M_{B_2} \log X^2/M^2) \tag{2}$$

where M_{B_1}, M_{B_2} are the masses of B_1 and B_2, X = cut-off mass, M = nucleon mass and g^2 is the coupling constant. The $+$ or $-$ sign in (2) is to be taken according as the interaction responsible for (2) is scalar or pseudoscalar. Formula (2) will be employed below to discuss the K^0-K^+ mass difference.

2. K^0-K^+ Parity Odd

In this case $\eta = i\gamma_5$ and there arises a non-electromagnetic K^0-K^+ mass split as can be seen from equation (2). If we now take $P(K^+)$ to be odd as the dispersion relations for K-mesons indicate [5]), then $\Gamma = i\gamma_5$ and from (1) and (2) we get

$$\begin{aligned}(\delta K^2/K^2)_1 &= \Delta m^2_{K^0} - \Delta m^2_{K^+}/m_K^2 \\ &= \left(\frac{g_1^2+3g_2^2}{4\pi}\frac{M_N M_Y}{m_K^2} \pm \frac{h_1^2+3h_2^2}{4\pi}\frac{M_\Xi M_Y}{m_K^2}\right) 8 \log X^2/M^2 \end{aligned} \tag{3}$$

where $+$ or $-$ are to be taken according as $P(\Xi)$ is even or odd; and M_Y is the mass of the hyperon Λ or Σ (taken to be equal). From this it is clear that for even $P(\Xi)$, $(\delta K^2/K^2)_1$ is certainly positive. For odd $P(\Xi)$, $(\delta K^2/K^2)_1$ is positive only if

$$\begin{aligned}(g_1^2+3g_2^2) &> (M_\Xi/M_N)(h_1^2+3h_2^2) \\ &\approx 1.41(h_1^2+3h_2^2).\end{aligned}$$

If the g's are of the same order of magnitude as the h's, then for odd $P(\Xi)$ we cannot get positive $(\delta K^2/K^2)_1$.

If we take $P(K^+)$ to be even, we get just the opposite results i.e. for even $P(\Xi)$, $(\delta K^2/K^2)_1$ is certainly negative, and for odd $P(\Xi)$ it is positive only if $(g_1^2+3g_2^2) < (M_\Xi/M_N)(h_1^2+3h_2^2)$.

From the above discussion we conclude that the most favourable case for making $(\delta K^2/K^2)_1$ positive is that for which we have odd $P(K^+)$ and even $P(\Xi)$. In this case (taking $g_1^2 \approx g_2^2$, $h_1^2 \approx h_2^2$, $M_Y \approx M_\Xi \approx M$) we get

$$(\delta K^2/K^2)_1 = (g^2+h^2/\pi)(8M^2/m_K^2) \log X^2/M^2. \tag{4}$$

To this must be added the electromagnetic self-mass of K^+ which is equal to $(3\alpha/4\pi)\ X^2$ (with $\alpha = 1/137$); so that the total

$$\begin{aligned} \delta K^2/K^2 &= m_{K^0}^2 - m_{K^+}^2/m_K^2 \\ &= (g^2+h^2/\pi)(8M^2/m_K^2) \log X^2/M^2 - (3\alpha/4\pi)X^2/m_K^2. \end{aligned} \tag{5}$$

If we now take $g^2 \approx h^2 \approx 1$ and $X^2 \approx 1.001\ M^2$, the experimental $\delta K^2/K^2$ can be obtained.

For even $P(K^+)$ and odd $P(\Xi)$, we get (taking all the coupling constants equal, $M_Y \approx M$ and $M_\Xi \approx 1.41\ M$)

$$(\delta K^2/K^2)_1 = (0.41g^2/\pi)(8M^2/m_K^2) \log X^2/M^2,$$

so that the total

$$\delta K^2/K^2 = (0.41\ g^2/\pi)(8M^2/m_K^2) \log X^2/M^2 - (3\alpha/4\pi)X^2/m_K^2.$$

If we now take $g^2 \approx 1$ and $X^2 \approx 1.007\ M^2$, the experimental $\delta K^2/K^2$ is again obtained.

We conclude that for odd $p(K)$, K^0 may be heavier than K^+ for either odd or even $P(K^+)$. But while the former favours even $P(\Xi)$, for the latter $P(\Xi)$ must be odd and the condition $g_1^2+3g_2^2 < (M_\Xi/M_N)(h_1^2+3h_2^2)$ must be satisfied.

3. K^+-K^0 Parity Even

Here $\eta = 1$ and K^+ and K^0 are regarded as members of the same charge multiplet. In this case the charge-independent K-baryon interaction (1) does not contribute anything to the K^0-K^+ mass difference. However, the K-baryon coupling constants, which are assumed to be equal between members of the same multiplet in the charge-independent theory, are bound to be affected due to their renormalisation by electromagnetic field. We denote such renormalisation effects by δg_i, $\delta h_i (i = 1,2)$ where δg_i, δh_i are defined as follows:

$$\begin{aligned} \delta g_1 &= g_1(p\Lambda K^+) - g_1(n\Lambda K^0) \\ \delta g_2 &= g_2(p\Sigma^0 K^+) - g_2(n\Sigma^0 K^0) \\ \delta g'_2 &= g_2(n\Sigma^- K^+) - g_2(p\Sigma^+ K^0) \end{aligned}$$

and δh_i are similar quantities with nucleons replaced by cascade particles. Then the mass difference between K^0 and K^+ can be written as

$$\delta K^2/K^2 = (\Delta E)_{\text{e.m.}} + (\Delta E) \tag{7}$$

where $-(\Delta E)_{\text{e.m.}}$ is the usual electromagnetic self-energy of K^+ and is equal to $(3\alpha/4\pi)X^2/m_K{}^2$ ($\alpha = 1/137$ and $X =$ cut-off mass); and ΔE is the contribution to the K^0-K^+ mass-difference due to the interaction (1) after the renormalisation of coupling constants occurring in (1), due to electromagnetic interaction, has been carried out. In second order perturbation theory ΔE can be obtained from (2) and (6) and is given by

$$\Delta E = (2/\pi)\left[\sum_{i=1}^{2}(g_i\delta g_i + h_i\delta h_i) + 2(g_2\delta g'_2 + h_2\delta h'_2)\right] X^2/m_K{}^2. \tag{8}$$

If there were no renormalisation effects due to electromagnetic field, δg_i etc. would be zero, making ΔE zero, as remarked earlier. Only if ΔE is positive and greater than $(\Delta E)_{\text{e.m.}}$, will K^0 be heavier than K^+.

We now estimate δg_i etc. in perturbation theory. The renormalisation due to the electromagnetic field, which does not include interaction of anomalous magnetic moments of the baryons, makes K^0 coupling constants slightly greater than those for K^+, as can be inferred from a similar calculation done by the author [6]) for π-coupling constants with nucleons. This will certainly make ΔE negative, which we do not want. If, however, we include in the electromagnetic field the Pauli type interaction of anomalous magnetic moments of baryons, we shall show that, with certain assumptions about relative parities of the hyperons (to be stated later), ΔE can be made positive. Nothing is, of course, known experimentally about the magnetic moments of hyperons. If, however, pion–baryon interaction is strong compared to K-baryon interaction, as experiments indicate, the main contribution to anomalous moments will come from pion–baryon interaction. If we now assume global symmetry for pion interactions, this predicts the magnetic moments of hyperons as follows [1]):

$$\mu_{\Sigma^+} = -\mu_{\Sigma^-} = \mu_{\Xi^0} = -\mu_{\Xi^-} = \mu_{\mathrm{x}} = -\mu_{\mathrm{n}} = \mu_{\mathrm{p}} = \mu = 1.8,$$
$$\mu_\Lambda = 0, \quad \mu_{\Sigma^0} = 0.$$

Here μ_{x} is the transition magnetic moment $\Sigma^0 \to \Lambda+\gamma$. In what follows we shall assume the above values for the magnetic moments of baryons. The contributions to $\delta g_1{}^2$ etc. of various self-energy and vertex part graphs due to electromagnetic interaction of lowest order are given in table 1.

We now discuss contributions of the various graphs given in table 1 to ΔE.

Let us first consider the graph S_K. From table 1 we see that its contribution to ΔE is $(g_1{}^2+3g_2{}^2+h_1{}^2+3h_2{}^2)(-2a/\pi)(X^2/m_K{}^2)$, which is certainly negative.

TABLE 1

Contributions of various self-energy and vertex part graphs to δg_1 etc.

Type of graph	S_K	S_B	V_I	V_{II}††
$\delta g_1/g_1$	$-a$	c	$-a$	$\binom{r}{s}$
$\delta g_2/g_2$	$-a$	c	$-a$	$\binom{r}{s}$
$\delta g'_2/g_2$	$-a$	$-c$	$-a$	$\binom{p}{q}$
$\delta h_1/h_1$	$-a$	c	$-a[1+\frac{0}{3\mu}]^{\dagger}$	$-\binom{r}{s}$
$\delta h_2/h_2$	$-a$	c	$-a[1+\frac{0}{3\mu}]^{\dagger}$	$-\binom{r}{s}$
$\delta h'_2/h_2$	$-a$	$-c$	$-a$	$\binom{p}{q}$

Notation:

S_K = K^+ self-energy graph, S_B = Baryon self-energy graph,
V_I = Vertex part graph with photon exchanging between K^+ line and baryon line,
V_{II} = Vertex part graph with photon exchanging between two baryon lines,
μ = Anomalous magnetic moment of nucleon,
$a = (\alpha/4\pi)\log\lambda^2/M^2$, $b = (\alpha/4\pi)\lambda^2/M^2$, $c = (\frac{3}{4}\mu-\frac{1}{2})a$,

$$\binom{p}{q} = -\tfrac{3}{4}\binom{5}{1}\mu a - 4a,\quad \binom{r}{s} = \tfrac{3}{4}\binom{5}{1}\mu a + 6\binom{1}{0}\mu^2 a + \tfrac{3}{2}\binom{-1}{+1}\mu^2 b,$$

(M = nucleon mass, λ = cut-off mass)

† The upper or lower number is to be taken according as the $K^{\Lambda}_{\Sigma}\Xi$ system is scalar or pseudoscalar.

†† In this column the upper or lower numbers are to be taken according as the system in question is scalar or pseudoscalar.

The contribution of S_B is $(g_1^2-g_2^2+h_1^2-h_2^2)(2/\pi)(-\frac{1}{2}+\frac{3}{4}\mu)aX^2/m_K^2$, which is positive if $g_1^2 > g_2^2$ and $h_1^2 > h_2^2$. If $g_1^2 \approx g_2^2$ and $h_1^2 \approx h_2^2$, this contribution is zero. Unless g_1^2 and h_2^2 differ very much from g_2^2 and h_2^2 respectively, this contribution is very small compared to those of other graphs; in what follows we shall neglect it.

Next we consider graph V_I. This gives for ΔE the expression

$$\left[g_1^2+3g_2^2+h_1^2\binom{1}{1+3\mu}+h_2^2\binom{1}{1+3\mu}+2h_2^2\right]2(-a)(1/\pi)X^2/m_K^2,$$

where upper or lower numbers in parenthesis are to be taken according as $K^{\Lambda}_{\Sigma}\Xi$ systems are scalar or pseudoscalar. In either case this contribution is negative, although the first case is slightly more favourable for our purposes.

So far, we have got negative contributions to ΔE. Hence, unless we get a contribution from graph V_{II} positive and larger than the previous ones, the results of this section are negative. From table 1 se see that the V_{II} contribution to ΔE is negative for either odd or even $P(K^+)$ if Ξ—N relative parity is even, provided that g_1^2, g_2^2 do not differ very much from h_1^2, h_2^2. However,

if $P(K^+)$ is odd and the $\Xi-N$ relative parity is also odd, we can get positive contribution from V_{II} to ΔE. In this case the contribution is

$$[-8(g_2^2+h_2^2)a+\{3(g_1^2-g_2^2)-15(h_1^2+3h_2^2)\}\tfrac{1}{4}\mu a-6(h_1^2+h_2^2)\mu^2 a + (g_1^2+g_2^2+h_1^2+h_2^2)\tfrac{3}{2}\mu^2 b](2/\pi)X^2/m_K^2.$$

To proceed further we assume $g_1^2 \approx g_2^2 \approx g^2 \approx h_1^2 \approx h_2^2$. Then the net ΔE is given by

$$\begin{aligned}\Delta E &= [-(32+15\mu+12\mu^2)\log\lambda^2/M^2+6\mu^2\lambda^2/M^2](\alpha/4\pi)(2g^2/\pi)X^2/m_K^2 \\ &= [-98\log\lambda^2/M^2+19.44\,\lambda^2/M^2](\alpha/4\pi)(2g^2/\pi)X^2/m_K^2.\end{aligned} \tag{9}$$

This is positive if the cut-off λ is such that $19.44\,\lambda^2/M^2 > 98\log\lambda^2/M^2$. If $M^2 \leqq \lambda^2 < 1.3\,M^2$ or if $\lambda^2 \geqq 13\,M^2$, we get ΔE positive. For $\lambda^2 \approx 1.1M^2$, we obtain

$$\Delta E \approx (\alpha/4\pi)g^2 \cdot 7.66\,X^2/m_K^2, \tag{10}$$

so that, using (7), we get

$$\delta K^2/K^2 \approx (\alpha/4\pi)(X^2/m_K^2)[-3+g^2 \cdot 7.66]. \tag{11}$$

If we now take $g^2 \approx 1.4$ and $X \approx M$, we can get the experimental $\delta K^2/K^2$.

We conclude this section with some remarks about π-baryon coupling constants. It has already been shown [6]) that the coupling constant of the π^0-meson with the nucleon is larger than that of $\pi^\pm$. In ref. [6]) the interaction of the anomalous magnetic moment of the nucleon was not considered. However, the conclusion of ref. [6]) is not altered even if we include this interaction. Similar results hold for the π-coupling constants with hyperons. Thus, for the $\pi^\pm-\pi^0$ mass difference, it follows that strong interactions tend to enhance the positive contribution of electromagnetic self-energy to the mass difference $m_{\pi^+}-m_{\pi^0}$.

4. Conclusions

We have given two different explanations of the K^0-K^+ mass excess. The first one, when the K^0-K^+ relative parity is odd, is the simpler of the two. But it destroys the doublet nature of K. The second explanation, although involved and not unambiguous, retains the doublet character of K. It is interesting to note that in both cases pseudoscalar K^+ with respect to ΛN, ΣN systems is favoured. But on the other hand, while the first (with pseudoscalar K^+) favours even $\Xi-N$ relative parity, the opposite is the case for the second one. Further, for the first explanation (odd $p(K)$), K^0 may be heavier than K^+ for scalar K^+ also; but in this case $P(\Xi)$ must be odd and the inequality $(g_1^2+3g_2^2) < (M_\Xi/M_N)(h_1^2+3h_2^2)$ must be satisfied.

This problem was suggested by Professor A. Salam, to whom the author is indebted for encouragement and advice.

References

1) A. H. Rosenfeld, F. T. Solmitz and R. D. Tripp, Phys. Rev. Lett. **2** (1959) 110;
F. S. Crawford, Jr., M. Cresti, M. L. Good, M. L. Stevenson and H. K. Ticho, Phys. Rev. Lett. **2** (1959) 112
2) S. Gasiorowicz and A. Petermain, Phys. Rev. Lett. **1** (1958) 457;
Riazuddin, to be published in Phys. Rev.
3) A. Pais, Phys. Rev. **112** (1958) 624;
see also J. G. Taylor, Nuclear Physics **9** (1959) 357
4) A. Salam and J. Tiomno, Nuclear Physics **9** (1959) 585
5) P. T. Matthews and A. Salam, Phys. Rev. **110** (1958) 569;
C. Gobel, Phys. Rev. **110** (1958) 572;
K. Igi, Prog. Theor. Phys. **20** (1958) 403;
J. G. Taylor, Nuclear Physics **9** (1959) 357;
S. Barshay, Phys. Rev. Lett. **1** (1958) 177;
D. Amati, Phys. Rev. (to be published)
6) Riazuddin, Nuclear Physics **7** (1958) 223
7) M. Gell-Mann and R. H. Dalitz, 1958 Annual International Conference on High Energy Physics at CERN (CERN, Geneva, 1958)

3.B *Nuclear Physics* **12** (1959) 349—355; © *North-Holland Publishing Co., Amsterdam*
Not to be reproduced by photoprint or microfilm without written permission from the publisher

CORRÉLATION ANGULAIRE DE PAIRES DE CONVERSION INTERNE DÉTECTÉES DANS UN FOND DE NEUTRONS ET DE RAYONNEMENT γ. APPLICATION À ^{14}N, ^{10}Be, ^{10}B

S. GORODETZKY, P. CHEVALLIER, R. ARMBRUSTER et G. SUTTER
Institut de Recherches Nucléaires de Strasbourg

Reçu le 6 avril 1959

Abstract: The determination of nuclear electromagnetic transitions by angular correlations of internal conversion pairs is extended to reactions induced by deuterons. The neutron and gamma background is eliminated by the adjunction of thin crystals to the usual β scintillation spectrometer. This technique is applied to certain transitions in ^{14}N, ^{10}Be and ^{10}B.

1. Introduction

La détermination de l'ordre de multipolarité des transitions électromagnétiques nucléaires par corrélation angulaire des paires de conversion interne présente de grandes difficultés dans le cas de réactions induites par deutérons. En effet, le nombre de niveaux excités obtenus peut alors être très important et le spectromètre utilisé pour mesurer les corrélations angulaires [1]) ne permet pas en général de dissocier les paires provenant de transitions trop voisines énergétiquement. La résolution du spectromètre est de 12 % pour la raie monopolaire (5.03 MeV) provenant du niveau de 6.05 MeV de ^{16}O. Cette difficulté a été contournée dans le cas où la réaction conduit à une série de transitions parmi lesquelles il s'en trouve deux énergétiquement voisines et séparables des autres par le spectromètre. En effet, la corrélation angulaire de ces deux transitions est alors effectuée simultanément, les paires provenant des deux transitions étant mélangées dans un même pic de somme. La corrélation angulaire mesurée sera donc la superposition de deux corrélations. Elle pourra, cependant, permettre d'en extraire les deux corrélations individuellement à la condition de connaître l'intensité relative des deux transitions. Il n'est pas nécessaire de connaître cette intensité relative avec une très grande précision. Elle sera mesurée dans un premier stade, au moyen d'un spectromètre à paires externes à trois cristaux NaI, appareil qui a un bien meilleur pouvoir de résolution que notre spectromètre à paires internes. Cette méthode a déjà été utilisée [2]) pour les transitions 6.09 MeV du ^{14}C et 5.69 MeV de ^{14}N. Nous avons cependant amélioré le spectromètre à paires externes utilisé dans cette première expérience en diminuant notablement la proportion de „bremsstrahlung"

qui élargit les pics obtenus. Pour cela, nous avons diaphragmé les cristaux latéraux au moyen d'anneaux de plomb de 1 cm d'épaisseur disposés comme sur la figure 1. En effet ce dispositif a l'avantage de ne donner lieu à une coïncidence que lorsque le positon a été annihilé au centre du cristal, ce qui permet aux rayonnements γ de „bremsstrahlung" provenant du positon d'avoir de fortes chances d'être réabsorbés dans le cristal. On arrive ainsi à améliorer la résolution du spectromètre. Celle-ci est de 4.8 % pour la raie correspondant à la transition 6.13 MeV de ^{16}O.

La seconde difficulté qui se présentera dans le cas des réactions induites par deutérons provient de la présence d'un fond intense de neutrons et de rayonnements γ qui donne lieu à des coïncidences et qui, par suite, perturbera le spectre de somme du spectromètre à paires internes. Cette difficulté avait été surmontée pour l'étude des transitions 6.09 MeV du ^{14}C et 5.69 MeV de ^{14}N en utilisant une discrimination de 2 MeV, celle-ci permettant d'éliminer toutes coïncidences possibles neutron—gamma et gamma—gamma.

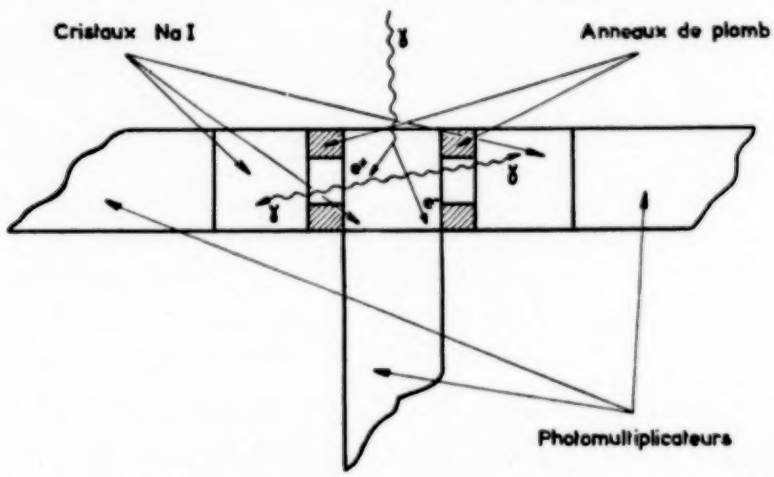

Fig. 1. Disposition des cristaux NaI du spectromètre à paires externes.

Cette méthode avait cependant le désavantage de diminuer considérablement le nombre de paires mesurées et surtout de diminuer l'importance des paires provenant du niveau 5.69 MeV par rapport à celles provenant du niveau 6.09 MeV. C'est ainsi que la précision de la mesure pour la transition 5.69 MeV était très faible. Aussi, utilisons-nous actuellement une méthode différente.

2. Spectromètre à Paires Internes

L'artifice utilisé pour éliminer les coïncidences neutron —γ et γ—γ consiste à placer devant chaque cristal épais destiné à mesurer l'énergie des particules un cristal mince télescopique. Ces cristaux minces (scintillateurs plastiques NE 102) ont une épaisseur de 0.5 mm, sont rectangulaires

1 cm × 2 cm et placés 1 cm en avant des cristaux épais. Ils sont adaptés à des conduits de lumière de forme conique, eux-memês reliés à deux nouveaux photomultiplicateurs. Les électrons perdent, en traversant ces cristaux minces, environ 130 keV. Ceci a été mesuré par le déplacement de la raie de conversion interne de 624 keV du ^{137}Cs et de la raie de somme de 5.03 MeV provenant du niveau 6.05 MeV de ^{16}O.

La probabilité de détection des rayonnements γ et des neutrons dans ces cristaux minces est très faible. Une coïncidence rapide est faite entre les deux cristaux minces et correspond donc, pour ainsi dire, uniquement à des électrons. Cette coïncidence est alors chargée d'ouvrir une porte située sur l'analyseur à 100 canaux R.I.D.L. utilisé. Le schéma du spectromètre est donné par la figure 2 qui doit être complétée par la figure 1 de la réf. [1]).

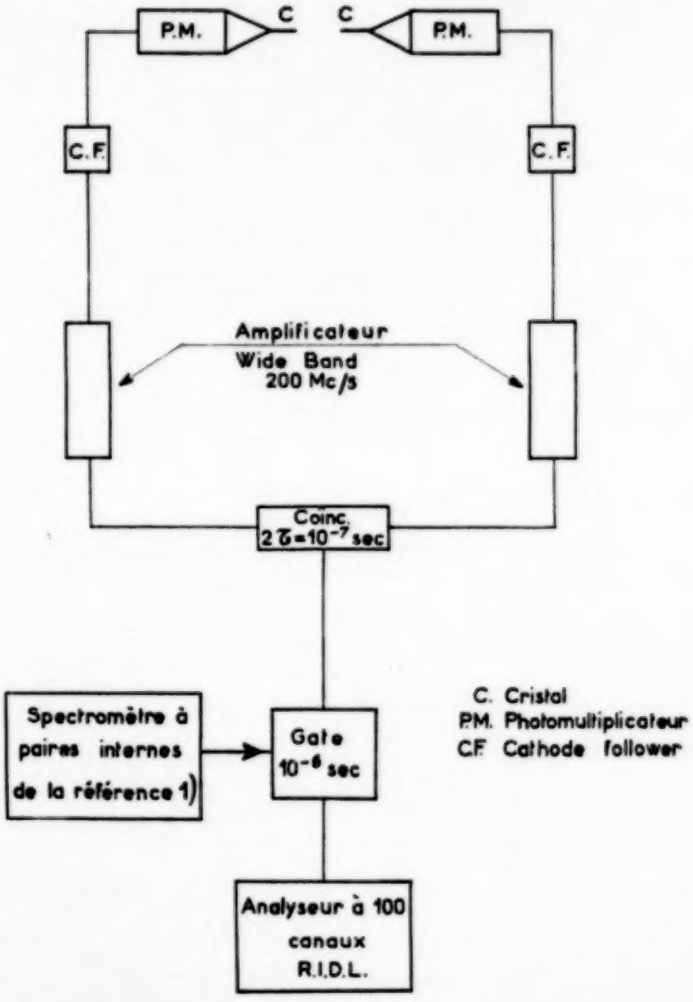

Fig. 2. Schéma du spectromètre à paires internes utilisant des cristaux minces.

Ainsi, l'adjonction de cristaux minces élimine les coïncidences parasites et, cela, en déplaçant seulement de 260 keV le pic de somme des paires des transitions étudiées.

3. Applications

La méthode décrite ci-dessus a d'abord été appliquée aux transitions 5.10 MeV et 4.91 MeV de ^{14}N obtenues par la réaction ^{13}C (d, n)^{14}N à une énergie $E_d = 550$ keV des deutérons incidents. La mesure de l'intensité relative de ces 2 transitions aux spectromètres à paires externes donne:

55 % de 5.10 MeV,
45 % de 4.91 MeV.

La figure 3 montre les courbes théoriques calculées à partir de l'intensité relative mesurée et les points expérimentaux normalisés à l'angle 75°. Le

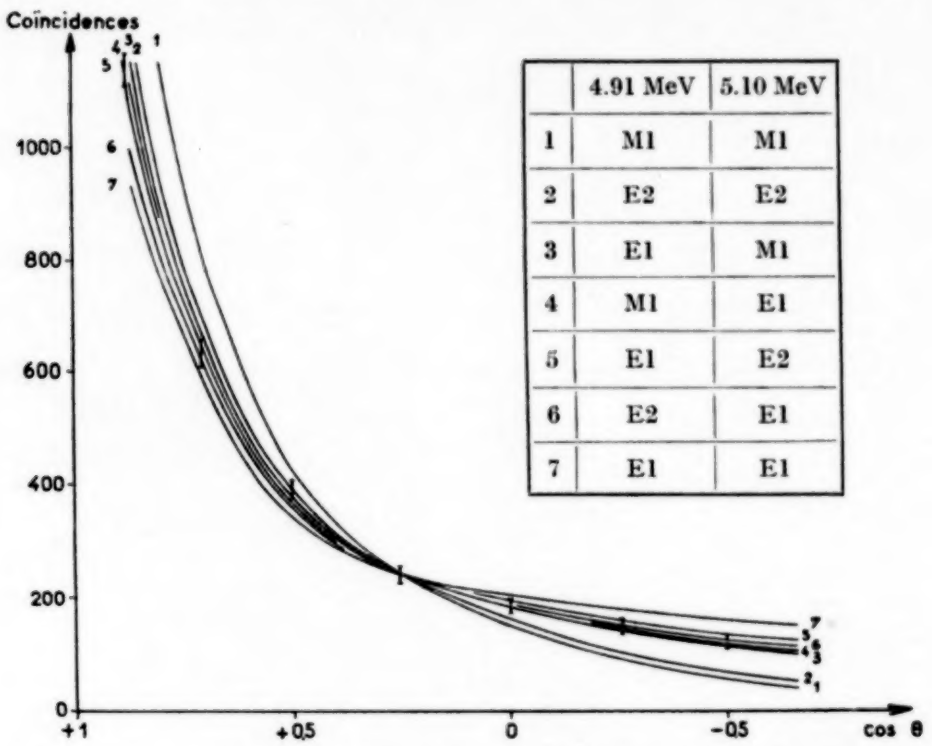

	4.91 MeV	5.10 MeV
1	M1	M1
2	E2	E2
3	E1	M1
4	M1	E1
5	E1	E2
6	E2	E1
7	E1	E1

Fig. 3. Corrélation angulaire des paires de conversion interne des transitions 5.10 MeV et 4.91 MeV de ^{14}N.

résultat indique que l'une des transitions est dipolaire électrique E1 alors que l'autre est dipolaire magnétique M1 ou quadrupolaire électrique E2, sans pouvoir attribuer ces caractères à une transition bien déterminée. Ceci provient de la concentration des courbes théoriques qui est due à l'intensité comparable des deux transitions. Cependant, d'après les résultats mentionnés dans l'article de F. Ajzenberg et T. Lauritsen [3]), on peut en conclure que c'est la transition de 4.91 MeV que a le caractère E1 alors que la transition 5.10 MeV a un caractère M1 ou E2. Ceci est en parfait accord avec l'attribution des moments angulaires $J = 0^-$ pour le niveau 4.91 MeV et $J = 1^+$ pour le niveau 5.10 MeV.

Nous avons, ensuite, appliqué cette méthode aux transitions 3.37 MeV du ^{10}Be, 3.58 MeV du ^{10}B et 2.86 MeV (3.58 MeV—0.72 MeV) du ^{10}B obtenues à partir des réactions ^{9}Be(d, p)^{10}Be et ^{9}Be(d, n)^{10}B à une énergie de bom-

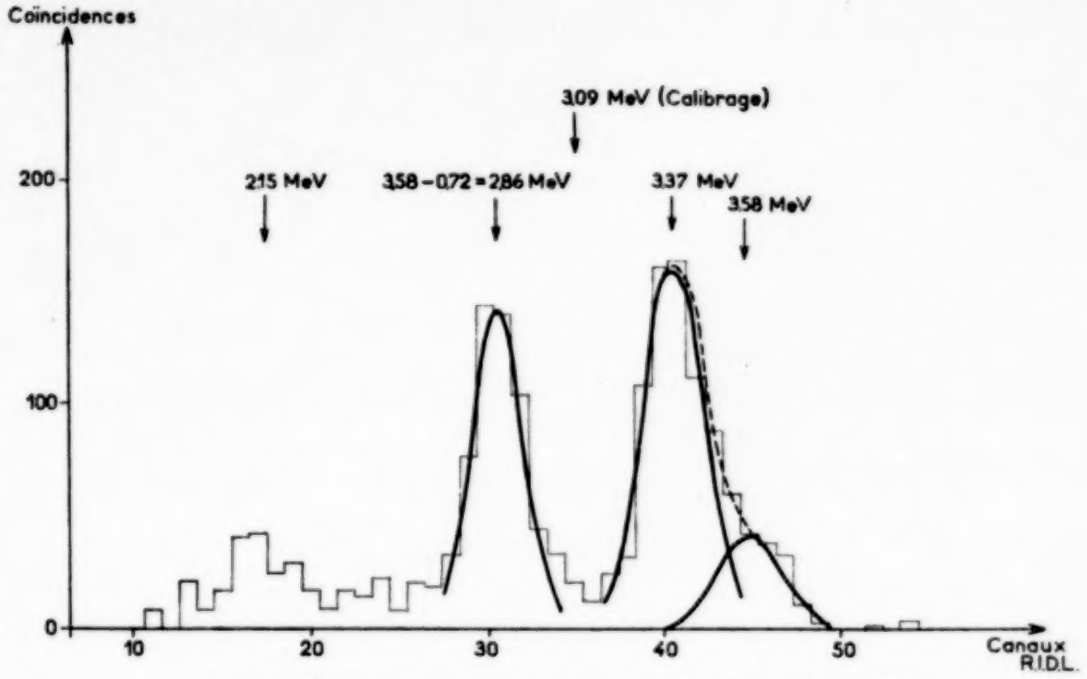

Fig. 4. ^{9}Be+deutérons en spectromètre à paires externes.

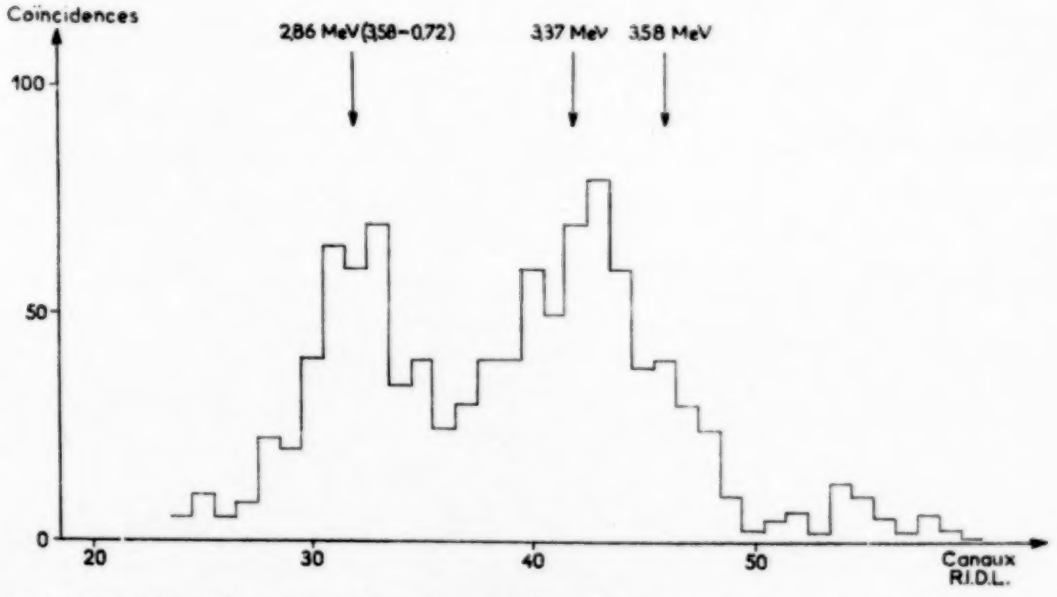

Fig. 5. Raie de somme des paires de conversion interne pour les transitions 3.58 MeV et 2.86 MeV du ^{10}B et 3.37 MeV du ^{10}Be.

bardement $E_d = 500$ keV. La figure 4 montre le spectre obtenu au moyen du spectromètre à paires externes qui nous donne l'intensité relative des

transitions 3.58 MeV et 3.37 MeV:

77.5 % de 3.37 MeV,
22.5 % de 3.58 MeV.

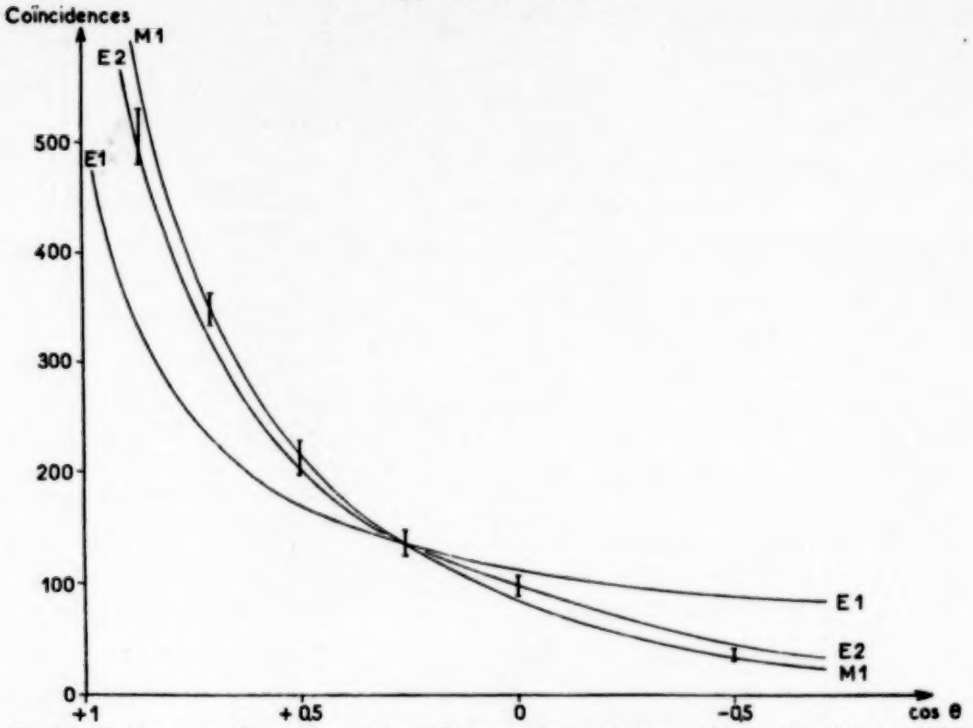

Fig. 6. Corrélation angulaire des paires de conversion interne de la transition 2.86 MeV (3.58 MeV—0.72 MeV) du ^{10}B.

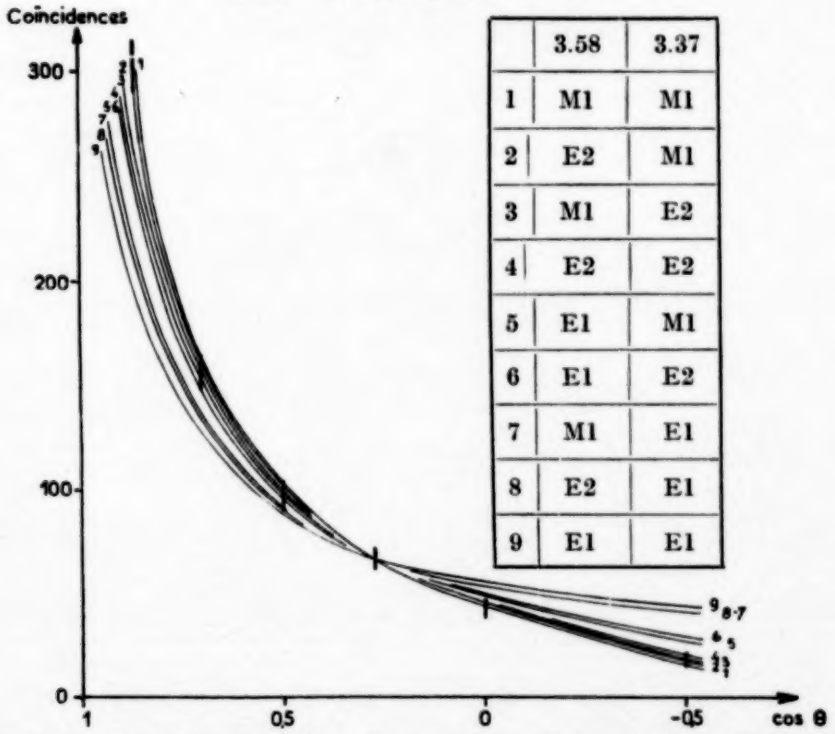

	3.58	3.37
1	M1	M1
2	E2	M1
3	M1	E2
4	E2	E2
5	E1	M1
6	E1	E2
7	M1	E1
8	E2	E1
9	E1	E1

Fig. 7. Corrélation angulaire des paires de conversion interne des transitions 3.58 MeV du ^{10}B et 3.37 MeV du ^{10}Be.

La figure 5 montre les raies de somme des paires de conversion interne. On voit que l'on peut dissocier les paires provenant, d'une part, de la transition 2.86 MeV et, d'autre part, des transitions 3.58 MeV et 3.37 MeV. Les figures 6 et 7 montrent les résultats de la mesure des corrélations angulaires. Elles indiquent que les trois transitions étudiées ont des caractères M1 ou E2. Ces résultats sont en accord avec l'attribution des moments angulaires $J = 2^+$ pour les niveaux 3.37 MeV du ^{10}Be et 3.58 MeV du ^{10}B et $J = 1^+$ pour le niveau 0.72 MeV du ^{10}B.

Nous tenons à remercier le Dr. G. Goldring, du Weizmann Institute of Science, Rehovoth (Israel), pour les conseils qu'il nous a prodigués lors de son séjour au laboratoire.

Bibliographie

1) S. Gorodetzky, P. Chevallier, R. Armbruster, A. Gallmann et G. Sutter, Nuclear Physics **7** (1958) 672
2) S. Gorodetzky, P. Chevallier, R. Armbruster, G. Sutter et A. Gallmann, Nuclear Physics **8** (1958) 412
3) F. Ajzenberg et T. Lauritsen, Revs. Mod. Phys. **27** (1959) 77

1.E.1:
4.E

Nuclear Physics **12** (1959)356—370; © *North-Holland Publishing Co., Amsterdam*
Not to be reproduced by photoprint or microfilm without written permission from the publisher

DECAY OF Pm^{148}

S. K. BHATTACHERJEE and BALDEV SAHAI
Tata Institute of Fundamental Research, Bombay
and
C. V. K. BABA
Atomic Energy Establishment, Trombay

Received 3 April 1959

Abstract: The radiations arising from the activities of Pm^{148} produced by proton bombardment of Nd^{148} (93 % enriched) have been studied mainly by a coincidence scintillation spectrometer. Three gamma rays of 560, 900 and 1460 keV are associated with the 4.2 day activity, while the gamma rays associated with the decay of the 46 day activity are 105, 195, 295, 400, 560, 630, 720, 930, 1015 and 1200 keV, of which 560 and 630 are the most intense and of equal intensity. Beta-gamma and gamma-gamma coincidence experiments show that the main levels in Sm^{148} arising from the negaton decay of the 46-day Pm^{148} are 560, 1190, 1590, 1910, 2120 and 2205 keV, the highest energy beta-group associated with this activity is 2330 keV which goes to the ground state of Sm^{148}. A tentative decay scheme is proposed for the 46 day Pm^{148} activity.

1. Introduction

Promethium-148 is known to decay by negaton-emission to Sm^{148} with a half-life of 5.3 days. Long and Pool [1]) bombarded enriched isotope of Nd^{148} with 6 MeV protons and observed, besides the 5.3 day activity, another activity with a half-life of 48 days, which was found to decay by negaton-emission of 1.7 ± 0.1 and 0.6 ± 0.1 MeV, and a gamma-radiation of about 0.54 MeV as shown by the absorption measurements of the radiation in aluminium and lead. Folger, Stevenson and Seaborg [2]) found an isotope with 42 ± 2 days half-life among products of the high energy fission of uranium. It emitted $\approx$ 2.3 MeV and 0.5 MeV negatons and $\approx$ 1 MeV gamma ray. V. Kistiakowsky Fischer [3]) bombarded 89.85 % enriched $(Nd^{148})_2O_3$ with about 9 MeV protons and observed a 5.3 day, 42 day and a long lived activity in addition to the 161 min half-life isotope previously assigned to Pm^{150}. By aluminium and lead absorption measurements she assigned the following decay modes to the three activities:

5.3 days: $\approx$ 2.3 MeV negaton followed by $\approx$ 1 MeV gamma ray;
42 day: $\approx$ 2.7 MeV negaton and 0.7 MeV negaton followed by two $\approx$ 1.0 MeV gamma rays;
long: $\approx$ 0.2 MeV negaton (identified as the 2.6 y Pm^{147} produced by $Nd^{148}(p, 2n)Pm^{147}$ reaction).

The present investigation was undertaken in order to provide further information on the decay mode of Pm^{148} activities, particularly the 42 day activity. The level structure of the even nucleus Sm^{148} is of special interest since in this region of neutron number (= 86) one expects the level structure predicted by the 'vibrational model' [4,5]) of the nucleus.

2. Experimental Procedure

10 mg of electromagnetically enriched † isotope Nd^{148}, in the form of Nd_2O_3 obtained from the Electromagnetic Separation Group, AERE, Harwell, were irradiated for 5 hours with protons of maximum energy 12 MeV in the Harwell cyclotron. Promethium activity was chemically separated from the Nd-target in an ion exchange column. Two days after the irradiation the experiments were started. The total source strength was a few microcuries, out of which a weak source was prepared for G.M. counter measurements to follow the decay of the activity. The rest of the Pm^{148} activity was deposited on a usual scotch tape backing and covered with another piece of scotch tape. This source was employed for all beta and gamma measurements.

The gamma ray energies and their relative intensities were measured in a 2 in. thick $\times$ $1\frac{3}{4}$ in. diameter NaI(Tl) crystal spectrometer at a source distance of 1 in. The resolution for 662 keV Cs^{137} gamma ray was about 9 %. The rates of decay of the different gamma ray photopeaks were followed for about three months under identical conditions of geometry, gain of the linear amplifier and window width of the pulse height analyser. The energy calibration was checked after each measurement.

The beta spectrum was observed in an anthracene crystal spectrometer, the crystal size being 1 cm thick $\times$ 4 cm diameter. The resolution of the K-conversion line of 662 keV Cs^{137} gamma ray was about 15.5 %. The Compton edges of several monoenergetic gamma rays and the highest energy negaton group of Eu^{154}(1880 keV) were employed for the energy calibration of this spectrometer.

A conventional fast-slow scintillation spectrometer with a resolving time of $2\tau = 20$ ns was employed for coincidence measurements. During some studies of the long-lived activity a slow coincidence circuit of about 2μs resolving time was made use of. In gamma-gamma coincidences both the NaI(Tl) crystals were of the same size (2 in. thick $\times$ $1\frac{3}{4}$ in. diameter), the source was usually placed right on the top of the crystal with sufficient Al

† Information supplied by the Electromagnetic Separation Group, Harwell about the Nd-isotopes is as follows:
Mass analysis: 142 (0.85 %), 143 (0.55 %), 144 (1.11 %), 145 (0.68 %), 146 (2.32 %), 148 (93.0 %), 150 (1.52 %).
Spectro-chemical analysis: Nd (0.2 %), Li (0.02 %), Mg (0.004 %).

absorber in between to stop the negatons. In all beta-gamma coincidences, the gamma-gamma background was determined by putting about 1.3 g/cm² Al absorber between the source and the anthracene crystal. In the figures showing beta-gamma coincidences, only the genuine beta-gamma coincidences are plotted.

3. Results

3.1. HALF-LIVES OF THE Pm^{148} ACTIVITIES

For the identification of the activities the decay of a part of the total source was followed in an end-window (window thickness ≈ 0.8 mg/cm²)

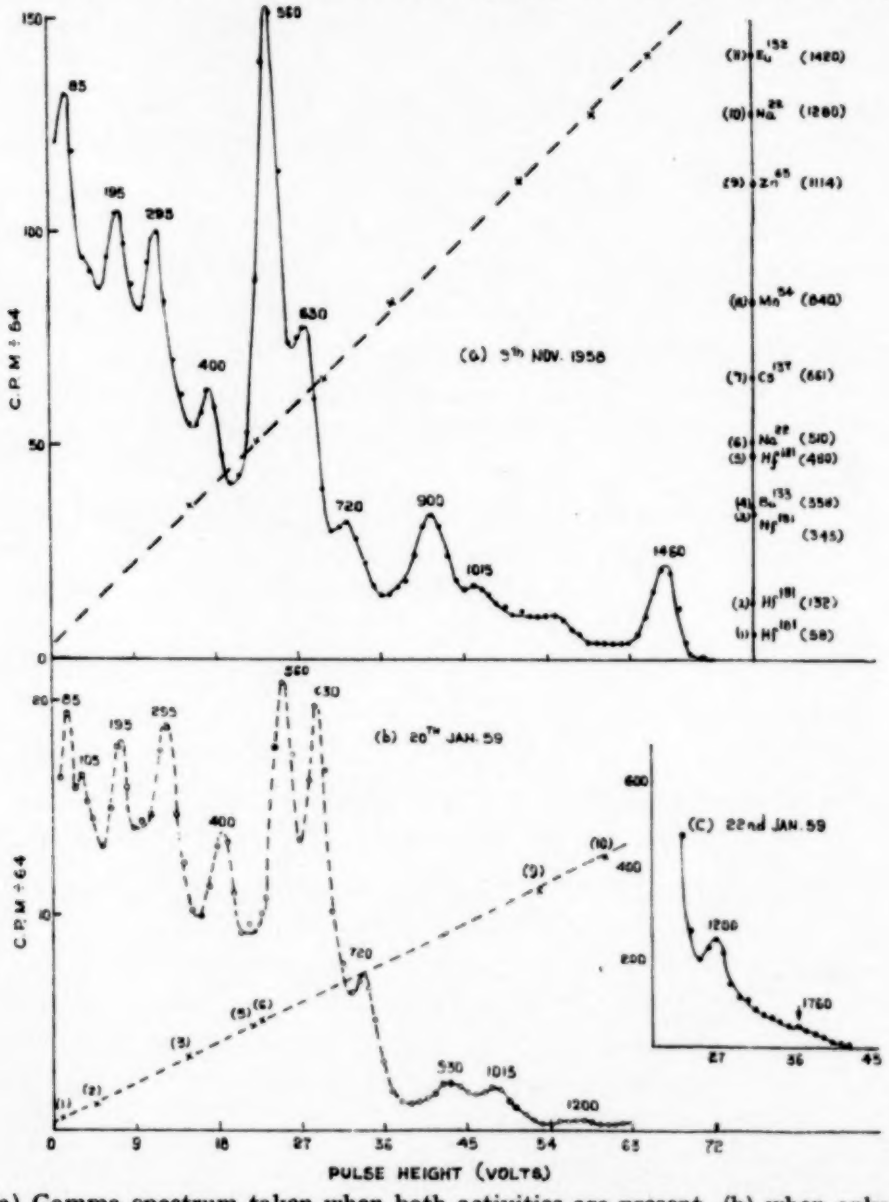

Fig. 1 (a) Gamma spectrum taken when both activities are present, (b) when only 46 day activity is present and (c) the spectrum taken in a lower gain to see the high energy gamma rays. In the first two spectra source to crystal distance was 1" whereas in the third spectrum it was placed right on top of the crystal with only 1.4 g/cm² perspex absorber in between.

G.M. counter over a period of about 70 days. The decay curve was resolved into 4.2 ± 0.2 days and 45.8 ± 2.9 days half-life components. The half-life for the short-lived activity as determined here shows a little lower value than reported earlier.

3.2. GAMMA RAYS ASSOCIATED WITH THE ACTIVITIES

Fig. 1(a) shows the gamma-ray spectrum generated in the NaI(Tl) crystal spectrometer four days after irradiation. The energy calibration is shown. Fig. 1(b) shows the gamma spectrum belonging presumably to the 46 day activity. The inset fig. 1(c) shows the weak highest energy gamma ray of 1760 keV belonging to this activity. The decay of each of the photopeaks was followed and on that basis the gamma rays have been assigned to the two activities. The only prominent gamma rays belonging to the 4.2 day activity are 560, 900 and 1460 keV. Thus it is evident that 560 keV gamma ray is

TABLE 1

Gamma ray energies and their relative intensities

Gamma-energy (in keV)	Relative Intensity †
46 day activity	
85	≈4
105	≈4
195	11 ††
295	20
400	20
560	100
630	100
720	30
930	23
1015	25
1200	≈3
1760	<1
4.2 day activity	
560	60
900	40
1460	100

† Above 400 keV the intensity measurements are believed to be correct to 20 %. Low energy intensity measurements have larger errors.

†† No correction has been made for the contribution of back scattered peaks due to high energy gamma rays.

common to both the activities. Table 1 summarizes the different gamma ray energies associated with each activity and their relative intensities.

3.3. GAMMA-GAMMA COINCIDENCES

Fig. 2(a) shows a portion of the gamma spectrum in coincidence with the 560 keV photopeak, when the 4.2 day activity was present. No appreciable

coincidences with 1460 keV gamma ray were noticed while there is a strong coincidence peak at 900 keV showing that in the short lived activity the two gamma rays of 560 keV and 900 keV are in cascade and 1460 keV is most likely the cross-over transition. However, in fig. 2(b), where the short lived activity is absent, one still observes coincidences around 930 keV corresponding to a gamma ray belonging to the 46 day activity. Fig. 2(b) also shows

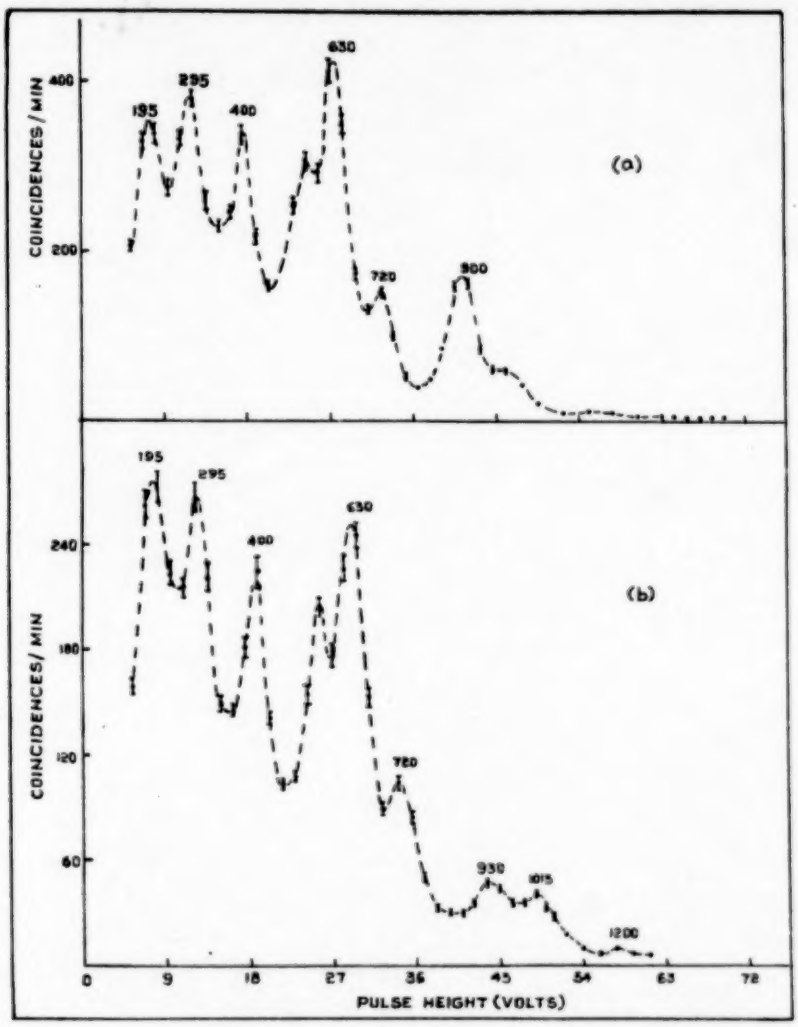

Fig. 2. (a) and (b) show the gamma spectrum in coincidence with 560 keV photopeak (a) is taken when both the activities are present and (b) when only 46 day activity is there.

that the 560 keV gamma ray is strongly in coincidence with 630 keV photopeak in the 46 day activity. In fact the 560 keV gamma ray seems to be in coincidence with almost all the prominent gamma rays. Similarly the 630 keV gamma ray has been found to be in coincidence with the entire gamma spectrum in the 46 day activity (fig. 3 (a)). This fact suggests that the 560 keV and 630 keV gamma rays are arising from the de-excitation of the 1st

and 2nd excited states in Sm^{148} and most of the other gamma rays are terminating at or above the 1190 keV level in Sm^{148}; further the equality of the intensities of these two gamma rays shows that the 560 keV level in Sm^{148} is not appreciably fed by negatons. This fact will be further supported by beta-gamma coincidence experiments.

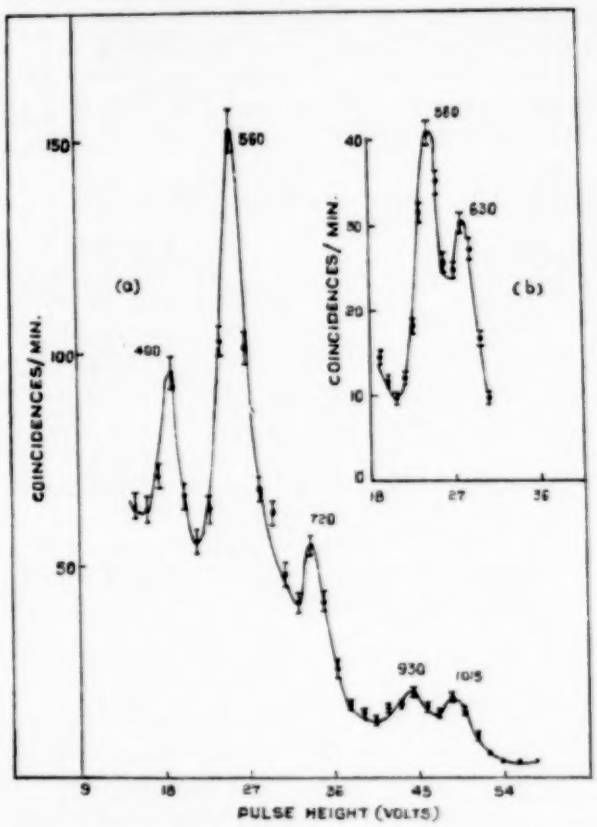

Fig. 3. (a) The gamma spectrum in coincidence with 630 keV gamma ray, (b) gamma spectrum in coincidence with 930 keV photopeak. Both the spectra were taken when only 46 day activity was present.

Fig. 3(b) shows that the 560 keV and 630 keV gamma rays are fully in cascade with the 930 keV gamma ray; this triple cascade giving rise to a level at 2120 keV in Sm^{148}. The details of gamma-gamma coincidence results are summarized in table 2.

3.4. ENERGIES AND ESTIMATE OF RELATIVE INTENSITIES OF THE BETA-RAY GROUPS IN 46 DAY ACTIVITY

Fig. 4A(a) shows the negaton spectrum as generated in the anthracene crystal spectrometer when the short lived activity was present. Fig. 4B(a) shows the spectrum when the short lived activity completely died away. Within the accuracy of measurements both these spectra appear to have the same highest energy point at about 2300 keV. Even though the source was not ideal at all for magnetic spectrometer measurements, two runs in the

Intermediate Image Spectrometer were made, one with the 4.2 day activity present and one a month later when the short lived activity had almost completely died away. The highest energy beta groups in both these spectra appear to have very nearly the same energy 2330 ± 60 keV which agrees well

TABLE 2

Summary of gamma-gamma coincidence experiments

Gating photopeaks (energies in keV)	Coincident radiations (energies in keV)	Remarks
	a. Both activities present	
295	195, 400, 560, 630, 720	No appreciable coincidences above 720 keV gamma energy. The coincidences at ≈ 400 keV may be due to the Compton edges of 560 or 630 keV gamma rays.
400	195, 295, ≈ 400, 560 630, ≈ 900	The weak coincidences observed at ≈ 400 and ≈ 900 keV are most probably due to coincidences of these gamma rays with the Compton-scattered edge of 560 keV gamma ray accepted in gating channel.
560	195, 295, 400, 560, 630 720, 900	The hump around 560 keV is most likely due to the fact that when 560 keV gamma ray is accepted in gate, a portion of 630 keV photopeak is also accepted in the gate.
900	295, ≈ 400, 560	A slight hump at 400 keV seems to be due to the coincidence with the Compton edge of 560 keV gamma ray.
	b. Only 46 day activity present	
560	195, 400, 560, 630, 720 930, 1015, 1200	The hump at 560 keV can probably be explained as above.
630	195, 400, 560, 720, 930 1015	Since 1015 keV gamma ray comes in coincidence with both the 560 and 630 keV photopeaks, this points to the triple cascade 560—630—1015, establishing the highest level in Sm^{148} at 2205 keV.
930	560, 630	This experiment clearly establishes a level at 2120 keV.

with the anthracene spectrometer measurements. However, it has been observed in the anthracene crystal spectrometer that the number of negatons above ≈ 1800 keV appear to decay faster than the longer lived activity i.e. 46 day. There is indeed a beta group ≈ 1900 keV which appears in coincidence with 560 keV gamma ray in the 4.2 day activity (see fig. 4A (b)). Because of poor resolution and poor statistics of our measurements of the

beta spectrum, it is difficult to say definitely which highest energy beta group is associated with the 4.2 day activity.

In order to ascertain the energies of the inner beta-groups and to estimate roughly the relative intensities of the 46 day activity a Kurie plot of the

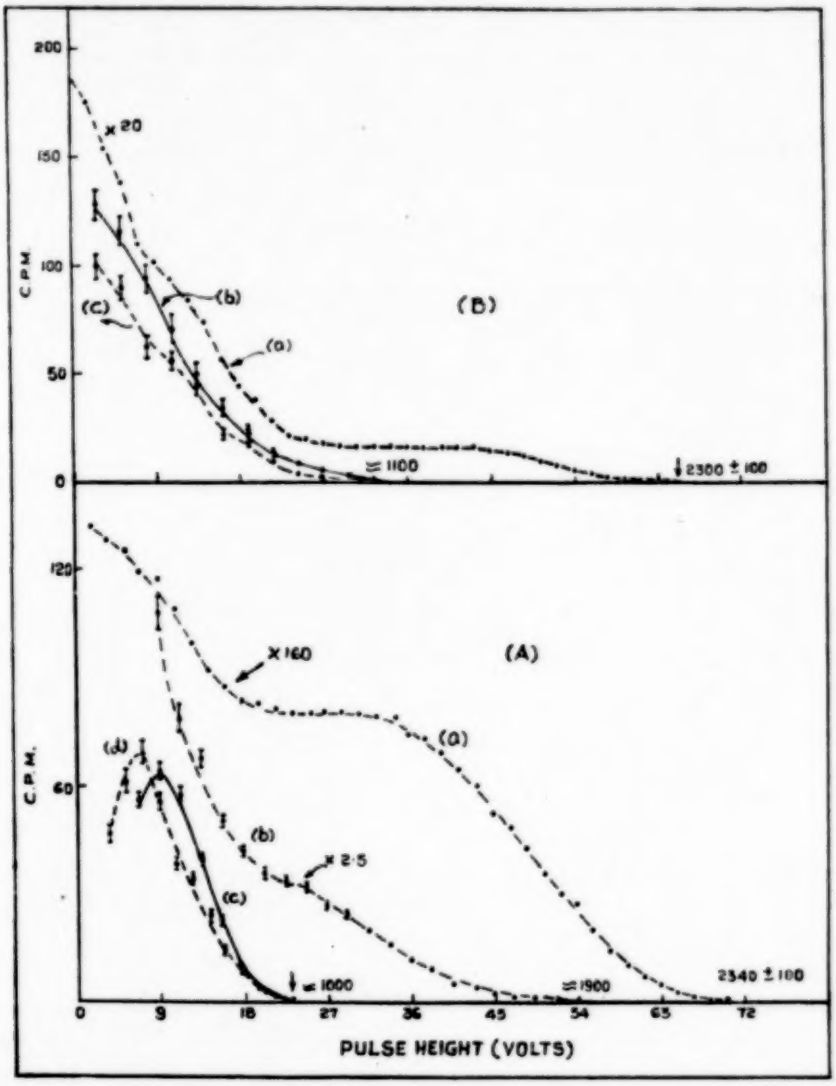

Fig. 4. A (a) The beta spectrum in anthracene crystal spectrometer when both the activities are present. A (b), A (c) and A (d) show the beta spectrum in coincidence with 560, 1460 and 900 keV photopeaks respectively at that time. Fig. 4B (a) shows the beta spectrum in anthracene crystal spectrometer when 46 day activity alone is present. B(b) and B(c) show the beta spectrum in coincidence with 560 and 630 keV photopeaks. The energies are quoted on the basis of calibration taken at the time each experiment was performed.

magnetic spectrometer data was effected. A similar plot of the anthracene crystal spectrometer data after correcting for resolution and gamma background was also made. The highest energy beta group shows a non-linear shape in both of them. Fig. 5(a) and 5(b) show the results.

Three beta groups of energies approximately at 400, 770 and 2300 keV are clearly seen in both these spectra. From the partial Kurie plots the intensities of the various groups were estimated. Table 3 summarises the results. In view of the uncertainties introduced in the intensity measure-

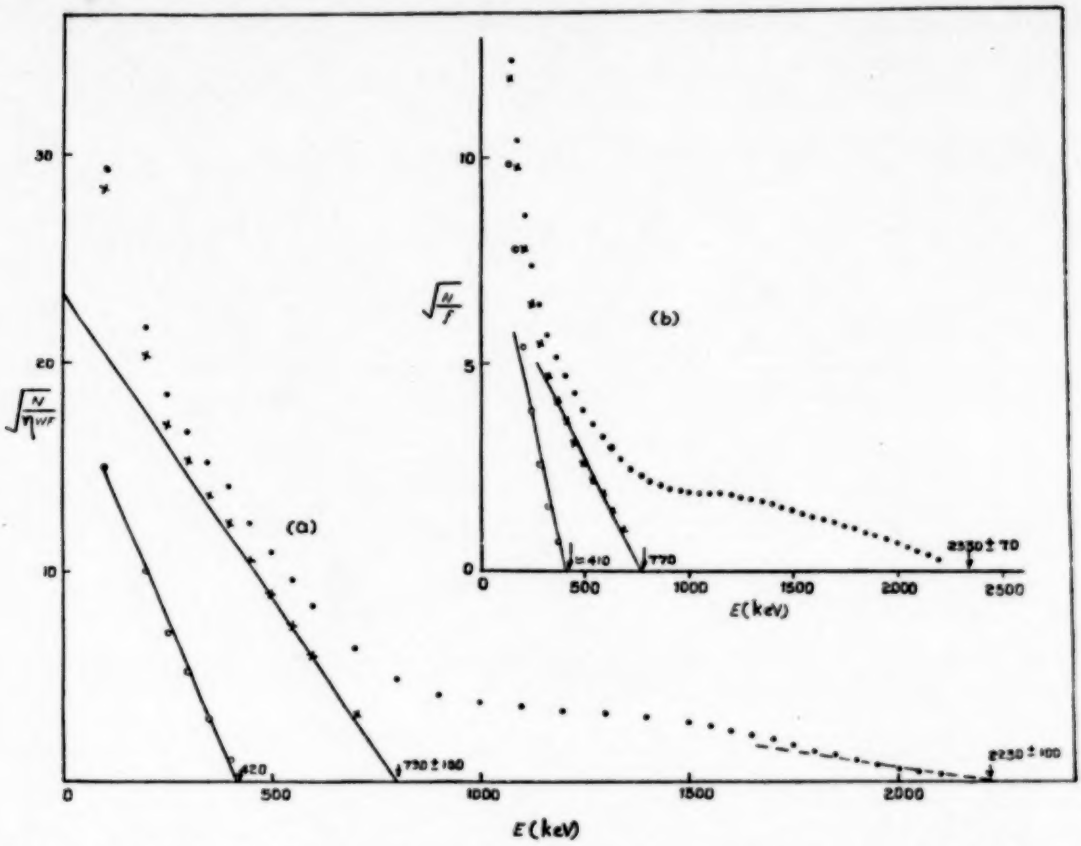

Fig. 5. (a) Kurie plot of the spectrum taken in anthracene crystal spectrometer (b) Kurie plot of the spectrum taken in magnetic spectrometer.

TABLE 3

Energies and estimates of the relative intensities of main beta groups in 46 day activity

Maximum energy of beta group in keV	Relative intensities	
	Magnetic spectrometer	Anthracene spectrometer
400	18	12
770	30	50
2330	52	38

ments owing to the non-linear shape of the highest energy beta group and also to the weak activity and poor backing of the source, it is felt that the estimates of the relative intensities of the three main beta groups in the 46 day activity by the two independent measurements is gratifying. Mean

values of these two intensity measurements have been used in calculating the transition probabilities of the different beta transitions in the 46 day Pm^{148}.

3.5. BETA-GAMMA COINCIDENCES

Fig. 6(a) shows the gamma spectrum in coincidence with a band of negatons of energy between 620 and 700 keV accepted in the gating channel when the 4.2 day activity is present. The most prominent gamma rays associated with this activity are clearly seen to be 1460, 900 and 560 keV. Fig. 6(b) shows the 560, 630 and 720 keV gamma rays in coincidence with a

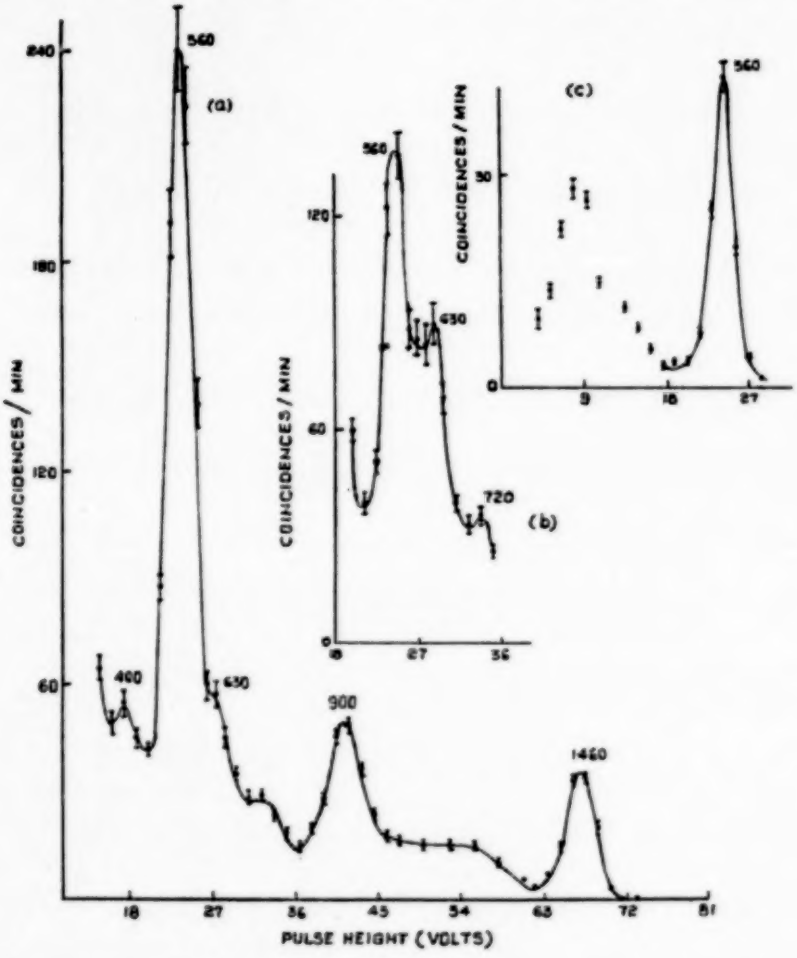

Fig. 6. (a), (b) and (c) show the gamma spectrum in coincidence with (620—700) keV beta rays, (340—420) keV beta rays and (1250—1400) keV beta rays respectively when both the activities were present.

lower energy beta band of 340—420 keV. Fig. 6(c) shows that the only gamma ray that is in coincidence with negatons of energy above 1250 keV is the 560 keV one, which shows that this is the gamma ray associated with the de-excitation of the first excited state in Sm^{148} in the short lived activity. The highest energy beta group found in coincidence with the 560 keV photo-

peak is of the order of 1900 keV (fig. 4a(b)) in 4.2 day activity whereas both the 900 and 1460 keV gamma rays (fig. 4A(c) and (d)) have a coincidence beta spectrum terminating at about 1000 keV. This fact coupled with the gamma-gamma coincidence results mentioned earlier suggests that the 560 and 900 keV gamma rays form a cascade and the 1460 keV gamma ray is the cross-over transition.

After the short lived activity has completely died down both 560 and 630 keV gamma rays show a coincident beta spectrum terminating around 1100 keV (fig. 4B(b) and (c)), a fact which suggests that the 2330 keV beta group in 46 day activity goes directly to the ground state of Sm^{148}. These points were further verified by carrying experiments where beta rays of energy higher than 1300 keV and higher than 500 and 850 keV were accepted in gate. In the first experiment no appreciable coincidences with any gamma ray were observed. In the latter experiments the 560 and 630 keV gamma rays were found to be in coincidence. This suggests that most of the other gamma rays are most likely arising from the de-excitation of levels fed by lower energy negatons. The details of the beta-gamma coincidence results are summarised in table 4.

4. Discussion of the Possible Decay Schemes of Pm^{148} Activities

Fischer [3]) mentioned that the 46 day activity might be an isomer of Pm^{147} produced by $Nd^{148}(p, 2n)Pm^{147}$ reaction. The 2.6y Pm^{147} decays predominantly by a single beta group of 227 keV energy to the ground state of Sm^{147}. The decay energy of the 46 day activity observed here is 2330 keV; hence if this activity is to be an isomer of Pm^{147}, the energy difference between the ground state and the isomeric state of Pm^{147} must be above 2 MeV. Even a spin change $\Delta I > 7$ will not explain the existance of the 46 day half-life for the isomer; further such a large spin change is very unlikely for the odd proton isotope. Hence one concludes that both the 4.2 day and 46 day activities are most likely isomers belonging to Pm^{148}, a conclusion reached earlier by Long and Pool [1]) by measuring the relative yields of the two activities as a function of isotopic abundance of Nd^{148} target isotope. Moreover, Heydenburg and Temmer [6]) did not observe any gamma ray associated with the Coulomb excitation of the enriched Sm^{147} isotope, whereas they, as well as Mark and Paulissen [7]), did observe the 1st excited state at 560 keV in the Coulomb excitation of Sm^{148}. Among others, Mack, Neuer and Pool [8]) observed a gamma ray of 560 keV in the electron capture decay of Eu^{148}. Folger, Stevenson and Seaborg [2]) also observed this gamma ray in the 46 day activity. Thus the observation of this gamma ray in both the activities lends further support to the conclusion that both the activities do belong to Pm^{148}.

TABLE 4

Summary of beta-gamma coincidences

Gating radiation	Coincident radiations (energies in keV)	Remarks
	a. Both activities present	
(620—700) keV negatons	195, 400, 560, 630, ≈ 700, 900, 1460	The weak coincidence hump around 700 keV is most probably due to the coincidences with the Compton edge of 900 keV gamma ray.
(340—420) keV negatons	560, 630, 720	This shows that 720 keV gamma ray is fed by beta particles of energy below 600 keV but higher than 340.
(1250—1400) keV negatons	≈ 180, 560	The coincidences around 180 keV are most likely due to coincidences with the back scattered peak of 560 keV gamma ray. The experiment shows the presence of a beta group of energy higher than 1250 keV which goes to 560 keV level in Sm^{148} in short lived activity, since no such coincidences are observed when this activity dies down.
560 keV photopeak	Maximum beta end point at ≈ 1900 keV	The trend of the curve shows the presence of a group around 1000 keV also.
900 keV photopeak	Maximum beta end point at about 1000 keV	These two experiments show that in short lived activity 1460 keV level de-excites directly as well as through the cascade 900 keV—560 keV.
1460 keV photopeak	Maximum beta end point at about 1000 keV	
	b. Only 46 day activity present	
Negatons of energy higher than 500 keV	195, 560, 630	Strong coincidences around 195 keV suggest that the corresponding gamma ray is most likely fed by negatons of energy higher than 500 keV.
Negatons of energy higher than 850 keV	560, 630	These two experiments suggest that highest energy beta group feeding any levels in Sm^{148} lies between 850 and 1300 keV. This fact is confirmed by reverse experiments stated below.
Negatons of energy higher than 1300 keV	No coincidences at all	
560 keV photopeak	≈ 1100 keV	These two experiments confirm that 560 and 630 keV gamma rays are in cascade and 1190 keV level is fed by beta particles of energy about 1100 keV. This confirms our earlier conclusion that 930 keV gamma ray is arising from 2120 keV level in Sm^{148} fed by low energy beta group.
630 keV photopeak	≈ 1100 keV	
930 keV photopeak	No coincidences with beta energies higher than 250 keV	

Mainly on the basis of our high energy gamma-gamma and beta-gamma coincidence results, gamma ray energy fits and intensity considerations, a tentative decay scheme for the 46 day activity of Pm^{148} is proposed in fig. 7. The main features of the decay mode of the 4.2 day isomer as observed in this experiment are also shown in the figure. The different gamma rays are assigned to the two activities on the basis of their decay periods.

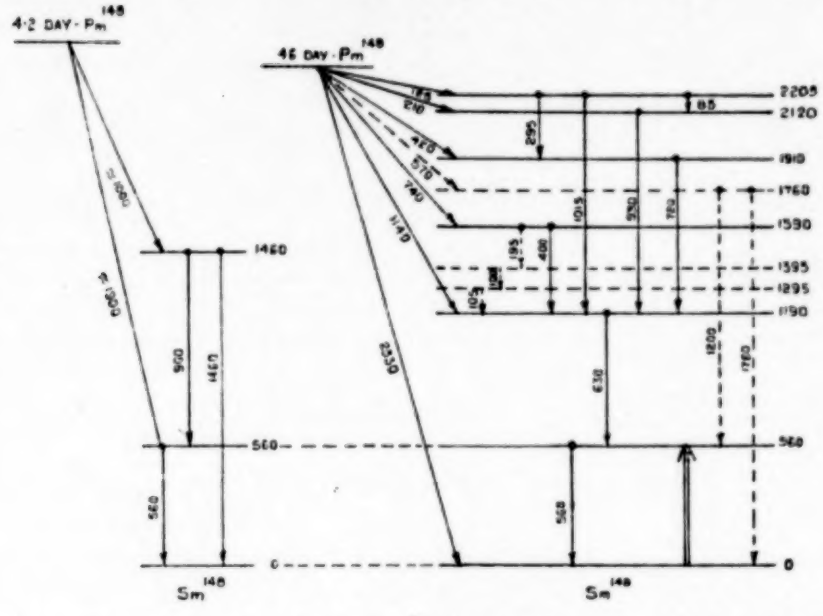

Fig. 7. Tentative decay scheme of Pm^{148}-activities. Energies are in keV.

The main nuclear levels in Sm^{148} reached by the negaton emission of 46 day Pm^{148} are seen to be located at 560, 1190, 1590, 1910, 2120 and 2205 keV. The existence of the levels and radiations shown by dotted lines must be regarded as uncertain. The level at 1460 keV in Sm^{148} is seen to be reached only by negaton emission of 4.2 day isomer of Pm^{148}, the state decaying by the emission of 900 keV—560 keV cascade and a strong cross-over transition of 1460 keV to the ground state of Sm^{148}.

The intensities of the two gamma rays of 560 and 630 keV in the 46 day activity are almost equal and both show coincidences with a beta group terminating at about 1100 keV. Hence the 560 keV level is most likely not fed directly by any beta group in appreciable intensity. All the other prominent gamma rays seem to terminate at the 1190 keV level; sum of the intensities of 400, 720, 930 and 1015 keV gamma rays agrees very well with the total intensity of 630 keV gamma ray.

The Kurie plots of the beta spectrum in the magnetic spectrometer and also in the anthracene crystal spectrometer enable us to estimate roughly the relative intensities of the three groups resolved i.e. 2330, 770 and 420 keV (fig. 5). It may be pointed out that the highest energy beta group shows a non-linear shape in both spectra; however, since the backing and

strength of the source were not ideal for any accurate beta-spectrum measurements, this result should not be regarded very seriously. Nevertheless, the energies of beta groups agree in the two measurements and show a very good agreement with the decay scheme proposed for 46 day activity. The branching ratios of the various other beta groups were found from the gamma ray intensities, neglecting conversion of low energy gamma rays. Estimates of the beta transition probabilities to the various levels in Sm^{148} were than made and summarized in table 5. The log *ft*-value of the 1140 keV

TABLE 5

Estimates of transition probabilities of the beta-transitions in 46 day Pm^{148}

Maximum energy of the beta group in keV	Abundance	log *ft*
125	33	5.8
210	14	7.0
420	9	7.4
740	20	8.5
1140	≈4	9.5
2330	20	10.4

beta group which shows up in coincidence with both 560 and 630 keV gamma rays was estimated by assuming a 10 % branching ratio.

The ratio of energies of the second to the first excited state in Sm^{148} is very closely 2, a value which is predicted by the simple 'vibrational model'[4,5] — a model which predicts level structure in the region of neutron numbers $N \leqq 88$ in even nuclei. These levels presumably arise from the quadrupole vibrations of a spherical nucleus [5]. However, in order to analyse the details of the level structure of Sm^{148} on the basis of this model, knowledge of the spin and parities of the different levels is necessary.

Thanks are due to Mr Shree Raman and Mr S. V. Godbole for their ungrundging help during the progress of this work. Thanks are also due to Mr M. C. Joshi for the help with magnetic spectrometer measurements.

Note added in proof: After about five half lives of the long lived activity (46 days) of Pm^{148}, the gamma spectrum of the source revealed the presence of a gamma ray at 475 keV. The low energy portion up to 200 keV and the region around 600—700 keV appeared to be following a half life longer than 46 days. In coincidence with K X-rays, gamma rays of energy ≈ 100, 200, 475, 600 and 700 keV were observed. On the other hand 475, 600 and 700 keV gamma rays were not found to be in coincidence with beta rays of energy ≈ 500 keV whereas the rest of the coincidence gamma spectrum showed the same features as reported in the main text. This longer lived activity may be

attributed to the presence of the electron capture isotope Pm^{144} (half life = 300 days) which has recently been studied by S. Ofer (Phys. Rev. **113** (1959) 895) and in which he has found these three gamma rays.

References

1) J. K. Long and M. L. Pool, Phys. Rev. **85** (1952) 137
2) R. L. Folger, P. C. Stevenson and G. T. Seaborg, UCRL-1195, revised (May 1951) (unpublished)
3) V. Kistiakowsky Fischer, UCRL-1629 (Jan. 1952) (unpublished); Phys. Rev. **87** (1952) 859
4) G. Scharff-Goldhaber and J. Weneser, Phys. Rev. **98** (1955) 212;
G. Scharff-Goldhaber, Proc. Pittsburgh Conference (June 1957)
5) K. Alder, A. Bohr, T. Huus, B. Mottelson and A. Winther, Revs. Mod. Phys. **28** (1956) 523
6) N. P. Heydenburgh and G. M. Temmer, Phys. Rev. **100** (1955) 150
7) H. Mark and G. Paulissen, Phys. Rev. **100** (1955) 813
8) R. C. Mack, J. J. Neuer and M. L. Pool, Phys. Rev. **91** (1953) 497 A

7.A *Nuclear Physics* **12** (1959) 371—388; © *North-Holland Publishing Co., Amsterdam*
Not to be reproduced by photoprint or microfilm without written permission from the publisher

ANALYTIC PROPERTIES OF THE SCHRÖDINGER AMPLITUDE AT A FIXED ANGLE

J. BOWCOCK and D. WALECKA †
Theoretical Study Division, CERN, Geneva

Received 20 April 1959

Abstract: The scattering from a given class of potentials including exchange forces is considered. For a fixed angle the scattering amplitude can be analytically continued into the complex energy plane with the exception of the usual cut along the positive real axis and certain poles and cuts on the negative real axis depending on the nature of the potential. Our results are a partial confirmation of the fixed angle dispersion relations recently proposed within the framework of field theory [5]).

1. Introduction

The study of the analytic properties of the scattering amplitude for a potential presents an interesting complement to the corresponding studies being carried out in field theory and recently this problem has been looked at in detail. Khuri [1]) has shown that dispersion relations for fixed momentum transfer exist for a very general class of central potentials, the upper limit on the momentum transfer depending on the rate of decrease of the potential at infinity. Jost [2]) has shown that the Lehmann ellipses are also free from singularities in potential theory, i.e. if one investigates the analytic behaviour in the momentum transfer for fixed energies, there are certain regions free of singularities. Hamilton [3]) has recently extended Khuri's results to include tensor forces and at the same time has indicated the difficulties encountered in trying to include exchange forces.

What one would like is to be able to give the analytic properties of the scattering amplitude in all the variables and perhaps combine the results into a relation similar to the one proposed by Mandelstam [4]). In this paper we attempt something far less ambitious. We investigate the analytic properties of the scattering amplitude in the complex energy plane, while keeping the angle of scattering fixed at some physical value, for the class of potentials which may be written in the form ††

$$V(r) = \int_{\mu}^{\infty} \rho_{\mathrm{D}}(\sigma) \frac{\mathrm{e}^{-\sigma r}}{r} \, \mathrm{d}\sigma + P_{\mathrm{M}} \int_{\mu}^{\infty} \rho_{\mathrm{E}}(\sigma) \frac{\mathrm{e}^{-\sigma r}}{r} \, \mathrm{d}\sigma \qquad (1.1)$$

† National Science Foundation Postdoctoral Fellow.
†† Potentials of finite range do not belong to this class.

with

$$\int_{\mu}^{\infty} [|\rho_{\mathrm{D}}(\sigma)|+|\rho_{\mathrm{E}}(\sigma)|]\,\mathrm{d}\sigma < \mu. \tag{1.2}$$

Here P_{M} is the Majorana exchange operator. The second condition implies that there are no bound states and allows one to use the Born series as a solution to the Schrödinger equation. (This is no great restriction since it is probably true that what holds for the Born series holds for Fredholm theory, the only difference being the poles appearing on the negative energy axis from the bound states in the latter.)

The investigation is carried out in four steps. First we study the scattering from a simple Yukawa potential

$$V(r) = \lambda \frac{\mathrm{e}^{-\mu r}}{r}, \tag{1.3}$$

$$|\lambda| < \mu. \tag{1.4}$$

We shall show that the scattering amplitude may be extended analytically from the real energy axis to any finite point in the complex energy plane with a cut from 0 to ∞, a pole at † $k^2 = -\mu^2/4 \sin^2\frac{1}{2}\theta$ and another cut from $k^2 = -\mu^2/\sin^2\frac{1}{2}\theta$ to $-\infty$.

The next step is to introduce an exchange potential, writing

$$V(r) = \lambda_{\mathrm{D}} \frac{\mathrm{e}^{-\mu r}}{r} + \lambda_{\mathrm{E}} \frac{\mathrm{e}^{-\mu r}}{r} P_{\mathrm{M}}, \tag{1.5}$$

$$|\lambda_{\mathrm{D}}|+|\lambda_{\mathrm{E}}| < \mu. \tag{1.6}$$

With this potential we find the same analytic properties, except that we now have two poles, one at $k^2 = -\mu^2/4 \sin^2\frac{1}{2}\theta$ and one at $k^2 = -\mu^2/4 \cos^2\frac{1}{2}\theta$ and the cut on the negative axis starts at

$$k^2 = -\mu^2 \min\left(\frac{1}{\sin^2\frac{1}{2}\theta}, \quad \frac{1}{\cos^2\frac{1}{2}\theta}\right).$$

The final steps consist of generalizing the potential, initially to

$$V(r) = \int_{\mu}^{\infty} \rho_{\mathrm{D}}(\sigma) \frac{\mathrm{e}^{-\sigma r}}{r}\,\mathrm{d}\sigma \tag{1.7}$$

and afterwards to the form (1.1). In this case the singularities along the negative axis depend upon the form of the $\rho(\sigma)$'s, the analytic properties elsewhere remaining unchanged. However, in no case is there a singularity on the negative real axis between 0 and $-\frac{1}{4}\mu^2 \min(1/\sin^2\frac{1}{2}\theta,\ 1/\cos^2\frac{1}{2}\theta)$.

† We take $\hbar = 2M_{\mathrm{r}} = 1$, where M_{r} is the reduced mass of the two body system, therefore $k^2 = E$. We denote the angle of scattering by θ.

2. Equations for the Scattering Amplitude

We start from the Schrödinger equation

$$\left(\nabla^2+k^2-\lambda\frac{e^{-\mu r}}{r}\right)\psi=0 \tag{2.1}$$

and write it as an integral equation with the Green's function containing the boundary condition of outgoing waves at infinity:

$$\psi(\mathbf{x})=e^{i\mathbf{k}\cdot\mathbf{x}}-\lambda\int G(\mathbf{x},\mathbf{y})\frac{e^{-\mu y}}{y}\psi(\mathbf{y})d\mathbf{y}, \tag{2.2}$$

$$G(\mathbf{x},\mathbf{y})=\lim_{\varepsilon\to 0}\frac{1}{(2\pi)^3}\int\frac{d\mathbf{q}e^{i\mathbf{q}\cdot(\mathbf{x}-\mathbf{y})}}{q^2-k^2-i\varepsilon}=\frac{1}{4\pi}\frac{e^{ik|\mathbf{x}-\mathbf{y}|}}{|\mathbf{x}-\mathbf{y}|}. \tag{2.3}$$

The scattering amplitude is then

$$f(k,\theta)=-\frac{\lambda}{4\pi}\int e^{-i\mathbf{k}'\cdot\mathbf{y}}\frac{e^{-\mu y}}{y}\psi(\mathbf{y})d\mathbf{y}, \tag{2.4}$$

where $\mathbf{k}'$ is the outgoing momentum. Since we are only interested in elastic scattering we have $\mathbf{k}'=k\hat{\mathbf{n}}_{k'}$ where $\hat{\mathbf{n}}_{k'}$ is a unit vector in the direction of scattering.

The integral equation for $\psi(\mathbf{x})$ can now be iterated and when put into the expression for $f(k,\theta)$ (2.4) we get the Born series [5]). The result is

$$f(k,\theta)=\frac{-\lambda}{4\pi}\left[\frac{4\pi}{\mu^2+(\mathbf{k}'-\mathbf{k})^2}+\sum_{n=1}^{\infty}\lambda^n f_n\right]. \tag{2.5}$$

The first term is just the Fourier transform of the potential and

$$f_n^{\mathrm{c}}=\left(\frac{-1}{4\pi}\right)^n\int dydzd\mathbf{x}_1\ldots d\mathbf{x}_{n-1}e^{-i\mathbf{k}'\cdot\mathbf{y}}\frac{e^{-\mu y}}{y}\frac{e^{ik|\mathbf{y}-\mathbf{x}_1|}}{|\mathbf{y}-\mathbf{x}_1|}\frac{e^{-\mu x_1}}{x_1}\cdots\frac{e^{ik|\mathbf{x}_{n-1}-\mathbf{z}|}}{|\mathbf{x}_{n-1}-\mathbf{z}|}\frac{e^{-\mu z}}{z}e^{i\mathbf{k}\cdot\mathbf{z}}, \tag{2.6}$$

where f_n^{c} indicates the coordinate representation.

We could also have iterated the equation for ψ by using the first form of $G(\mathbf{x},\mathbf{y})$ given above. This leads to an expression for f_n in a momentum representation which we denote by f_n^{k}:

$$f_n^{k}=\lim_{\varepsilon\to 0}4\pi\left(\frac{-1}{2\pi^2}\right)^n\int d\mathbf{k}_1\ldots d\mathbf{k}_n\frac{1}{\mu^2+(\mathbf{k}'-\mathbf{k}_1)^2}\frac{1}{\mathbf{k}_1^2-\mathbf{k}^2-i\varepsilon}\frac{1}{\mu^2+(\mathbf{k}_1-\mathbf{k}_2)^2}\cdots$$
$$\frac{1}{k_n^2-k^2-i\varepsilon}\frac{1}{\mu^2+(\mathbf{k}-\mathbf{k}_n)^2}. \tag{2.7}$$

We shall need one more form of f_n and that is the one obtained from f_n^{k} by parametrizing the integrand and doing the momentum integrations. This parametrization is carried out in detail in appendix 1, together with the proof of the properties stated below:

$$f_n^{\mathrm{p}} = \mathop{\mathrm{L}}_{\varepsilon\to 0} A_n \int_0^1 \mathrm{d}x_1 \int_0^{x_1} \mathrm{d}x_2 \ldots \int_0^{x_{2n-1}} \mathrm{d}x_{2n} \frac{1}{(a'_1 a'_2 \ldots a'_n)^{\frac{3}{2}}} \left(\frac{1}{D_n}\right)^{\frac{1}{2}n+1}$$

$$\begin{aligned} D_n &= \alpha(x_1 \ldots x_{2n})k^2 + \beta(x_1 \ldots x_{2n})k'^2 + \gamma(x_1 \ldots x_{2n})\mathbf{k}\cdot\mathbf{k}' + \mu^2 x_n - i\varepsilon(1-x_n) \\ &= k^2(\alpha+\beta+\gamma\cos\theta) + \mu^2 x_n - i\varepsilon(1-x_n) \\ &= -k^2 F_\theta(x) + \mu^2 x_n - i\varepsilon(1-x_n); \end{aligned}$$

A_n is a numerical constant, the a'_i are complicated functions of the differences of the x's but are all positive in the region of integration, and α, β and γ are all real. Since we are to take the limit as $\varepsilon \to 0$ and since, for $x_n = 0$, $F_\theta \neq 0$, we can just as well write (for positive k^2)

$$\begin{aligned} D_n &= -(k^2 + i\varepsilon)F_\theta(x) + \mu^2 x_n \\ &= -k^2 F_\theta(x) + \mu^2 x_n, \end{aligned}$$

where we now consider k^2 to be complex and take the limit as it approaches the positive real axis from above.

Since the x-integration is over a finite region and the denominator of the integrand can never vanish for k^2 complex, f_n^{p} is an analytic function of k^2 in the whole complex energy plane with the exception of the real axis [5] †. It is shown in the appendix that on the real axis there is a cut extending from $k^2 = 0$ to ∞ and from $k^2 = -\infty$ to $-\mu^2(n+1)^2/4\sin^2\frac{1}{2}\theta$. It is also shown there that $f_n^{\mathrm{p}} \to 0$ as $|k^2| \to \infty$.

We shall show in the next section that, in the region where f_n^{c} exists (this region lies in the upper half k plane and includes the real axis), it is an analytic function of k.

The function f_n^{c} is also continuous onto the real axis. Since the same values there are taken by the boundary values of the analytic function $f_n^{\mathrm{p}}(k)$, we can conclude that f_n^{c} and f_n^{p} represent the same analytic function in the common region of existence. That is, if there is an analytic function which takes the (continuous) values of the scattering amplitude as boundary values, that analytic function is unique [7].

3. Analyticity of $f(k, \theta)$

In this section we shall prove that for

$$V(r) = \lambda \frac{\mathrm{e}^{-\mu r}}{r} \tag{3.1}$$

$f(k, \theta)$ is an analytic function of k in a strip $0 \leqq \mathrm{Im}\, k < m\mu$, where m

† We shall frequently go from the k to the k^2 plane and vice versa. We use $k = \sqrt{k^2}$. Confining k to the upper half-plane means that k^2 covers the whole k^2 plane with a cut from 0 to ∞. The strip $0 \leqq \mathrm{Im}\, k < b$ is transformed into a parabola opening on the real k^2 axis and intersecting the k^2 axis at $k^2 = -b$.

(an integer) can be made arbitrarily large, with a branch cut running from $k = i\mu/\sin\frac{1}{2}\theta$ to $i\infty$ and a pole at $k = i\mu/2\sin\frac{1}{2}\theta$ coming from the Fourier transform of the potential. The problem is to show that the Born series is a sum of analytic functions in such a strip and that this sum is uniformly convergent there. Although f_n^{p} exists and is analytic for all complex k^2, it is difficult to put an upper bound on its magnitude. What we shall do is show that f_n^{c} exists in the above strip provided that $n \geqq 2m$, that it is analytic there, and that $\sum_{2m}^{\infty} \lambda^n f_n^{\mathrm{c}}$ is uniformly convergent. This means that we write

$$-\frac{4\pi}{\lambda} f(k,\theta) - \frac{4\pi}{\mu^2+(\mathbf{k}'-\mathbf{k})^2} - \sum_{n=1}^{2m-1} \lambda^n f_n^{\mathrm{p}} = \sum_{n=2m}^{\infty} \lambda^n f_n^{\mathrm{c}} \tag{3.2}$$

and show that for $0 \leqq \operatorname{Im} k < m\mu$, the right hand side of this expression is an analytic function and, therefore, $f(k,\theta)$ has the analytic properties of the *finite* sum standing on the left, that is, just those properties we set out to prove.

One can see from f_n^{c} that in our strip the Green's functions are decreasing exponentials but that the plane wave factors standing at either end of the integrand may become infinite. We use the fact that for a given k, if we have enough factors arising from the potential in between these two end terms, they can counteract this effect.

To prove our statement, we use a theorem due to Titchmarsh [6]) and given by Khuri in the following form [1]):

Theorem 1. If $\Phi(k,x)$ is analytic in k, regular in a certain region Γ of the complex k plane and if $\Phi(k,x)$ is continuous in the closed region composed of Γ and its boundary B, then

$$f(k) = \int_A \Phi(k,x)\mathrm{d}x \tag{3.3}$$

is analytic in k, regular and uniformly bounded in Γ, provided there exists $\psi(x)$ such that $|\Phi(k,x)| \leqq \Psi(x)$ for all k on B (and hence all k in Γ since $\Phi(k,x)$ is analytic) and provided that

$$\int_A \Psi(x)\mathrm{d}x < \infty. \tag{3.4}$$

We wish to apply this theorem to f_n^{c} when the region Γ is the region enclosed by the real axis, the line $\operatorname{Im} k = m\mu$, and the two lines $\operatorname{Re} k = \pm L$.

It is evident that the integrand of f_n^{c} satisfies the first three conditions, and we shall show that for $n \geqq 2m$ we can find a $\Psi(x)$ satisfying the last condition. If we denote the integrand by J_n^{c}, we have, for $\operatorname{Im} k = 0$,

$$|J_n^{\mathrm{c}}| \leqq \frac{\mathrm{e}^{-\mu y}}{y}\,\frac{1}{|\mathbf{y}-\mathbf{x}_1|}\,\frac{\mathrm{e}^{-\mu x_1}}{x_1}\,\frac{1}{|\mathbf{x}_1-\mathbf{x}_2|}\cdots\frac{1}{|\mathbf{x}_{n-1}-\mathbf{z}|}\,\frac{\mathrm{e}^{-\mu z}}{z} \equiv I_1^{(n)}; \tag{3.5}$$

for

$$\operatorname{Im} k = m\mu = b, \tag{3.6}$$

we have

$$|J_n^c| \leqq e^{by} \frac{e^{-\mu y}}{y} \frac{e^{-b|y-x_1|}}{|y-x_1|} \frac{e^{-\mu x_1}}{x_1} \cdots \frac{e^{-b|x_{n-1}-z|}}{|x_{n-1}-z|} \frac{e^{-\mu z}}{z} e^{bz} \equiv I_2^{(n)}. \quad (3.7)$$

Therefore, on both of these lines,

$$|J_n^c| < I_1^{(n)} + I_2^{(n)}. \quad (3.8)$$

Now, on the two end lines $\mathrm{Re}\, k = \pm L$, we have also

$$|J_n^c| < I_1^{(n)} + I_2^{(n)}, \quad (3.9)$$

since $e^{\alpha x} < 1 + e^{\alpha x_0}$ for $0 \leqq x \leqq x_0$ and all real α. We can therefore let $L \to \infty$.

We now show that the integrals over $I_1^{(n)}$ and $I_2^{(n)}$ are finite. Take first

$$\int I_1^{(n)} = \frac{1}{(4\pi)^n} \int dy dz dx_1 \ldots dx_{n-1} \frac{e^{-\mu y}}{y} \frac{1}{|y-x_1|} \frac{e^{-\mu x_1}}{x_1} \cdots \frac{1}{|x_{n-1}-z|} \frac{e^{-\mu z}}{z}. \quad (3.10)$$

From appendix 2 we have

$$\int \frac{dz}{|x-z|} f(z) \leqq 4\pi \int_0^\infty z dz\, f(z), \quad (3.11)$$

and therefore, defining

$$M = \int_0^\infty y V(y) dy = \frac{1}{\mu}, \quad (3.12)$$

$$N = \int_0^\infty y^2 V(y) dy = \frac{1}{\mu^2}, \quad (3.13)$$

we find

$$\int I_1^{(n)} \leqq 4\pi N M^n. \quad (3.14)$$

For the second integral

$$\int I_2^{(n)} = \frac{1}{(4\pi)^n} \int dy dz dx_1 \ldots dx_{n-1} e^{by} \frac{e^{-\mu y}}{y} \frac{e^{-b|y-x_1|}}{|y-x_1|} \cdots \frac{e^{-b|x_{n-1}-z|}}{|x_{n-1}-z|} \frac{e^{-\mu z}}{z} e^{bz}. \quad (3.15)$$

We start doing the integrations from the right, noting (appendix 2) that

$$\int dz \frac{e^{-b|x-z|}}{|x-z|} \frac{e^{-\mu z}}{z} e^{bz} = \frac{4\pi}{\mu} e^{(b-\mu)x} \left[\frac{1-e^{-(2b-\mu)x}}{(2b-\mu)x} \right]. \quad (3.16)$$

Since

$$\frac{1-e^{-y}}{y} \leqq 1 \quad \text{for} \quad y \geqq 0, \quad (3.17)$$

we have

$$\int dz \frac{e^{-b|x-z|}}{|x-z|} \frac{e^{-\mu z}}{z} e^{bz} \leqq \frac{4\pi}{\mu} e^{(b-\mu)x} \quad (3.18)$$

for $2b-\mu \geqq 0$. For the $\mathbf{x}_{n-1}$ integration we find

$$\int d\mathbf{x}\, \frac{e^{-b|\boldsymbol{\rho}-\mathbf{x}|}}{|\boldsymbol{\rho}-\mathbf{x}|}\, \frac{e^{-\mu x}}{x}\, \frac{4\pi}{\mu}\, e^{(b-\mu)x} = \frac{4\pi}{\mu} \int d\mathbf{x}\, \frac{e^{-b|\boldsymbol{\rho}-\mathbf{x}|}}{|\boldsymbol{\rho}-\mathbf{x}|}\, \frac{e^{-2\mu x}}{x}\, e^{bx}$$

$$\leqq \frac{4\pi}{\mu}\, \frac{4\pi}{2\mu}\, e^{(b-2\mu)\rho} \tag{3.19}$$

for $2b-2\mu \geqq 0$. We repeat this process m times starting from the right and m times starting from the left. We obtain

$$\int I_2^{(n)} \leqq \left(\frac{4\pi}{\mu}\right)^{2m} \left(\frac{1}{m!}\right)^2 \left(\frac{1}{4\pi}\right)^n \int d\mathbf{x}_1 \ldots d\mathbf{x}_r\, \frac{e^{-\mu x_1}}{x_1}\, \frac{1}{|\mathbf{x}_1-\mathbf{x}_2|}\, \frac{e^{-\mu x_2}}{x_2} \cdots \frac{1}{|\mathbf{x}_{r-1}-\mathbf{x}_r|}\, \frac{e^{-\mu x_r}}{x_r}, \tag{3.20}$$

$$r = n+1-2m. \tag{3.21}$$

Provided $r \geqq 1$, which is satisfied for $n \geqq 2m$, and also provided $2b-m\mu = m\mu \geqq 0$, which is always satisfied, we get

$$\int I_2^{(n)} \leqq \left(\frac{4\pi}{\mu}\right)^{2m} \left(\frac{1}{m!}\right)^2 \left(\frac{1}{4\pi}\right)^n (4\pi)^r N M^{r-1}, \tag{3.22}$$

$$\int I_2^{(n)} \leqq 4\pi N M^n. \tag{3.23}$$

Therefore,

$$|f_n^c| \leqq \int I_1^{(n)} + \int I_2^{(n)} \leqq 8\pi N M^n, \tag{3.24}$$

$$\sum_{n=2m}^{\infty} \lambda^n f_n^c \leqq \sum_{n=2m}^{\infty} |\lambda|^n |f_n^c| \leqq 8\pi N \sum_{n=0}^{\infty} |\lambda|^n M^n = \frac{8\pi N}{1-|\lambda|M}. \tag{3.25}$$

This converges for

$$|\lambda|M < 1, \quad |\lambda| < \mu. \tag{3.26}$$

Thus each f_n^c in $\sum_{2m}^{\infty} \lambda^n f_n^c$ is analytic, and the sum is uniformly convergent for $0 \leqq \operatorname{Im} k < b = m\mu$, which is what we set out to prove.

4. Exchange Forces

We next show how the previous analysis can be extended to include exchange forces. We shall suppose for simplicity that the exchange force has the same range as the direct force but a different strength. We write

$$(\nabla^2+k^2)\psi = \int V(\mathbf{x}, \mathbf{y})\psi(\mathbf{y})d\mathbf{y}, \tag{4.1}$$

$$V(\mathbf{x}, \mathbf{y}) = \frac{e^{-\mu x}}{x}\, [\lambda_D \delta(\mathbf{x}-\mathbf{y}) + \lambda_E \delta(\mathbf{x}+\mathbf{y})]. \tag{4.2}$$

Going to the integral equation for scattering one has

$$\psi(\mathbf{x}) = e^{i\mathbf{k}\cdot\mathbf{x}} - \int G(\mathbf{x}, \mathbf{y})V(\mathbf{y}, \mathbf{z})\psi(\mathbf{z})d\mathbf{y}d\mathbf{z} \tag{4.3}$$

$$= e^{i\mathbf{k}\cdot\mathbf{x}} + \int (\lambda_D k_D(\mathbf{x}, \mathbf{y}) + \lambda_E k_E(\mathbf{x}, \mathbf{y}))\psi(\mathbf{y})d\mathbf{y}. \tag{4.4}$$

$$k_D(\mathbf{x}, \mathbf{y}) = -G(\mathbf{x}, \mathbf{y})\frac{e^{-\mu y}}{y}, \tag{4.5}$$

$$k_E(\mathbf{x}, \mathbf{y}) = k_D(\mathbf{x}, -\mathbf{y}), \tag{4.6}$$

and the scattering amplitude is again

$$f(k, \theta) = -\frac{1}{4\pi}\int e^{-i\mathbf{k}'\cdot\mathbf{y}}V(\mathbf{y}, \mathbf{z})\psi(\mathbf{z})d\mathbf{y}d\mathbf{z}. \tag{4.7}$$

Iterating the equation for $\psi(\mathbf{x})$ and substituting in the equation for f one finds

$$f(k, \theta) = -\frac{1}{4\pi}\left[V(\mathbf{k}', \mathbf{k}) + \sum_{n=1}^{\infty} f_n^c\right], \tag{4.8}$$

$$f_n^c(k, \theta) = \left(\frac{-1}{4\pi}\right)^n \sum_{i=0}^{n} \lambda_D{}^i \lambda_E^{n-i} \sum_P \int d\mathbf{x}d\mathbf{y}d\mathbf{z}d\mathbf{x}_1 \ldots d\mathbf{x}_{n-1} e^{-i\mathbf{k}'\cdot\mathbf{x}}$$
$$\cdot V(\mathbf{x}, \mathbf{y})\underbrace{k_D(\mathbf{y}, \mathbf{x}_1) \ldots k_D(\mathbf{x}_{i-1}, \mathbf{x}_i)}_{i \text{ terms}}\underbrace{k_E(\mathbf{x}_i, \mathbf{x}_{i+1}) \ldots k_E(\mathbf{x}_{n-1}, \mathbf{z})}_{n-i \text{ terms}} e^{i\mathbf{k}\cdot\mathbf{z}},$$

where $\sum_P$ denotes a sum over all permutations of the indices D and E on the k's.

Now, notice that one can change all the E's to D's in each term of the above sum (including the E in $V(\mathbf{x}, \mathbf{y})$) by starting with the first exchange term on the left and changing the integration variables to their negatives working out to the left. That is, we use

$$k_E(\mathbf{x}, \mathbf{y}) = k_D(\mathbf{x}, -\mathbf{y}) = k_D(-\mathbf{x}, \mathbf{y}). \tag{4.10}$$

Now, if the exchange force acts an *even* number of times the net result is to change the sign of $\mathbf{k}' \cdot \mathbf{x}$ an even number of times and thus we can replace all the E's by D's and $\mathbf{k}'$ by $+\mathbf{k}'$. This is just the expression we have studied before. If, however, the exchange form acts an *odd* number of times, we can change all the E's into D's but must simultaneously replace $\mathbf{k}'$ by $-\mathbf{k}'$, which means replacing $\cos\theta$ by $-\cos\theta$ or $\sin^2\frac{1}{2}\theta$ by $\cos^2\frac{1}{2}\theta$.

As for proving the uniform convergence of $\sum_{2m}^{\infty} f_n^c$, it will be noticed that the bounds we put on the integrals were independent of the *direction* of $\mathbf{k}'$ and hence still hold. The only difference now is that we have more terms and the condition for the convergence of the bounding series is changed slightly. Thus,

$$|f_n^c| \leqq \sum_{i=0}^{n} |\lambda|_D{}^i |\lambda|_E^{n-i} \left[|\lambda_D| \frac{n!}{i!(n-i)!} + |\lambda_E| \frac{n!}{i!(n-i)!}\right] 8\pi N M^n \tag{4.11}$$
$$= 8\pi N(|\lambda_D| + |\lambda_E|)M^n(|\lambda_D| + |\lambda_E|)^n,$$

$$\sum_{2m}^{\infty} f_n^{\mathrm{e}} \leqq 8\pi N(|\lambda_{\mathrm{D}}|+|\lambda_{\mathrm{E}}|)\,\frac{1}{1-M(|\lambda_{\mathrm{D}}|+|\lambda_{\mathrm{E}}|)}. \tag{4.12}$$

The factors $n!/i!(n-i)!$ appear because this is the number of terms in $\sum_{\mathrm{P}}$. The condition for convergence is now

$$(|\lambda_{\mathrm{D}}|+|\lambda_{\mathrm{E}}|)M < 1, \quad |\lambda_{\mathrm{D}}|+|\lambda_{\mathrm{E}}| < \mu. \tag{4.13}$$

The Fourier transform of the potential now gives

$$V(\mathbf{k}', \mathbf{k}) = 4\pi\left[\frac{1}{\mu^2+4k^2\sin^2\frac{1}{2}\theta}+\frac{1}{\mu^2+4k^2\cos^2\frac{1}{2}\theta}\right], \tag{4.14}$$

and thus $f(k^2, \theta)$ is an analytic function in the whole k^2 plane except for a cut from $k^2 = 0$ to ∞, poles at $k^2 = -\frac{1}{4}\mu^2\sin^{-2}\frac{1}{2}\theta$ and $k^2 = -\frac{1}{4}\mu^2\cos^{-2}\frac{1}{2}\theta$ and a cut from $k^2 = -\mu^2\min(\sin^{-2}\frac{1}{2}\theta, \cos^{-2}\frac{1}{2}\theta)$ to $-\infty$.

5. Extension to Spectral Representations

In this section we further extend our results to include potentials which can be written as integrals over Yukawa potentials.

5.1. CENTRAL FORCE

We write

$$V(r) = \int_{\mu}^{\infty} \rho(\sigma)\frac{\mathrm{e}^{-\sigma r}}{r}\,\mathrm{d}\sigma \tag{5.1}$$

and can again write a Born series classifying terms by the number of times the potential acts. Thus,

$$f(k, \theta) = -\frac{1}{4\pi}[V(\mathbf{k}', \mathbf{k})+\sum_{n=1}^{\infty} f_n], \tag{5.2}$$

$$f_n(k, \theta) = \left(-\frac{1}{4\pi}\right)^n \int_{\mu}^{\infty} \mathrm{d}\sigma_1 \ldots \mathrm{d}\sigma_{n+1}\rho(\sigma_1)\ldots\rho(\sigma_{n+1}) \int \mathrm{d}\mathbf{y}\mathrm{d}\mathbf{z}\mathrm{d}\mathbf{x}_1 \ldots \mathrm{d}\mathbf{x}_{n-1}$$
$$\cdot\, \mathrm{e}^{-i\mathbf{k}'\cdot\mathbf{y}}\frac{\mathrm{e}^{-\sigma_1 y}}{y}\,\frac{\mathrm{e}^{ik|\mathbf{y}-\mathbf{x}_1|}}{|\mathbf{y}-\mathbf{x}_1|}\,\frac{\mathrm{e}^{-\sigma_2 x_1}}{x_1}\cdots\frac{\mathrm{e}^{-\sigma_{n+1}z}}{z}\,\mathrm{e}^{i\mathbf{k}\cdot\mathbf{z}}. \tag{5.3}$$

Investigating first the uniform convergence of the series $\sum_{2m}^{\infty} f_n$, we find

$$|f_n| \leqq \left(\frac{1}{4\pi}\right)^n \int_{\mu}^{\infty} |\rho(\sigma_1)|\ldots|\rho(\sigma_{n+1})|\mathrm{d}\sigma_1 \ldots \mathrm{d}\sigma_{n+1} \int \mathrm{d}\mathbf{y}\mathrm{d}\mathbf{z}\mathrm{d}\mathbf{x}_1 \ldots \mathrm{d}\mathbf{x}_{n-1}$$
$$\cdot\, \mathrm{e}^{by}\frac{\mathrm{e}^{-\mu y}}{y}\,\frac{\mathrm{e}^{-b|\mathbf{y}-\mathbf{x}_1|}}{|\mathbf{y}-\mathbf{x}_1|}\,\frac{\mathrm{e}^{-\mu x_1}}{x_1}\cdots\frac{\mathrm{e}^{-\mu z}}{z}\,\mathrm{e}^{bz}, \tag{5.4}$$

where use has been made of $\mathrm{e}^{-\sigma x} \leqq \mathrm{e}^{-\mu x}$. This uncouples the spectral functions and allows one to make the same analysis as previously, except that we must replace λ by $\int_{\mu}^{\infty}|\rho(\sigma)|\mathrm{d}\sigma$. Therefore, the condition for convergence of the

series is

$$\int_{\mu}^{\infty}|\rho(\sigma)|\mathrm{d}\sigma < \mu. \tag{5.5}$$

One can carry out the parametrization as before and finds

$$f_n^{\mathrm{p}}(k,\theta) = A_n\int_{\mu}^{\infty}\mathrm{d}\sigma_1\ldots\mathrm{d}\sigma_{n+1}\rho(\sigma_1)\ldots\rho(\sigma_{n+1})$$
$$\int_0^1\mathrm{d}x_1\int_0^{x_1}\mathrm{d}x_2\ldots\int_0^{x_{2n-1}}\mathrm{d}x_{2n}\frac{1}{(a'_1\ldots a'_n)^{\frac{3}{2}}}\frac{1}{(\tilde{D}_n)^{\frac{1}{2}n+1}}, \tag{5.6}$$

$$\tilde{D}_n = -k^2F_\theta(x)+G(\sigma,x), \tag{5.7}$$

where (see appendix 1)

$$G(\sigma,x) = \sigma_1{}^2x_{2n}+\sigma_2{}^2(x_{2n-1}-x_{2n})+\ldots+\sigma_{n+1}^2(x_n-x_{n+1}) \geqq \mu^2x_n. \tag{5.8}$$

Therefore, $G(\sigma,x)$ can only vanish for $x_n\to 0$, in which case $F_\theta(x)\neq 0$. Also, to locate the position of the branch cut on the negative axis we must find the *minimum* of

$$\frac{G(\sigma,x)}{2|\gamma|\sin^2\frac{1}{2}\theta} \geqq \frac{\mu^2x_n}{2|\gamma|\sin^2\frac{1}{2}\theta} \tag{5.9}$$

with the equality holding for all $\sigma=\mu$. Therefore, the condition on the start of the branch cut for each term of the Born series is the same as before. What is different is

$$V(\mathbf{k}',\mathbf{k}) = 4\pi\int_{\mu}^{\infty}\frac{\rho(\sigma)\mathrm{d}\sigma}{\sigma^2+(\mathbf{k}'-\mathbf{k})^2}. \tag{5.10}$$

If $\rho(\sigma)$ is continuous from μ we have a branch cut (no longer a pole) starting from $k^2=-\mu^2/4\sin^2\frac{1}{2}\theta$. If, however, $\rho(\sigma)$ has the form

$$\rho(\sigma) = 2\lambda\delta(\sigma-\mu)+g(\sigma), \tag{5.11}$$

where $g(\sigma)=0$ for $\sigma<2\mu$, as one might expect from meson theory, we have

$$V(\mathbf{k}',\mathbf{k}) = \frac{4\pi\lambda}{\mu^2+4k^2\sin^2\frac{1}{2}\theta}+\int_{2\mu}^{\infty}\frac{g(\sigma)\mathrm{d}\sigma}{\sigma^2+4k^2\sin^2\frac{1}{2}\theta}. \tag{5.12}$$

Again, there is an isolated pole and a branch cut starting from $k^2=-\mu^2/\sin^2\frac{1}{2}\theta$ which *coincides* with the branch cut coming from the first iteration of the Yukawa potential.

5.2. GENERAL EXCHANGE MIXTURE

We write

$$V(\mathbf{x},\mathbf{y}) = \int_{\mu}^{\infty}\rho_{\mathrm{D}}(\sigma)\frac{\mathrm{e}^{-\sigma x}}{x}\mathrm{d}\sigma\delta(\mathbf{x}-\mathbf{y})+\int_{\mu}^{\infty}\rho_{\mathrm{E}}(\sigma)\frac{\mathrm{e}^{-\sigma x}}{x}\mathrm{d}\sigma\delta(\mathbf{x}+\mathbf{y}). \tag{5.13}$$

Exactly the same analysis holds as in section 4. We again use $\mathrm{e}^{-\sigma r}\leqq\mathrm{e}^{-\mu r}$,

which decouples the spectral functions, and must replace

$$|\lambda_{D,E}| \text{ by } \int_{\mu}^{\infty} |\rho_{D,E}(\sigma)| d\sigma. \tag{5.14}$$

The arguments on the parametrization are the same as above; again, if the exchange force acts an odd number of times we must replace $\sin^2 \frac{1}{2}\theta$ by $\cos^2 \frac{1}{2}\theta$. The condition for the convergence of the series is

$$\int_{\mu}^{\infty} (|\rho_D(\sigma)| + |\rho_E(\sigma)|) d\sigma < \mu, \tag{5.15}$$

and if, in particular,

$$\rho_{D,E}(\sigma) = 2\lambda_{D,E}\delta(\sigma-\mu) + g_{D,E}(\sigma), \tag{5.16}$$

with $g_{D,E}(\sigma) = 0$ for $\sigma < 2\mu$, we find, as the analytic properties of $f(k^2, \theta)$, a branch cut from 0 to ∞, poles at $k^2 = -\frac{1}{4}\mu^2 \sin^{-2} \frac{1}{2}\theta$ and $-\frac{1}{4}\mu^2 \cos^{-2} \frac{1}{2}\theta$ and a branch cut from $k^2 = -\mu^2 \min (\sin^{-2} \frac{1}{2}\theta, \cos^{-2} \frac{1}{2}\theta)$ to $-\infty$.

6. General Considerations

It should be noted that it is now an easy task to study the analytic properties of each phase shift. One multiplies $f(k^2, \theta)$ by a Legendre polynomial and integrates over angles. The partial wave amplitude that one obtains will again be analytic in the whole complex k^2 plane, with the exception of the cut on the positive k^2 axis, and poles and cuts on the negative k^2 axis which depend on the nature of the potential. These extra singularities appear in addition to any real bound states in the problem and have long been a subject of discussion [9]). An alternative way of investigating the analytic properties of the scattering amplitude might be to demonstrate analytic properties of each partial wave separately and then consider the behaviour of their sum.

It is interesting to compare our results with the fixed angle dispersion relations recently proposed within the framework of field theory [8]). These dispersion relations follow if one assumes the Mandelstam relations [4]) to have a general validity. The analytic properties obtained and exploited in ref. [8]) are just those demonstrated here for a potential. We note, for example, that the residue of the pole coming from potential (5.11) is just $-\lambda/4 \sin^2 \frac{1}{2}\theta$ and if the Yukawa potential arises from a meson exchange, λ is just the square of the coupling constant. We have not been able to prove the complete dispersion relations at fixed angle which the above authors suggest, since we are not able to make a definite statement about the behaviour of the scattering amplitude at infinity. All we are able to say is that each term in the Born series goes to zero there, and one is therefore perhaps justified in hoping that the scattering amplitude will also have this property †.

† It is easy to show from our analysis that in the first and fourth quadrants of the k^2 plane, the scattering amplitude must go to zero at infinity.

One may make one other interesting comparison with the proposed field theory results [8]). In the relativistic theory, the branch points on the negative energy axis correspond to the thresholds for processes involving antinucleons and in particular for the processes

$$\mathrm{N}+\overline{\mathrm{N}} \to (n+1)\pi$$

and for direct forces, they occur at [8])

$$(\mathbf{k}-\mathbf{k}')^2 = -[(n+1)\mu]^2 \qquad (\mu = m_\pi)$$

or

$$k^2 = -\frac{1}{4\sin^2\frac{1}{2}\theta}[(n+1)\mu]^2.$$

Exactly the same result follows from our potential theory, where n is now the order of iteration of the potential and μ is its range.

We are greatly indebted to Professor S. Fubini for suggesting the problem and for fruitful discussions during the course of this work. We would also like to thank Professors H. Lehmann and R. Jost for a very illuminating discussion. One of us (D. W.) would like to thank Professor Bakker, Professor Fierz and the Theoretical Group of CERN for the hospitality extended to him during his stay.

Appendix 1

The Parametric Integrals

I.1. PARAMETRIZATION

We want to parametrize

$$\frac{f_n^{\,k}}{4\pi} = \left(\frac{-1}{2\pi^2}\right)^n \int \mathrm{d}\mathbf{k}_1 \ldots \mathrm{d}\mathbf{k}_n \frac{1}{\mu^2+(\mathbf{k}'-\mathbf{k}_1)^2}\,\frac{1}{k_1^{\,2}-k^2-i\varepsilon}\cdots\frac{1}{k_n^{\,2}-k^2-i\varepsilon}\,\frac{1}{\mu^2+(\mathbf{k}_n-\mathbf{k})^2}$$

and carry out the momentum integrations. To do this we use [10])

$$\frac{1}{a_1 \ldots a_N} = (N-1)!\int_0^1 \mathrm{d}x_1 \int_0^{x_1} \mathrm{d}x_2 \ldots \int_0^{x_{N-2}} \mathrm{d}x_{N-1}[a_1 x_{N-1}+a_2(x_{N-2}-x_{N-1}) + \ldots + a_N(1-x_1)]^{-N},$$

$$1 > x_1 > x_2 \ldots > x_{N-1} > 0.$$

We let $N = 2n+1$, the number of terms in $f_n^{\,k}$, and take all the potentials first and the Green's functions last. We find, if J^{-N} is the integrand above,

$$J = \mu^2 x_n - (1-x_n)(k^2+i\varepsilon) + k'^2 x_{2n} + k^2(x_n-x_{n+1}) - 2\mathbf{k}\cdot\mathbf{k}_1 x_{2n} - 2\mathbf{k}\cdot\mathbf{k}_n(x_n-x_{n+1}) + \sum_{i,j=1}^{n-1} a_{ij}\mathbf{k}_i\cdot\mathbf{k}_j$$

where

$$a_{ii} = x_{2n-i} - x_{2n+2-i} + x_{n-i} - x_{n+1-i} > 0,$$
$$a_{ij} = -2(x_{2n-i} - x_{2n+1-i})\delta_{i,i+1} < 0.$$

We now complete the square and do the $\mathbf{k}_1$ integration. We use

$$\int_0^\infty \frac{p^2 \mathrm{d}p}{(p^2+C)^{n+1}} = \begin{cases} \frac{1}{2}\pi \dfrac{(2n-3)!!}{n!2^n} \dfrac{1}{C^{n-\frac{1}{2}}} & (n \text{ integral}), \\ 2^{n-\frac{1}{2}} \dfrac{(n-\frac{3}{2})!}{2n!!} \dfrac{1}{C^{n-\frac{1}{2}}} & (n \text{ half-integral}). \end{cases}$$

These formulae are easily established by taking appropriate derivatives of

$$\int_0^\infty \frac{\mathrm{d}p}{p^2+C} = \frac{\pi}{2\sqrt{C}}, \qquad \int_0^\infty \frac{\mathrm{d}p}{(p^2+C)^{\frac{3}{2}}} = \frac{1}{C}.$$

These integrals are well defined as long as C is never purely negative, and since the coefficient $-(1-x_n)$ of $i\varepsilon$ does not vanish in the region of integration, this can never happen. Repeating the process n times one finds

$$f_n^{\,k} = A_n I_n(k^2, \cos\theta),$$

$$A_n = \begin{cases} +\left(\dfrac{-1}{2\sqrt{\pi}}\right)^n (\tfrac{1}{2}n)! & (n \text{ even}) \\ +\tfrac{1}{2}\sqrt{\pi}\left(\dfrac{-1}{2\sqrt{2\pi}}\right)^n n!! & (n \text{ odd}), \end{cases}$$

$$I_n = \int_0^1 \mathrm{d}x_1 \int_0^{x_1} \mathrm{d}x_2 \ldots \int_0^{x_{2n-1}} \mathrm{d}x_{2n} \frac{1}{(a'_1 \ldots a'_n)^{\frac{3}{2}}} \left(\frac{1}{D_n}\right)^{\frac{1}{2}n+1},$$

$$D_n = \alpha(x_1 \ldots x_{2n})k^2 + \beta(x_1 \ldots x_{2n})k'^2 + \gamma(x_1 \ldots x_{2n})\mathbf{k}\cdot\mathbf{k}' + \mu^2 x_n - i\varepsilon(1-x_n),$$

$$\alpha = -(1-x_n) - \tfrac{1}{2}a_{n,n+1}\left(1 + \frac{a_{n,n+1}}{2a'_n}\right),$$

$$\beta = -\tfrac{1}{2}a_0 - \sum_{i=1}^{n} (\tfrac{1}{2})^{2i} \frac{1}{a'_i} \prod_{j=1}^{i-1} \frac{a_{01}^2 a_{j,j+1}^2}{(a'_j)^2},$$

$$\gamma = (-\tfrac{1}{2})^n \prod_{i=1}^{n} \frac{a_{01} a_{i,i+1}}{a'_i},$$

$$a_{01} = -2x_{2n}, \qquad a_{n,n+1} = -2(x_n - x_{n+1}),$$

$$a'_i = a_{ii} - \frac{a_{i-1,i}^2}{4a'_{i-1}}, \qquad a'_1 = a_{11}.$$

Note that all the a_{ij} and a'_i have a dependence on n which is suppressed in the notation. The a'_i appear because when one completes the square for the $\mathbf{k}_i$ integration, the coefficient of $\mathbf{k}_{i+1}$ is altered.

I.2. PROPERTIES OF THE PARAMETRIZATION

1) $a'_i > 0$

To study the properties of the parametric integrals it is more convenient to introduce

$$\begin{aligned} -2b_{ij} &= a_{ij} \qquad (i \neq j) \\ b_i &= a_{ij} \qquad (i = j), \end{aligned}$$

in which case

$$b_{ij} > 0, \quad b_i > 0.$$

One easily verifies from the definitions that

$$\begin{aligned} b_i &= b_{i-1,i} + b_{i,i+1} + c_i, \\ c_i &= x_{n-i} \; - x_{n+1-i} > 0. \end{aligned}$$

All three terms in the expression for b_i are thus positive.

One next notices, by substituting in the recurrence relation defining a'_i, that the general form of a'_i is

$$\underset{i \leq n}{a'_i} = \frac{1}{a' \ldots a'_{i-1}} \left[\prod_{j=1}^{i} b_j + \sum \prod_{j=1}^{i} b_j \right],$$

the sum being extended over all contractions of pairs of neighbouring indices in the product, i.e. all replacements $b_i b_j \to -b_{ij}^2$. For example,

$$a'_4 = \frac{1}{a'_1 a'_2 a'_3} [b_1 b_2 b_3 b_4 - b_{12}^2 b_3 b_4 - b_1 b_{23}^2 b_4 - b_1 b_2 b_{34}^2 + b_{12}^2 b_{34}^2].$$

If one now substitutes the above expression for b_i, it is seen that the $\sum$ over contractions is just the process which removes all the terms in b_{ij}^2 from $\prod_{j=1}^{i} b_j$ and what is left is a series of positive terms. One can thus write

$$\begin{aligned} a'_1 \ldots a'_j = {} & c_1 c_2 \ldots c_j + \sum{}^1 c_2 \ldots c_j + \sum{}^2 c_1 c_3 \ldots c_j + \ldots \\ & + \sum{}^{1,2} c_3 \ldots c_j + \sum{}^{1,3} c_2 c_4 \ldots c_j + \ldots \\ & + \sum{}^{1,2,3} c_4 \ldots c_j + \sum{}^{1,2,4} c_3 c_5 \ldots c_j + \ldots \\ & + \ldots + \sum{}^{1,2,3 \ldots j} \end{aligned}$$

where $\sum^{i,j}$ is a sum over all possible products of the b_{ij}'s associated with the missing c_i, c_j through $b_i = b_{i-1,i} + b_{i,i+1} + c_i$ and *not* containing any b_{ij}^2. For example,

$$\begin{aligned} a'_3 a'_2 a'_1 = {} & c_1 c_2 c_3 + (b_{01} + b_{12}) c_2 c_3 + c_1 (b_{12} + b_{23}) c_3 + c_1 c_2 (b_{23} + b_{34}) \\ & + (b_{01} b_{12} + b_{01} b_{23} + b_{12} b_{23}) c_3 + (b_{01} b_{23} + b_{12} b_{23} + b_{01} b_{34} + b_{12} b_{34}) c_2 \\ & + (b_{12} b_{23} + b_{12} b_{34} + b_{23} b_{34}) c_3 + (b_{01} b_{12} b_{23} + b_{01} b_{12} b_{34} + b_{01} b_{23} b_{34} + b_{12} b_{23} b_{34}). \end{aligned}$$

Since this is a series of positive terms and holds for all $i \leqq n$, one sees that all the $a'_i > 0$ †.

† Note that the $a'_i \cdots a'_n$ may vanish at the boundary of the integration region but that the integrals over the vanishing denominators are convergent. This has been shown for $n = 1, 2, 3$ and probably holds in general.

2) *Show that* $-(\alpha+\beta+\gamma\cos\theta) = F_\theta \neq 0$ *when* $x_n = 0$.

From their definition

$$-(\alpha+\beta+\gamma) = 1+g(x)-2x_n-x_{2n}, \quad g(x) \geqq 0;$$

also

$$-(\alpha+\beta+\gamma\cos\theta) = -(\alpha+\beta+\gamma)+2\gamma\sin^2\tfrac{1}{2}\theta \equiv A-2|\gamma|\sin^2\tfrac{1}{2}\theta.$$

(Notice that $\gamma < 0$.) We shall show in the next section that $x_n/|\gamma|$ has a finite minimum and therefore $\gamma \to 0$ as $x_n \to 0$ †. Thus

$$F_\theta \underset{x_n\to 0}{\to} 1+g(x) \geqq 1.$$

3) *Location of the branch cuts*

We first make the observation that for forward scattering the scattering amplitude is analytic in the whole complex k^2 plane with a cut from 0 to ∞. The Fourier transform of the potential reduces to $4\pi/\mu^2$ and the series $\sum_{n=1}^{\infty}\lambda^n f_n$ is easily shown to be uniformly convergent under the condition $|\lambda| < \mu$ by using the inequality

$$|\exp[i\{k(|\mathbf{y}-\mathbf{x}_1|+|\mathbf{x}_1-\mathbf{x}_2|+\ldots+|\mathbf{x}_n-\mathbf{z}|)-\mathbf{k}\cdot(\mathbf{y}-\mathbf{z})\}]|$$
$$\leqq \exp[-\mathrm{Im}k|\mathbf{y}-\mathbf{z}|(1-\hat{n}_{\mathbf{k}}\cdot\hat{n}_{\mathbf{y}-\mathbf{z}})] \leqq 1$$

for k in the upper half plane. Since we have already shown that $f_n^{\,c}$ and $f_n^{\,p}$ represent the same analytic function, we can conclude that $f_n^{\,p}$ only has a branch cut on the positive k^2 axis for forward scattering. We thus get the condition

$$-(\alpha+\beta+\gamma) \equiv A \geqq 0.$$

To find the location of the branch cuts in the general case we write

$$D_n = -F_\theta k^2+\mu^2 x_n, \qquad F_\theta = A-2|\gamma|\sin^2\tfrac{1}{2}\theta.$$

We must therefore find which values of $k^2 = \mu^2 x_n/[A-2|\gamma|\sin^2\frac{1}{2}\theta]$ are permissible on the negative axis. Since both A and x_n are positive we get an upper limit by finding the minimum of

$$-k^2 = \frac{\mu^2 x_n}{2|\gamma|\sin^2\frac{1}{2}\theta}.$$

Now, $|\gamma| = 2\,b_{01}b_{12}\ldots b_{n,\,n+1}/a'_1\ldots a'_n$; to get a minimum for the above expression we want $|\gamma|$ as large as possible. Since we can set all the $c_i = 0$ in $a'_1\ldots a'_n$ without changing the values of $b_{01}b_{12}\ldots b_{n,\,n+1}$ and x_n, we first do this. This leaves

† This is easily seen from the definition of γ. All the a_{ij} are differences of x_i with $i \geqq n$ while $a'_i\ldots a'_n$ has a term $c_i\ldots c_j$ which contains differences of x_i's with $i \leqq n$. Therefore, as $x_n \to 0$, the numerator must go to zero while the denominator contains a non-vanishing term inside the region of integration.

$$|\gamma| = \frac{2b_{01}b_{12}\dots b_{n,n+1}}{\sum^{1,2,3,\dots n}} = 2\left(\frac{1}{\frac{1}{b_{01}}+\frac{1}{b_{12}}+\frac{1}{b_{23}}+\dots+\frac{1}{b_{n,n+1}}}\right).$$

We must therefore minimize

$$\frac{\mu^2}{4\sin^2\frac{1}{2}\theta}x_n\left(\frac{1}{b_{01}}+\frac{1}{b_{12}}+\dots+\frac{1}{b_{n,n+1}}\right).$$

It is evident that the minimum of this expression occurs when the interval from 0 to x_n is split into $n+1$ equal parts each of length $x_n/(n+1)$. Therefore†

$$-k^2_{\min} = \left(\frac{\mu(n+1)}{2\sin\frac{1}{2}\theta}\right)^2.$$

4) $f_n^{\mathrm{p}} \underset{|k^2|\to\infty}{\to} 0$

Write $k^2 = \rho e^{i\phi}$ and $\mathrm{d}x = \mathrm{d}x_1 \dots \mathrm{d}x_{2n}/(a'_1 \dots a'_n)$. First split the domain of the x integration into two parts, one of which, the region δ, is defined by

$$|F_\theta| < \varepsilon\mu^2 x_n$$

and the rest is the region $(\Gamma-\delta)$. Then,

$$\frac{f_n^{\mathrm{p}}}{A_n} = \int_\delta \mathrm{d}x \frac{1}{(-k^2F_\theta+\mu^2x_n)^{\frac{1}{2}n+1}} + \int_{\Gamma-\delta}\mathrm{d}x\frac{1}{(-k^2F_\theta+\mu^2x_n)^{\frac{1}{2}n+1}}$$
$$= I_\delta + I_{M-\delta}.$$

Maximizing the integrand in I_δ as a function of F we can write

$$I_\delta \leqq \left(\frac{1}{\sin\phi}\right)^{\frac{1}{2}n+1}\int_\delta \mathrm{d}x\left(\frac{1}{\mu^2x_n}\right)^{\frac{1}{2}n+1}.$$

Letting $\rho\to\infty$, we can write for the second region

$$I_{\Gamma-\delta} \leqq \left(\frac{1}{\rho\varepsilon}\right)^{\frac{1}{2}n+1}\int_{\Gamma-\delta}\mathrm{d}x\left(\frac{1}{\mu^2x_n}\right)^{\frac{1}{2}n+1}.$$

Now,

$$\int \mathrm{d}x\left(\frac{1}{\mu^2x_n}\right)^{\frac{1}{2}n+1} = \frac{f_n^{\mathrm{p}}(k^2=0)}{A_n} < \infty.$$

Therefore,

a) choose ε so that $I_\delta < \frac{1}{2}\eta$,

b) choose ρ so that $I_{\Gamma-\delta} < \frac{1}{2}\eta$,

and hence $I < \eta$, $\rho > \rho(\eta)$.

It will be noticed that this proof only holds for $\sin\phi \neq 0$. However, for $\phi = 0$, one sees from the coordinate representation that $f_n^{\mathrm{c}} \to 0$ as $\rho\to\infty$

† Notice that we have just set an upper limit to the start of the cut. We speak in the text of the cut actually starting there since in the lowest order terms it is true.

owing to the rapid oscillation of the exponentials [1]). Also, noting from the form of f_n^{p} that we can relate the integrals for complex k^2 to the integrals for complex μ^2 and real k, and that if we make μ^2 complex we can still go from the coordinate to the parametric representations, we conclude again that the integrand of f_n^{c} will oscillate and f_n^{c} tend to zero as $k^2 \to -\infty$ along the negative axis. Therefore, $f_n^{\mathrm{p}} \to 0$ as $\rho \to \infty$.

Appendix 2

2.1. PROOF OF

$$I_1 \equiv \int_0^\infty \frac{\mathrm{d}\mathbf{z}}{|\mathbf{x}-\mathbf{z}|} f(z) \leqq 4\pi \int_0^\infty z\mathrm{d}z|f(z)|.$$

We have

$$I_1 = 2\pi \left[\int_0^x \frac{z^2 \mathrm{d}z \sin\theta \,\mathrm{d}\theta}{|\mathbf{x}-\mathbf{z}|} f(z) + \int_x^\infty \frac{z^2 \mathrm{d}z \sin\theta \,\mathrm{d}\theta}{|\mathbf{x}-\mathbf{z}|} f(z) \right].$$

Let

$$u^2 = |\mathbf{x}-\mathbf{z}|^2 = x^2+z^2-2xz\cos\theta,$$

$$u\mathrm{d}u = xz \sin\theta \,\mathrm{d}\theta.$$

The limits for u are $x+z \geqq u \geqq |x-z|$, and

$$I_1 = 2\pi \left[\int_0^x \frac{zf(z)\mathrm{d}z}{x} \int_{x-z}^{x+z} \mathrm{d}u + \int_x^\infty \frac{zf(z)\mathrm{d}z}{x} \int_{z-x}^{z+x} \mathrm{d}u \right]$$

$$= 4\pi \left[\int_0^x \frac{z}{x} zf(z)\mathrm{d}z + \int_x^\infty zf(z)\mathrm{d}z \right].$$

Therefore,

$$I_1 \leqq 4\pi \int_0^\infty z\mathrm{d}z|f(z)|.$$

2.2. PROOF OF

$$I_2 \equiv \int_0^\infty \frac{\mathrm{d}\mathbf{z}}{|\mathbf{x}-\mathbf{z}|} \mathrm{e}^{-b|\mathbf{x}-\mathbf{z}|} \frac{\mathrm{e}^{-\mu z}}{z} \mathrm{e}^{bz} = \frac{4\pi}{\mu} \mathrm{e}^{(b-\mu)x} \left[\frac{1-\mathrm{e}^{-(2b-\mu)x}}{(2b-\mu)x} \right].$$

Use the same transformation to the variable u as above. Then,

$$I_2 = \frac{2\pi}{x} \left[\int_0^x \mathrm{d}z \mathrm{e}^{(b-\mu)z} \int_{x-z}^{x+z} \mathrm{e}^{-bu} \mathrm{d}\mu + \int_x^\infty \mathrm{d}z \mathrm{e}^{(b-\mu)z} \int_{z-x}^{z+x} \mathrm{e}^{-bu} \mathrm{d}u \right]$$

$$= \frac{4\pi}{\mu} \mathrm{e}^{(b-\mu)x} \left[\frac{1-\mathrm{e}^{-(2b-\mu)x}}{(2b-\mu)x} \right].$$

References

1) N. N. Khuri, Phys. Rev. **107** (1957) 1148
2) R. Jost, unpublished
3) J. Hamilton, preprint
4) S. Mandelstam, Phys. Rev. **112** (1958) 1344
5) R. Jost and A. Pais, Phys. Rev. **82** (1951) 840
6) E. C. Titchmarsh, The Theory of Functions, 2nd. Ed. (Oxford University Press, 1939) p. 99
7) A. Besicovitch, Almost Periodic Functions (Dover Publications, 1954) p. 134
8) M. Cini, S. Fubini and A. Stanghellini, preprint
9) S. T. Ma, Phys. Rev. **69** (1946) 668
10) J. M. Jauch and F. Rohrlich, The Theory of Photons and Electrons (Addison-Wesley Cambridge, Mass., 1955) p. 454

1.D.2:
1.E.1:
3.A

Nuclear Physics **12** (1959) 389—412; © *North-Holland Publishing Co., Amsterdam*

Not to be reproduced by photoprint or microfilm without written permission from the publisher

LEVELS IN Gd^{156} EXCITED IN THE DECAY OF 5.6 d Tb^{156}

P. GREGERS HANSEN †, O. B. NIELSEN and R. K. SHELINE ††

Institute for Theoretical Physics, University of Copenhagen

Received 27 April 1959

Abstract: The decay of 5.6 day Tb^{156} has been studied by means of a six gap β-ray spectrometer, scintillation spectrometers, and coincidence techniques. Conversion electron and γ-ray coincidence measurements have been used extensively for obtaining quantitative estimates of γ-ray intensities.

A description of the electronic equipment is given, including a scaler and gate unit, which improves the performance of a relatively slow ($\tau = 700$ μsec) multichannel analyzer.

24 transitions are assigned to Tb^{156}. Multipole orders are given in most cases. The following levels are proposed and their quantum numbers (K, I, π) given in parenthesis: 89 keV (0, 2^+), 199 keV (0, 4^+), 584 keV (0, 6^+) 1126 keV (tentative), 1152 keV (2, 2^+), 1246 keV (2, 3^+), 1507 keV (4, 4^+), 1620 keV (4, 5^+), 1931 keV (3^-), and 2042 keV (4^-). Violation of K-selection rules and significant deviations from the expected branching ratios for transitions to a rotational band are observed. These features are discussed in terms of a probable mixing of the rotational bands.

CONTENTS

1. Introduction 390

2. Experimental technique 391

2.1. SOURCE PREPARATION 391

2.2. THE β-RAY SPECTROMETER 391

2.3. THE ELECTRONIC EQUIPMENT 391

3. Experimental data 392

3.1. INTERNAL CONVERSION LINES 392

3.2. γ-RAY SPECTRUM 393

3.3. INTERNAL CONVERSION LINE AND γ-RAY COINCIDENCE MEASUREMENTS 393

4. The decay scheme 399

5. Multipole orders and intensities 402

5.1. K/L RATIOS 402

5.2. CONVERSION COEFFICIENTS BASED ON γ-RAY INTENSITIES FROM THE SINGLE γ-RAY SPECTRUM 403

† Permanent address: Danish Atomic Energy Commission, Risø pr. Roskilde, Denmark.

†† Permanent address: Department of Chemistry, Florida State University, Tallahassee, Florida.

5.3. γ-RAY INTENSITIES FROM COINCIDENCE EXPERIMENTS 404
a) *The* 113 *and* 422 keV *transitions* 404
b) *The γ-rays from the* 1152, 1246, 1507, *and* 1620 keV *levels* 404
6. The level scheme 406
7. Discussion 409

1. Introduction

A 5.2 day period was assigned to Tb^{156} by Handley and Lyon [1]). Mihelich *et al.* [2]) have studied the low energy conversion-line spectrum and established transitions from the 2^+ and 4^+ states and, tentatively, from the 6^+ state in the ground-state rotational band. The γ-ray spectrum contains numerous high energy lines [3,4]), but only little was known of the pattern of the disintegration. Recently, Ofer has proposed a decay scheme similar to the present work [5,6]).

Obviously, a closer study of the high energy levels in Gd^{156} is desirable as a contribution to the systematic collection of experimental information on deformed even nuclei. The excited levels belong to rotational bands which are characterized by a K-quantum number equal to the projection of the angular momentum on the nuclear symmetry axis. The assignment of the K-quantum number has generally been made on the basis of the branching of γ-transitions to different levels in rotational bands of lower energy, since these branching ratios can be calculated for every value of K with the assumption that K is a good quantum number, e.g., that no mixing of states with different K takes place [7]). Although the observed branching ratios in most cases agree well enough with the theoretical to point unambiguously to a definite value of K, deviations greater than the experimental uncertainty have been observed. It is natural to investigate whether the actual branching ratios can be understood as a result of the coupling of the rotational bands due to the Coriolis force.

The decay of Tb^{156} turned out to be exceptionally suited for the study of branching ratios. Relatively strong, carrier-free sources almost pure in Tb^{156} could be produced by the (α, n) reaction on Eu^{153} and subsequent chemical separation, and the half-life of 5.6 days is favourable for e—γ coincidence measurements. Furthermore, although a large number of transitions were observed, they could in almost every case be placed into the decay scheme without ambiguity, and the conditions for quantitative measurements were good.

2. Experimental technique

2.1. SOURCE PREPARATION

Separated samples of Eu^{153} were supplied by the Oak Ridge National Laboratory. The cyclotron targets and β-ray sources were prepared by the general technique described elsewhere [8, 9, 10]). A bombardment with about 20 μA α-particles of $\approx$ 20 MeV in the Copenhagen cyclotron produced about 10 μC Tb^{156} per hour. The target material contained a few per cent of Eu^{151}, but the Tb^{154} activities caused no difficulties due to the shorter half-lives ($\approx$ 17 and $\approx$ 12 h). More troublesome was the amount of 5.6 day Tb^{155}, which was formed in the (α, 2n) reaction with an intensity of about 10 % of Tb^{156}. The conversion lines of Tb^{155} are known from the work of Mihelich *et al.*, and they could also be recognized by their coincidence relations, but a few of them could not be resolved from lines in Tb^{156} and thus complicated the quantitative measurements.

2.2. THE β-RAY SPECTROMETER

The measurements were performed in a six-gap spectrometer, which is essentially an enlarged version of one constructed earlier [10]). With the linear dimensions doubled, it covers β-ray energies until 4 MeV with a power consumption of 1.5 kW. The measurements were performed with sources of an area of about 3×6 mm^2, and a resolution of $\approx$ 1.3 % was obtained with a transmission of $\approx$ 9 %.

2.3. THE ELECTRONIC EQUIPMENT

The source and the focus are situated in regions outside the magnetic field in the six-gap spectrometer, and photomuliplier tubes can thus be used without light pipes. Consequently, the large transmission of the spectrometer can be favourably utilized for β—γ and e—γ coincidence experiments. In the actual measurements, a $1.5'' \times 1.5''$ NaI crystal was placed about 5 mm above the source for recording the γ-rays. In some cases, a $3'' \times 3''$ crystal was employed.

The 100-channel kicksorter is of the Wilkinson type, developed in Harwell and manufactured by Philips in England. This analyzer is relatively slow, the dead time being 700 μs and the maximum counting rate about 500 per second. This speed is large enough for the recording of coincidence spectra, but insufficient for the counting rate in the single γ-ray channel which necessarily was high in the coincidence measurements, generally between 20 000 and 80 000 per second. In order to utilize the multichannel for recording the single spectra without changing the geometry, a scaling circuit (block diagram fig. 1) was introduced, which reduced the number of pulses from the gate to the input of the analyzer by a variable factor 2, 4, 8 . . . 64. The scaler is a slightly modified binary unit, which is triggered by all γ-ray

pulses above the level of the discriminator. In addition to decreasing the counting rate to a level acceptable for the kicksorter, the scaler reduces the effective dead time in the manner well known from a mechanical register preceded by a fast scaler. By this mode of operation, the slowness of the multichannel is no serious inconvenience, and a γ-ray spectrum containing 10^5 counts can still be obtained in about three minutes.

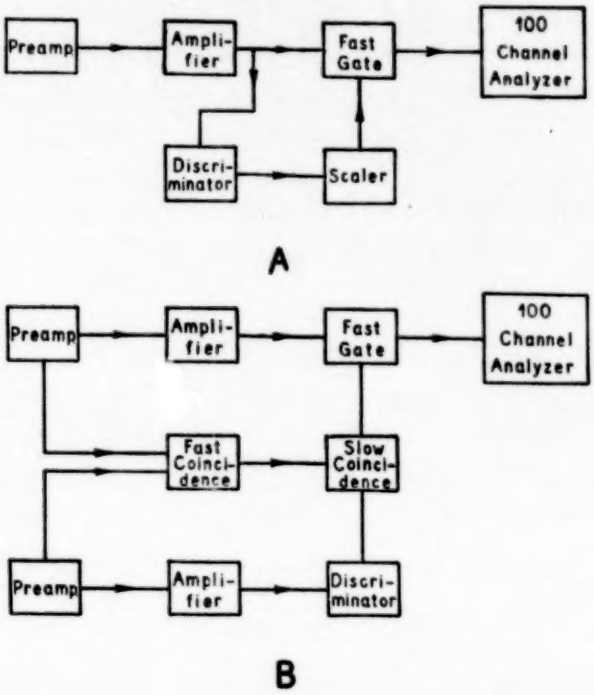

Fig. 1. Block diagram of electronic set-up. A: Single γ-ray spectrum. B: e—γ coincidence measurement.

3. Experimental data

3.1. INTERNAL CONVERSION LINES

The conversion-line spectrum was studied from 30 keV to 2600 keV electron energy. 57 conversion lines were observed, of which 45 were assigned to 24 transitions taking place in Gd^{156}. The remaining 12 were due to the decay of Tb^{154} and Tb^{155}. The complexity of the spectrum is illustrated by fig. 2, which shows the high energy part. The observed energies and intensities are listed in table 1.

During the procedure of establishing the decay scheme it became evident that the line 1102 was double, containing contributions from the K-conversion lines of transitions of 1152 and 1157 keV. A measurement with a resolution of 0.5 % was then performed and, although the line was not resolved completely, the shape clearly revealed two components with a relative intensity of 2 : 1.

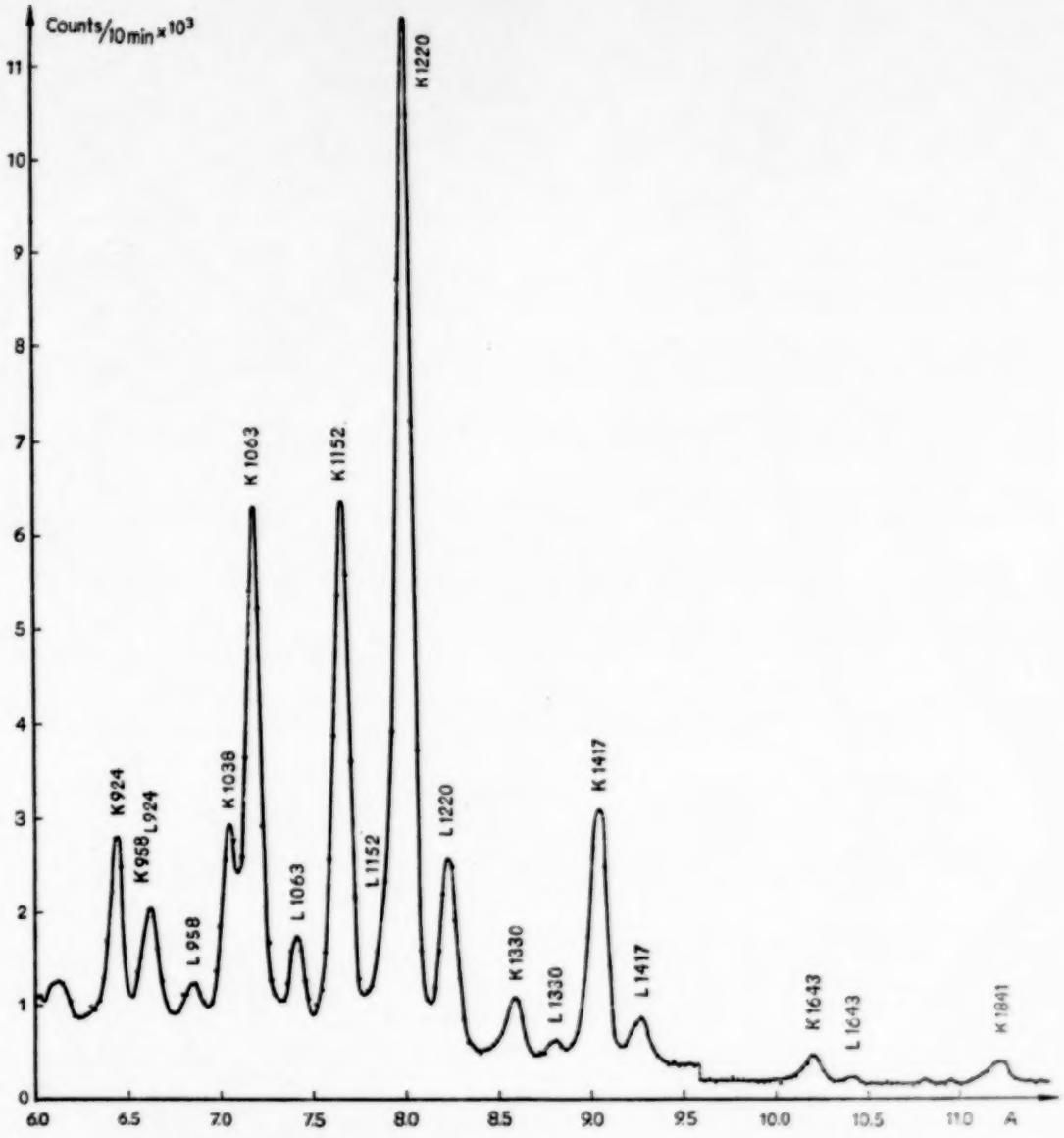

Fig. 2. High energy conversion-line spectrum.

3.2. γ-RAY SPECTRUM

The large number of γ-rays indicated by the conversion-line spectrum could, of course, not be resolved in a scintillation spectrometer (fig. 3 and fig. 4). Pronounced lines were observed, however, at 45 (K X-ray), 90, 200, 260, 350, 530, 1200, 1400, 1650, 1850, and $\approx$ 1980 keV. Table 4 lists energies and intensities of the major γ-rays as measured with the 3″ dia × 3″ NaI-crystal.

3.3. INTERNAL CONVERSION LINE — γ-RAY COINCIDENCE MEASUREMENTS

Conversion lines succeeding orbital electron capture are not disturbed by a continuous β-ray background and, accordingly, the conditions for coinci-

TABLE 1

Energies and relative intensities of internal conversion lines

Electron energy	Assignment	Absolute intensity	Data of Mihelich *et al.* [b]	
			Ass.	Intensity
39	K 89	22.1[a]	K 89.10	16.5
63	K 113	1.4	K 111.9	1.65
81	L 89	33.8	L 89.10	29.4
87	M, N 89	11.2	M, N 89.10	8.8
105	L 113	0.71[b]	L 111.9	0.32
149	K 199	5.9	K 199.4	(5.9)
192	L 199	1.88	L 199.4	2.18
197	M, N 199	0.82	M, N 199.4	0.82
210	K 261	0.30 [b]	K 262.7	0.41
246	K 296	0.218	K 296.7	0.212
254	L 261		L 262.7	weak
261	M 261			
289	L 296	0.065		
305	K 355	0.29	K 356.6	weak
331	K 381	0.013		
348	L, M 355	0.082		
372	K 422	0.038	K 422.2	weak
415	L, M 422	0.0071		
484	K 534	0.206		
526	L, M 534	0.036		
728	K 778	0.0035		
772	L, M 778	0.00071		
794	K 844	0.0012		
816	K 866	0.0016		
874	K 924	0.0077		
907	K 958[c]	0.0030		
951	L, M 958			
988	K 1038[c]	0.0080		
1013	K 1063	0.023		
1056	L, M 1063	0.0065		
1102	K 1152	0.0017		
1107	K 1157	0.00085		
1145	L, M 1152			
1170	K 1220	0.041		
1211	L, M 1220	0.0094		
1280	K 1330	0.0028		
1323	L, M 1330	0.00071		
1367	K 1417	0.012		
1411	L, M 1417	0.0020		
1593	K 1643	0.0012		
1635	L, M 1643			
1791	K 1841	0.0011		
1940 – 1980	K 1990 – 2030	0.0004		

[a]) Intensity uncertain because of strong K Auger-lines.

[b]) Line unresolved from transitions of similar energy in Tb^{155}. The intensity estimate is from coincidence experiments described in the text.

[c]) Double line. See text.

The intensities are in per cent of all Tb^{156} decays. In order to facilitate comparison, the data of Mihelich *et al.* have been normalized with respect to K_{199}. We have failed to observe lines due to the 155.2 keV transition reported by these authors. The K-line probably contributes to the L_{113} peak.

dence experiments with the conversion electrons are extremely favourable The large transmission of the β-ray spectrometer implies that coincidence measurements involving strongly converted low-energy transitions can be performed almost with the efficiency of a $\gamma-\gamma$ coincidence experiment, but with the higher resolution and lower background of the magnetic spectrometer. Even the γ-ray spectra coincident with weak high-energy lines can be obtained in some cases, the time needed for the measurement being about one night.

The purpose of the e—γ-coincidence experiments was not only to yield information on the coincidence relations, but also quantitatively to establish branching ratios and intensities for the γ-rays. The quantitative measurements demand a knowledge of the efficiency of the coincidence setup. This

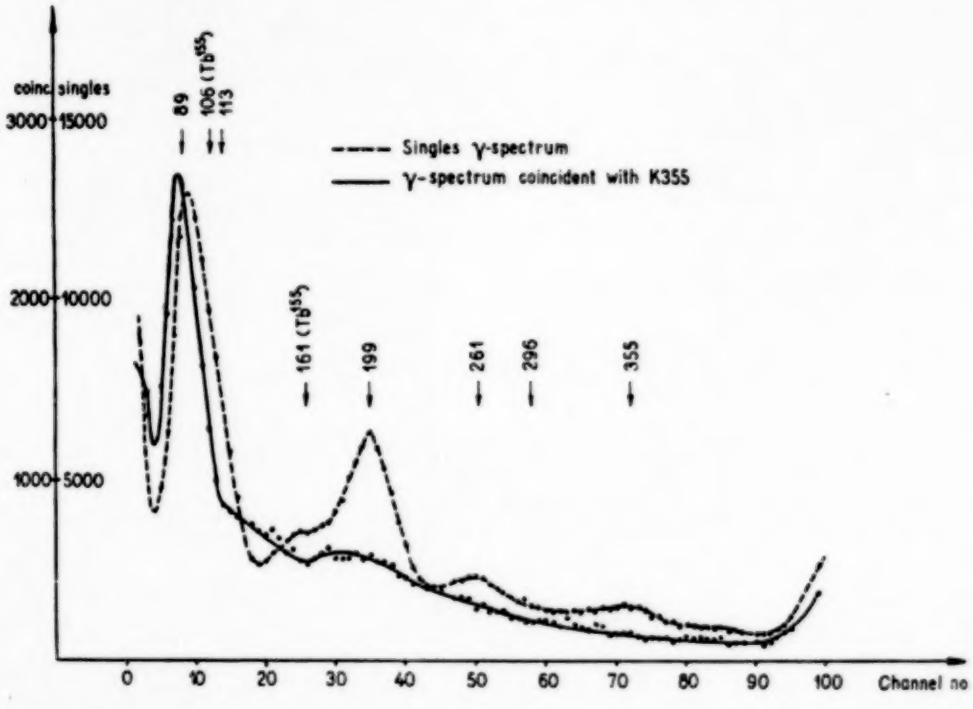

Fig. 3. Low energy γ-ray spectra, measured with a $1.5'' \times 1.5''$ NaI-crystal.

clearly depends on the geometry and on the intrinsic photopeak efficiency of the NaI-crystal. Let this energy-dependent efficiency η_E be defined as the ratio of the number of pulses recorded in the photopeak to the total number of photons of energy E emitted by the source, and let b denote the fraction of the conversion electrons which are accompanied by a transition of energy E. If η_E is known, the γ-ray spectrum coincident with the conversion line gives b, since

$$\eta_E = \frac{C_\gamma f}{C_e b},$$

C_γ being the number of events in the photopeak of the γ-ray, C_e the number of conversion electrons counted simultaneously, and f the correction for internal conversion of the γ-ray.

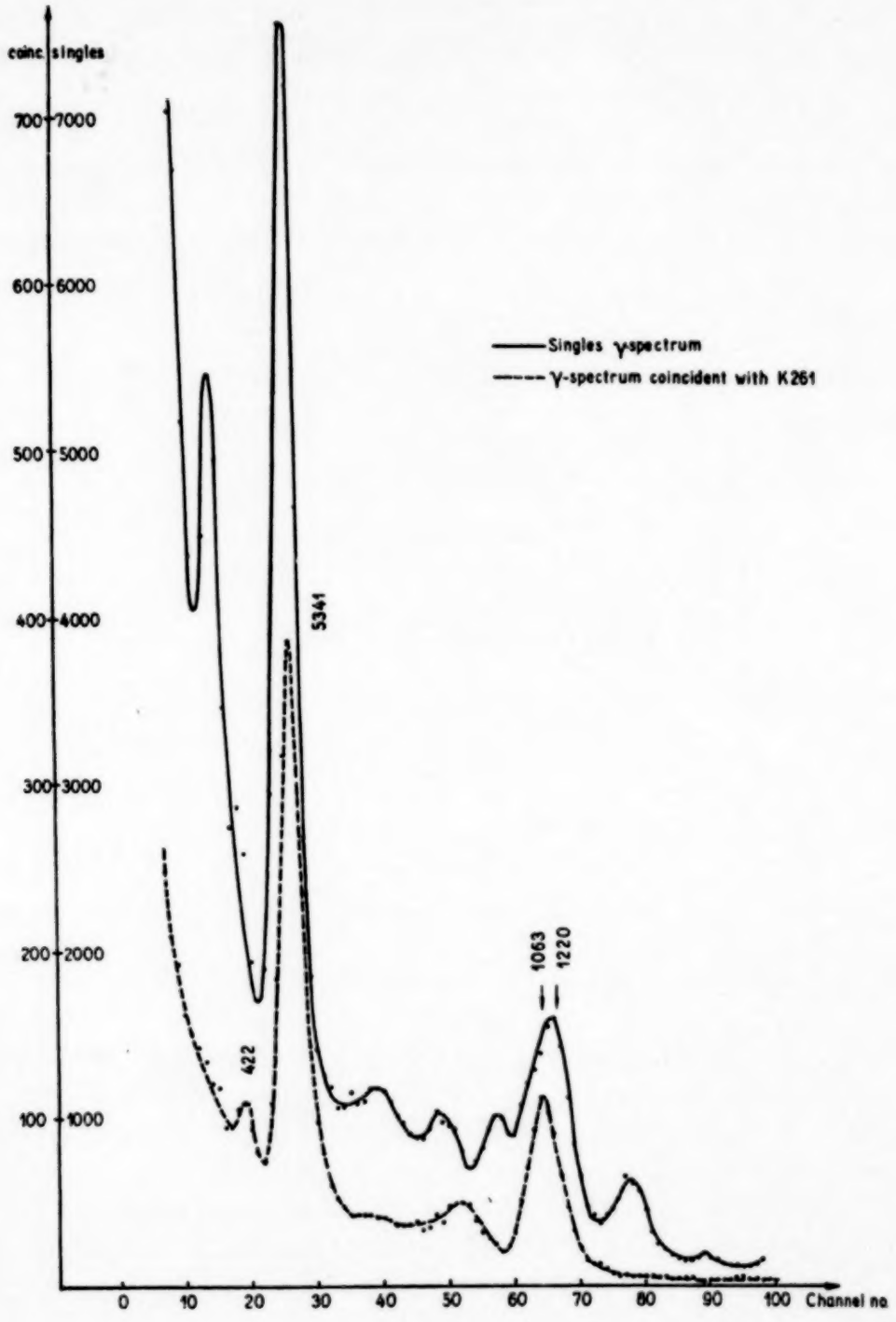

Fig. 4. High energy γ-ray spectra, measured with a 3″×3″ NaI-crystal.

The evaluation of η_E implies a calibration of the setup with sources of known strength or by coincidence methods. It turned out that the Tb^{156} activity under investigation was suited for the latter purpose, since the decay scheme could be found from a qualitative treatment of the coincidence data, and the intensities of the major conversion lines and γ-rays were known from other types of experiments (sections 4 and 5). η_E could accordingly by evaluated in a first approximation for the stronger γ-rays by using values of b calculated from tentative estimates of the strengths of the weaker transitions. These η_E values were in turn used for determining more accurate intensities for the weaker γ-rays, and the final η_E (fig. 5) could now be obtained in a second treatment which, however, did not change the result very much.

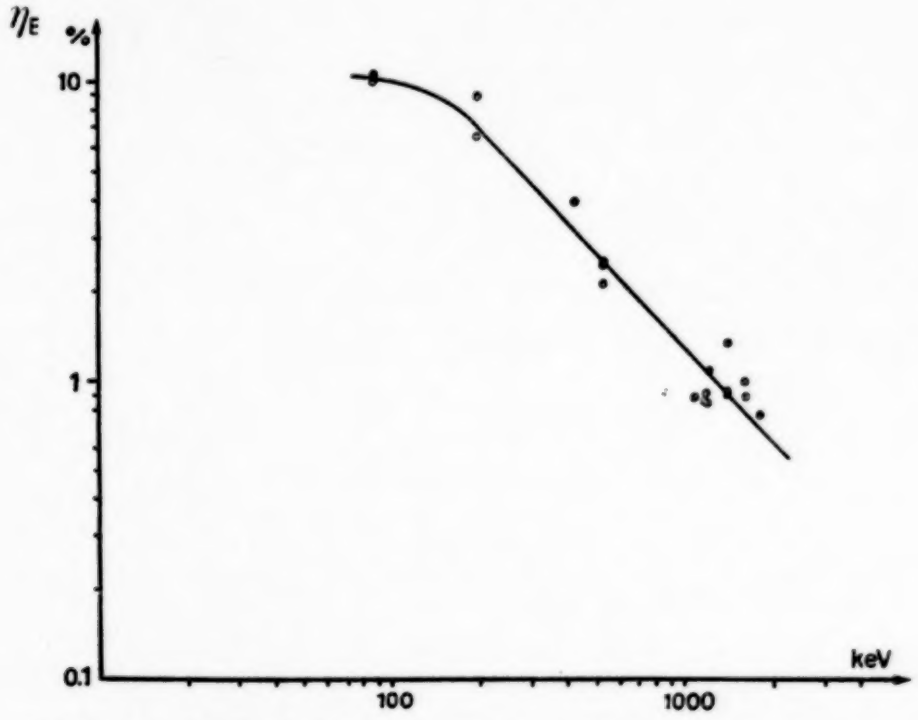

Fig. 5. Coincidence efficiency η_E as a function of the γ-ray energy. NaI crystal 1.5″×1.5″.

The results of e—γ-coincidence experiments are summarized in table 2. The numbers quoted in parentheses after the energies of the coincident γ-rays are the coincidence frequencies b in per cent. A typical coincident spectrum is shown in fig. 4.

The method is subject to several sources of error, of which random coincidences and dead time losses are dependent on the source strength. The resolving time of the fast coincidence stage was 2×10^{-7} sec, and the number of randoms was not negligible at high counting rates. Also the dead time correction could amount to as much as 10 %, since each pulse blocked the

circuit in about 2 μsec. For these reasons, some of the more crucial experiments were repeated with weaker sources.

TABLE 2

Internal conversion line–γ-ray coincidences

Selected event	Coincident γ-rays Coincidence frequencies are quoted in parenthesis	Remarks
L 89	115, 200, 260, 360, 420, 530 (65) 1200 (30) 1400 (14) 1650, 1850 (4.3)	
K 113	90, 200, 260, 360, 420 (100) 1200, 1400	Not coincident with the 1643 and 1841 keV transitions
K 199	90, 300, 420 (14) 530 (72) 920 (10) 1200 (58) 1650 (9)	
K 261	90, 200 (23) 530, 960 (18) 1160 (76)	The coincidence frequencies have been corrected for the Tb^{155} contribution to K 261
K 296	90, 200, 420 (21) 530 (50) 920 (66) 1040 (32)	
K 355	90, (53) 200 (3+1) 420 (10) 530 (94) 1100 (98)	
K 381	90, 200, 530, 850, 1050	The relative intensities of the 199, 850, and 1050 keV transitions are 1 : 1 : 3
K 422	90, 115, 200, 1040 (50) 1340 (50)	
K 534	90, 200, 260, 360, 1200, 1400	
K 1038	200, 300, 400	Poor statistics. 400 keV line broad. (Probably 381+422)
K 1063	90, 360 (51) 530	
K 1152+1157	90, 260 (30) 360 (30) 530 (60)	
K 1220	90, 200, 530	

Coincidence frequencies are in per cent of the number of conversion electrons. Correction for internal conversion has been applied.

The solid angle subtended by the γ-counter was about 10 %, and therefore sum lines appeared frequently. However, the identification was not difficult, but the effect contributed significantly to the experimental uncertainty. In principle, errors could furthermore be introduced by angular correlations between conversion electrons and γ-rays, but these were necessarily small because of the large range of angles between γ-rays and conversion electrons which are utilized in the setup.

If, in addition, the uncertainties which normally attach to the quantitative analysis of scintillation spectra are taken into account, the coincidence frequencies in table 2 can be considered accurate to within 20—30 %, depending on the actual experimental conditions. This estimate is confirmed by the scatter of the points in fig. 2. Relative intensities, of course, are found with much better accuracy.

4. The Decay Scheme

The energies, as well as the high intensities and the E2 nature (section 5), unambiguously assign the 199 keV and 89 keV transitions as the 4^+—2^+—0^+

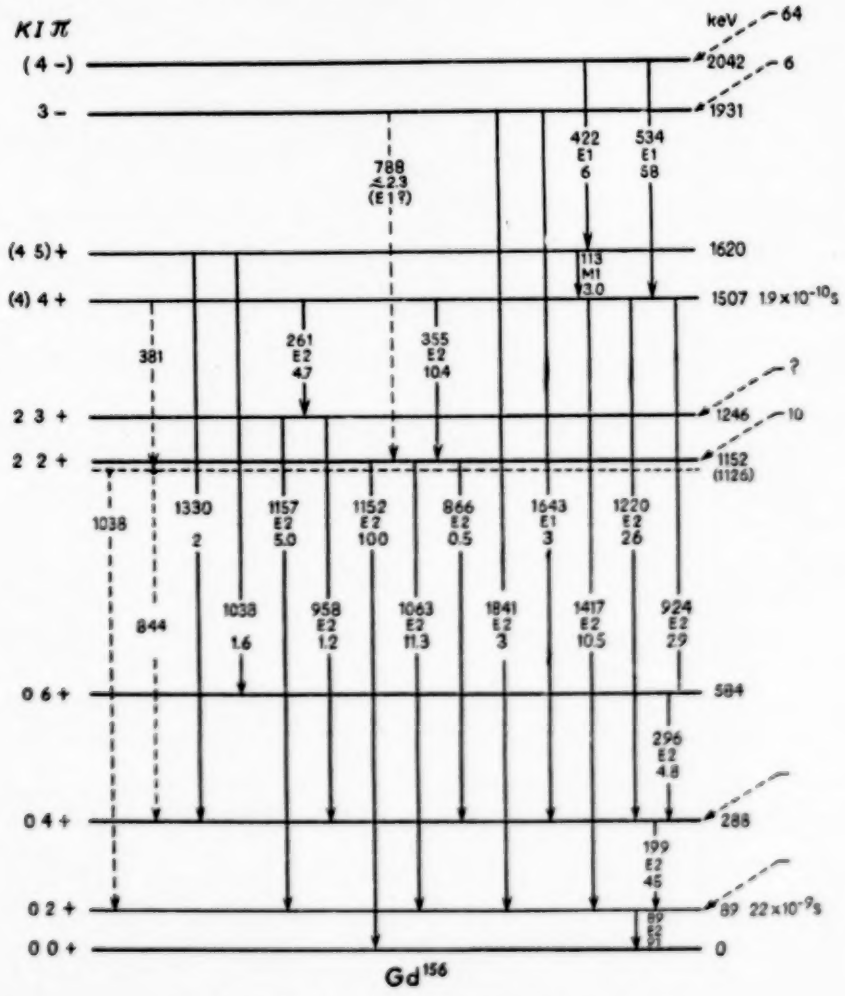

Fig. 6. The decay scheme $Tb^{156} \rightarrow Gd^{156}$.
The transitions are labelled with the energy in keV, the predominant multipole order when known, and the intensity in per cent of all K-capture decays.

cascade in the ground-state rotational band, as shown earlier by Mihelich *et al.* [2]). This interpretation is also confirmed by numerous coincidence experiments.

In the single γ-ray spectrum and in the spectrum coincident with the 89 keV conversion lines, prominent γ-ray peaks of $\approx$ 1200, $\approx$ 1400, $\approx$ 1640 and $\approx$ 1840 stand out. Only the $\approx$ 1200 and $\approx$ 1640 keV lines appear in coincidence with the 199 keV transition (table 2). These relations, in connection with the energy fit obtained by using the more accurate conversion-line energies of table 1, establish levels at 1507 and 1931 keV.

The strong 534 keV transition is coincident with the 1200 and 1400 keV γ-rays from the 1507 keV level. The intensity shows that it is the main source of excitations of this level, and it must thus originate in a level at 2042 keV. The coincidence between the 534 and 1220 keV transitions was further confirmed by the γ-ray spectrum coincident with the line K_{1220}.

The 113 and 422 keV transitions are coincident with each other, but, unlike almost all other transitions in table 2, not with the 534 keV transition. They thus form a cascade with 534 keV as a cross-over. The intermediate level could be identical with the above mentioned 1931 keV level, but this assumption was disproved by the fact that the 113 keV transition was not coincident with the 1643 and 1841 keV γ-rays, and furthermore by the pronounced dissimilarity of the γ-spectra coincident with the 422 and 534 keV conversion lines. On the other hand, the similarity of the spectra coincident with the 113 and 534 keV transitions suggests that these feed the same level. The intermediate level must thus be placed at 1620 keV, and the 113 keV transition can only partly account for the de-excitation of the level. This is confirmed by the information in table 2 that the 422 keV line is strongly coincident with γ-rays of 1040 and 1340 keV. Assuming the latter transition to be identical with the 1330 keV transition observed in the conversion-line spectrum, the energy fits accurately between the 1620 and 288 keV levels.

On the basis of energy systematics the 295 keV transition has earlier [3]) been suggested as the transition from a 583 keV to the 4^+ state in the ground-state band. This position is completely in agreement with the coincidence relations. The conversion line was strongly coincident with the 89 and 199 keV γ-rays, and furthermore with two rays $\approx$ 920 and $\approx$ 1040 keV. A 1040 keV γ-ray is thus observed in coincidence with the 422 as well as with the 295 keV conversion lines, and it can safely be placed between the 1620 and 583 keV levels. A close energy fit is obtained by using the more accurate energy 1038 keV from the conversion-line measurement, and further support comes from the coincident spectrum of the K_{1038} line which contained γ-rays $\approx$ 300 and $\approx$ 400 keV. The 920 keV γ-ray in coincidence with K_{295} probably corresponds to the conversion line K_{924}, which closely reflects the energy difference between the 1507 and 583 keV levels.

The 355 keV transition is coincident with the 534 keV, but not with the 1220 keV ray, and must thus be placed below the 1507 keV level. If it feeds a

level at 1152 keV from the 1507 keV state, this level could decay to the ground state and to the 89 keV level with the 1152 and 1063 keV transitions, which were observed in the conversion-line spectrum and not included in the decay scheme until now. The coincidence spectrum of K_{355} agrees with this assumption. Since the 199 keV γ-ray also appears weakly in this spectrum, the 1152 keV level must also decay to the 288 keV level with a γ-ray, which is probably represented by the conversion line K_{866}. This assumption is not inconsistent with the fact that only the 199, and not the 866, keV γ-rays were observed in the coincident spectrum, since a weak low-energy γ-peak stands up more distinctly in a scintillation spectrum than a high-energy line of the same intensity.

The 1152 keV level decays to the 0^+, 2^+, and 4^+ levels in the ground-state rotational band with γ-rays which are of E2 nature (see next section.) The spin is thus 2^+, and since the energy spacings in rotational bands are similar for states with the spin sequences 0—2 and 2—3, provided that the moments of inertia are the same, a level with spin 3 is expected $\approx$ 90 keV above the 1152 keV state. This level, at 1246 keV, seems to be populated from the 1507 keV state by the 261 keV transition and to decay to 288 keV and 89 keV with transitions of 958 and 1157 keV (table 2).

All transitions represented by the stronger conversion lines have now been included in the decay scheme with almost no ambiguity. Still, a weak line with an energy of 331 keV was observed. It could be either an L-line, in which case the K-line would be hidden below the line L_{296}, or it could be a K-line with the corresponding L-line below K_{422}. A 340.8 keV transition has been reported by Ward *et al.* [12]) in the decay of Tb^{155}. As, however, the line turned out to be clearly coincident with high energy γ-rays (table 2), at least a considerable fraction of it must belong to Tb^{156}. The coincidence relations are very similar to those of the 261 and 355 keV lines and suggest that the weak transition has its origin in the 1507 keV level, and that it is followed by two transitions 850 and 1050 keV to the 288 and 89 keV levels. The γ-ray energies are hardly determined accurately enough for an unambiguous identification of the corresponding conversion lines, but there is some evidence that the 1038 keV K-conversion line is double (section 5), and a weak conversion line corresponding to a transition energy of 844 keV has also been observed. Assuming these more accurate energies for the two γ-rays, a good energy fit is obtained if the 331 keV line is the K-line of a 381 keV transition feeding a level at 1126 keV. Additional, though not conclusive evidence came from the γ-ray spectrum coincident with the 1038 keV conversion line. A broad peak at 400 keV was observed, probably indicating the presence of a 381 and a 422 keV γ-ray, but the statistics was not sufficient for an analysis of the shape of the line. The 1126 keV level is thus still tentative.

Also a weak conversion line corresponding to the K-line of a 778 keV transition was observed. On the basis of the energy it has been placed tentatively between the 1931 and the 1152 keV levels.

A broad peak in the conversion-line spectrum indicated at least 2 or 3 transitions of 1990—2030 keV, which probably originates in levels above the 2042 keV state, since they appear coincident with the 89 keV transition.

5. Multipole Orders and Intensities

5.1. K/L RATIOS

Table 3 lists the cases in which the K/L ratios could be used for assigning multipole orders. The E2 nature is confirmed for the three transitions between levels in the ground-state rotational band. The conversion lines of the 261 keV transition are not resolved from the lines of a transition of similar energy taking place in the decay of Tb^{155}. Since there are no high energy γ-rays from Tb^{155}, the components of the lines belonging to Tb^{156} could be recorded in coincidence with high energy γ-rays, which were selected by integral bias discrimination.

TABLE 3

K/L ratios

E_γ(keV)	Assignment	Experimental value	Theoretical value		
			E1	E2	M1
89	E2	0.65±0.15	6.7	0.83	7.0
113	M1	4.4 ±2 [a])	6.9	1.3	6.9
199	E2	3.1 ±0.3	6.9	2.9	7.0
261	E2	3.5 ±0.3 [a])	7.0	3.7	7.0
296	E2	3.4 ±0.7	7.1	4.1	7.1
355	E2	4.8 ±0.5	7.4	4.7	7.2
422	E1	7.1 ±0.7	7.4	5.2	7.2

[a]) See text (section 5) for details of measurement.

A similar difficulty was met in connection with the 113 keV transition. The intensities in table 1 indicate a K/L ratio of 2. As, however, the line L_{113} is likely to contain a contribution from a line K_{155} (see footnote d of table 1), the K/L ratio was determined by a coincidence experiment. The β-ray spectrometer was adjusted to select the peaks of the lines K_{113} and L_{113}, and the coincident γ-ray spectra were recorded. The K/L ratio was now estimated from the intensity of the 422 keV peaks appearing in the two spectra. The experimental value (4.4) is in good agreement with the data of Mihelich *et al.* [2]), indicating 5 (table 1). The transition is thus predominantly of dipole character; the assignment of M1 rather than E1 is made on the basis of the

K-conversion coefficient which will be discussed later. The E1 (rather than M1) nature of the 422 keV transition is also demanded by the conversion coefficient.

5.2. CONVERSION COEFFICIENTS BASED ON γ-RAY INTENSITIES FROM THE SINGLE γ-RAY SPECTRUM

The K-conversion coefficient of the 534 keV transition was found by comparison with a Cs^{137} source which was measured in identical geometries in a scintillation spectrometer and in the β-ray spectrometer. Assuming $\alpha_K = 0.095$ for the 662 keV transition in Ba^{137}, the 534 keV conversion coefficient was 0.0030, in agreement with the theoretical value 0.0035 for E1 multipole order.

TABLE 4
Transition intensities

E (keV)	Assignment	α_K theor.	I_K	I_γ singles	I_γ coinc.	I_γ calcul.
89	E2	1.70	3.31			19
113	M1 +E2	1.20 0.88	1.4		1.5 [a])	1.2
199	E2	0.155	5.9	43		37
261	E2	0.070	0.30			4.3
296	E2	0.048	0.22			4.6
355	E2	0.029	0.29	11		10.0
381			0.013			
422	E1	0.0061	0.038	5		6
534	E1	0.0035	0.202	(58)		58
778	(E1?)	≈0.0015	0.0035			≲2.3
844			0.0012			
866	E2	0.0033	0.0016		0.6∓ 0.2	0.48
924	E2	0.0027	0.0077		3.3	2.9
958	E2 or M1	0.0025 0.0046	0.0030		0.9	≈1.2 ≈0.6
1038 [a])	E2 or M1	0.0023 0.0037	0.0080		1.6	
1063	E2	0.00205	0.023		10.5	11.2
1152	E2	0.00174	0.017	46	9	9.8
1157	E2	0.00174	0.0085		4.0	5.0
1220	E2	0.00155	0.041		27	26
1330	E2 or M1	0.0014 0.0021	0.0028	14	1.6	2 1.3
1417	E2	0.00115	0.012		12.5	10.5
1643	E2	0.00042	0.0012	4	4	3
1841	E1	0.00036	0.0011	4	4	3
1990-2030	(E1)	0.0003	0.0004	≈1	≈1	≈1

[a]) See experiments described in the text.

The γ-ray intensities in columns 5 and 6 are obtained from the single γ-ray spectrum and coincidence spectra, respectively. The intensities in column 7 are calculated on the basis of conversion-line intensities and theoretical conversion coefficients. The consistency of the multipole assignments is checked by comparing the experimental and the calculated γ-ray intensities. The intensities are given in per cent of all Tb^{156} decays.

Table 4 summarizes the data pertinent to the evaluation of conversion coefficients and transition intensities. The γ-ray intensities in column 5 are those with which some confidence could be deduced from the complicated single γ-ray spectrum. The γ-ray intensities are normalized relative to the conversion lines by assuming the theoretical E1-conversion coefficient for the 534 keV transition. The α_K's establish E1 nature for the 1643 and 1841 keV transitions, whereas the 1400 and 1200 keV γ-rays are mainly E2's.

5.3. γ-RAY INTENSITIES FROM COINCIDENCE EXPERIMENTS

a) *The* 113 *and* 422 keV *transitions*

A rough estimate of the K-conversion coefficient of the 113 keV transition was obtained in a γ—γ coincidence experiment, in which the low-energy spectrum coincident with γ's above 600 keV was recorded. This eliminates the 106 keV contribution from Tb^{155}, and since the 89 as well as the 113 transition on the average are coincident with one high energy γ-ray, the relative intensities of the two γ-rays in the coincident spectrum should approximately reflect the true ratio. The experimental value $\gamma_{89}/\gamma_{113} \approx 14$ corresponds to $\alpha_K = 1.4$ for the 113 keV transition, in agreement with the theoretical M1 value 1.2 (Theoretical E1 and E2: 0.19 and 0.88). Thus, whereas the 113 keV transition is largely of M1 character, considerable E2 admixtures cannot be excluded.

The 422 keV γ-ray is 100 % coincident with 113 keV, and its intensity is then higher than 3.5 % of all decays, which is the total intensity of the 113 keV transition (table 5). The conversion coefficient is thereby definitely lower than the value for M1, and since the K/L ratio indicates dipole nature, E1 is the only possible assignment.

b) *The γ-rays from the* 1152, 1246, 1507 *and* 1620 keV *levels*

The M1 or E2 nature of the 113, 261 and 355 keV transitions demonstrates that these four levels have the same parity, which must be even, since, for example, the 1152+1220 and 1330+1417 keV γ-rays are predominantly E2. Consequently, all transitions from these to the ground-state band are M1's, E2's or mixtures, the higher multipoles M3 and E4 being excluded for lifetime and other reasons. Since the transitions take place between low lying states in a deformed even nucleus, the E2 transition probability is presumably large, and the subsequent discussion thus deals with a possible M1 contribution, only. Unfortunately, the K-conversion coefficients for M1 and E2 differ by less than a factor of two in the energy region > 1 MeV, and α_K is thus not a very sensitive function of the M1 contribution.

The 1507 keV level decays to the 2^+, 4^+ and 6^+ states in the ground-state band. The only likely spin assignment is then 4^+, with at least the 924 and 1417 keV transitions being pure E2's. The E2 nature of the 1417 keV γ-ray is already indicated in table 4. The 924 keV γ-ray is about 70 % coincident

with the 296 keV conversion line and represents ≈ 3.3 % of all transitions. The K-conversion line in table 1 then corresponds to a conversion coefficient of 0.0023, in agreement with the theoretical E2 value 0.0027. Since these two γ-rays connect states with a spin difference of two, their multipole orders must be considered pure, and the most accurate γ-ray intensities are probably calculated from the conversion line and the theoretical conversion coefficients. The 1220 keV transition can be admixed with M1 radiation. However, a good determination of the γ-ray is obtained from the γ-ray spectrum coincident with the line K_{199}. This spectrum is relatively simple, and the 1220 keV γ-ray corresponds to ≈ 60 % of the 199 keV transition, or ≈ 27 % of all decays, in good agreement with the value calculated on the basis of the conversion line and the theoretical E2 conversion coefficient (table 5).

The 1038 keV γ-ray to 584 keV from the 1620 keV level is ≈ 33 % coincident with K_{296}, and the corresponding intensity is 1.6 %. With the intensity of the line K_{1038} in table 1, a conversion coefficient $\alpha_K \approx 0.006$ is obtained. This is considerably higher than the theoretical values for E2 and M1 : 0.0023 and 0.0037, respectively. As mentioned in section 4, the conversion line is probably due partly to a second transition of 1038 keV proceeding from a 1126 keV to the 89 keV levels.

The 422 keV γ-ray, which represents 6 % of all decays, appears 100 % coincident with the 113 keV conversion lines, and is thus responsible for almost all excitations of the 1620 keV level.

This is de-excited with 3.5 % by the 113 keV and the above 1.5 % by the 1038 keV transitions. The amount ≈ 2 % left to the 1330 keV γ-ray is not known accurately enough to allow a distinction between M1 and E2 multipole orders.

The 1152 keV level decays to the 0^+, 2^+ and 4^+ levels in the ground-state band, suggesting the spin 2^+. If the weak 866 keV transition to the 4^+ level is considered doubtful, a 1^+ assignment would be an alternative, but this possibility is excluded by the conversion coefficient of the 1152 keV transition, which is definitely lower than the M1 value. The 89 keV conversion lines are coincident with all the γ-rays of the single spectrum except the 1152 keV line, and a good determination of this γ-ray was obtained by a subtraction of this coincidence spectrum from the single spectrum. The resulting intensity was 9 %, and since the 1157 keV γ-ray appearing in coincidence with 261 keV conversion lines is at least 4 %, the α_K for the composite 1152+1157 keV transition is $\lesssim 0.025/13 \approx 0.002$, in good agreement with the E2 value 0.0017. The relative intensities of the 1152, 1063, and 866 keV γ-rays are of considerable interest in the subsequent discussion of the branching ratios. The most accurate values were probably found from the γ-ray spectrum coincident with K_{355}. The 1152 and 1063 keV rays were

not completely resolved, but the 1063 keV was about 15 % more intense than the 1152 keV ray. The strength of the 866 keV γ-ray was determined from the peak due to the 199 keV γ-ray ,since

$$I_{866} = I_{199} = 3 \pm 1 \text{ per cent.}$$

These values are in good agreement with the results based on the conversion lines and the theoretical E2 conversion coefficients, and a predominant E2 nature is thus established for the 1063 as well as the 866 keV transitions.

The three transitions de-exciting the 1152 keV level amount together to $\approx$ 20 %, although the 355 keV transition feeding it represents $\approx$ 11 % only. The level is thus probably fed also by K-capture. This assumption was confirmed by the spectrum coincident with K_{1063}, in which the 355 keV γ-ray appeared only with 50 % efficiency compared to $\approx$ 100 % for the 89 keV γ-ray.

The 261 keV transition exciting the 1246 keV level represents $\approx$ 5 % of the decays. If the possibility of K-capture directly to the level is neglected, the 958 and 1157 keV γ-rays as indicated by the coincidence spectrum of K_{261} are $\approx$ 1 and $\approx$ 4 %, respectively. The shape of the conversion line corresponding to K_{958} revealed the presence of weak components of unknown origin, and the intensity in tables 1 and 4 represents an upper limit. The corresponding value of α_K is between M1 and E2, whereas the α_K for the 1157 keV transition points to a predominant E2 nature. A weak K-capture branch to the 1246 keV level would strengthen the E2 assignments, and as the spin of Tb^{156} is probably 3 (see next section), such a transition seems extremely likely. Considerable M1 admixtures in the γ-rays from the 1246 keV state are still not excluded experimentally.

No information on the multipole orders of the 381, 778, 844 and 1038 keV transitions is available. The proposed position in the decay scheme of the 778 keV transition implies E1 nature, and the corresponding γ-ray intensity, which must be an upper limit, is 2.3 %. The average conversion coefficient for the $\approx$ 2000 keV transitions corresponds to E1.

Information on the level scheme in Gd^{156} has been obtained also from the decay of Eu^{156} [13,14]). Ewan *et al.* reported levels at 89, 288, 1142, 1229, 1495, 1958, 2024 and 2183 keV. The levels of 1142 and 1229 keV apparently are identical with the states of 1152 and 1246 keV in fig. 6. The levels of higher energy seem not to be excited in the decay of Tb^{156}.

6. The Level Scheme

The energies of the levels in the ground-state rotational band are in the first approximation described by [15])

$$E = I(I+1)\frac{\hbar^2}{2\mathcal{I}},$$

I being the angular momentum of each state, and $\mathcal{I}$ the moment of inertia of the ground state. The value of $\mathcal{I}$ calculated from $E = 89$ keV for the 2^+ level corresponds to 297 and 623 keV for the 4^+ and 6^+ states. The correction to the above formula due to the rotational-vibrational interaction is of the order $I^2(I+1)^2$. Taking this term into account, the energy of the 6^+ level is calculated as 576 keV against the experimental 584 keV.

The branching ratios, reduced for the energy dependence, for the E2 transitions depopulating the 1152 keV 2^+ are given in table 5. Comparison with the theoretical values for different K-quantum numbers shows only reasonable agreement with $K = 2$, although the deviations seem definitely larger than the experimental uncertainty.

TABLE 5

Branching ratios from the 1152 and 1246 keV states

Reduced transition probabilities	Experimental values	Theoretical values		
		$K=0$	$K=1$	$K=2$
$\frac{B(2\to 4)}{B(2\to 2)}$	$\frac{0.48}{11.2}\times\left(\frac{1063}{866}\right)^5 = 0.12$	0.7	2.8	0.05
$\frac{B(2\to 0)}{B(2\to 2)}$	$\frac{9.8}{11.2}\times\left(\frac{1063}{1152}\right)^5 = 0.58$	1.8	3.2	0.7
$\frac{B(3\to 4)}{B(3\to 2)}$	$\frac{18}{76}\times\left(\frac{1157}{958}\right)^5 = 0.62$		2.5	0.40

The transitions are assumed to be pure E2's.

A rotational band, interpreted as a γ-vibration, with $K = 2$ and $I = 2^+$, 3^+ ... is regularly observed at about 1 MeV in deformed even nuclei [16]). As mentioned earlier, the 1246 keV level is probably the 3^+ state in this band. The energy spacing between the 2^+ and 3^+ states indicates that the moment of inertia is about 6 % larger than in the ground-state band. Assuming that the de-exciting γ-rays are of E2 nature, although this is not verified experimentally, the branching ratio is given in table 7. Only $K = 2$ yields an acceptable fit.

In addition to the γ-vibrational states, low lying levels with $K = 0$, $I = 0^+, 2^+, 4^+$ ... and $K = 0$, $I = 1^-, 3^-$ ... have been observed and interpreted as β and octupole vibrational states, respectively, in deformed even nuclei [16]). These bands have not been identified in Gd^{156}, although the possible 1126 keV level may represent one of them; but their existence is not excluded, as the excitation must be hindered by K-forbiddenness.

Bell and Jørgensen [19]) have measured a half-life of 1.88×10^{-10} sec for the 1507 keV 4^+ level. The K-quantum number is then probably 4, since levels with lower spin in the same rotational band would be strongly excited from a level with this half-life. The high energy E2 transitions to the ground-state band are thus K-forbidden, as indicated by their long partial half-lives

The branching ratios for the γ-rays to the ground-state band and to the assumed γ-vibrational band are listed in table 6. In every case, $K = 2$ gives

TABLE 6

Branching ratios from the 1507 and 1620 keV states

Reduced transition probabilities	Experimental values	Theoretical values				
		$K=0$	$K=1$		$K=2$	
$\frac{B(4 \to 6)}{B(4 \to 4)}$	$\frac{2.9}{26} \times \left(\frac{1220}{924}\right)^5 = 0.44$	1.65	12.4		0.09	
$\frac{B(4 \to 2)}{B(4 \to 4)}$	$\frac{10.5}{26} \times \left(\frac{1220}{1417}\right)^5 = 0.19$	1.10	12.2		0.34	
$\frac{B(5 \to 6)}{B(5 \to 4)}$	$1 \times \left(\frac{1330}{1038}\right)^5 = 3.5$				0.57	
		$K=0$	1	2	3	4
$\frac{B(4 \to 3)}{B(4 \to 2)}$	$\frac{4.6}{10.6} \times \left(\frac{355}{261}\right)^5 = 2.0$	14	6.9	2.2	0.14	0.56

The transitions are assumed to be pure E2's.

the best fit, although the deviations from the theoretical values are considerable. This result can most easily be understood by assuming that the transition probability to the lower bands is due to a $K = 2$ admixture in the $K = 4$ band. The reduced transition probabilities for the 261 and 355 keV transitions are ≈ 3 and ≈ 1.5 single-particle units, respectively. Since the transition probability within the ground-state rotational band is about 150 [19, 20]), the lifetime of the 1507 keV level is consistent with an admixture of about 1 per cent.

The 261 and 355 keV transitions are favoured about 200 times compared to the high energy E2 transitions. This is of the same order as, although a little larger than, the expected ratio between the transition probabilities within a rotational band and from the $K = 2$ band to the ground-state band (see next section).

The 1620 keV level decays to the 4^+ and 6^+ levels in the ground-state band, and with an M1 transition to the 1507 keV 4^+ state. Spin 5^+ is thus suggested. If the state is interpreted as belonging to the rotational band of the 1507 keV level, the moment of inertia is about 30 % larger than for the ground-state band.

The 1931 keV level has spin 3^-, as it decays with E1 transitions to states with spin 2^+ and 4^+. Similarly, the 2042 keV level has probably spin 4^-, since it decays with E1 γ-rays to states of 4^+ and 5^+. 5^- is unlikely, as the level is excited by K-capture. In order to maintain balance between excitations and de-excitations for each level, K-capture transitions must be assumed to the 1042 (65 %), 1152 (11 %), 288, and 89 keV states. Since levels with spins 2, 3, and 4 are excited, the spin of Tb^{156} is probably 3, and a transition to a 5^- level is unlikely.

7. Discussion

The branching ratios for the γ-rays from the states which are interpreted as γ-vibrations have been studied in numerous cases. Although the experimental values are consistent only with $K = 2$, the deviations are systematically larger than the experimental uncertainty. Only for the decay from the 2, 2^+ state to the 0, 0^- and 0, 2^+ states is the experimental material sufficiently detailed for a systematic comparison with the calculated value. The branching ratio

$$\frac{B(2, 2 \rightarrow 0, 0)}{B(2, 2 \rightarrow 0, 2)}$$

is shown in fig. 7 as a function of the $(2, 2^+)$ state. In all known cases, the branching ratio is lower than the theoretical value 0.7, the discrepancy being larger when $E_{2,2^+}$ is low. This trend is consistent with an interpretation as an effect of a certain mixing of the $K = 0$ and $K = 2$ bands. Such admixtures can even in cases with no K-forbiddenness change the intensity rules considerably because of the large transition probability between the states in a rotational band.

The effect of mixing can be treated by introducing a parameter $z \approx AQ_{00}/Q_{20}$, with A representing the admixed amplitude, Q_{00} the mean intrinsic quadrupole moment for the two rotational bands, and Q_{20} the transition amplitude from the $K = 2$ band to the $K = 0$ band. Since the E2 transition probability corresponding to Q_{00} systematically is larger than 100 in single-particle units, whereas that corresponding to Q_{20} in the cases studied by Coulomb excitation [17, 18]) is smaller than 10, the transition probability from the $K = 2$ to the $K = 0$ band can be affected considerably even for small values of the admixed amplitude [7]).

In the absence of coupling between the bands, the reduced transition probability for a transition of E2 multipole order is described by [7])

$$B(\mathrm{E2}, I_1 \rightarrow I_f) = \langle I_1, \mathrm{E2}, K_1, K_f - K_1 | I_1, \mathrm{E2}, I_f, K_f \rangle^2.$$

The effect of the coupling is taken into account by multiplying this squared

Clebsch-Gordan coefficient by a factor $f(z, I_1, I_f)$ which is given in table 7 † for $K = 2$. The branching ratio is obtained by multiplying the uncorrected value with the ratio of the two factors $f(z, I_1, I_f)$.

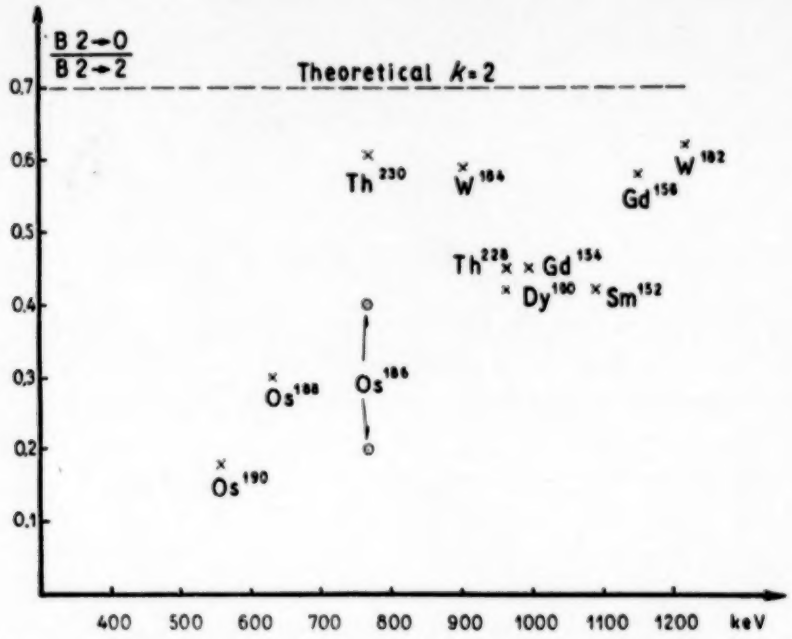

Fig. 7. $B(2, 2^+ \to 0, 0^+)/B(2, 2^+ \to 0, 2^+)$ versus the energy of the 2, 2^+ state. A smooth behaviour of the relationship cannot be expected, since the coupling depends on numerous parameters. References:

Os^{190}: O. B. Nielsen, N. O. Roy Poulsen, B. Skytte Jensen and R. K. Sheline, Nuclear Physics **10** (1959) 475.
Os^{188}: K. O. Nielsen, O. B. Nielsen and O. Skilbreid, Nuclear Physics **5** (1958) 319.
Os^{186}: F. T. Porter, M. S. Freedman, T. B. Novey and F. Wagner, Phys. Rev. **103** (1956) 921; M. W. Johns, C. C. McMullen, I. R. Williams and S. V. Nablo, Can. J. Phys. **34** (1956) 69.
Th^{230}: E. Arbman, S. Bjørnholm and O. B. Nielsen, to be published.
W^{184}: C. J. Gallagher, D. S. Strominger and J. P. Unik, Phys. Rev. **110** (1958) 725.
Th^{228}: S. Bjørnholm, O. Nathan, O. B. Nielsen and R. K. Sheline, Nuclear Physics **4** (1957) 313.
Dy^{160}: O. Nathan, Nuclear Physics **4** (1957) 125.
Gd^{154}: J. O. Juliano and F. S. Stephens, Phys. Rev. **108** (1957) 341.
Sm^{152}: O. Nathan and S. Hultberg, Nuclear Physics **10** (1959) 118.
W^{182}: F. Boehm, P. Marmier and J. W. M. DuMond, Phys. Rev. **95** (1954) 864.

TABLE 7

Correction factor $f(z, I_1, I_f)$ for the transition probability between states with $K = 2$ and $K=0$

Initial state $K = 2$, $I_1 =$	Final state $K = 0$, $I_f =$	$f(z, I_1, I_f)$
$I-2$	I	$(1+(2I+1)z)^2$
$I-1$	I	$(1+(I+2)z)^2$
I	I	$(1+2z)^2$
$I+1$	I	$(1-(I-1)z)^2$
$I+2$	I	$(1-(2I+1)z)^2$

† This table was kindly worked out by Dr. B. R. Mottelson.

Obviously, it is possible to determine a value of z which can explain every observed branching ratio, but if the deviations from the uncorrected theoretical branching ratios really are due to the rotational-vibrational interaction, the same value of z should apply for all transition rates from one band to another.

In the present case of Gd^{156}, the three branching ratios of table 6 can be used for this test. Table 8 contains the ratios between the experimental and

TABLE 8

Deviations from the theoretical branching ratios for pure $K = 2$. Comparison with the theoretical correction factors for $K = 0$ admixture with $z = 0.04$

Branching ratios	Correction factor $f(z, I_1, I_f)$	
	Exp.	Theor.
$\frac{B(2 \to 4)}{B(2 \to 2)}$	2.4	1.6
$\frac{B(2 \to 0)}{B(2 \to 2)}$	0.83	0.79
$\frac{B(3 \to 4)}{B(3 \to 2)}$	1.55	1.68

the uncorrected theoretical values as well as the correction factor calculated for $z = 0.04$. The remaining deviations are scarcely outside the experimental uncertainty.

If the $K = 2$ part of the $K = 4$ band is responsible for the transition rates to the ground-state band, one would expect similar deviations from the uncorrected branching ratios as observed in connection with the transitions from the $K = 2$ band. The correction factors calculated for $z = 0.04$ are compared with the experimental factors in table 9. The corrected values

TABLE 9

$K = 4$ band

Deviations from the theoretical branching ratios for pure $K = 2$. Comparison with the theoretical correction factors for $K = 0$ admixture with $z = 0.04$

Branching ratios	$f(z, I_1, I_f)$	
	Exp.	Theor.
$\frac{B(4 \to 6)}{B(4 \to 4)}$	5.0	1.97
$\frac{B(4 \to 2)}{B(4 \to 4)}$	0.54	0.55
$\frac{B(5 \to 6)}{B(5 \to 4)}$	6	2.25

represent a drastic improvement, although complete quantitative agreement is not obtained.

The apparent success in explaining the deviations from the theoretical branching ratios in Gd^{156} as an effect of mixing of states with different K need, of course, confirmation by results from other nuclei. W^{182} is a case [7]) which can be analyzed in a similar way. The intensity ratio of the transitions from the 2, 2^+ to the 0, 0^+ and 0, 2^+ states is 0.6 compared to the theoretical value 0.7. Similarly,

$$\frac{B(2, 3^+ \rightarrow 0, 2^+)}{B(2, 3^+ \rightarrow 0, 4^+)} = 2.1$$

and theoretically 2.5. In both cases, the deviations are accounted for by $z = 0.03$.

The authors wish to express their gratitude to Professor Niels Bohr for the excellent working conditions in his Institute, and to Professor Aage Bohr and Dr. Ben R. Mottelson who initiated the analysis of the branching ratios. One of us (P. G. H.) is grateful to the Danish Atomic Energy Commission, especially to Dr. C. F. Jacobsen, for having given him the opportunity to participate in this work. We are indebted to Professor N. O. Lassen and the cyclotron crew for a large number of bombardments.

References

1) T. H. Handley and W. S. Lyon, Phys. Rev. **99** (1955) 1415
2) J. W. Mihelich, B. Harmatz and T. H. Handley, Phys. Rev. **108** (1957) 989
3) L. T. Dillman, R. W. Henry, N. B. Gove and R. A. Beeker Bull. Am. Phys. Soc. **2** (1957) 341
4) R. W. Henry, L. T. Dillman, N. B. Gove and R. A. Beeker, Bull. Am. Phys. Soc. **2** (1957) 341
5) S. Ofer, private communication.
6) S. Ofer, Bull. Am. Phys. Soc. **3** (1958) 357
7) G. Alaga, K. Alder, A. Bohr and B. R. Mottelson, Mat. Fys. Medd. Dan. Vid. Selsk. **29**, No. 9 (1955)
8) S. Bjørnholm, P. Dam, H. Nordby and N. O. Roy Poulsen, to be published in Nuclear Instruments
9) P. Gregers Hansen and R. K. Sheline, Nuclear Instruments **2** (1958) 39
10) S. Bjørnholm, O. B. Nielsen and R. K. Sheline, Nature **178** (1956) 1110
11) O. B. Nielsen and O. Kofoed Hansen, Mat. Fys. Medd. Dan. Vid. Selsk. **29**, No. 6 (1955)
12) T. J. Ward, K. P. Jacob, J. W. Mihelich, B. Harmatz and T. H. Handley, Bull. Am. Phys. Soc. **2** (1957) no. 5
13) F. Boehm and E. N. Hatch, Bull. Am. Phys. Soc. **1** (1956) 390
14) G. T. Ewan, J. W. Knowles and D. R. MacKenzie, Bull. Am. Phys. Soc. **2** (1957) 259
15) A. Bohr and B. R. Mottelson, Mat. Fys. Medd. Dan. Vid. Selsk. **27**, No. 16 (1953)
16) K. Alder, A. Bohr, T. Huus, B. R. Mottelson and A. Winther, Revs. Mod. Phys. **28** (1956) 432
17) R. Barloutaud, P. Lehman and A. Lévêque, C. R. **245** (1957) 523
18) P. H. Stelson, private communication
19) R. E. Bell and M. Jørgensen, Nuclear Physics **12** (1959) 413
20) O. Nathan, Nuclear Physics **4** (1957) 125

1.D.2:
1.E.4:
3.A

Nuclear Physics **12** (1959) 413—417; © *North-Holland Publishing Co., Amsterdam*
Not to be reproduced by photoprint or microfilm without written permission from the publisher

HALF-LIVES OF TWO EXCITED STATES OF Gd^{156}

R. E. BELL † and M. H. JØRGENSEN

Institute for Theoretical Physics, University of Copenhagen

Received 27 April 1959

Abstract: The half-lives of the 1507 keV and 89 keV excited states of Gd^{156} have been measured with a fast time-to-amplitude converter. The half-life of the 1507 keV 4+ state is $(1.88 \pm 0.10) \times 10^{-10}$ sec, in agreement with estimates made in the preceding paper by Gregers Hansen *et al.* [1]). This result throws serious doubt on the supposed measurement of the half-life of the 288 keV state by Ofer [4]). The half-life of the 89 keV first rotational state is $(2.19 \pm 0.07) \times 10^{-9}$ sec, differing slightly from a previous measurement by Nathan [2]). The new value leads to a reduced transition probability for the reverse (Coulomb excitation) process $B(E2) : e^2 = (4.64 \pm 0.20) \times 10^{-48}$ cm^4, in excellent agreement with the value directly measured by Coulomb excitation by Ramšak *et al.* [7]).

1. Introduction

The electron-capture disintegration of Tb^{156} to excited states in Gd^{156} has recently been studied with great care by Gregers Hansen *et al.* [1]). The radiations in this decay are such that it is easy to measure the lifetimes of the 1507 keV excited state and the 89 keV first rotational excited state, and this has now been done. The lifetime of the latter state was measured earlier by Nathan [2]) with a slightly different result.

The measurements were made with a fast time-to-amplitude converter similar to that described by Green and Bell [3]), but with a number of modifications and additions which we hope to describe at a later time. The apparatus is capable of producing a time resolution curve for Co^{60} gamma rays having a full width at half maximum of 4×10^{-10} sec and sides dropping off with an instrumental half-life of 5×10^{-11} sec. For 500 keV gamma rays, the latter figure increases to 6 or 7×10^{-11} sec. Thus, gamma rays with half-lives above, say, 10^{-10} sec can have their half-lives measured directly from the logarithmic slope of the resolution curve, rather than by the less certain centroid-shift method.

2. Experiments and Results

2.1. HALF-LIFE OF THE 1507 keV STATE

A weak source of Tb^{156} (≈ 0.5 μC) was placed between two gamma ray counters consisting of diphenylacetylene crystals (2.0 cm diameter $\times$ 1.5 cm

† Permanent address: Radiation Laboratory, Department of Physics, McGill University, Montreal, Canada.

high) coupled to RCA-6342A photo-multipliers. Pulses from counter no. 1 lying between 210 keV and 320 keV electron energy were accepted by the pulse height selector. This counter was therefore sensitive to gamma rays above 335 keV, but most sensitive around 500 keV. In a similar way, counter no. 2 was set to be sensitive to gamma rays above 900 keV, but most sensitive around 1250 keV. Reference to the Tb^{156} disintegration scheme of Gregers Hansen *et al.*[1]) and Ofer[4]) shows that essentially all the coincidences between two such counters involve the 534 keV gamma ray leading to the 1507 keV state and one of several $\approx$ 1 MeV gamma rays leading from it. Nevertheless a few coincidences, possibly 2 % of the total, may involve the 1620 keV state as well; unless the lifetime of this state were much longer than that of the 1507 keV state, these coincidences would not show up separately in the measurements, and an allowance is made for them in assigning errors.

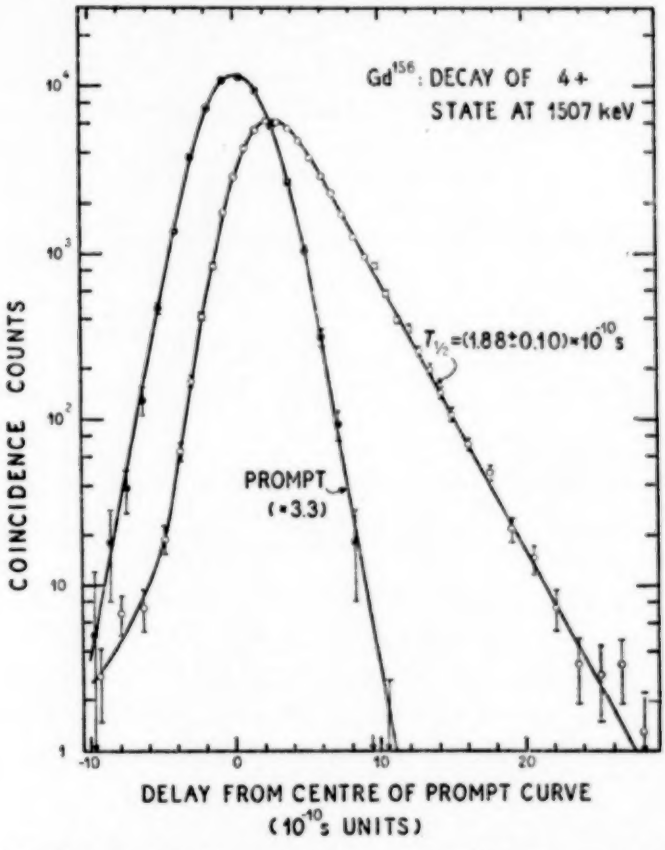

Fig. 1. Time distribution of coincidences between the 534 keV gamma ray leading to the 1507 keV state of Gd^{156}, and any one of several $\approx$ 1 MeV gamma rays leading from it. A prompt coincidence curve made with Co^{60} at the same counter biases is included for comparison.

The result is given in fig. 1 in the form of a time spectrum of the delay of the counter 2 pulses relative to the counter 1 pulses. A prompt curve made with Co^{60} using the same counter biases is included for reference. We use this prompt curve only to demonstrate that the long decay observed for the

Tb^{156} source is real and not instrumental; exact details of the shape and position of the prompt curve are therefore unimportant. The delayed curve shows a clean straight line decay through over 3 decades (> 10 half-lives) with a half-life of 1.88×10^{-10} sec. The statistical error in this value is negligible, but we allow an error of 5 % to cover the time-to-amplitude calibration (3 %) and the possible presence in the curve of a few coincidences of different lifetime (3 %). The result may therefore be quoted as $(1.88 \pm 0.10) \times 10^{-10}$ sec.

A discussion of the lifetime of the 1507 keV state and of the radiations proceeding from it is given in the paper of Gregers Hansen *et al.* [1]) immediately preceding this one. The measured lifetime agrees with expectation for the disintegration scheme proposed there.

Ofer [4]), working at Brookhaven, has recently attempted to estimate the half-life of the 288 keV second excited state of Gd^{156} by observing coincidences between conversion electrons of the 199 keV gamma ray and gamma rays of energy 534 keV and higher. The necessary assumption of this method — that all the higher excited states have negligibly short half-lives — is now seen to be incorrect. Ofer's result was 1.5×10^{-10} sec. This result describes some mixture of the half-life of the 1507 keV state and other, presumably shorter, half-lives. We conclude that the half-life of the 288 keV state is probably shorter than 2×10^{-10} sec, but still unknown.

2.2. HALF-LIFE OF THE 89 keV STATE

The arrangements for this measurement were very similar to those used previously for the same measurement by Nathan [2]), and the main justification for the repetition is the improved time resolution now available. A weak source ($\approx$ 0.25 μC) of Tb^{156} was deposited on a plate of plastic phosphor, 1.5 mm thick, and the deposit was covered with a second plate. This 4π electron counter showed a large peak in the region of 75 keV, with a width of 30 keV, due to the L, M, . . . conversion electrons of the 89 keV gamma ray. A broad pulse height window was set on this peak, but this counter also necessarily detected some of the background under the peak, caused by higher energy gamma rays. A gamma-ray counter (one of those mentioned previously) was brought close to the electron counter, and biased to accept gamma rays above 335 keV. Under these conditions, most of the coincidences are due to the 89 keV gamma ray, but the background pulses already mentioned will give rise to some prompt coincidences and some others showing the half-life of 1.88×10^{-10} seconds of the 1507 keV state. On the long time scale used for measuring the 89 keV lifetime, these will appear as a "prompt bump" at the beginning of the resolution curve.

The results are shown in fig. 2. The prompt bump appears as expected, followed by the long decay due to the 89 keV lifetime. This decay was not

followed as far out as it could have been, because it was not at the moment convenient to lengthen the time scale of the time-to-amplitude converter sufficiently. (At the right-hand end of the curve of fig. 2 the coincidence rate is still more than two decades above the chance coincidence rate.) The prompt resolution curve of fig. 1 has been repeated in fig. 2 in order to give an impression of the instrumental resolution, but neither its shape nor its position is exactly right for this measurement. The half-life read from fig. 2 is $(2.19 \pm 0.07) \times 10^{-9}$ sec, the assigned error of ≈ 3 % being mainly an allowance for calibration errors.

The same prompt bump effect would be present in Nathan's work, and in fact his published curve indicates its presence. He ignored it in evaluating the slope of his curve, however, and thus produced a result for the half-life about 13 % smaller than ours.

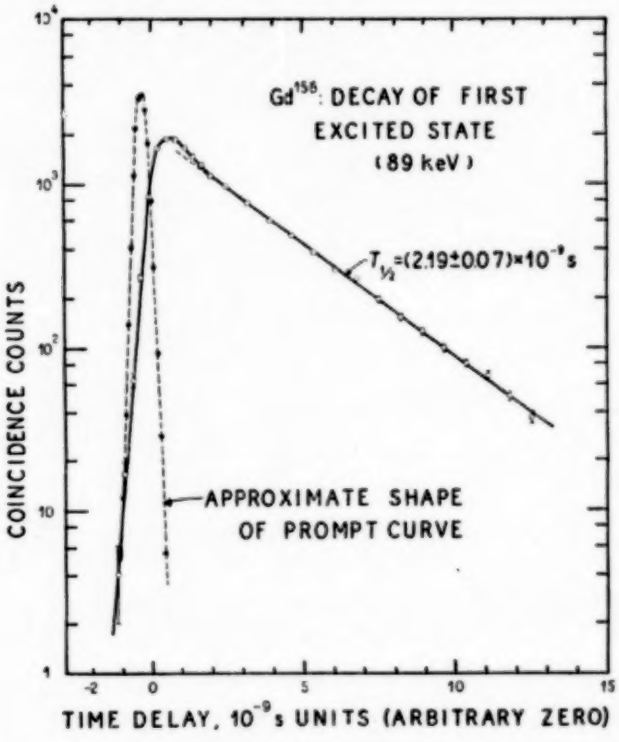
Gd156: DECAY OF FIRST EXCITED STATE (89 keV)
T½=(2.19±0.07)×10⁻⁹s
APPROXIMATE SHAPE OF PROMPT CURVE
COINCIDENCE COUNTS
TIME DELAY, 10⁻⁹s UNITS (ARBITRARY ZERO)

Fig. 2. Time distribution of coincidences between the L, M . . . conversion electrons of the 89 keV gamma ray of Gd^{156} and gamma rays above 335 keV. The prompt curve is repeated from fig. 1, and is intended only to give an impression of the time resolution with which this measurement was made.

The radiative mean life of the 89 keV state is $\tau_\gamma = T_{\frac{1}{2}}(1+\alpha)/\ln 2$, where α is the total conversion coefficient. To evaluate α, we use the average of the K and L conversion coefficients from the tables of Rose[5]) and of Sliv and Band[6]). (The worst disagreement between the two tables is 5 % for the L_{II} shell.) In addition, we know experimentally[1]) that the M, N . . . conversion for this transition is 0.33 ± 0.03 of the L conversion. We finally get

$\alpha = 3.93$, with an estimated standard error of 3 %. This gives

$$\tau_\gamma = (1.56 \pm 0.08) \times 10^{-8} \text{ sec.}$$

Following the procedure of Nathan [2]), this value of τ_γ leads to a reduced transition probability for the reverse (Coulomb excitation) process

$$B(\text{E2}; I_0 \rightarrow I_1) : e^2 = (4.64 \pm 0.20) \times 10^{-48} \text{ cm}^4.$$

The value of B(E2) measured directly from Coulomb excitation by Ramšak *et al.* [7]) is $(4.50 \pm 0.25) \times 10^{-48}$ cm^4, in excellent agreement with the present result.

One of us (R. E. B.) is grateful for the hospitality of the Institute for Theoretical Physics, and we thank Professor Niels Bohr for the excellent working conditions in the Institute. Thanks are also due mag. scient. B. Elbek for urging that the 89 keV half-life be re-measured.

References

1) P. Gregers Hansen, N. O. Lassen, O. B. Nielsen and R. K. Sheline, Nuclear Physics **12** (1959) 389
2) O. Nathan, Nuclear Physics **5** (1958) 401
3) R. E. Green and R. E. Bell, Nuclear Instruments **3** (1958) 127
4) S. Ofer, Phys. Rev. (1959) to be published
5) M. E. Rose, Internal Conversion Coefficients (North-Holland Publishing Company, Amsterdam, 1958)
6) L. A. Sliv and I. M. Band, Internal Conversion Coefficients, tables circulated by the University of Illinois, Reports 57 ICC K1 (1957) and 58 ICC L1 (1958)
7) V. Ramšak, M. C. Olesen and B. Elbek, Nuclear Physics **6** (1958) 451

7.C *Nuclear Physics* **12** (1959) 418—425; © *North-Holland Publishing Co., Amsterdam*
Not to be reproduced by photoprint or microfilm without written permission from the publisher

PHOTO PRODUCTION OF PION PAIRS BY A NUCLEON

S. K. SRINIVASAN † and K. VENKATESAN ††

Department of Physics, University of Madras

Received 22 April 1959

Abstract: Double photo production of pions by nucleons is examined on the basis of the "fixed extended" source theory of Chew and Low. A linear integral equation for the matrix element is derived using the Tamm-Dancoff approximation. Using the solution of Chew and Low for single production, an expression for the cross-section of the process is obtained as a first approximation. The total cross-section compares favourably with the experimental results of Sellen, Cocconi and Hart.

1. Introduction

Recent experiments on the photo production of pion pairs by nucleons reveal many interesting features. There is a flattening of the yield per photon curve of the π^- at about 700 MeV [1]). This may be explained from the existing knowledge of pion-nucleon collisions on the basis of a resonance in the production of the π^- or by a two body interaction with the (p, π^+) system which forms an excited isobaric state. Apart from this, the pion pair production process can throw some light on some of the essential features of the cut-off theory such as the linearity of the pion-nucleon interaction. Thus a calculation of the amplitude of double photo-production of pions can be expected to confirm the success of the cut-off theory and also the view point that only low energy intermediate states are important for low energy processes. In this paper, we derive the amplitude for double photo production of pions using the method of Low taking both mesons in P-state †††. Our calculations will be based on the available knowledge of single photo pion production and as such we can expect our results to be in qualitative agreement with experiments. The reproduction of the order of magnitude of experimental cross-section will decisively prove the validity of Chew's theory even at five or six hundred MeV.

2. Derivation of the Matrix Element

The S-matrix for the photo production of a pair of mesons of momenta q_1, q_2 and isobaric spin indices α, β by a nucleon due to a photon of momen-

† National Institute of Sciences Senior Research Fellow; now at the Department of Applied Mathematics, Indian Institute of Technology, Madras.

†† Government of India Senior Research Scholar.

††† The matrix element for the case where one of the mesons is in S-state has been considered by Cutkosky and Zachariasen [2]).

tum k and polarization λ is given by

$$\langle p'; q_1\alpha, q_2\beta|S|k\lambda; p\rangle = \sum_{n=0}^{\infty}\frac{(-i)^n}{n!}\int dx_1\int dx_2\ldots\int dx_n(\Phi_{p'}, a_\alpha(q_1)a_\beta(q_2). \quad (1)$$
$$T(L(x_1)L(x_2)\ldots L(x_n))b^{(\lambda)\dagger}(k)\Phi_p)$$

where p and p' are the initial and final momentum states of the nucleon and $L(x)$ the interaction Lagrangian density is given by †

$$\begin{aligned}L(x) = {} & +ig\bar{\psi}(x)\gamma_5\tau_i\psi(x)\phi_i(x) - \delta m\bar{\psi}(x)\psi(x)\\ & +ie\bar{\psi}(x)\gamma_\mu A_\mu\tfrac{1}{2}(1+\tau_3)\psi(x)\\ & +ie\left(\phi^*\frac{\partial\phi}{\partial x_\mu}-\frac{\partial\phi^*}{\partial x_\mu}\phi\right)A_\mu(x)\\ & +\tfrac{1}{2}e\bar{\psi}(x)\gamma_\mu A_\mu(x)\gamma_\nu A_\nu(x)[\tfrac{1}{2}(1+\tau_3)\mu_p+\tfrac{1}{2}(1-\tau_3)\mu_n]\psi(x).\end{aligned}$$

The τ_i's are the usual iso-spin matrices and μ_p and μ_n are the magnetic moments of the proton and neutron respectively; a is the annihilation operator for a meson and $b^\dagger$ is the creation operator for a photon. As e, the electromagnetic coupling constant, is about 100 times less than the meson nucleon coupling constant g, we shall neglect the contribution of the fourth term of (2) to the meson current in comparison with that of the first; it will be taken into account at a later stage when we intend calculating the cross-section more accurately.

Using the standard procedure of Low [3]) or Lehmann, Symanzik and Zimmerman [4]) the S-matrix element can be written as

$$\langle p'; q_1\alpha, q_2\beta|S|k\lambda; p\rangle = -\frac{1}{(2\pi)^3}\int dx\int dy\frac{e^{-iq_1x-iq_2y}}{(4\omega(q_1)\omega(q_2))^{\frac{1}{2}}}\langle p'|(j_\alpha(x)j_\beta(y))_+|k\lambda; p\rangle \quad (3)$$

where $|k\lambda; p\rangle$ is an outgoing state whose plane wave part consists of a nucleon of momentum p and a photon of momentum k and polarization λ; $(\ )_+$ is the time-ordered product defined according to Dyson. $j_\alpha(x)$, $j_\beta(y)$ are the usual meson current operators given by

$$(-\Box+\mu^2)\varphi_\alpha(x) = j_\alpha(x) = +ig\bar{\psi}(x)\gamma_5\tau_\alpha\psi(x).$$

Using the translational invariance theorem

$$j_\alpha(x) = e^{-iPx}j_\alpha(0)e^{iPx}$$

† Throughout this paper, we shall write a four-vector x and an ordinary vector by the corresponding bold letter $\mathbf{x}$. The scalar product of two four-vectors x and y will be denoted by $xy = x_iy_i - x_0y_0$. Integration over three dimensional volumes are denoted by $\int d\mathbf{x}$ while those over four dimensional ones are denoted by $\int dx$.

where P is a four momentum operator, we obtain

$$\begin{aligned}&\langle p'; q_1\alpha, q_2\beta|S|k\lambda; p\rangle\\ &= -(2\pi)\delta(p+k-p'-q_1-q_2)\frac{1}{(4\omega_1\omega_2)^{\frac{1}{2}}}\\ &\int e^{-iq_2y}\langle p'|(j_\alpha(0)j_\beta(y))_+|k\lambda; p\rangle dy\ \dagger.\end{aligned} \tag{4}$$

Expanding in terms of a complete set of "incoming" states yields

$$\begin{aligned}&\langle p'; q_1\alpha, q_2\beta|T|k\lambda; p\rangle\\ &= -\frac{i}{(4\omega_1\omega_2)^{\frac{1}{2}}}[\sum_n \langle p'|j_\alpha(0)|n; \mathbf{p}_n = \mathbf{k}+\mathbf{p}-\mathbf{q}_2\rangle\\ &\quad\cdot(\omega_2+E_n-p_0-k_0+i\varepsilon)^{-1}\langle n; \mathbf{p}_n = \mathbf{k}+\mathbf{p}-\mathbf{q}_2|j_\beta(0)|k\lambda; p\rangle\\ &\quad-\sum_n \langle p'|j_\beta(0)|n; \mathbf{p}_n = \mathbf{p}'+\mathbf{q}_2\rangle(\omega_2+p'_0-E_n-i\varepsilon)^{-1}\\ &\quad\cdot\langle n; \mathbf{p}_n = \mathbf{p}'+\mathbf{q}_2|j_\alpha(0)|k\lambda; p\rangle]\end{aligned} \tag{5}$$

where the T-matrix is defined by

$$\langle p'; q_1\alpha, q_2\beta|S|k\lambda; p\rangle = (2\pi)^4\delta(p+k-p'-q_1-q_2)\langle p'; q_1\alpha, q_2\beta|T|k\lambda; p\rangle. \tag{6}$$

Next we make the usual Tamm-Dancoff approximation of restricting the n states to one nucleon and one nucleon + one meson states. The procedure yields an integral equation for double photo-production amplitude, the inhomogeneous term being the product of the nucleon vertex operator and single photo-production amplitude.

In this paper we shall confine ourselves to the processes

(a) $\gamma+\mathrm{p}\to\mathrm{p}+\pi^+ +\pi^-$

(b) $\gamma+\mathrm{p}\to\mathrm{n}+\pi^+ +\pi^0$

since these can be checked against the available experimental data.

3. Calculation of Cross-Sections

3.1. $\gamma+\mathrm{p}\to\mathrm{p}+\pi^+ +\pi^-$

In this case we note that non-vanishing contribution to the amplitude comes from only one of the two terms in (5) since a proton cannot emit a π^-. The amplitude is given by

$$\begin{aligned}&\langle p'; q_1-, q_2+|T|k\lambda; p\rangle i(4\omega_1\omega_2)^{\frac{1}{2}}\\ &= \langle p'|j_-(0)|p+k-q_2\rangle(\omega_2+E(\mathbf{p}+\mathbf{k}-\mathbf{q}_2)-p_0-k_0+i\varepsilon)^{-1}\\ &\quad\langle p+k-q_2|j_+(0)|k\lambda; p\rangle\\ &+\sum_{\alpha'}\int dp''\int dq'\langle p'|j_-(0)|q'\alpha'; p''\rangle(p''_0+\omega'+\omega_2-p_0-k_0+i\varepsilon)^{-1}\\ &\quad\langle p''; q'\alpha'|j_+(0)|k\lambda; p\rangle\delta(\mathbf{p}''+\mathbf{q}'-\mathbf{p}-\mathbf{k}+\mathbf{q}_2).\end{aligned} \tag{7}$$

† For brevity we shall denote $\omega(q_i)$ the energy of pion of momentum q_i by ω_i.

As a first approximation, we drop the second term and in a later contribution we propose to include it and refine the cross-section.
In the static limit

$$\langle p'|j_-(0)|p+k-q_2\rangle = -(4\pi)^{\frac{1}{2}} f i\boldsymbol{\sigma}\cdot\mathbf{q}_1\sqrt{2}\tau_+. \tag{8}$$

The single photo-production amplitude consisting only of the dominant terms is given by Chew and Low [5]) as

$$\begin{aligned}(2k)^{\frac{1}{2}}\langle p+k-q_2|j_+(0)|k\lambda;\, p\rangle &= (2k)^{\frac{1}{2}} T^+_{q_2}(k\lambda)\\ &= \left\{\frac{\mu_p-\mu_n}{mf^2}\pi e f\left[\frac{1}{\sqrt{2}}(\tau_-\tau_3+\tau_3\tau_-)-\frac{\sqrt{2}}{3}\tau_-\tau_3\right]\frac{e^{i\delta(q_2)}\sin\delta(q_2)}{{q_2}^3}\right.\\ &\quad [2\mathbf{q}_2\cdot\mathbf{k}\times\boldsymbol{\lambda}-i\boldsymbol{\sigma}\cdot(\mathbf{q}_2\times(\mathbf{k}\times\boldsymbol{\lambda}))]\\ &\quad \left.+\frac{4}{\sqrt{2}}\pi i e f(\tau_-\tau_3-\tau_3\tau_-)\left[\boldsymbol{\sigma}\cdot\boldsymbol{\lambda}+\frac{2\boldsymbol{\sigma}\cdot(\mathbf{k}-\mathbf{q}_2)\mathbf{q}_2\cdot\boldsymbol{\lambda}}{(\mathbf{k}-\mathbf{q}_2)^2+1}\right]\right\}\end{aligned} \tag{9}$$

where the matrix elements can be regarded as matrices in spin and isobaric spin space of the nucleon and e and f are the renormalized (and the latter unrationalized) coupling constants. $\delta(q_2)$ can be taken to be $\delta_{33}(q_2)$, the phase shifts corresponding to 11, 13 and 31 states being negligible.

Using (8) and (9) and averaging over the initial spin and polarization directions and summing over the intermediate and final spin states, we obtain

$$d\sigma^{+-} = 2\pi|M_a|^2(2\pi)^{-6}\omega_1\omega_2 q_1 q_2 d\omega_1 d\Omega^- d\Omega^+ \tag{10}$$

where $|M_a|^2$ is given by

$$\begin{aligned}|M_a|^2 = \frac{4\pi}{(\omega_2-k)^2}&\left\{\frac{\pi^2 e^2(\mu_p-\mu_n)^2 {q_1}^2 k}{36m^2\omega_1\omega_2{q_2}^4}\sin^2\delta(q_2)(2+3\sin^2\theta_2)\right.\\ &+\frac{8\pi^2 e^2 f^4 {q_1}^2}{\omega_1\omega_2 k}\left[1-\frac{2{q_2}^2\sin^2\theta_2}{(k^2+{q_2}^2-2kq_2\cos\theta_2+1)^2}\right]\\ &+\frac{4\pi^2 e^2 f^2(\mu_p-\mu_n){q_1}^2}{3{q_2}^2 m\omega_1\omega_2}\sin\delta(q_2)\cos\delta(q_2)\\ &\left.\cdot\left[\frac{kq_2\sin^2\theta_2}{k^2+{q_2}^2-2kq_2\cos\theta_2+1}-\cos\theta_2\right]\right\}\end{aligned} \tag{11}$$

where θ_2 is the angle that $\mathbf{q}_2$ makes with $\mathbf{k}$.

3.2. $\gamma+p\to n+\pi^++\pi^0$

The calculation for the process is similar to (a) except that we have taken into account both the terms of the equation (5) since a π^0 can be emitted either by a proton or by a neutron. The amplitude in this case is given by

$$\begin{aligned}
&\langle p'; q_1 0, q_2+|T|k\lambda; p\rangle(4\omega_1\omega_2)^{\frac{1}{2}} \\
&= -i[\langle p'|j_0(0)|p+k-q_2\rangle(\omega_2+E(\mathbf{p}+\mathbf{k}-\mathbf{q}_2)-p_0-k_0+i\varepsilon)^{-1} \\
&\quad \langle p+k-q_2|j_+(0)|k\lambda; p\rangle-\langle p'|j_+(0)|p'+q_2\rangle \\
&\quad (\omega_2+p'_0-E(\mathbf{p}'+\mathbf{q}_2)-i\varepsilon)^{-1}\langle p'+q_2|j_0(0)|k\lambda; p\rangle]
\end{aligned} \tag{12}$$

where $\langle p'+q_2|j_0(0)|k\lambda; p\rangle$ is given by

$$\begin{aligned}
&(2k)^{\frac{1}{2}}\langle p'+q_2|j_0(0)|k\lambda; p\rangle = (2k)^{\frac{1}{2}}T^0_{q_1}(k\lambda) \\
&\quad = +\frac{\mu_p-\mu_n}{4mf^2}\,\frac{8\pi ef}{3q_1^3}\,e^{i\delta(q_1)}\sin\delta(q_1)[2\mathbf{q}_1\cdot(\mathbf{k}\times\boldsymbol{\lambda})-i\boldsymbol{\sigma}\cdot(\mathbf{q}_1\times(\mathbf{k}\times\boldsymbol{\lambda})].
\end{aligned} \tag{13}$$

Using (13), (9) and (8), we obtain the cross-section as

$$d\sigma^{+0} = 2\pi|M_b|^2(2\pi)^{-6}\omega_1\omega_2 q_1 q_2\, d\omega_1\, d\Omega^+ d\Omega^0 \tag{14}$$

where $|M_b|^2$ is given by

$$\begin{aligned}
|M_b|^2 = \frac{4\pi}{(\omega_2-k)^2}\Bigg\{&\frac{\pi^2e^2(\mu_b-\mu_n)^2q_1{}^2k}{72m^2\omega_1\omega_2q_2{}^4}\sin^2\delta(q_2)(2+3\sin^2\theta_2) \\
&+\frac{4\pi^2e^2f^4q_1{}^2}{\omega_1\omega_2k}\left[1-\frac{2q_2{}^2\sin^2\theta_2}{(k^2+q_2{}^2-2kq_2\cos\theta_2+1)^2}\right] \\
&+\frac{2\pi^2e^2f^2(\mu_p-\mu_n)}{3m\omega_1\omega_2}\sin\delta(q_2)\cos\delta(q_2)\cdot\frac{q_1{}^2}{q_2{}^2}\left[\frac{kq_2\sin^2\theta_2}{k^2+q_2{}^2-2kq_2\cos\theta_2+1}-\cos\theta_2\right]\Bigg\} \\
&+\frac{4\pi}{\omega_2{}^2}\left\{\frac{\pi^2e^2(\mu_p-\mu_n)^2q_2{}^2k}{18m^2\omega_1\omega_2q_1{}^4}\sin^2\delta(q_1)(2+3\sin^2\theta_1)\right\} \\
&-\frac{4\pi}{\omega_2(\omega_2-k)}\Bigg\{\frac{4\pi^2e^2f^2(\mu_p-\mu_n)\sin\delta(q_1)\cos\delta(q_1)}{3m\omega_1\omega_2q_1{}^2}
\end{aligned} \tag{15}$$

$$\begin{aligned}
&\mathbf{q}_1\cdot\mathbf{q}_2[\{q_2\sin\theta_1\sin\theta_2(k\sin\varphi-q_2\cos\theta_2\sin\varphi+q_2\cot\theta_1\sin\theta_2)\} \\
&(k^2+q_2{}^2-2kq_2\cos\theta_2+1)^{-1}-(\cos\theta_1+\tfrac{1}{2}\mathbf{q}_1\cdot\mathbf{q}_2\sin\theta_1(\sin\theta_2\cos\theta_2-\cos\theta_1\sin\theta_2\sin\varphi))] \\
&+\frac{4}{9}\,\frac{\pi^3e^2(\mu_p-\mu_n)^2k\,(\mathbf{q}_1\cdot\mathbf{q}_2)}{m^2\omega_1\omega_2q_1{}^2q_2{}^2}\sin\theta_1\sin\theta_2\sin\varphi\sin\delta(q_1)\cos[\delta(q_1)-\delta(q_2)]\sin\delta(q_2) \\
&+\frac{2}{9}\,\frac{\pi^3e^2(\mu_p-\mu_n)^2k}{m^2\omega_1\omega_2q_1{}^2q_2{}^2}\,\mathbf{q}_1\cdot\mathbf{q}_2(2\cos\theta_1\cos\theta_2+\sin\theta_1\sin\theta_2\sin\varphi) \\
&\qquad\cdot\sin\delta(q_1)\sin\delta(q_2)\cos[\delta(q_1)-\delta q_2)]\Bigg\}
\end{aligned}$$

where θ, φ are the spherical polar angles of $\mathbf{q}_1$ in the coordinate system with $\mathbf{k}$ along the z-axis, the zOy plane being determined by $\mathbf{k}$ and $\mathbf{q}_2$.

4. Numerical Results

The variation of the differential cross-section (for a pair of charged pions) with the incident photon energy is illustrated in tables 1 and 2. For convenience, we have fixed the kinetic energy of the negative pion at 72 and 120 MeV. Integrating over the angles eq. (10) becomes

TABLE 1

Differential cross-sections in μb/sr for the photo production of a (π^+, π^-) pair at various photon energies and π^+ scattering angles (π^- kinetic energy. 72 MeV)

Photon energy (MeV)	π^+ scattering angle			
	0°	30°	60°	90°
420	0.07	0.088	0.201	0.204
500	0.209	0.367	0.591	0.635
550	0.38	0.502	0.726	0.801
600	0.451	0.481	0.631	0.519
700	0.542	0.302	0.355	0.267

TABLE 2

Differential cross-sections in μb/sr for the photo production of a (π^+, π^-) pair at various photon energies and π^+ scattering angles (π^- kinetic energy 120 MeV)

Photon energy (MeV)	π^+ scattering angle			
	0°	30°	60°	90°
420	0.133	0.13	0.133	0.133
500	0.056	0.178	0.49	0.635
550	0.204	0.251	0.85	0.898
600	0.689	0.8	1.90	1.17
700	0.698	0.63	0.61	0.543

$$\mathrm{d}\sigma^{+-} = \frac{e^2 q_1 q_2 \mathrm{d}\omega_1}{{\omega_1}^2}\left\{\frac{2}{9}\frac{(\mu_p-\mu_n)^2 {q_1}^2 k}{m^2 {q_2}^4}\sin^2\delta(q_2)\right.$$

$$+\frac{8f^4 {q_1}^2}{k}\left[2+\frac{2}{k^2}-\frac{k^2+{\omega_2}^2}{2k^3 q_2}\log\frac{k^2+{\omega_2}^2+2kq_2}{k^2+{\omega_2}^2-2kq_2}\right] \quad (16)$$

$$\left.+\frac{4}{3}\frac{f^2(\mu_p-\mu_n){q_1}^2}{m{q_2}^2}\sin\delta(q_2)\cos\delta(q_2)\left[\frac{k^2+{\omega_2}^2}{2kq_2}-\frac{(k^2-{\omega_2}^2)^2+4k^2}{8k^2{q_2}^2}\log\frac{k^2+{\omega_2}^2+2kq_2}{k^2+{\omega_2}^2-2kq_2}\right]\right\}.$$

Curves showing the variation of the differential cross-section with the kinetic energy of the negative pion are given in fig. 1 for various photon energies. The total cross-section for the production of a pair of charged pions is of the order of 46, 23 and 6 μb corresponding to 550, 500 and 420 MeV photon energies, respectively. This compares favourably with the results of Sellen *et al.* [6]) who have obtained a value of 50 μb at about 500 MeV. However, Friedman and Crowe [7]) obtain a total cross section of the order of one microbarn at 500 MeV. To our knowledge, the only experimental results now available are those of Friedman and Crowe, on the one hand, and Sellen *et al.* on the other. Since these differ by an order of magnitude, detailed comparison with experiment is not possible unless one of these two sets of results is corroborated.

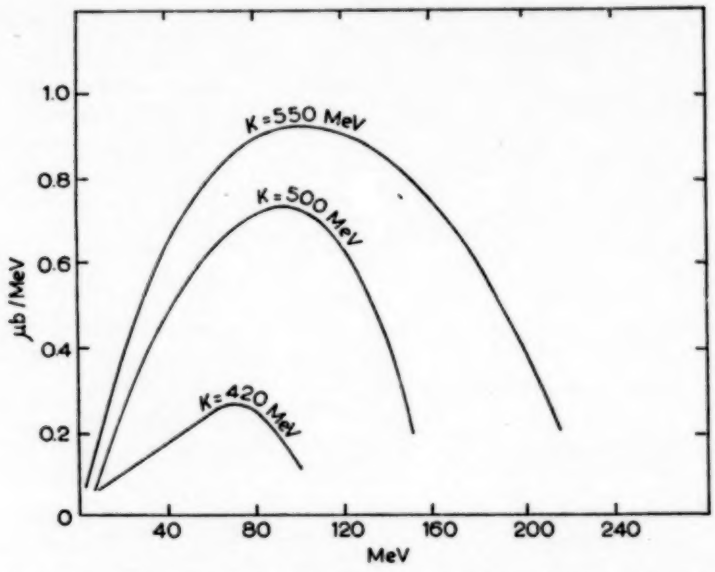

Fig. 1. $(1/4\pi) \times$ differential cross section for $(\pi^+\pi^-)$ pair versus kinetic energy of the π^- meson. The corresponding photon energy is marked on the curve.

For completeness, we have plotted in table 3 the differential cross-section for the case that one of the pions is neutral, the other being positively charged.

TABLE 3

$\frac{d\sigma^{+0}}{d\omega}$ in μb/MeV for various incident photon energies

Photon energy (MeV)	π^0 kinetic energy (MeV)		
	40	72	120
420	1.43	2.38	2.06
500	1.26	4.9	6.53
550	2.26	2.58	15.6

We are deeply indebted to Professor Alladi Ramakrishnan for the interest shown in the work and for his constant encouragement. Our thanks are also due to Messrs. N. R. Ranganathan and R. Vasudevan for many interesting discussions. One of us (S.K.S.) would like to express his gratefulness to the National Institute of Sciences of India for the award of a Senior Research Fellowship and the other (K. V.) to the University of Madras for a Government of India Senior Scholarship.

References

1) Woodward, Proceedings of the Seventh Rochester Conference (1957); Tollestrup, *ibid.*
2) R. E. Cutkosky and F. Zachariasen, Phys. Rev. **103** (1957) 1108
3) F. E. Low, Phys. Rev. **97** (1955) 1392
4) H. Lehmann, K. Symanzik and W. Zimmerman, Nuovo Cimento **1** (1955) 205
5) G. F. Chew and F. E. Low, Phys. Rev. **101** (1956) 1579
6) J. M. Sellen, G. Cocconi, V. T. Cocconi and E. L. Hart, Phys. Rev. **110** (1958) 779
7) R. M. Friedman and K. M. Growe, Phys. Rev. **105** (1957) 1369

1.E.1:
2.A.1

Nuclear Physics **12** (1959) 426—431; © *North-Holland Publishing Co., Amsterdam*
Not to be reproduced by photoprint or microfilm without written permission from the publisher

A STUDY OF THE ENERGY LEVELS OF A^{37}, Sc^{48} AND Cr^{51}

A. T. G. FERGUSON and E. B. PAUL
A.E.R.E., *Harwell, Didcot, Berks.*

Received 23 March 1959

Abstract: Thresholds for neutron emission resulting from proton bombardment of Cl^{37}, Ca^{48} and V^{51} have been observed. Four excited states in A^{37}, nine excited states in Sc^{48} and nine excited states in Cr^{51} were established and the corresponding Q values determined to about ± 10 keV. The threshold detector used is briefly described.

1. Introduction

The positions of energy levels in A^{37}, Sc^{48} and Cr^{51} have been determined by observing the thresholds for the emission of neutrons leaving these nuclei in excited states. Targets of Cl^{37}, Ca^{48} and V^{51} were bombarded with protons and the neutron thresholds observed using a detector developed by Kinsey [1]). A full account of this apparatus is to be published shortly by that author and only a brief description will be given below.

2. Apparatus

The threshold detector shown in fig. 1 consists of two neutron detectors A and B set in a large mass of shielding. These two detectors measure respec-

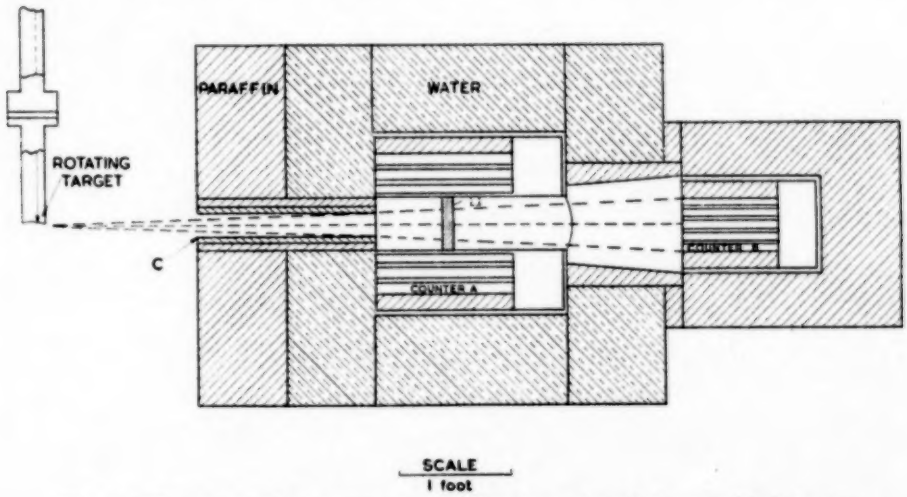

Fig. 1. The general arrangement of the target and threshold detector.

tively the number of neutrons scattered and transmitted by a disc of lithium placed on the axis of the detector. Thresholds are indicated by a sharp peak

in the ratio of scattered to transmitted flux which occurs when the energy of neutrons emitted from a source reaches 258 keV. The detector A consists of BF_3 filled proportional counters set in an annulus of paraffin, three inches thick. Detector B is a rectangular block of paraffin in which are set BF_3 counters. On the axis of detector A is a disc of lithium 5.25 inches diameter and one inch thick. The shielding is such that neutrons from the target can reach detector A only by scattering from the Li block. In the same way neutrons can only reach B by transmission through the Li block. The scattering cross section of Li has only one resonance above a neutron energy of 10 keV, viz. that at 258 keV (see ref. [8])). Above and below this energy, the cross section is small, and slowly varying. Thus, if the neutron energy is varied, the fraction of neutrons incident on the lithium which are detected by A has a peak at 258 keV and the fraction detected by B has a corresponding dip. The ratio of counts in A to counts in B has therefore a sharp peak at this neutron energy. The width of this peak is determined by the width of the Li resonance, the dimensions of the Li scatterer and the neutron energy spread introduced by finite target thickness. If the latter effect is neglected, the width of the peak is estimated to be 30 keV for a scatterer of the dimensions used here.

In order to use the apparatus as a threshold detector in studying a (p, n) reaction, the ratio counts in A/counts in B is measured as a function of proton energy. As soon as the threshold is exceeded, counts will be observed in both A and B. As the proton energy is increased, the ratio A/B will only change slowly till the proton energy corresponding to the emission of neutrons of energy close to 258 keV is reached. The ratio will have a sharp peak here. When the threshold for emission of a second group of neutrons is exceeded the same process will take place. This time the height of the peak will be smaller as the rapid variation in transmission of the second group will be superimposed on the relatively constant transmission of the first neutron group. The magnitude of the peak will be related to the relative intensities of the two groups.

3. Results

The apparatus described briefly above was used to study the energy levels of a number of nuclei produced in (p, n) reactions. The detailed results are presented and discussed below.

3.1. $Cl^{37}(pn)A^{37}$

An evaporated target of natural sodium chloride on a tantalum backing was used. Since the thresholds for neutron production from Na^{23} and Cl^{35} are 5.053 MeV and 6.14 MeV, the effects observed were entirely due to Cl^{37}. The ratio A/B was measured as a function of proton energy from 1.8 MeV to 4.6 MeV. Fig. 2 shows the results obtained. The peak at lowest energy corre-

Fig. 2. The ratio A/B of the number of counts in detector A to the number in detector B as a function of proton energy for the reaction $Cl^{37}(pn)A^{37}$.

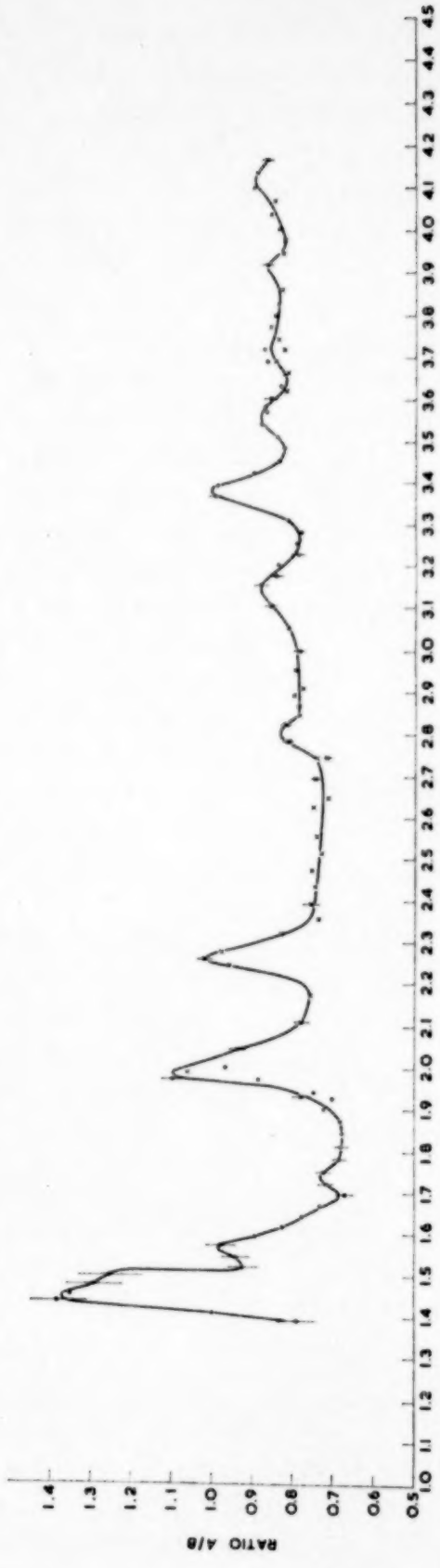

Fig. 3. The ratio A/B of the number of counts in detector A to the number in detector B as a function of proton energy for the reaction $Ca^{48}(pn)Sc^{48}$, assuming $Q_0 = -660$ keV.

sponds to the case in which A^{37} is left in its ground state. Schoenfield *et al.* [2]) found the value of Q_0 for this reaction to be -1.641 ± 0.02 MeV and this was consistent with our results when a correction is made for the estimated energy loss in the target. From the positions of the other peaks the energy levels in A^{37} were determined. Table 1 shows these results and compares

TABLE 1

Positions of energy levels in A^{37}

Reaction	Cl^{37}(p, n)	Cl^{37}(p, n)	Cl^{37}(p, n)	A^{36}(d, p)	A^{36}(d, p)
Energies of levels (MeV)	1.42 ± 0.01 1.61 ± 0.01 2.25 ± 0.01 2.41 ± 0.01	1.40 ± 0.05 1.65 ± 0.05	1.41 ± 0.05	1.53 1.67 2.27 2.56	1.44 — — 2.56
Reference	This paper	[7])	[6])	[3])	[4])

them with those of other authors. There is generally good agreement except for the level found at 2.41 MeV. The nearest corresponding level found by Davison *et al.* [3]) and Zucker and Watson [4]) is one at 2.56 MeV.

3.2. Ca^{48}(pn)Sc^{48}

Targets of $Ca^{48}F_2$ of thickness 240 $\mu g/cm^2$ were evaporated onto gold backings. The ratio A/B was measured for proton energies between 1.4 MeV and 4.2 MeV and 1.0 and 1.4 MeV and is shown in fig. 2. Below 1.4 MeV the yield fell off rapidly and at 1.0 MeV the number of counts in the detector due to background neutrons etc. greatly exceeded the number from the target. No significant structure in the ratio A/B was observed below 1.4 MeV.

By making allowance for target thickness the Q values of the levels in Sc^{48} were calculated and these are tabulated in table 2. The Q value of the reac-

TABLE 2

Q values for the reaction Ca^{48}(p, n)Sc^{48} and the positions of energy levels in Sc^{48}

$-Q$ values determined in this experiment (MeV)	Level positions in Sc^{48} (Assuming $Q_0 = -0.66 \pm 0.03$) (MeV)	Level positions found by Elwyn *et al.*[5]) (MeV)
		0
		0.112 ± 0.005
1.127 ± 0.010	0.467 ± 0.035	0.485 ± 0.008
1.245 ± 0.010	0.583 ± 0.035	
1.380 ± 0.010	0.720 ± 0.035	
1.650 ± 0.010	0.996 ± 0.035	0.985 ± 0.015
1.901 ± 0.010	1.241 ± 0.035	1.23 ± 0.02
2.454 ± 0.010	1.794 ± 0.035	
2.788 ± 0.010	2.128 ± 0.035	
3.023 ± 0.010	2.363 ± 0.035	
3.199 ± 0.010	2.539 ± 0.035	

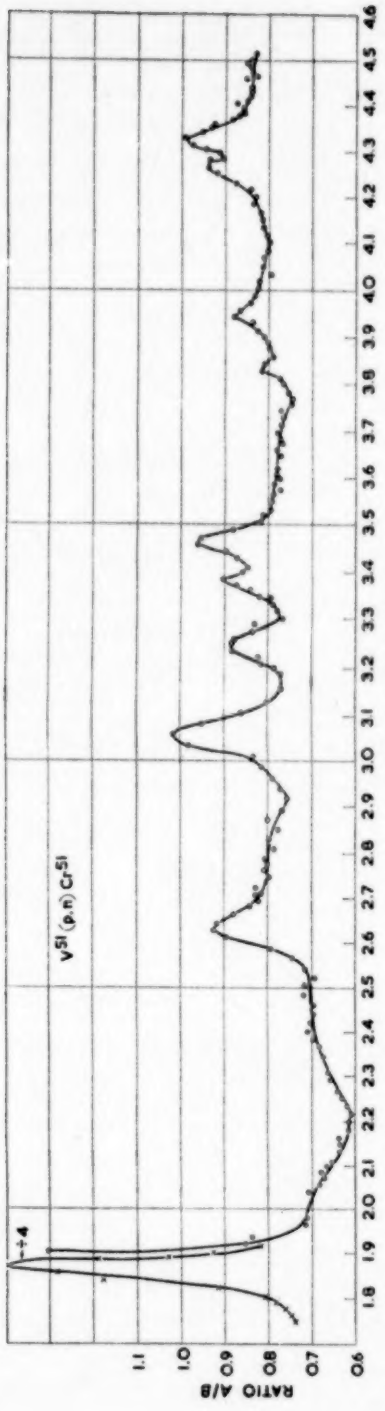

Fig. 4. The ratio A/B of the number of counts in detector A to the number in detector B as a function of proton energy for the reaction $V^{51}(pn)Cr^{51}$.

tion leading to the ground state of Sc^{48} has been found by Elwyn *et al.* [5]) to be 660±30 keV. This figure was obtained by measuring the energy of the neutron group of highest energy from this reaction when the proton bombarding energy was approximately 3.0 MeV. Combining this value with our results, the positions of the excited states of Sc^{48} were determined. These agree well with those found by Elwyn *et al.*, though we have found some additional levels.

3.3. $V^{51}(pn)Cr^{51}$

A target of V_2O_5 of thickness 250 $\mu g/cm^2$ was evaporated onto a gold backing and bombarded with protons of energy between 1.5 MeV and 4.4 MeV. Fig. 3 shows the ratio A/B as a function of proton energy. The level positions in Cr^{51} computed from these results are shown in table 3. The level

TABLE 3

Energy levels of Cr^{51}

Energy levels found by these authors (MeV)	Energy levels found by Stelson and Preston [6]) (MeV)
0.755±0.010	0.750
1.167±0.010	1.165
1.350±0.010	
	1.420
1.486±0.010	
	1.530
1.569±0.010	
1.927±0.010	
2.030±0.010	
2.353±0.010	
2.417±0.010	

positions found by Stelson and Preston [6]) who measured the neutron spectrum from this reaction using photographic emulsions are shown for comparison. The positions of the first two states agree well but at higher energies the better resolution of this method shows additional levels.

References

1) B. B. Kinsey, Can. Journ. Res. (1959) to be published
2) Schoenfeld, Duborg, Preston and Goodman, Phys. Rev. **85** (1952) 873
3) Davison, Buchanan and Pollard, Phys. Rev. **76** (1949) 890
4) A. Zucker and W. W. Watson, Phys. Rev. **80** (1950) 996
5) Elwyn, Landon, Oleksa and Glasoe, private communication
6) P. H. Stelson and W. M. Preston, Phys. Rev. **86** (1952) 807
7) J. C. Grosskrentz and K. B. Mather, Phys. Rev. **77** (1950) 580
8) D. J. Hughes and R. B. Schwartz, Neutron Cross Sections, BNL 325 (U.S. Atomic Energy Commission, Washington, 1958)

4.E *Nuclear Physics* **12** (1959) 432—445; © *North-Holland Publishing Co., Amsterdam*

Not to be reproduced by photoprint or microfilm without written permission from the publisher

INTERNAL BREMSSTRAHLUNG FROM P^{32}

BÖRJE PERSSON and SVEN A. E. JOHANSSON
Department of Physics, University of Lund

Received 29 April 1959

Abstract: The spectrum of internal bremsstrahlung from P^{32} has been measured in a coincidence experiment. The β-particles are detected by an anthracene scintillation spectrometer and the bremsstrahlung spectrum measured by a sodium iodide scintillation spectrometer. Pulses in a certain energy range are selected in the anthracene spectrometer by a single channel analyzer. They are used to gate the 100 channel analyzer which records the bremsstrahlung spectrum. The angle of emission between the β-particles and the bremsstrahlung is defined by the orientation of the spectrometers. The experiment has been performed for a number of different angles. The experimental results are compared with the theory of Knipp and Uhlenbeck and by Bloch. The agreement is very good.

1. Introduction

The internal bremsstrahlung from P^{32} has been investigated several times during the last few years. Unfortunately, however, the results do not agree very well. Novey [1]), Madansky and Rasetti [2]), and Bolgiano *et al.* [3]) found a rather good agreement with the theory. The measurements were restricted to energies below 250 keV. The upper limit was extended to 400 keV by Michalowicz [4]) and to 900 keV by Goodrich and Payne [5]). In both cases satisfactory agreement with the theory was obtained. In contrast to this, Lidén and Starfelt [6]) got a result that agreed with the theory below 600 keV but disagreed for higher energies. At 1000 keV there was an excess over the theoretical curve of 70 per cent. Finally, Langevin-Joliot [7]) obtained an experimental curve which was higher than the theoretical curve with a factor of about 2 over the whole energy range investigated (up to 1100 keV).

In all these measurements basically the same method has been used. The bremsstrahlung spectrum is measured by means of a scintillation spectrometer. The beta rays are in some way prevented from reaching the spectrometer. In most cases they are stopped by an absorber made of a light material so that only a small amount of external bremsstrahlung is produced. Langevin-Joliot used a method in which the source is mounted inside a magnetic field. The electrons spiral away around the magnetic field lines and they are therefore not able to reach the scintillation spectrometer.

In the present work we use a quite different method. The experimental arrangement is shown in fig. 1. The beta rays emitted from a thin source are

recorded by means of an anthracene scintillation spectrometer. The bremsstrahlung spectrum is recorded by means of a sodium iodide scintilllation spectrometer. Only those bremsstrahlung pulses that are in coincidence with a beta-ray pulse are registered.

This type of experiment has a number of advantages.

a) It gives a differential spectrum. A certain beta-ray energy can be selected by the beta spectrometer. A certain angle of emission is defined by the orientation of the spectrometers. A comparison can therefore be made with the differential formula for the bremsstrahlung intensity. It might then be easier to find the cause of any discrepancy between the experimental and theoretical results. A disturbing effect in the experiment is not likely to be independent of electron energy and angle of emission. In contrast to this the earlier experiments have to be compared with a formula obtained by integrating the differential formula over the beta-ray spectrum and over all angles.

b) There is no need of an absolute determination of the strength of the P^{32} source. The counting rate of the beta spectrometer and the efficiency of the gamma spectrometer are enough to enable the bremsstrahlung intensity to be expressed as photons per beta disintegration.

c) The experimental arrangement is in some ways simpler. There is no correction for external bremsstrahlung. The electrons producing external bremsstrahlung in the absorber and the surroundings are not able to reach the beta spectrometer. Hence the external bremsstrahlung will not be recorded. No collimator is needed for the gamma spectrometer. Some of the uncertainties and corrections of the earlier works are therefore eliminated.

d) Finally, it is always desirable to investigate a certain phenomenon by as many different experimental arrangements as possible. The systematic errors will probably not be the same. Hence the experimental results as far as they agree will be more reliable.

There are, of course, some disadvantages with the present method. First of all, the measurements are considerably more difficult. The number of coincidences is low. Counting periods of the order of weeks are therefore necessary. This puts rather rigid requirements on the stability of the apparatus. The electronics is more complicated. An especially important part is the coincidence circuit. It must be fast in order to keep down the number of accidental coincidences. On the other hand it must have 100 per cent efficiency over a wide energy range. These conditions are contradictory and it is necessary to make a compromise.

In the present work we have measured the bremsstrahlung spectrum for the following angles: 25, 45 and 90°. The pulse height analyzer after the beta spectrometer has been set to accept pulses above an energy of about 150 keV. Hence essentially all beta particles are counted by the spectro-

meter. In a future work we plan to measure bremsstrahlung spectra corresponding to beta rays of a certain energy.

2. Experiment

The experimental arrangement is shown schematically in fig. 1. The source is supported by a thin plastic film with a thickness of 25 $\mu g/cm^2$. The film is mounted on a thin plastic ring. The source was prepared by evaporating a carrier-free solution of P^{32} in dilute hydrochloric acid. The activity of the source was about 200μC. The weight of the active material was less than 3μg

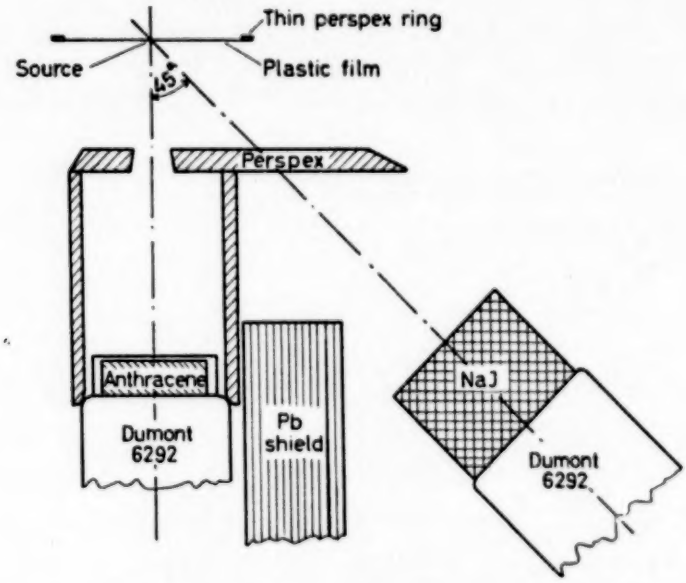

Fig. 1. Schematic diagram of the experimental arrangement.

and it was spread out over a circular area with a diameter of about 2 mm. Hence the external bremsstrahlung produced in the source and the supporting foil is negligible. The spectrometers were mounted as far as possible from surrounding material and walls in order to minimize disturbing scattering and external bremsstrahlung production.

A possible error might come from the external bremsstrahlung produced in the air between the source and the anthracene crystal. It is obvious that the first few centimeters are most important. Closer to the crystal the angle between the axis and the direction to the sodium iodide crystal becomes greater. Since the bremsstrahlung intensity is peaked in the forward direction the contribution in the measured spectrum will decrease with the distance from the source. Furthermore, the lead shield will prevent to a great extent the external bremsstrahlung produced near the anthracene crystal from reaching the gamma spectrometer. The production of external bremsstrahlung in the present geometry can be calculated in principle. The

problem is mathematically complicated, however, and various approximations have to be introduced. Instead we tried to determine it in an experiment. A plastic film with a thickness corresponding to the amount of air between the source and the crystal was placed one centimeter below the source. The external bremsstrahlung contribution from this foil is an upper limit to that one present in the main experiment. We could not find any change by introducing the plastic film, however. Therefore we conclude that this effect is without importance.

The lead shield between the crystals prevents the scattering of gamma radiation between them. We varied the thickness in order to make sure that

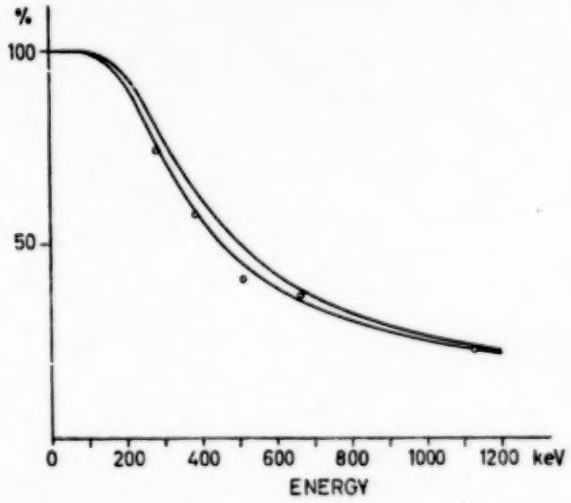

Fig. 2. The photoelectric efficiency of the sodium iodide crystal. The lower curve is fitted to the experimental points. The upper curve is calculated according to Maeder *et al.* [8]).

it was enough. The thickness should also be sufficient to prevent the external bremsstrahlung produced in the anthracene crystal from reaching the sodium iodide crystal. This effect can be calculated. There is, of course, some possibility of multiple scattering. Then the photons are degraded in energy, however. Therefore they have little importance in the bremsstrahlung spectrum which has an exponential shape.

There are a number of corrections that have to be applied to the pulse height distribution in order to get the bremsstrahlung spectrum. First of all, it is the correction for the photoelectric efficiency. The relative efficiency has been determined experimentally by recording spectra for a number of gamma rays of different energies. Fig. 2 shows the result. The lower curve is fitted to the experimental points. The upper curve is calculated on the basis of the theoretical work of Maeder *et al.* [8]). The agreement is as good as can be expected. The absorption coefficients are taken from the tables of White [9]). The correction factor resulting from the experimental curve is shown in fig. 3 (curve 1).

Another important effect is the scattering of the electrons in the space between the collimator and the anthracene crystal. Some of the electrons will be scattered away and will not hit the crystal. This effect is of importance since it depends on the electron energy. The low energy electrons will scatter more than the high energy ones. The efficiency or the anthracene spectrometer will therefore vary with the energy. The scattering of electrons is so well known both theoretically and experimentally that is is possible to treat this problem in an exact way. The probability for scattering of an electron in a certain angle can be calculated. One then calculates the intensity distribution in the plane of the anthracene crystal for electrons coming in

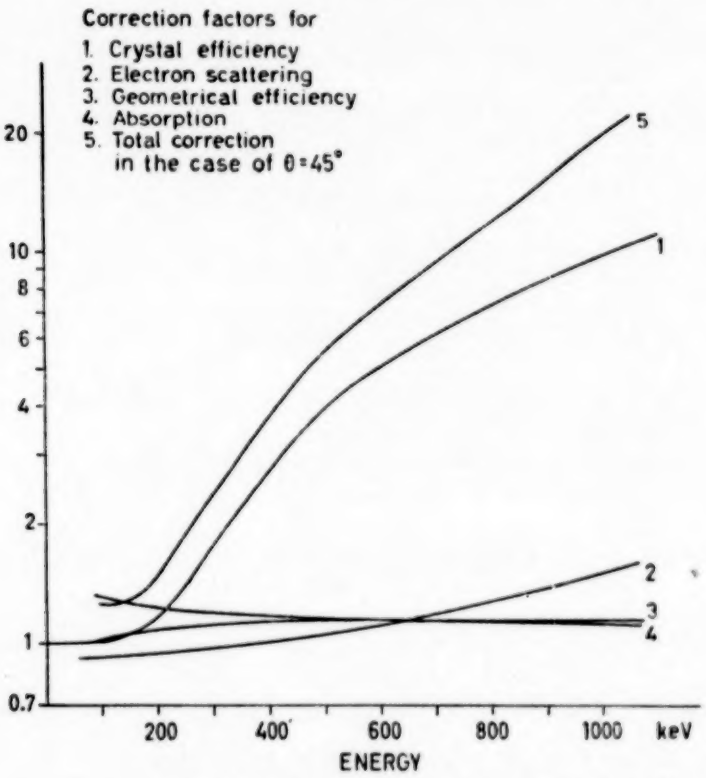

Fig. 3. Correction factors for converting pulse height spectrum to photon spectrum.

a certain direction through the collimator hole. By integrating over all directions one gets the total intensity distribution. The integral contains a modified Bessel function. It is evaluated numerically. The total number of electrons going through the hole divided by the number hitting the crystal then gives the correction factor. The details of the calculation will not be given here. It is straightforward but somewhat tedious. The result is shown in fig. 4. The correction factor is given as a function of the energy. This effect produced a rather effective cut-off for an energy of about 200 keV.

A check on the calculation is provided by the shape of the beta spectrum recorded by the scintillation spectrometer. The true spectrum is modified by the scattering. The spectrum resulting from the application of the correction

factor is shown in fig. 5 as the theoretical curve. Included is also a correction for the energy loss of the electrons in the air between the source and the crystal. It is compared with the experimental spectrum. The agreement is good indicating that the calculated correction is essentially correct. The remaining difference can be attributed to backscattering of electrons from the crystal.

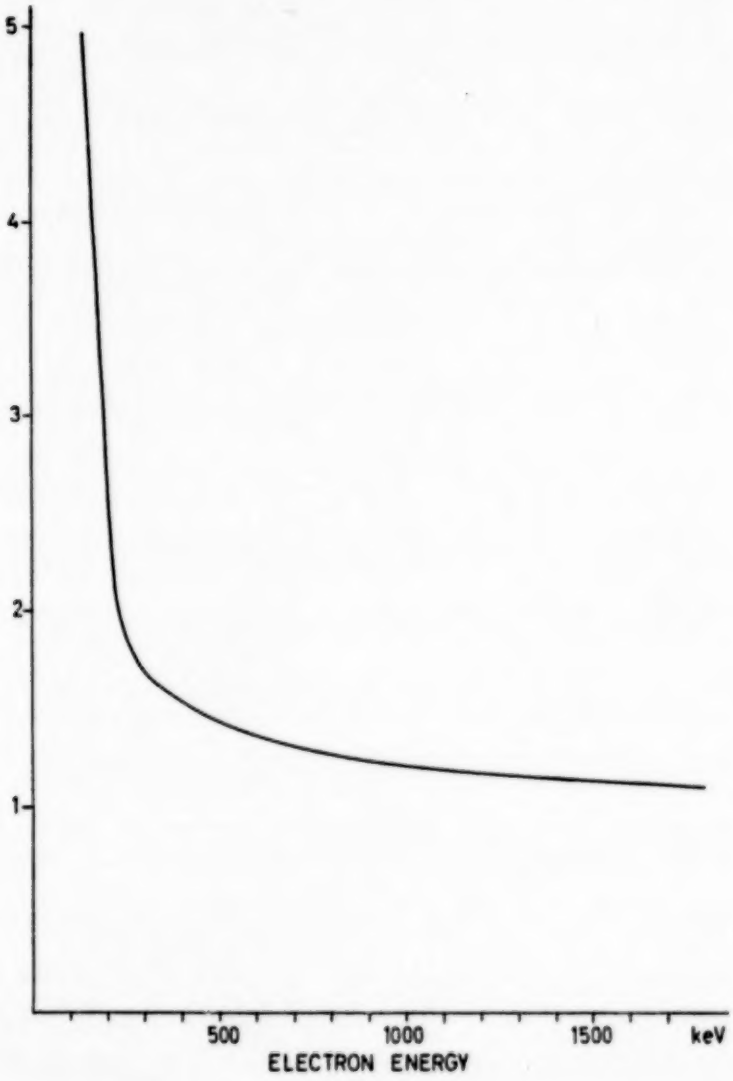

Fig. 4. The correction factor for electron scattering.

The influence of the scattering on the bremsstrahlung spectrum is given by the correction factor (curve 2) shown in fig. 3. It is small for lower energies and increases to 60 per cent at 1000 keV. Even a fairly large relative error in the scattering correction will not cause any serious error in the bremsstrahlung spectrum.

It is, of course, possible to avoid the difficulties with the electron scattering by putting the whole apparatus in an evacuated chamber. This introduces

some difficulties with scattering and bremsstrahlung production in the walls of the chamber, however. Another possible solution is to fill the space between the source and the anthracene crystal with hydrogen gas in order to reduce the scattering. In the present case such measures are hardly worthwhile. For nuclei having a lower beta-ray energy they will be necessary, however.

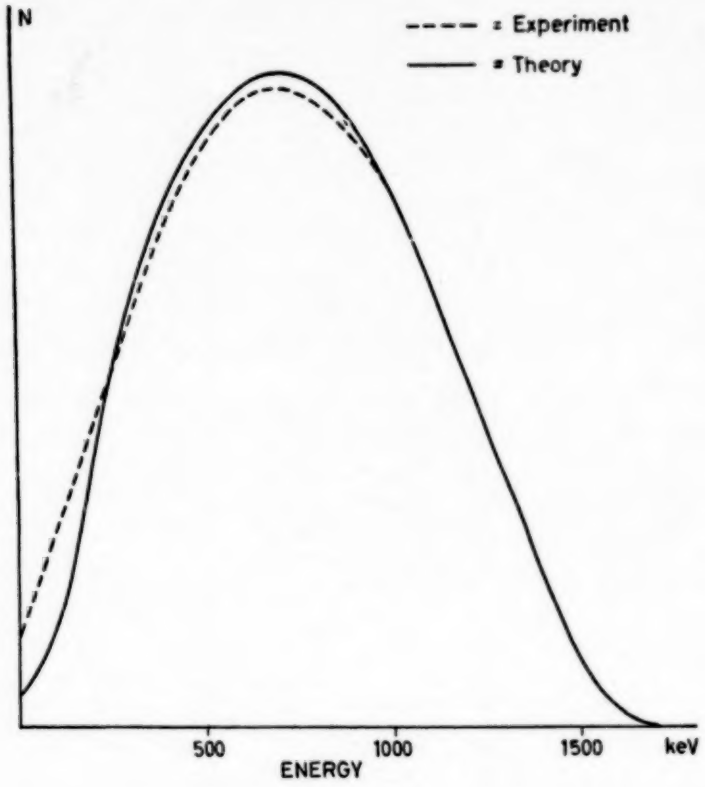

Fig. 5. The shape of the beta spectrum. The dashed curve shows the experimental result and the full turve the theoretical spectrum modified by the calculated correction due to electron scattering.

The remaining corrections are all rather small. The geometric efficiency varies since the absorption in the sodium iodide crystal depends on the energy. The mean solid angle is greater for the low energy photons that are absorbed mainly at the surface than for the high energy photons that penetrate into the crystal. Finally, there is a small correction for the absorption of the photons in the beta-ray absorber and the can of the sodium iodide crystal.

The total correction factor is also shown in fig. 3. Some of the correction factors depend slightly on the angle between the spectrometers. The values in fig. 3 apply to the angle 45°.

Before applying the correction factor shown in fig. 3, it is necessary to make some small corrections that depend on the spectrum shape. It is mainly

the correction for the Compton distribution. It is fairly constant over the whole energy range and of the order of 10 per cent. The corrections for resolving power, K X-ray escape and backscattering are small and have been neglected.

A block diagram of the electronic equipment is shown in fig. 6. The coincidence circuit is of the fast-slow type. The pulses for the fast coincidence circuit are taken from the anodes of the photomultipliers. They are standardized in height by means of a cathode follower and are then clipped in the usual way by a shorted coaxial cable. The fairly high current needed to drive the cathode follower is provided by a White follower. The pulses coming

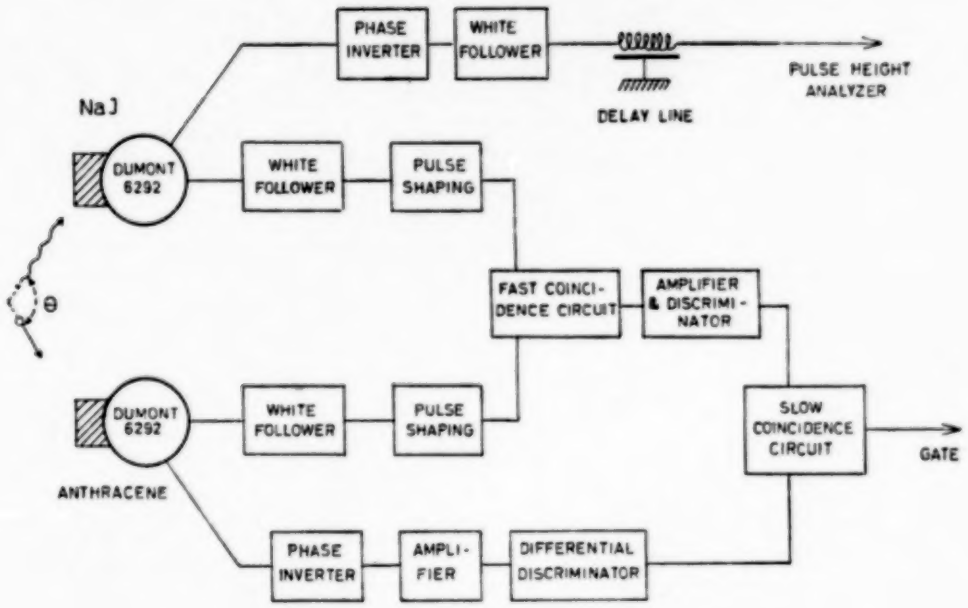

Fig. 6. Block diagram of the electronics.

from the pulse shaper are faily small. If one wants to avoid the difficulties connected with the amplification of fast pulses, it is necessary to use a sensitive coincidence circuit. We used a balanced diode bridge [10]). The pulses from the fast coincidence circuit are amplified and, after discrimination, led to one of the inputs of the slow coincidence circuit. The pulses to the other input come from a single channel pulse height analyzer that selects pulses corresponding to a certain energy interval in the anthracene spectrometer. For the energy measurements the pulses are taken from the third dynode from the end in the two photomultipliers in order to avoid saturation effects, which cause a non-linearity in the energy scale. It is known that for DuMont photomultipliers the pulse height depends to some extent on the counting rate. This effect is also reduced by taking the pulses from one of the dynodes. The bremsstrahlung spectrum is recorded on a 100-channel pulse

height analyzer of the Hutchinson-Scarrot type. It is gated by the pulses from the slow coincidence circuit.

The most important problems in connection with the electronics are the resolution and efficiency of the coincidence circuit. These two questions are, of course, related. The resolution is limited by the fact that the time constant of the sodium iodide crystal is rather long, 0.25 μs. By shaping the pulses the resolving time can be made much shorter. For resolving times of the order of a few ns, however, statistical fluctuations in the time of emission of the first few photoelectrons begin to become important. This effect causes a drop in efficiency for small pulses. It turned out that a resolving time of

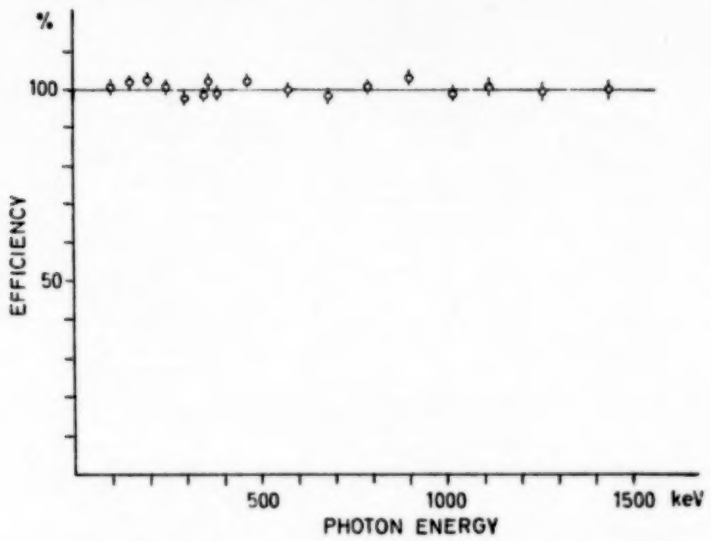

Fig. 7. The efficiency of the coincidence circuit.

about 15 ns was suitable. This choice is rather conservative, but is is better to be sure about the 100 per cent efficiency even if a somewhat higher counting rate of accidental coincidences has to be accepted.

The efficiency of the coincidence circuit was tested extensively. Several radioactive isotopes with well-known decay schemes were investigated for β—γ and γ—γ coincidences under the same conditions as in bremsstrahlung measurements. A comparison between the shape of the pulse height spectra for the coincidences and for the direct pulses gives the relative efficiency. Knowing the efficiency of the scintillation spectrometers and the various correction factors, one can calculate the absolute efficiency of the coincidence circuit. It was found to be 100 per cent with a variation of 2—3 per cent between the different determinations. An example of such a determination is shown in fig. 7. Below 100 keV the efficiency starts to drop in agreement with the result of an analysis of the statistical fluctuations in the photomultipliers.

The correction for the accidental coincidences has to be made very care-

fully, since it is a large effect. To do this the sodium iodide spectrometer was removed and shielded from the rest of the apparatus. In order to keep the counting rate in the spectrometer constant a weak source was mounted close to the sodium iodide crystal. The source consisted of a small amount of P^{32} between two plastic disks. It emits bremsstrahlung and gives roughly the same photon spectrum as is obtained in the coincidence experiments. It was necessary, however, to correct the accidental coincidence spectrum for the difference in the photon spectra. The spectrum of accidental coincidences obtained in this way was used to correct the coincidence spectrum.

The experiment was carried out in the following way. First the coincidence spectrum was recorded for a time of 4—8 hours. The spectrometers were then separated and the spectrum of accidental coincidences recorded for the same length of time. This procedure was repeated many times. The apparatus was run continuously for periods of the order of a week in order to get a single bremsstrahlung spectrum. It was calibrated and checked frequently during this time.

3. Comparison with Theory

The theory for the internal bremsstrahlung in allowed beta transitions was developed independently by Knipp and Uhlenbeck [11]) and by Bloch [12]) with the assumption of polar vector interaction. Second order perturbation theory was used. Knipp and Uhlenbeck give an alternative method in which the emission of the beta particle and the bremsstrahlung emission are assumed to be independent processes. They first calculate the probability for the emission of a beta particle, $P(W)\mathrm{d}W$, from the conventional beta theory. The conditional probability per unit time, $\Phi(W_e, k)$, that an electron coming from the nucleus with the energy W_e will emit a photon with energy k is then calculated, using first order perturbation theory. The probability $S(k)\mathrm{d}k$ for the emission of a photon with energy between k and $k+\mathrm{d}k$ can then be written

$$S(k) = \int_{1+k}^{W_0} P(W_e)\Phi(W_e, k)\mathrm{d}W_e;$$

W_0 is the upper limit of the beta spectrum. The great advantage of this procedure is that for $P(W)$ one can use the experimentally determined spectrum. Many of the difficulties connected with the beta theory are thereby avoided. If this procedure is justified, it is not necessary to know the form of the beta interaction. The justification of Knipp and Uhlenbeck for using this procedure was that it gives exactly the same result as the more rigorous second order perturbation method. Later, Chang and Falkoff [13]) showed that the two methods do not give exactly the same result for forbidden beta transitions. The agreement is good enough, however, to warrant the use

of the simpler method in most cases, especially for low energy photons.

The probability $d\Phi$ that a beta particle emitted with the energy W_e will radiate a photon of energy k per unit photon energy interval at an angle θ between the direction of the beta particle and the photon is given by

$$d\Phi(W_e, k, \theta) = \frac{\alpha p_s}{4\pi^2 p_e k}\left[\frac{W_e^2+W_s^2}{W_e(W_s-p_s\cos\theta)} - \frac{1}{(W_s-p_s\cos\theta)^2} - 1\right] d\Omega_k;$$

W_e is the energy of the electron before the emission of the photon, p_e is the corresponding momentum, W_s is the observed electron energy ($W_s = W_e - k$),

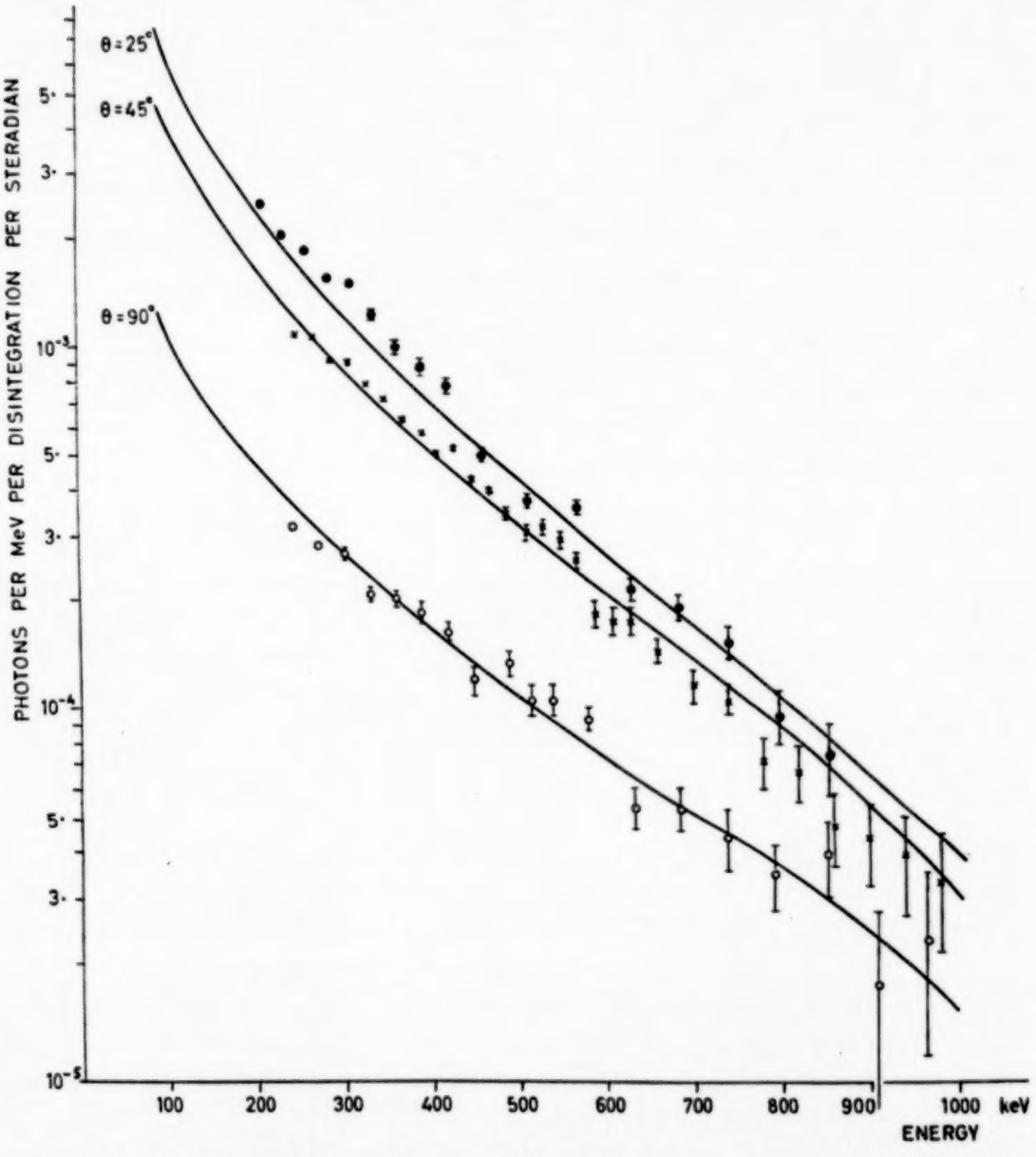

Fig. 8. The experimental internal bremsstrahlung spectra. The curves show the theoretical spectra corrected for the Coulomb effect.

p_s is the corresponding momentum, α is the fine structure constant. All energies are in units of mc^2, and all momenta in units of mc.

In the calculations of Knipp and Uhlenbeck plane wave functions are used rather than Coulomb wave functions. Hence the effect of the nuclear charge on the radiation is neglected. The reason that this does not give a large discrepancy is that the calculations are used only to predict the number of photons per beta disintegration. There is a partial cancellation of the Coulomb effects on the photon and beta intensity.

The influence of the nuclear charge has recently been treated by Nilsson [14]) and by Lewis and Ford [15]). For an allowed beta transition Nilsson suggests replacing $\Phi(W_e, k)$ by

$$\Phi(W_e, k)\frac{F(Z, W_s)}{F(Z, W_e)}.$$

Here $F(Z, W)$ is the Coulomb function in the theory of the beta decay. For $P(W_e)$ the Coulomb corrected distribution should be used. Lewis and Ford arrive at the result that a factor $1+(\pi\alpha ZW_e/p_e)$ should be inserted in the formula of Knipp and Uhlenbeck. This is essentially in agreement with the result of Nilsson. For P^{32}, however, the correction is only of minor importance. It amounts to about 10 per cent at 1000 keV and decreases rapidly for lower energies.

In calculating the theoretical results the expression for $\Phi(W_e, k)$ was calculated for different electron energies. For $P(W_e)$ the experimental beta spectrum was used. The integral for $S(k)$ was evaluated numerically. The correction for the Coulomb effect was performed according to Lewis and Ford. The resulting theoretical spectra are shown in fig. 8 as full lines. The experimental spectra are also shown in fig. 8. The indicated errors are the statistical errors only. The total number of photons in the intervals 250—500

TABLE 1

Experimental and theoretical values of the total number of photons in certain energy intervals
The errors in the experimental values are the statistical errors only

Angle	Energy range (keV)	Photons per disintegration per steradian × 10^5		
		Experiment	Theory	
			Uncorrected	Coulomb corrected
25°	250—500	26.0±0.3	23.1	23.1
	500—900	7.9±0.2	7.7	7.9
45°	250—500	17.0±0.1	16.5	16.5
	500—1000	6.1±0.2	6.4	6.6
90°	250—500	5.2±0.1	5.1	5.1
	500—1000	2.6±0.2	2.4	2.5

keV and 500—900 keV are compared with the theory in table 1. Shown there are the results before and after the application of the Coulomb correction. It will be noted that the correction is very small but that the agreement with the experimental values seems to be slightly improved by the correction.

4. Discussion

The agreement with the theory is very good. Both the shape of the spectra and the total yield agree with the theoretical values within the statistical errors. It is difficult to get an estimate of the systematic errors. The most likely sources of systematic errors are scattering of radiation between the crystals and the production of external bremsstrahlung. The scattering should be most serious for small angles, where the crystals are close together. The results for 25°, however, show the same good agreement with the theory as the results for the other angles. The spectrum of the external bremsstrahlung that is produced when the electrons are stopped in the material around the spectrometers is steeper than the spectrum for internal bremsstrahlung. Hence any disturbance from external bremsstrahlung should be more serious for low photon energies. There is no sign of such an effect. Under these circumstances it would be very strange if the systematic errors exactly compensated deviations from the theory and gave a result which apparently agreed well with the theory. Hence from our measurements we must conclude that the production of internal bremsstrahlung in the decay of P^{32} is in excellent agreement with the theory.

It is difficult to understand the deviations from the theory found in some of the previous experiments. Lidén and Starfelt found a deviation only for higher energies. The total number of excess photons is small, of the order of 1 photon per 10 000 disintegrations. One cannot exclude the possibility of a gamma-ray emitting impurity in the P^{32} source. The reason that it does not show up in our experiment might be that our source material is purer, but it might also be that these gamma rays are not in coincidence with beta rays that can be detected by the anthracene spectrometer. The decay might take place by emission of very low energy beta rays or by K-capture.

Langevin-Joliot reports a large deviation from the theory, the experimental values being a factor of about 2 above the theoretical values. This is in definite disagreement with our work.

References

1) T. B. Novey, Phys. Rev. **89** (1953) 672
2) L. Madansky and F. Rasetti, Phys. Rev. **83** (1951) 187
3) Bolgiano, Madansky and Rasetti, Phys. Rev. **89** (1953) 679
4) A. Michalowicz, J. phys. et radium **15** (1954) 156

5) M. Goodrich and W. B. Payne, Phys. Rev. **94** (1954) 405
6) K. Lidén and N. Starfelt, Phys. Rev. **97** (1955) 419
7) H. Langevin-Joliot, Ann. de Physique **2** (1957) 16
8) Maeder, Müller and Wintersteiger, Helv. Phys. Acta **27** (1954) 3
9) G. R. White, Nat. Bur. Stand. Rep. No 1003.
10) E. F. Shrader, Rev. Sci. Instr. **21** (1950) 883
11) J. K. Knipp and G. E. Uhlenbeck, Physica **3** (1936) 425
12) F. Bloch, Phys. Rev. **50** (1936) 272
13) C. S. Chang and D. L. Falkoff, Phys. Rev. **76** (1949) 365
14) S. B. Nilsson, Arkiv för Fysik **10** (1956) 467
15) R. R. Lewis and G. W. Ford, Phys. Rev. **107** (1957) 756

10.D *Nuclear Physics* **12** (1959) 446—448; © *North-Holland Publishing Co., Amsterdam*

BOOK REVIEWS

K. H. HÖCKER and K. WEIMER (Editors), *Lexikon der Kern- und Reaktortechnik* (Franck'sche Verlagshandlung, Stuttgart, 1959. 2 volumes, 1686 pages. DM 125)

A considerable amount of information is collected in this encyclopedia of nuclear and reactor techniques. The encyclopedia is intended as a help to people working in the field of nuclear energy or to people outside this field, but for various reasons interested in such subjects. It is of little value to the specialist inside his own field, but it may serve him in understanding of the terminology in fields related to his own under the general heading of nuclear energy. Furthermore, it is hoped that the encyclopedia will provide proper German words for all the many items mentioned; at the same time, for each German word the corresponding English and French words are given, and a dictionary is added as an appendix, giving the English-German and French-German references.

The task of writing up all words and definitions of use in the many scientific and engineering aspects of nuclear energy is tremendous. A list of subjects will illustrate this point: Nuclear Physics, Radiation Chemistry, Electronics, Biology, Reactor Theory, Reactor Materials, Radiation Protection, Fuel Processing, Nuclear engineering, Radiology, Waste Disposal, Magnetohydrodynamics. All these and many more subjects are treated in some detail in the encyclopedia. Furthermore, tables of interest such as isotope tables, reactor tables, cross section tables, etc. are given as an appendix.

The detail in which the items are treated may be illustrated by an example chosen among the major subjects: Power reactor station. Under this heading one finds 1) a list of components of such a station, 2) a defining section describing what is meant by power reactor, 3) an extensive discussion of the cost of a complete station, with several calculations leading to a formula for the kWh-cost, and illustrated by a table of examples, 4) a description of the conditions required of the site from the points of view of safeguards, economics and technical aspects and, finally, 5) a discussion of efficiency for all stages in the complete installation.

The encyclopedia is not intended for specialists. This can be illustrated by mentioning an item which is not treated: one finds in the English-German dictionary that parity is called Parität in German, but there is no heading Parität in the encyclopedia. However, such items as the Dirac equation, the Majorana force or the Bohr magneton are mentioned.

The cross references are not always sufficiently carefully arranged. Let me illustrate by an example. It is advertised that one of the main subjects of the encyclopedia is fuel reprocessing. According to the dictionary part this is called in German Brennstoffaufarbeitung. However, the interested reader who looks up this key-word will not find it; but he may be unfortunate enough to find: Brennstoff, aufgearbeiteter, s. Kernbrennstoffaufbereitung. Well, he then takes a look under this word, but finds only Kernbrennstoff, s. Brennstoff. At this time in the process he may be clever enough to look under: Aufbereitung, and here he finds: Aufbereitung des radioaktiven Brennstoffs aus einem Reaktor, s. Kernbrennstoff-aufbereitung. Of course, he now knows that this does not work and may happen to understand that not only is there an item Brennstoff, aufgearbeiteter, but also the proper item Brennstoffaufbereitung, under which word he finds the pertinent information.

The definitions could sometimes have gained in clarity by being shortened, but thorough popular descriptions of the words are often given and this should be of great help for the non-specialist.

The user of the encyclopedia should be warned that it contains an addendum („Nachtrag") in which many new items such as thermonuclear devices are described. However, even in spite of this addendum much recent information has not been included. Thus the Windscale reactors

are according to this encyclopedia still going strong and the Windscale accident is not mentioned.

As a conclusion it may be said that the present encyclopedia is quite valuable. It is easy, in large collective works of this kind, to find small subjects for jokes, but it is a major undertaking to write an encyclopedia and it cannot be denied that a wealth of information is amassed here.

O. Kofoed-Hansen

WILLIAM GALBRAITH, *Extensive air showers* (Butterworth, London, 1958. xvi+211 p. 40 s).

Twenty years after the first recognition of extensive showers in cosmic radiation, these events, as a result of widespread and sustained investigation, are understood in broad outline. Meanwhile, the remarkable position which they occupy in the development of physics has become clear. They offer on the one hand an important tool for the advancement of cosmology, for we surely ask what properties must be attributed to the galaxy if particles which give rise to the largest known extensive showers are to be found moving isotropically near the earth, and by what means these particles have attained great energy. On the other hand the interactions from which large showers derive in the atmosphere take place at energies far beyond prospective human initiation, but equally certainly not beyond the realm of interest.

It seems likely that understanding of extensive showers has reached a point from which further work will be undertaken in a more purposeful and co-ordinated manner than was much in the past, and Dr. Galbraith's very timely book will be of main value for the way in which he has brought together, summarized and commented upon the wide and varied range of experiments which have been reported. The book is quite essential to all who now plan to work in the field; through almost the whole of the book the degree of detail given seems admirably chosen, and even those already generally familiar with the literature will be grateful for a freshness of approach as well as for a convenient summary.

Whether the book will appeal to a wider range of readers is not so certain, but here the fault does not lie so much with the author as with the subject matter. What is reported here is instructive in the range of techniques which have been deployed for complementary observations and in the processes of deduction which, largely from experimental shortcomings, have been forced upon workers. But it is precisely the points which might interest a wider audience — a confident description of the very high energy primaries and of the details of first collisions at these energies — which can only be the subjects of a tentative and probably unsatisfying discussion at the present time.

A feature which invites criticism is the system of references, which seems inferior to others in common use.

J. G. Wilson

W. R. WOOTTON, *Steam cycles for nuclear power plant* (Nuclear Engineering Monographs) (Temple Press Limited, London, 1958. vii—66 pages. 10 s 6d.)

This book is volume VI in a series of monographs on nuclear engineering.

It is intended for non-specialists, who want a better understanding of this topic of nuclear engineering.

The book is small, the space limited. However, the author has been able, without use of deeper theory, to account for the special problems which are connected with the selection of the steam cycle for a nuclear power plant.

As one can expect the greater part of the book treats of reactors of the gas-cooled, graphite-moderated type and their associated steam cylces, the single pressure cycle and the dual pressure cycle. The reheating steam cycle is mentioned and the super-critical pressure steam cycle touched on.

The steam cycles for water-cooled, water-moderated and liquid-metal-cooled, graphite-moderated reactors are discussed in very few pages.

The book has six appendixes, among which the use of steam tables, the Mollier-diagram and the temperature-entropy diagram are illustrated by use of examples.

The aim taken into consideration, a good book.

H. Abel-Larsen

M. HAÏSSINSKY (Editor), *Les Peroxydes Organiques en Radiobiologie* (Organic Peroxides in Radiobiology), Fourth Series of *Actions Chimiques et Biologiques des Radiations*. (Masson et Cie, Paris 1958. 156 p. 36 nouv. fr.)

In the fourth colloquium of the series organised by Professor M. Haïssinsky, radiochemists and radiobiologists joined in discussing aspects of radiation-induced peroxide formation in simple and biological systems. This book contains the papers that were presented at the meeting together with the discussions which followed.

The colloquium opened with a paper by C. Paquot describing recent work on the chemistry of fatty acid peroxides, a topic which was developed by M. Durup who has studied the radiochemical peroxidation of cumene and by J. Durup who had investigated the degradation of polystyrene by irradiation.

The articles which follow deal mainly with the influence of oxygen on radiation effects *in vitro* and *in vivo* in biological material. Radiobiologists are very familiar with the action of oxygen in augmenting radiation damage in living organisms, a topic well summarised by L. H. Gray. A possible mechanism for this effect was discussed by T. Alper. Philpot has for some time speculated that X-radiation damage might be mediated by a peroxide. He and his collaborators have now studied the autoxidation of various lipid materials (squalene and linoleic acid) and have measured the toxicity of the autoxidation products in mice. R. Latarjet *et coll.* conclude from a study of the inactivation of bacterial transforming principals (DNA) by peroxides and by radiation that peroxide could be the mediators of the radiation damage. F. H. Sobels discussed the mutagenic effect of peroxides in relation to that of radiation. J. A. V. Butler gave a short account of the effect of oxygen in the degradation of DNA by ionizing radiation. J. Weiss followed with a description of the formation of hydroperoxides from nucleic acids and related compounds. It now appears that lipid peroxides are not the only peroxides to be considered by the radiobiologist; the idea that amino-acids and peptides also give rise to hydroperoxides on irradiation was introduced by S. Okada.

These and other articles not specifically mentioned here together make a valuable contribution to our knowledge of the actions of radiations. The possibility that there exists an identity of action between peroxides and ionizing radiation was well discussed but the final word remains to be said about this difficult problem.

Derek B. Hope

NORTH-HOLLAND BOOKS

TURNING POINTS IN PHYSICS

A series of lectures given at

OXFORD UNIVERSITY in TRINITY TERM 1958

5×8″ viii + 192 pages Guilders 10.50 (20s.)

THE CONTENTS

INTRODUCTION
by A. C. Crombie,
All Souls College, Oxford

i. THE END OF MECHANISTIC PHILOSOPHY AND THE RISE OF FIELD PHYSICS
by R. J. Blin-Stoyle,
Clarendon Laboratory, Oxford

ii. THE QUANTUM NATURE OF MATTER AND RADIATION
by D. ter Haar,
Clarendon Laboratory, Oxford

iii. PROBABILITY ENTERS PHYSICS
by K. Mendelssohn,
Clarendon Laboratory, Oxford

iv. FROM THE RELATIVE TO THE ABSOLUTE
by G. Temple,
Mathematical Institute, Oxford

v. THE DECLINE AND FALL OF CAUSALITY
by F. Waismann,
New College, Oxford

vi. TOWARDS NEW CONCEPTS: ELEMENTARY PARTICLES
by D. H. Wilkinson,
Clarendon Laboratory, Oxford

THIS VOLUME CONTAINS the text of a series of six lectures organised by the Reader in the Philosophy of Science and the Lecturer in the History of Science in the University of Oxford and given by senior members of the University to an audience composed mainly of philosophers and scientists, who were not physicists. As a consequence these lectures are non-technical and can be understood by laymen who are interested to read about the development of physics in the last hundred years.

The first lecture describes how the concept of fields was introduced by Faraday and Maxwell, the next two lectures and the fifth lecture describe the changes in outlook brought about by the advent of quantum mechanics. These changes incorporate a change in the concepts of probability, causality and determinism, as well as the introduction of the idea of quantisation. The fourth lecture deals with relativity and the last lecture describes the galaxy of so-called elementary particles which nowadays dominate such a large part of physics.

Sole Agency for U.S.A.: Interscience Publishers Inc. - New York

NORTH-HOLLAND PUBLISHING COMPANY - AMSTERDAM

REPRINTS OF NUCLEAR PHYSICS

Available at the Publishers

NUCLEAR ENERGIES AND THE SHELL MODEL

by

NISSAN ZELDES

Department of Physics, The Hebrew University of Jerusalem, Israël

and

Department of Mathematical Physics, University of Birmingham, England

volume 7 (1958) no. 1,
84 pages, 20s., $ 2.80

PARTICLES AND SYMMETRIES

by

E. CORINALDESI

University College of North Staffordshire, Keele, England

volume 7 (1958) no. 4
68 pages, 17s., $ 2.25

ENERGY LEVELS OF LIGHT NUCLEI. VI

by

E. AJZENBERG-SELOVE

Department of Physics, Haverford College, Haverford, Pennsylvania

and

T. LAURITSEN

Kellog Radiation Laboratory, California
Institute of Technology, Pasadena, California

volume 11 (1959) no. 1
320 pages, 40s., $ 5.30

NORTH-HOLLAND PUBLISHING COMPANY

NIEUWE ZIJDS VOORBURGWAL 68-70 AMSTERDAM-C HOLLAND